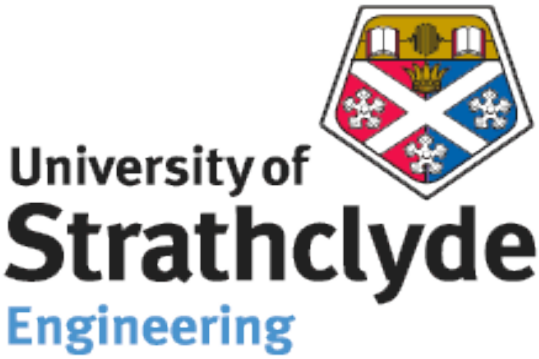

Batch to Continuous Organic Salt Crystallisation:

Model Based Design

John McGinty

Thesis submitted to the Chemical and Process Engineering Department

at the University of Strathclyde in accordance with the requirements for

the degree of Doctor of Philosophy

June 2017

Declaration of Author's Rights

This thesis is the result of the author's original research. It has been composed by the author and has not been previously submitted for examination which has led to the award of a degree.

The copyright of this thesis belongs to the author under the terms of the United Kingdom Copyright Acts as qualified by University of Strathclyde Regulation 3.50. Due acknowledgement must always be made of the use of any material contained in, or derived from, this thesis.

Signed:

Date:

Acknowledgements

Firstly I would like to thank my supervisor Prof Jan Sefcik for his constant support and guidance throughout my PhD project. In addition, I would like to thank my second supervisor Dr Chris Price for his input and advice when required.

Everyone in the Department of Chemical and Process Engineering in addition to the EPSRC Centre for Continuous Manufacturing and Advanced Crystallisation (CMAC) deserve gratitude and appreciation for their academic and technical support during my PhD project. In particular, I would like to thank Dr Thomas McGlone, Dr Naomi Briggs and Vishal Raval for their training in operating the continuous oscillatory baffled crystalliser (COBC). I would also like to thank Dr Anna Jawor-Baczynska, Dr Pól MacFhionnghaile and Vaclav Svoboda for their assistance in assembling and maintaining the continuous mixers. In addition, I would like to thank Dr Elke Prasad for performing the experimental pH-solubility measurements of 3,5-dinitrobenzoic acid (3,5-DNBA).

I would like to thank Prof Zoltan Nagy and his research group for hosting me during my 2 month placement at Purdue University in Indiana, USA where I conducted many of the semi-batch crystallisation experiments. I would also like to thank Dr Helen Wheatcroft and all members of the AstraZeneca Right Particle team in Macclesfield, UK for hosting me during my 3 month placement where I performed some of the continuous crystallisation experiments.

Finally, I would like to thank all my friends and family for their encouragement and support throughout my PhD project.

Abstract

Organic salt crystallisation is of great importance to the pharmaceutical industry as the majority of pharmaceutical products are sold as salts with salt formation being an essential step in drug development. In this research a solution speciation model was developed to predict pH and solution composition during salt crystallisation processes. This tool allows for the entire salt crystallisation design space to be explored in terms of process pathways in the concentration vs. pH phase diagram. This allows for greater process understanding to be obtained and for theoretical solid yields to be determined.

The model compound used in this work is the polymorphic organic salt ethylenediammonium 3,5-dinitrobenzoate (EDNB) which is the 2:1 salt of 3,5-dinitrobenzoic acid (3,5-DNBA) with ethylenediamine. In this system one of the two EDNB polymorphs (monoclinic and triclinic) or the 3,5-DNBA starting material may crystallise. The solution speciation model was used to predict the crystallisation pathway for each solid form and to guide the development of semi-batch and fully continuous crystallisation processes. In addition, aqueous pH-solubility measurements of EDNB triclinic and 3,5-DNBA were made to better understand EDNB salt solubility in high ionic strength solutions and to establish the operating space where 3,5-DNBA crystallisation is avoided.

In this study EDNB crystallisation was experimentally performed in semi-batch and fully continuous processes. The semi-batch experiments demonstrated the scale up of the EDNB crystallisation process to 400 ml compared to 50 ml in literature. The fully continuous processes demonstrated that continuous mixing approaches could be used to crystallise the EDNB salt with consistent yield and PSD. Control over which polymorphic form crystallised was successfully demonstrated in both semi-batch and continuous mixing processes.

Contents

List of Figures

List of Tables

1. Introduction

One of the oldest chemical engineering unit operations in history is evaporative crystallisation which was employed to recover salt from sea water [1]. The process of crystallisation has remained an important unit operation throughout history with the techniques evolving and improving but the fundamental principles staying the same. Currently crystallisation processes are widely used for particle formation, purification and separation in the fine chemical and pharmaceutical industry. Many fine chemical products and active pharmaceutical ingredients (API) are synthesised in solution and then crystallised further downstream as solid materials. The ability to separate the desired compound from the bulk solution is essential because the bulk often contains by-products from the chemical reactions, and impurities from the input materials.

It is well established that the conditions under which a solid is crystallised can affect its physical properties with factors including temperature, solvent, pH and agitation speed often being manipulated to control crystal size, shape, purity and solid form [2, 3]. Therefore, a large amount of work has been carried out by both academia and industry in order to better understand the principles of solubility and supersaturation, in addition to crystal nucleation and growth.

Organic salt crystallisation, in particular, is of great importance to the pharmaceutical industry as many pharmaceutical products are sold as salts. Salt formation is a popular technique as it modifies and optimises physiochemical properties. Important properties including solubility, dissolution rate and stability can be improved by using a range of pharmaceutically acceptable counter-ions [4]. In fact it is possible to form a wide range of salts from an active acidic or basic compound and therefore a salt screen is typically carried

out in order to discover which salt has the best overall properties for the intended application [5, 6]. Despite the importance of organic salt crystallisation there is a lack of literature describing appropriate design principles which is in stark contrast with the crystallisation of single component molecules. For example, an in-depth study of the pH-solubility of the desired salt usually isn't carried out.

Currently, the main method for producing crystals in the pharmaceutical industry is to use stirred tank reactors (STRs) operated in batch mode. In the pharmaceutical industry there are long timelines and uncertain project outcomes to commercial products. That is, the majority of projects do not move past the R&D stage so batch technology is used due to its flexibility. Moreover, even for products which are commercialised, only relatively small volumes are produced (100s tonnes per year for popular drugs) which traditionally favours the use of batch reactors rather than continuous reactors [7, 8].

Despite their widespread use there are several challenges with batch STRs. The major challenge is that of scale up which is especially true for salt crystallisation. It's usually difficult to scale up from the laboratory with variability in the product arising due to mixing imperfections. In fact, in a large STR a significant portion of the batch time is the time required simply to fully mix and remix the contents of the vessel in a dynamic manner. The additional challenges of batch processing include poor understanding of the effects of volume, a lack of control over the entire vessel and low yields due to the varying rates of heat and mass transfer throughout the batch time.

The challenges of poor scalability, poor control and poor yield can be addressed by switching from batch to continuous crystallisation. Continuous crystallisation offers the advantages of reduced waste and energy consumption (due to increased yields and smaller equipment) in addition to greater process control (by using PAT at steady state) and

reduced costs (combined effect of other advantages) [7]. Due to the prevalence of stirred tank reactors in the pharmaceutical industry, the simplest continuous setup possible would be a single stage or cascade of mixed-suspension, mixed-product-removal crystallisers (MSMPRs). As the MSMPRs in the cascade are smaller than their batch equivalent the mixing imperfections are reduced. Another possible continuous setup is the tubular plug flow crystalliser (PFC) which exhibits improved mass and heat transfer rates due to the higher area/volume ratio (specific surface area). Therefore, either continuous crystallisation setup yields a higher quality product than the traditional batch stirred tank reactor.

To overcome the challenges discussed here the first main aim of this project was to increase the understanding of ionic equilibria in solution and the pH-solubility of salts. The theory of these topics is well covered in textbooks but still isn't commonly applied to designing salt crystallisation processes. In order to address this lack of understanding a full solution speciation model was developed that can be used to predict pH and solution composition during an organic salt crystallisation process. Simply with knowledge of component concentrations, dissociation constants and solubility products this tool can be used to generate the entire crystallisation design space, explore different solution addition/mixing approaches and model full crystallisation processes. This allows for the number of experiments to be minimised, easier transfer from batch to continuous crystallisation and increased process understanding.

In this work the model compound studied was the polymorphic organic salt ethylenediammonium 3,5-dinitrobenzoate (EDNB). In addition to the solution speciation model, understanding of ionic equilibria and pH-solubility was increased by experimentally measuring the aqueous pH-solubility of the materials involved in this model system.

Furthermore, a new activity corrected solubility equation was developed and applied to properly account for the effect of high ionic strength on the solubility of the EDNB salt.

The other main aim of this project was to experimentally scale up the semi-batch EDNB crystallisation process and transfer it to a continuous mixing process. The first step in batch to continuous transfer was to utilise the solution speciation model developed here to select suitable operating conditions with respect to the mixing approach, solution concentrations and flow ratio. Once the operating conditions are selected a continuous mixer with a confined volume should be utilised to mix the solutions. The confined volume provides more intense, consistent and scalable mixing in comparison with larger continuous reactors (CSTRs, COBCs, etc.). PAT tools were used in combination with the solution speciation model to obtain greater process understanding and to determine if steady state had been reached in the continuous crystallisation processes.

Overall, the aim of the project was to develop a quantitative salt crystallisation model to assist in the transfer from small scale semi-batch EDNB crystallisation to larger scale fully continuous EDNB crystallisation. The model allows for the EDNB crystallisation process to be better designed and understood. The transfer from batch to continuous processing allows for the mixing of the solutions to be more controlled and scalable which leads to a more consistent product in terms of the polymorphic outcome and particle properties.

2. Background

2.1. Solubility and supersaturation

In a pure solvent, at any given temperature and pressure, there is an equal chemical potential throughout the system and a spontaneous change should not occur. If a solid is added into the solvent there is an effect on the chemical potential between the solvent, dissolved solute and undissolved solid so the system seeks to return to equilibrium by allowing the solid to dissolve into the solvent by a certain extent. If the amount of solid is below a certain value it will become completely dissolved in the solvent. However, if the amount of solid is above a certain value then the system will reach equilibrium between the dissolved solute and the remaining undissolved solid. This value at which equilibrium takes place is known as the saturation concentration or the solubility. For any system, with any number of solvents and solutes, the solubility value depends on many different parameters including temperature, pressure, solute concentrations, solvent composition and pH. As with any concentration, the solubility can be expressed in various units but is almost always an amount of solute per unit amount of solvent (or solution). Example units include mg/ml solvent, kg/m^3 solvent and mol/L solvent.

A saturated solution is a solution where the solute concentration equals the saturation concentration. In order to crystallise the solute from a saturated solution, a system parameter (temperature, solvent composition, pH etc.) must be manipulated in order to reduce the saturation concentration and make the solution supersaturated rather than saturated. After a certain period of time a supersaturated solution will undergo phase separation where the solute will come out of the solution in the crystalline phase. The formation of a crystalline phase has two main steps: nucleation, the birth of stable crystal nuclei, and crystal growth, the addition of more solute onto the existing crystals. The

generation of supersaturation is essential for all crystallisation processes as a solute can only nucleate from a solution when the solution is supersaturated.

The supersaturation may be defined in several different ways with one of the most common ways being the relative supersaturation (S) which is the ratio of the actual concentration (C) to the saturation concentration (C_S) as shown in equation 1. The relative supersaturation is unitless as it is a ratio of two concentrations.

$$S = \frac{C}{C_S} \tag{1}$$

For single component systems using this definition of relative supersaturation is usually the best method for describing the crystallisation driving force but for multicomponent systems, like co-crystals and salts, this is not the case. The definition of salt supersaturation is discussed and shown in section 4.2.

2.2. Crystal forms (polymorphs, co-crystals & salts)

Understanding the crystalline form of an API is vital for successful drug development. That is, the solid API can exist in several subphases which include polymorphs, solvates, hydrates, co-crystals and salts [9, 10]. Polymorphs are different crystalline structures of the same chemical entity [11]. The other subphases are different in that solvates, hydrates, co-crystals and salts consist of more than one type of molecule; one molecule being the API and the other being either an organic solvent (to form a solvate), water (to form a hydrate) or another crystalline solid (to form co-crystals or salts). Co-crystals and salts are often referred to as multicomponent solid forms. The two molecules comprising the co-crystal or salt participate in the short-range and long-range orders of the crystal and so the co-crystal or salt is considered a single crystalline form consisting of two molecules.

The use of salts has been investigated extensively [12-14] as the salt of an API may exhibit improved chemical and physical properties in comparison with the original API. As the benefits of salt formation became apparent over the years many studies [15-18] have been conducted to discover, form and characterise new salts for a range of applications. The optimisation of properties such as solubility, dissolution rate and stability is clearly a very attractive prospect for the pharmaceutical industry. It is for this reason that during the development of an API, a salt screen will typically be carried out using a range of pharmaceutically acceptable counter-ions in an effort order to discover a salt with the best possible overall properties for the intended therapeutic application.

With regards to pharmaceutical salt screening there is no predictive method for determining if a specific acidic or basic API would form a salt with a specific counter ion. However, it has been repeatedly shown that salt formation generally requires the pKa value of the acid to be smaller than the pKa value of the base to make sure that there is sufficient proton transfer from the acidic species to the basic species. Additionally to this there have been salt formation guidelines proposed by several researchers saying how best to choose a counter ion. Typically, a minimum difference of 2 pH units is required between the acid and base to allow for salt formation. However, this isn't always the case and therefore exhaustive and wide reaching salt screens are still often required [4].

In addition to salts, a large volume of research has been performed to try and better understand polymorphism and to discover new polymorphs [19-23]. This knowledge is very important to the pharmaceutical industry because they need to know all the possible polymorphs of an API that may crystallise so they can ensure they consistently crystallise the desired polymorph for regulatory reasons. There have been attempts to predict polymorphism as part of crystal structure prediction so that all the possible polymorphs of a

molecule can be predicted from molecular structure alone [24, 25]. However, the computational power required for these predictions is massive and the predictions are currently not able to deal with the complexity of most organic molecules. Therefore, determining all the possible polymorphic outcomes of a crystallisation process still requires an experimental approach which utilises extensive screening methods.

The pharmaceutical industry usually prefers to use the most thermodynamically stable polymorph (under ambient temperature and humidity) for a medicinal product because of its inherent thermodynamic stability. Using a metastable form poses the risk of transforming to a more stable form during manufacturing or storage. However, there are cases when the stable form doesn't possess the therapeutic properties required and it's necessary to produce and market the metastable form of the API. With regards to relative stability, it is common for a metastable form of the API to nucleate first during a crystallisation process. This is explained by Ostwald's rule of stages which tells us that in an unstable system the first transition state results from the smallest loss of free energy and the system doesn't need to move to the most stable state first. However, the most stable polymorph does have the lowest solubility in solution and so if a metastable polymorph is present it will transform to the most stable polymorph eventually. The mechanism for this transformation is thought to be that the stable form nucleates on the surface of the metastable form before the stable from then grows as the metastable form dissolves. Developing the ability to control which polymorph is crystallised from solution by manipulating the crystallisation process conditions has been researched extensively [26-33].

2.3. Solution speciation & pH

Developing design principles for organic salt crystallisation requires an understanding of ionic equilibria and the speciation of acids and bases which is well covered in textbooks [4, 34]. Strong acids and bases are assumed to be fully dissociated in whatever solvent they occupy but the speciation of weak acids and bases are more difficult to determine. Their speciation depends on solvent, pH and temperature and needs to be calculated from measured pK_a values. The pKa value of an acid or base essentially defines its strength with this being the pH at which half of the acid or base is in its ionised form. The ionisation of an acid may be represented by the equilibrium between its protonated and unprotonated form as shown in equation 2.

$$AH \leftrightarrow A^- + H^+ \tag{2}$$

The dissociation constant, K_a, which represents this equilibrium is expressed by equation 3 and is related to the pKa by equation 4.

$$K_a = \frac{a_{A^-}\, a_{H^+}}{a_{AH}} \tag{3}$$

$$pKa = -\log K_a \tag{4}$$

Therefore, in a solution the extent to which a weak acid or base has dissociated is characterised by its inherent pKa value and the overall pH of the solution. In fact, knowledge of these values allows for the calculation of the relative quantities of the protonated and unprotonated species in solution. The relative concentrations of the species as a function of pH are typically presented graphically in the form of a speciation diagram. An example of a speciation diagram for a weak acid with a pKa of 4 is shown in Figure 1.

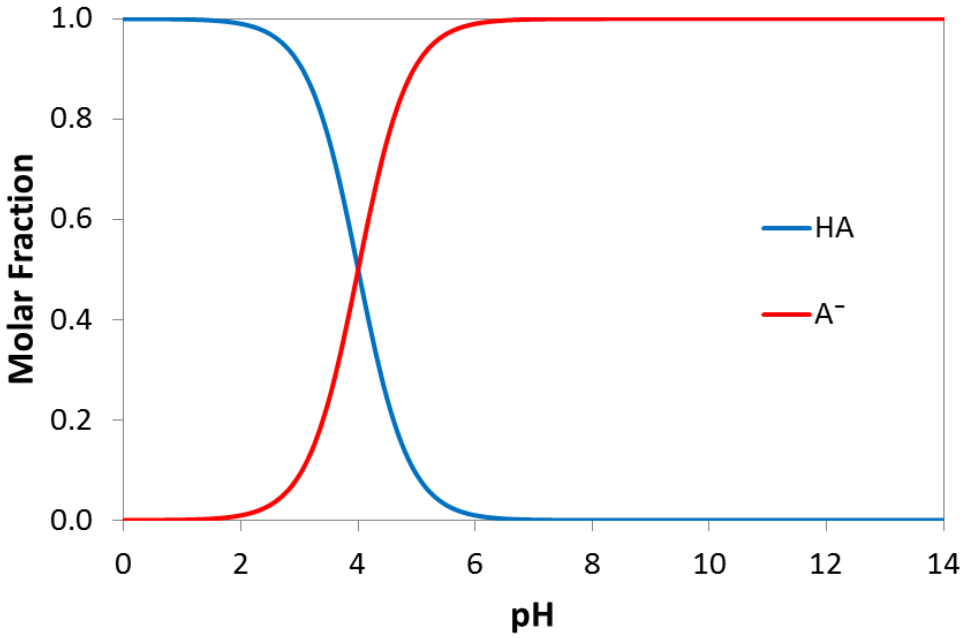

Figure 1. Example speciation diagram for weak acid with a pKa of 4.

The speciation diagram demonstrates that half of the weak acid is ionised at pH 4 because it has a pKa value of 4. As an API is almost always a weak acid or base it clearly necessary to measure all of the pK_a values associated with it. In addition to knowing the pKa values it is also vital to know which of the species of the API will combine with the counter-ion in solution to form the salt of interest. With this combined knowledge the salt can be formed experimentally by reaching a target pH for a particular solvent and temperature.

2.4. Continuous crystallisation

Despite the widespread use of batch stirred tank reactors (STRs) in the pharmaceutical industry they have several challenges. The major challenge is that of scale up which is especially true for salt crystallisation. It's usually difficult to scale up from the laboratory with variability in the product arising due to mixing imperfections. In fact, in a large stirred tank reactor a significant portion of the batch time is the time required simply to fully mix and remix the contents of the vessel in a dynamic manner. Another issue with scaling up

stirred tank reactors is that as the impeller diameter increases, the tip speed increases despite the lower rotation speed. This results in increasingly high shear with impellers of increasing size. With regards to crystallisation, this is a huge problem as the high shear regions around the impeller tip will cause significant attrition resulting in the generation of fines. Other issues caused by the poor scalability of batch processes are a lack of control and low yields.

The interest in continuous crystallisation techniques from academia and industry has increased over recent years with a greater effort being put into researching the transfer from batch to continuous processes. The reason is that continuous processing has the potential advantages of lower costs, faster manufacturing, increased scalability and improved process control [7, 8]. For the pharmaceutical industry the simplest and least risky transfer from batch to continuous crystallisation is to use an existing batch stirred tank reactor (STR) and change its operation to the continuous mode which is described as a single-stage mixed-suspension, mixed-product-removal crystalliser (MSMPR). Due to the ease of this equipment modification and simplicity in design there has been extensive research conducted into continuous crystallisation using a single-stage MSMPR. The work has included cooling [35-41], antisolvent [42, 43] and reactive [44-47] crystallisation processes.

An extension of the single-stage MSMPR is simply to utilise a cascade of MSMPRs. The main advantage of utilising a cascade of MSMPRs, rather than a single stage MSMPR, is that with each additional MSMPR the flow moves closer to being plug flow. Using at least 5 MSMPRs typically ensures that the flow is approximately plug flow. This regime of near plug flow is desired for a crystallisation process because it means that the crystals travelling through the crystalliser will have a narrow residence time distribution which results in a narrow

crystal size distribution. In addition to obtaining plug flow, another advantage of using a cascade is that for a particular throughput each vessel can be smaller than the comparative single stage MSMPR that would be required. This means that it will be easier to maintain efficient mixing and avoid the unwanted attrition of crystals. It is because of these advantages that many studies have looked at implementing and developing MSMPR cascades for continuous crystallisation. MSMPR cascades have been used for traditional cooling, antisolvent and reactive crystallisations [48-50] in addition to crystallising multicomponent systems [51]. Furthermore, crystallising under steady state periodic flow rather than standard steady state flow has been investigated [52]. The availability and versatile nature of MSMPRs (single and multi-stage) means that they are the most widely used type of continuous crystallisation device. Despite this they still suffer from similar limitations to batch STRs in that it can be difficult to ensure efficient mass and heat transfer across the entire STR volume. This is especially apparent when there is an attempt to mix solutions in the vessels.

In addition to MSMPR cascades, tubular plug flow crystallisers (PFCs) are commonly used for continuous crystallisation. Each setup has its advantages and disadvantages with the selection typically being down to the kinetics of the crystallisation process. An MSMPR cascade is usually chosen for systems that require longer residence times and the PFC is chosen for systems that exhibit higher conversions and shorter residence times. The main advantage of a PFC over a MSMPR cascade is that it has a higher area/volume ratio (specific surface area) which results in improved mass and heat transfer. With the only criteria for a PFC being that it is tubular and operates in plug flow, it can come in many forms. However, most PFCs used in continuous crystallisation have narrow internal diameters (<5 mm) and are constructed from plastic or glass (to allow for visualisation of process). Plug flow is created either from a combination of a small diameter and high flow rate or from

segmentation via air or immiscible fluid. The development and use of PFCs has been studied for cooling [53, 54], antisolvent [42, 55-57] and reactive crystallisation [58-60] in both segmented and non-segmented flow. PFCs are usually the most suitable device for mixing-induced supersaturation crystallisations (antisolvent and reactive) as their confined volumes allow for intense and controlled mixing. However, producing solids in these small volumes can lead to major fouling and blockage issues which is the main challenge that still has to be overcome.

With regards to PFCs there is one special case called the continuous oscillatory baffled crystalliser (COBC) which has received much interest in recent years. A COBC is a tubular device with periodically spaced orifice baffles across which fluid oscillation is superimposed. The COBC system comprises a series baffled glass tubes (straights) and bends connected to an oscillation source. The geometry of the DN15 COBC straights and an example of the set-up are shown in Figure 2. The DN15 COBC has this name because it is designed to have an internal diameter of 15 mm.

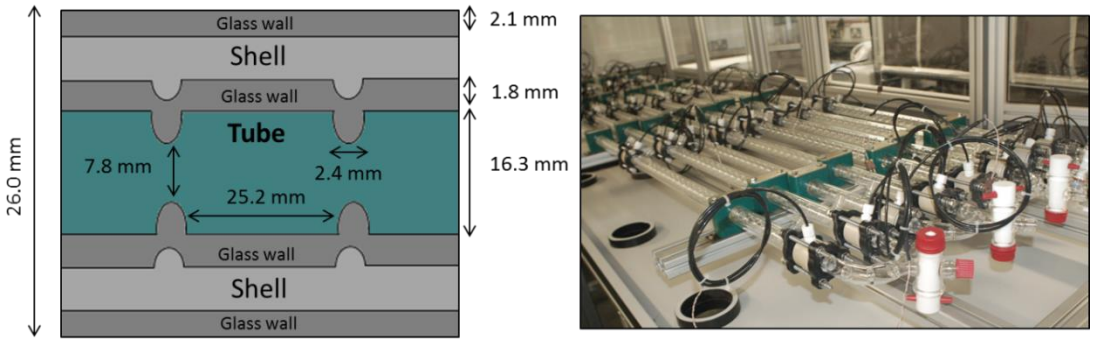

Figure 2. Schematic of a cross section of a DN15 COBC straight (left) with dimensions indicated and a photograph of a typical COBC set-up (right) [61].

The key feature of a COBC is that it can achieve plug flow with low net flow rates. Plug flow is desired for a crystalliser to obtain crystals with a narrow size distribution and low net

flow is desired for a crystalliser to obtain a residence time that is long enough for the relatively slow process of crystallisation to reach completion without having very long tubes [62]. Plug flow is possible because the oscillatory motion (forward and backstroke) of flow through the baffles provides strong radial mixing. Eddies are formed downstream of the baffle on the forward stroke and while these eddies are dissipated on the back stroke new eddies are created upstream of the baffle. This repetitive creation and destruction of eddies results in a chaotic flow that provides efficient mixing within each interbaffle zone. The benefits of achieving plug flow with a low net flow have resulted in the COBC being studied extensively in recent years with a wide range of compounds being continuously crystallised [63-69]. Most of the work has taken the form of a seeded cooling crystallisation due to the excellent heat transfer characteristics of the COBC and the desire to avoid nucleation in the relatively narrow diameter of the tubes.

Continuous oscillatory flow is mainly described by three dimensionless numbers: Re_O, the oscillatory Reynolds number; St, the Strouhal number; and Re_n, the net flow Reynolds number [70, 71]. These are governed by equations 5–7.

$$Re_O = \frac{2\pi f \chi_o \, \rho D}{\mu} \tag{5}$$

$$St = \frac{D}{4\pi\chi_o} \tag{6}$$

$$Re_n = \frac{\rho u D}{\mu} \tag{7}$$

In these equations, D = column diameter (m), χ_o= centre-to-peak amplitude (m), ƒ = frequency (Hz), ρ = density (kgm^{-3}), μ = fluid viscosity ($kgm^{-1}s^{-1}$), and u = mean velocity (ms^{-1}). Re_o describes the intensity of oscillatory mixing applied within the tube, where $2\pi f\chi_o$ is the maximum oscillatory velocity (ms^{-1}). St is the ratio of the column diameter to the

oscillation amplitude, and is a measure of the eddy propagation inside each interbaffle zone. St is inversely proportional to χ_o. Re_n, the classic dimensionless number describing flows in pipes, is the ratio of inertial to viscous force within a flow. Oscillatory flow must be dominant to fully gain the benefits of the eddy shedding cycle and therefore flow should be fully reversing, which to hold true requires $\mathrm{Re_O}$ to be ≥ $\mathrm{Re_n}$. To underline this rule a velocity ratio, ψ, was proposed to relate the oscillatory velocity to the net flow velocity and is described by equation 8.

$$\psi_{=} \frac{Re_O}{Re_n} \tag{8}$$

Experimental data has shown that the velocity ratio should be maintained in the range of $2 \leq \psi \leq 6$ to have approximate plug flow [72, 73].

2.5. Continuous mixing

Continuous mixing plays a crucial role in all mixing-induced supersaturation processes including continuous salt crystallisation [74-79]. The mixing of miscible liquids is typically classified by three length scales which are illustrated in Figure 3. “Macromixing” occurs on the scale of the vessel, “mesomixing” occurs on the scale of the turbulent eddies and “micromixing” occurs on the scale of molecular diffusion in the stretching of fluid lamellae. In turbulent mixing, kinetic or mechanical energy put into the system is dissipated by viscous deformation during various physical steps on the three mixing scales. In macromixing, energy is dissipated through the distribution of fluid throughout the vessel by bulk convection (blending). In mesomixing, energy is dissipated through the formation of vortices which grow (by turbulent diffusion or inertial-convective mixing) and engulf new fluid. In micromixing, energy is dissipated through further deformation of the vortices which ultimately results in a lamellar structure (momentum diffusion) where molecular

diffusion can eliminate regions of segregation in a local flow that is laminar (molecular diffusion) [80].

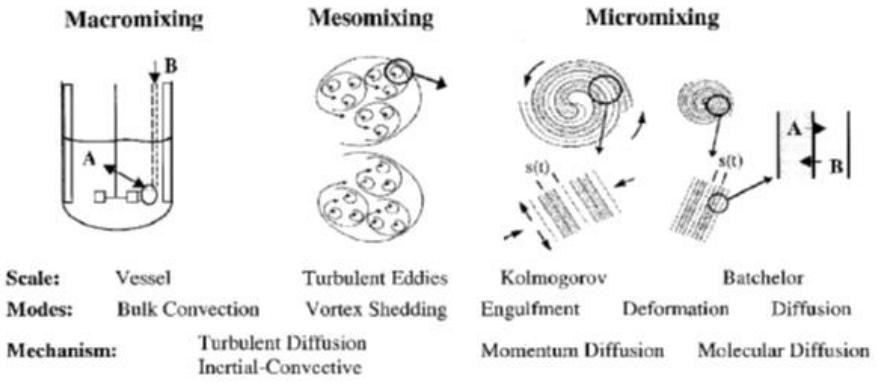

Figure 3. Illustration of mixing scales in turbulent mixing [80].

Molecular scale processes (chemical reactions, crystal nucleation & growth) require micromixed fluids, and since each step in mixing is a prerequisite for the next, any of the mixing scales can be rate limiting and control product quality [81, 82]. The framework for classifying mixing-sensitive processes consists of comparing time constants (or characteristic times) for mixing, reaction and crystallisation. For example, a neutralisation's time constant is orders of magnitude shorter than that for mixing; mixing is rate-determining, and neutralisation is instantaneous relative to mixing. Ester hydrolysis is the opposite case: reaction kinetics determines its rate, and hydrolysis is slow relative to mixing [83]. The time constant associated with a crystallisation process will depend on the compound being crystallised, the mode of crystallisation and the supersaturation level. The reactive crystallisation of an inorganic salt will be extremely fast whereas the cooling crystallisation of an organic molecule may be slow [84].

The fact that chemical reactions are sensitive to mixing allows for them to be used as test systems to characterise mixing and evaluate quantitative models which claim to describe

the coupling between mixing and reaction. The test reactions should be fast relative to mixing so that the time constants of chemical reactions are either smaller or of comparable magnitude to the time constants for mixing. In fact, fast parallel reactions are the best test reactions because in their case the product distribution stores the mixing history in addition to the spatial distribution of the reactants (extent of the reaction zone) and the variation of concentrations over time. The drawbacks of using chemical reactions to characterise mixing are that exact reaction kinetics must be known and accurate quantitative analysis of reactants and products should be possible [84-88].

Although micromixing directly affects the molecular level processes of crystal nucleation & growth, larger scales of mixing may indirectly affect or even control the crystallisation process. That is, mesomixing and macromixing dictate the redistribution of supersaturation in the system by diluting regions of high supersaturation with less supersaturated solution and by allowing the contact of particles with regions of high supersaturation where they grow. It is more difficult to predict and model mixing in crystallisation processes than in chemical reactions. This is because in the case of chemical reactions it is possible to distinguish between the chemically active zone close to the feeding point and the chemically passive bulk, whereas in a crystallisation process, one needs to follow the progress of the crystallisation in the bulk as well [84].

2.6. Heat transfer in a continuous oscillatory baffled crystalliser (COBC)

The topic of heat transfer in a continuous oscillatory baffled crystalliser (COBC) is highly significant in the field of continuous crystallisation. In particular, it is important to understand how the temperature of a solution varies as it travels along the COBC. This is of critical importance during cooling crystallisation as the temperature at any point along the COBC will determine the supersaturation of the solution and consequently the growth rate

of the crystals at that point. Therefore, greater understanding of the heat transfer would allow for greater control of the temperature profile along the COBC and consequently greater control over crystal properties.

The work of Mackley et al. [89] was the first to report experimental heat transfer measurements for oscillatory flow in baffled tubes. It was known previous to this work that having oscillatory flow in a tube with periodically spaced baffles results in vigorous eddy mixing. The sharp edges of the baffles cause eddy shedding which produces exceptional global mixing with the mean radial and axial velocity components being of the same order of magnitude. It was expected that these fluid mechanical conditions would significantly change the rate of heat transfer which is why this investigation took place. The investigation itself was concerned with comparing the tube-side Nusselt number obtained from four different configurations; a configuration with no baffles and with no oscillation, a configuration with baffles and with no oscillation, a configuration with no baffles and with oscillation and a configuration with baffles and with oscillation. It was found that the configuration with no baffles and with no oscillation yielded the lowest tube-side Nusselt number whereas the configuration with baffles and with oscillation yielded the highest tube-side Nusselt number. The results also showed that the introduction of baffles significantly increased the tube-side Nusselt number even if there was no oscillation as it effectively increased the surface area of the heat conduction surface and modified the flow pattern. Fluid oscillation alone had very little effect on the tube-side Nusselt number.

The aim of Mackley and Stonestreet [90] was to extend the preliminary findings of Mackley et al. [89]. The paper reported the results of experiments which determined the heat transfer enhancement that was achieved under both steady and oscillatory flow conditions. A large range of oscillatory conditions were tested and it was found that the rate of heat

transfer was highly dependent on the product of oscillation frequency and amplitude so that choosing a particular frequency and amplitude allows for precise control of heat transfer enhancement. The paper also found that the advantages of oscillatory flow were most evident at moderate net flow Reynolds numbers. Using a particular product of oscillation frequency and amplitude in combination with a moderate new flow Reynolds number yielded a 30-fold increase in Nusselt number (relative to steady, unbaffled flow) compared with the 7-fold increase which was achieved in Mackley et al. [89].

More recent studies concerning heat transfer for oscillatory flow in baffled tubes have investigated what effect changing the baffle type could have [91]. Of particular interest was a numerical study that was carried out on the heat transfer enhancement in oscillatory baffled tubes with helical coil inserts. Helical baffles are better suited to the processing of solid-liquid systems than orifice type baffles because they do not have as pronounced constrictions where particles may become lodged. Another advantage of helical baffles is that plug flow behaviour can be obtained over a much broader range of oscillation conditions than for other baffle types. This is due to the interaction between helical baffles and oscillatory flow as it produces a swirling flow in addition to vortex generation. The study found that a 4-fold increase in Nusselt number could be obtained using oscillatory flow with helical baffles compared to non-oscillatory flow with helical baffles. This increase due to oscillatory flow in the presence of baffles is significantly larger than that which has been obtained using orifice type baffles at similar conditions [89].

In addition to helical baffles, studies have been conducted on conic ring baffles [92]. Conic ring baffles have the same advantage as helical baffles in that they are more suitable for solid-liquid systems because suspended particles are much less likely to become lodged in the baffle constrictions. Of particular interest was a numerical study carried out on the

temperature field of oscillatory baffled tubes with conic ring baffles. It was found that a small oscillatory Reynolds numbers (<3000) coupled with a large Strouhal number (≥1) produced a relatively soft mixing condition. This resulted in the temperature field having significant temperature gradients at the centres of the interbaffle regions at which convection heat transfer is much more dominant than conductive heat transfer. When the oscillatory Reynolds number was larger or the Strouhal number was lower, the mixing condition became more chaotic which resulted in a more chaotic temperature field. It was also found that the heat transfer performance was close at the same oscillatory Reynolds number regardless of the Strouhal number.

3. Analytical techniques

3.1. Offline techniques

3.1.1. Gravimetric analysis

In a crystallisation process, solubility and supersaturation describe the amount of material that can theoretically be recovered. For the pharmaceutical industry, and for almost any other application, it is of great importance to recover a high yield from the crystallisation procedure in order to minimise waste and make the process as economical as possible. With this in mind, gravimetric analysis was carried out for every experiment performed in this study as it is a fast, simple and reliable method for determining the concentration of material recovered as a solid and consequently the concentration of material still remaining in the solution.

Gravimetric analysis was performed by firstly collecting a representative sample from the crystal suspension and weighing it. The sample was then filtered using a vacuum until the filter cake was as dry as possible. After this the filter cake was dried further, for at least 24 hours, in either a vacuum oven or in a regular oven set at 40 °C. After the filter cake was completely dry, the dry filter cake was weighed. Knowledge of the weight of the dried filter cake, in addition to the total weight of the sample, allowed for the solution concentration to be calculated according to the overall material balance. Knowledge of the solution concentration and the solubility of the material at the point where the sample was taken allowed for the sample supersaturation and yield to be calculated. In the case where the solution concentration was equal to the saturation concentration, the sample was completely desupersaturated. If the solution concentration was greater than the saturation concentration, the sample was still supersaturated to some extent.

When discussing yield it is very important to be clear about the precise definition. In this work yield was defined as the percentage of material recovered with respect to the total amount of material dissolved in the solvent. This was calculated from the final solution concentration (C_{final}) and the initial solution concentration ($C_{initial}$) according to equation 9.

$$Yield = \left(\frac{C_{initial} - C_{final}}{C_{initial}}\right) \times 100 \quad (9)$$

In addition to yield, a term referred to as solid recovery was used in this work. Solid recovery was defined as the percentage of material recovered with respect to the amount of material than can potentially be crystallised based on thermodynamic solubility. This was calculated from the final solution concentration (C_{final}), the initial solution concentration ($C_{initial}$) and the saturation concentration (C_S) according to equation 10.

$$SR = \left(\frac{C_{initial} - C_{final}}{C_{initial} - C_S}\right) \times 100 \quad (10)$$

Comparing the terms of yield and solid recovery a few things can be noted. As the solubility of the crystallising material is always greater than 0 the yield will always be less than 100%. On the other hand it is possible, although unlikely, that the solid recovery will have a value of 100%. Consequently, the yield will always have a smaller value than solid recovery.

With regards to the EDNB crystallisation experiments in this work the gravimetric analysis was performed in order to calculate yield. It should be noted that for multicomponent systems, like the EDNB salt, yield and solid recovery are based on the concentration of the limiting component. Gravimetric analysis performed in the EDNB solubility measurement experiments was not for yield determination. In these experiments, the conditions were such that it was expected that the samples were completely desupersaturated. In other

words, the experimental solution concentration equalled the saturation concentration. For the EDNB solubility measurements the results were consistent over observed time periods and between repeat measurements. Therefore, it was concluded that the samples were completely desupersaturated and that these solution concentration measurements were valid as solubility measurements.

3.1.2. Optical microscopy

Optical microscopy is perhaps the most widely used technique in crystallisation studies. It is used to observe the range of size and shapes present in a crystal sample. Differences in the size, shape and colours of crystals between samples, or within a sample, may be due to several factors. The overriding factor being the solid form as different polymorphs of the same compound can exhibit very different shapes and colours. For the same solid form the size and shape can be greatly influenced by the supersaturation profile employed in the crystallisation process.

In this work two forms of optical microscopy were utilised. One form was standard microscopy using a standard microscope. Standard microscopy involved placing the dry crystal sample on a glass slide and placing the slide on the microscope stage. When the sample was in position the light source and camera were switched on before a suitable magnification was chosen. The crystals of interest were then brought into focus and images were captured [93]. The image capture software could then be used to measure the size of a specific crystal if desired. The standard microscope was used in experiments mainly to obtain qualitative information about the crystal size and shape. However, the sizes of particular crystals of interest were measured when it was deemed appropriate.

The other form of optical microscopy was combined automated microscopy with image analysis using the Malvern Morphologi G3 instrument. An image of the Morphologi is shown in Figure 4.

Figure 4. Malvern Morphologi G3 instrument [94].

The procedure involved placing the dry powder sample into the integrated powder dispersion unit and selecting a suitable dispersion pressure which would allow for a circle of flat separate particles to be formed on the glass plate as a result of the dispersion. The instrument would then scan the powder sample while capturing images with the use of 1 or more magnifications depending on the sample. For all of the particles captured, the full ranges of size and shape properties were determined by the software. For this reason the Morphologi instrument was used to obtain quantitative information of the crystal population by obtaining full size and shape distributions [95].

3.1.3. Attenuated Total Reflectance Fourier Transform Infrared Spectroscopy (ATR FTIR)

The ATR FTIR instrument (Bruker TENSOR II) was used to analyse the samples of dry powder recovered from the crystallisation experiments. The IR spectrum obtained from the instrument allowed for the solid form of the sample to be determined. This technique is extremely useful for determining the solid form of a sample as it requires very little sample preparation, a very small sample quantity and the IR spectrum is acquired very quickly (<1 minute). The solid sample was placed on the ATR crystal and pressure was applied to ensure sufficient contact between the sample and the crystal. Before each sample spectrum was collected, the background spectrum was collected. The background spectrum was collected in the air at room temperature. No samples were ground before analysis.

The FTIR spectrometer consists of a source, interferometer, sample compartment, detector, amplifier and A/D convertor which is all connected to a computer [96]. The source generates the IR beam which goes through the interferometer, then through the sample, then to the detector. The signal is then amplified by the amplifier and converted to a digital signal by the analogue-to-digital converter. The signal is then transferred to the computer where Fourier transformation is performed. A diagram of the FTIR spectrometer is shown Figure 5.

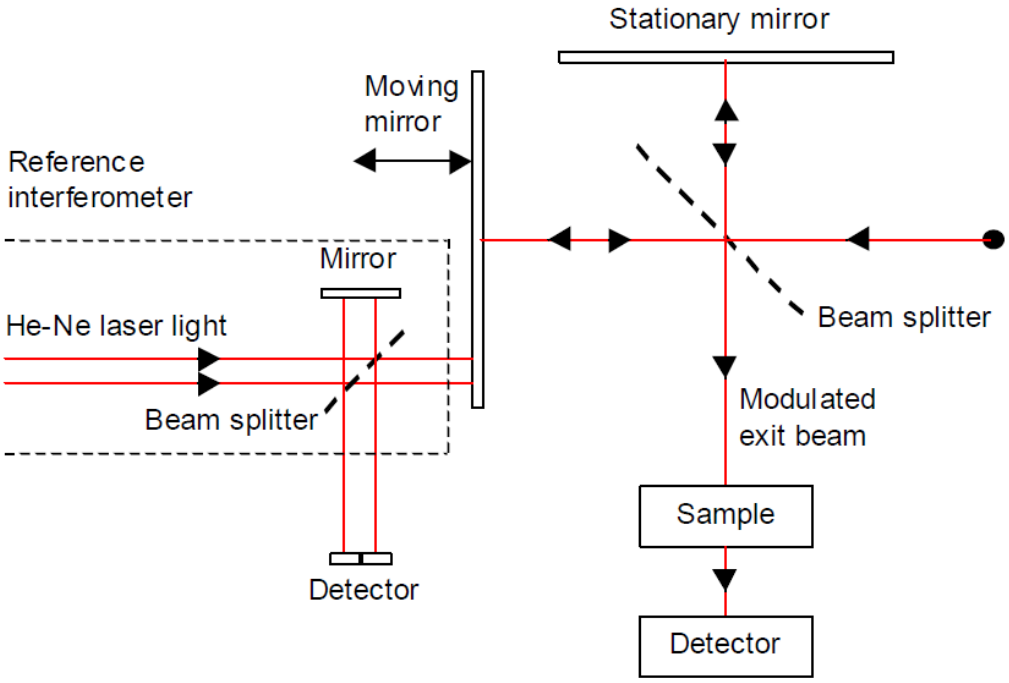

Figure 5. Diagram of the Fourier Transform Infrared Spectrometer [97].

The key difference between the FTIR spectrometer and the traditional dispersive IR spectrometer is the Michelson interferometer. By using a Michelson interferometer in Fourier Transform Infrared spectroscopy, the whole frequency range can be scanned concurrently [98, 99]. In practice, this means that the IR beam goes into the Michelson interferometer before passing through the sample. In the interferometer the beam is separated by the beam splitter with half of the beam being reflected on to the stationary mirror and half of the beam being transmitted to the moving mirror. The two beams, which could have travelled different path lengths, are recombined at the beam splitter with half being directed back to the source and half being directed through the sample to the detector. An interference pattern is created by the combination of the beams which have travelled different path lengths. This is because when the recombined beams are directed through the sample this gives spectral data as a function of time, which is converted by the

Fourier transformation to a spectrum of absorption as a function of either wavenumber or frequency.

The ATR technique works by measuring the changes that occur in an internally reflected IR beam when the beam makes contact with the liquid or solid sample. The IR beam is directed onto an optically dense crystal with a high refractive index at a certain angle. This internal reflectance produces an evanescent wave which extends beyond the surface of the ATR crystal and into the sample which is in direct contact with the crystal. As a result, the evanescent wave will be attenuated in the regions of the IR spectrum where the sample absorbs energy. The attenuated beam returns to the ATR crystal before exiting the opposite end of the crystal where it is directed to the detector in the FTIR spectrometer. The detector registers this attenuated IR beam as an interferogram signal that can then be used to produce an IR spectrum [100].

The infrared spectra contain information about the bonds and functional groups present in the molecule in addition to the intermolecular interactions. IR spectra can be divided into four regions which are the fingerprint region (1500-600 cm^{-1}), the double bond region (2500-1500 cm^{-1}), the triple bond region (3000-2500 cm^{-1}) and the X-H region (4000-3000 cm^{-1}) [98]. The characteristic bands of the functional groups of ethylenediammonium 3,5-dinitrobenzoate (EDNB) are given in Table 1.

Table 1. Characteristic IR bands for ethylenediammonium 3,5-dinitrobenzoate (EDNB) [101].

Functional Group	**Characteristic Wavenumbers (cm^{-1})**
CO_2^- (anti-symmetric stretch)	1650-1620
NH_3^+ (N-H)	1585-1580

NO_2 (anti-symmetric stretch)	1550-1510
Aromatic C=C (stretch)	1480-1470
Alkyl C-H (deformation)	1460-1450
CO_2^- (symmetric stretch)	1390-1370
NO_2 (symmetric stretch)	1370-1340
Aromatic C-H (deformation)	1175-1125
	1070-1000

Differences in the IR spectra of polymorphs may be observed due to different intermolecular interactions and different molecular conformations. With regards to the EDNB salt, the EDNB polymorphs can be distinguished by the bands at 1549 and 1518 cm^{-1} due to nitro group stretching for the monoclinic form which are absent in the triclinic form and by bands at 1533 cm^{-1} due to nitro group stretching and at 1479, 1126 and 1051 cm^{-1} due to aromatic ring vibrations for the triclinic form which are absent from spectra of the monoclinic form. Therefore, IR was the technique used to determine which solid form was recovered in each crystallisation experiment.

3.1.4. Sirius T3 automatic titrator

The Sirius T3 automatic titrator was used to experimentally measure the 3,5-DNBA aqueous pH-solubility. Experiments were conducted at a temperature of 25 ± 0.5 °C under an argon atmosphere. The apparatus was controlled using Sirius software. The T3 set up includes an Ag/AgCl double junction reference pH electrode, a Peltier temperature control device, with thermocouple temperature probe and an overhead stirrer (variable speed, computer controlled). The spectrophotometer was a MMS UV–Vis Carl Zeiss Microimaging

spectrophotometer with an ultra-mini immersion probe attached. An image of the Sirius T3 automatic titrator is shown in Figure 6.

Figure 6. Image of Sirius T3 automatic titrator [102].

In addition to solubility measurements the T3 automatic titrator can be used to measure pKa values (as was done in this work for 3,5-DNBA) or partition-coefficients (which wasn't done in this work).

3.2. Online techniques

3.2.1. pH measurement

As this work dealt with pH controlled salt crystallisation it was clearly very important to measure pH in the experiments whenever possible. For all the semi-batch experiments a pH probe was always inside the system to record the pH profile over the course of the titration and the crystallisation process. In the continuous mixer experiments it wasn't possible to have online pH measurement as the mixers have a very narrow diameter. Instead, the pH

values of the feed solutions and final slurry samples were recorded. In the full continuous processes it was possible to have online pH measurement as the pH probes could be placed in the CSTRs after the X-mixer to monitor the slurry pH.

For the 100 ml beaker experiments, 100 ml EasyMax experiments and continuous mixer experiments the pH was measured using a Mettler-Toledo M800 pH meter and Mettler-Toledo InPro pH probe. For the 400 ml STR experiments pH was measured using an Orion Star A111 pH meter and Orion 9157BNMD pH probe from Thermo Fisher Scientific. For the full continuous processes pH was measured using an Almemo 2390-5 data logger and Mettler-Toledo InLab Semi-Micro-L pH probe. The accuracy of a pH measurement is expected to be ±0.05 in aqueous systems when using a glass pH electrode [34].

3.2.2. Ultraviolet–visible (UV-vis) spectroscopy

Ultraviolet-visible (UV-vis) spectroscopy was performed online using a UV probe connected to a Carl Zeiss MCS 621 UV spectrometer for the 400 ml STR experiments or a Carl Zeiss MCS 500 UV Spectrometer for the fully continuous processes [103]. Use of a UV probe allows for an in-situ absorbance measurement to be made for a UV active compound [104]. In this work the only UV active compound in solution was 3,5-DNBA so 3,5-DNBA UV absorption spectra were collected over the course of each experiment where the probe was used. The absorption signal depended on temperature, concentration and pH so by applying a calibration model to account for the effect of these variables the 3,5-DNBA absorbance spectra could be transformed into a 3,5-DNBA concentration profile for each experiment where possible. Knowledge of the 3,5-DNBA concentration profile allowed for the EDNB salt concentration profile to be calculated as a 2:1 molar ratio was maintained at all times. Therefore, use of the UV probe was very important in terms of gaining deeper understanding of the EDNB salt crystallisation process.

3.2.3. Focused beam reflectance measurement (FBRM)

The focused beam reflectance measurement (FBRM) probe from Mettler-Toledo is a commonly applied tool in crystallisation processes. A diagram of the FBRM probe with an illustration of the measurement method is shown in Figure 7.

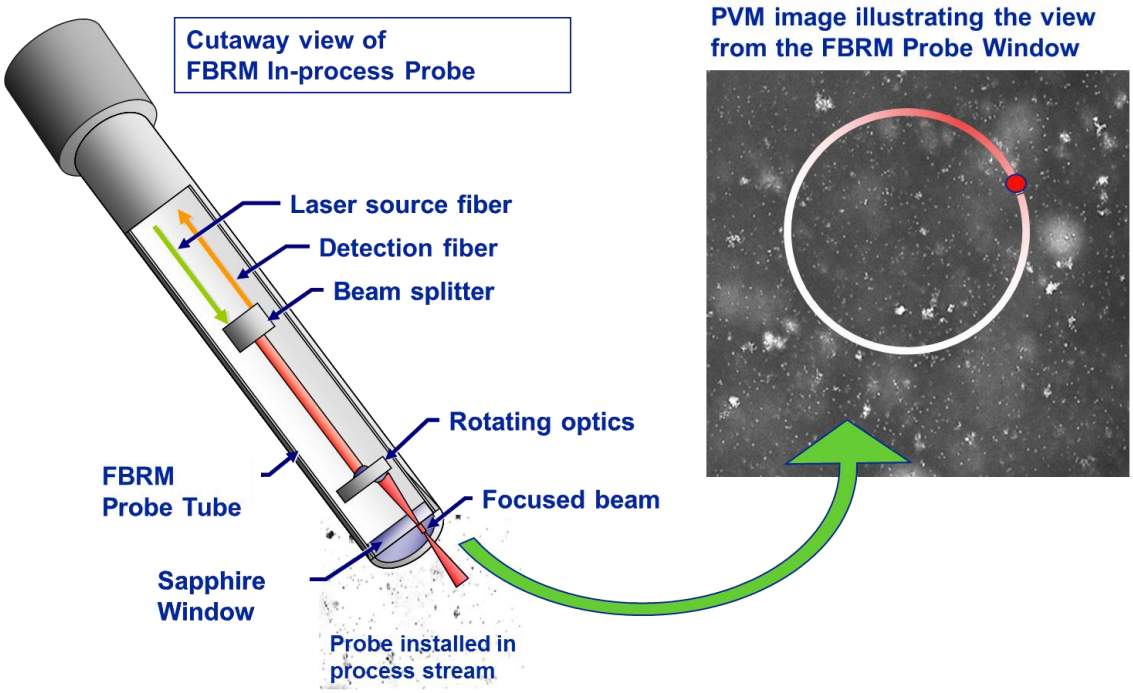

Figure 7. Diagram of the FBRM probe with an illustration of the measurement method [105].

In the FBRM probe a laser beam is directed down the probe tube and focused to a tight beam spot at the sapphire window. The optics rotate at a fixed speed (typically 2m/s) resulting in the beam spot rapidly scanning across particles as they flow past the sapphire window. As the focused beam scans across the particle system individual particles or particle structures will backscatter the laser light to the detector. These distinct pulses of backscattered light are detected, counted, and the duration of each pulse is multiplied by the scan speed to calculate the distance across each particle. This distance is defined as the

chord length which is related to, but almost never equal to, the particle size. Usually thousands of chord lengths are measured every second and this measurement is used to generate a chord length distribution (CLD) in real time. Once again, a CLD relates to the particle size distribution (PSD) but is highly unlikely to be the same. A detailed illustration of chord length measurement is shown in Figure 8.

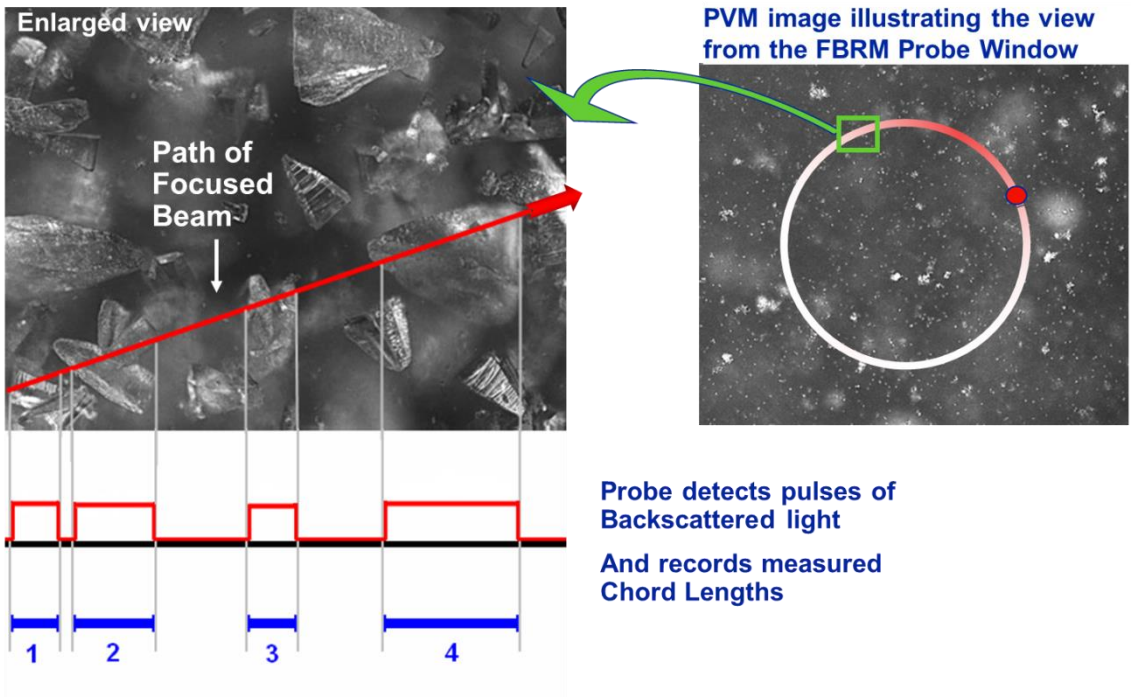

Figure 8. Detailed illustration of chord length measurement [105].

In this study the FBRM probe was used to monitor the EDNB crystallisation process in the semi-batch experiments and the full continuous processes. The recent G400 model was used in the semi-batch experiments while the older S400 model was used in the full continuous processes. For both probe models analysing the value of total counts and CLDs allowed for greater process understanding. Important results included nucleation point determination, the determination of steady state continuous operation and a comparison of CLDs between similar experiments which allowed for PSD trends to be known.

The FBRM results can be analysed with both the “Primary” and the “Macro” view. The primary view has a narrower measurement zone than the macro view which makes it more sensitive to individual particles and crystal facets. The macro view is useful for measuring total agglomerate size and ignoring the individual particles which make up the agglomerate. In addition to these two types of view, the CLDs produced can be either unweighted or square weighted. Clearly the unweighted distributions will be more sensitive to fines and the square weighted distributions will give greater importance to larger particles.

3.2.4. Particle vision and measurement (PVM)

In the 100 ml EasyMax experiments and the 400 ml STR experiments a particle vision and measurement (PVM) probe from Mettler-Toledo was used to obtain in-situ imaging of the EDNB crystallisation process. A diagram of the PVM probe with an example image is shown in Figure 9.

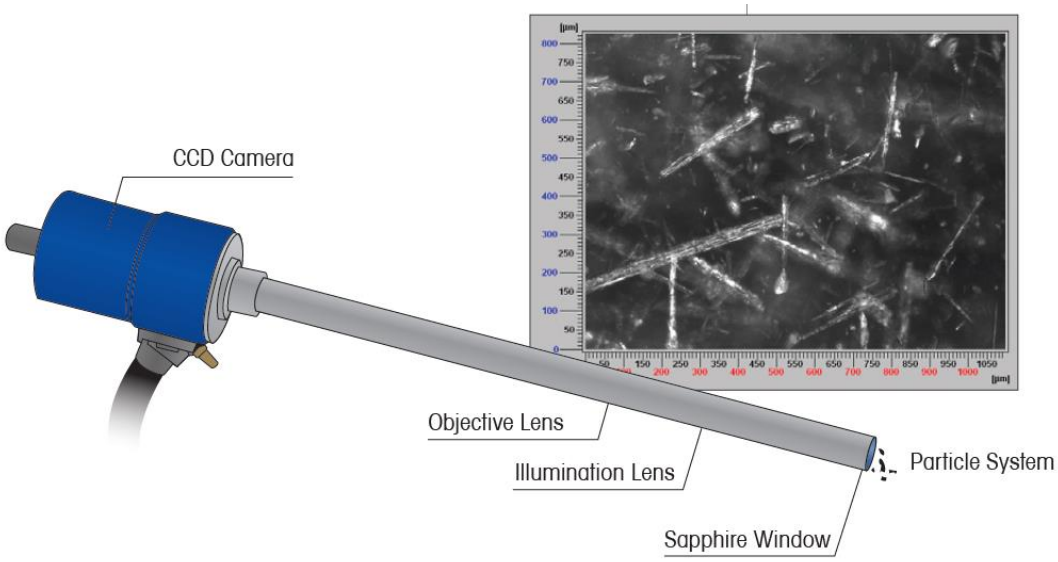

Figure 9. Diagram of the PVM probe with an example image [106].

The PVM probe was very in this work useful because it allowed for the polymorphic form of EDNB to be estimated in-situ. This is because the two polymorphs of EDNB have

significantly different crystal shapes with EDNB triclinic having a rectangular plate shape and EDNB monoclinic having a block shape. In this way the images were a reality check when used in combination with the offline IR analysis. Furthermore, the images from PVM were used to determine the extent of agglomeration in the system and confirm the results from sizing techniques such as FBRM.

4. Model compound

4.1. Ethylenediammonium 3,5-dinitrobenzoate (EDNB)

The system being studied in this work is the crystallisation of the polymorphic organic salt ethylenediammonium 3,5-dinitrobenzoate (EDNB). EDNB is the 2:1 salt of 3,5-dinitrobenzoic acid (3,5-DNBA) with ethylenediamine where 3,5-DNBA is a weak acid and ethylenediamine is a weak base [107, 108]. Figure 10 shows the molecular structure of the 2:1 EDNB salt.

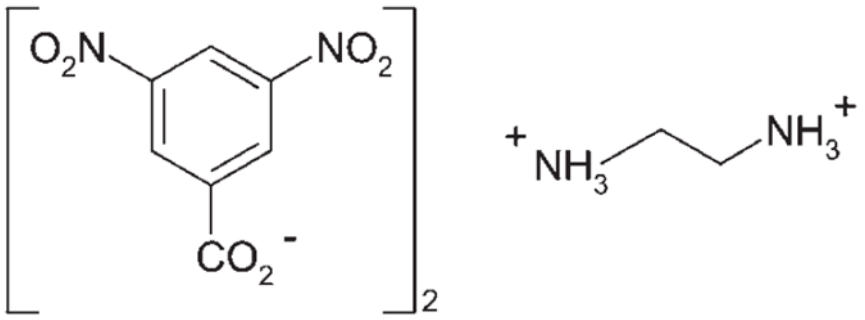

Figure 10. Molecular structure of ethylenediammonium 3,5-dinitrobenzoate (EDNB).

The two polymorphs of EDNB are recorded in the Cambridge Crystallographic Database: a monoclinic form (VUJXIH01; $P2_1/c$) and a triclinic form (VUJXIH; $P\bar{1}$) [109]. The crystal structure diagrams of both polymorphs are shown in Figure 11.

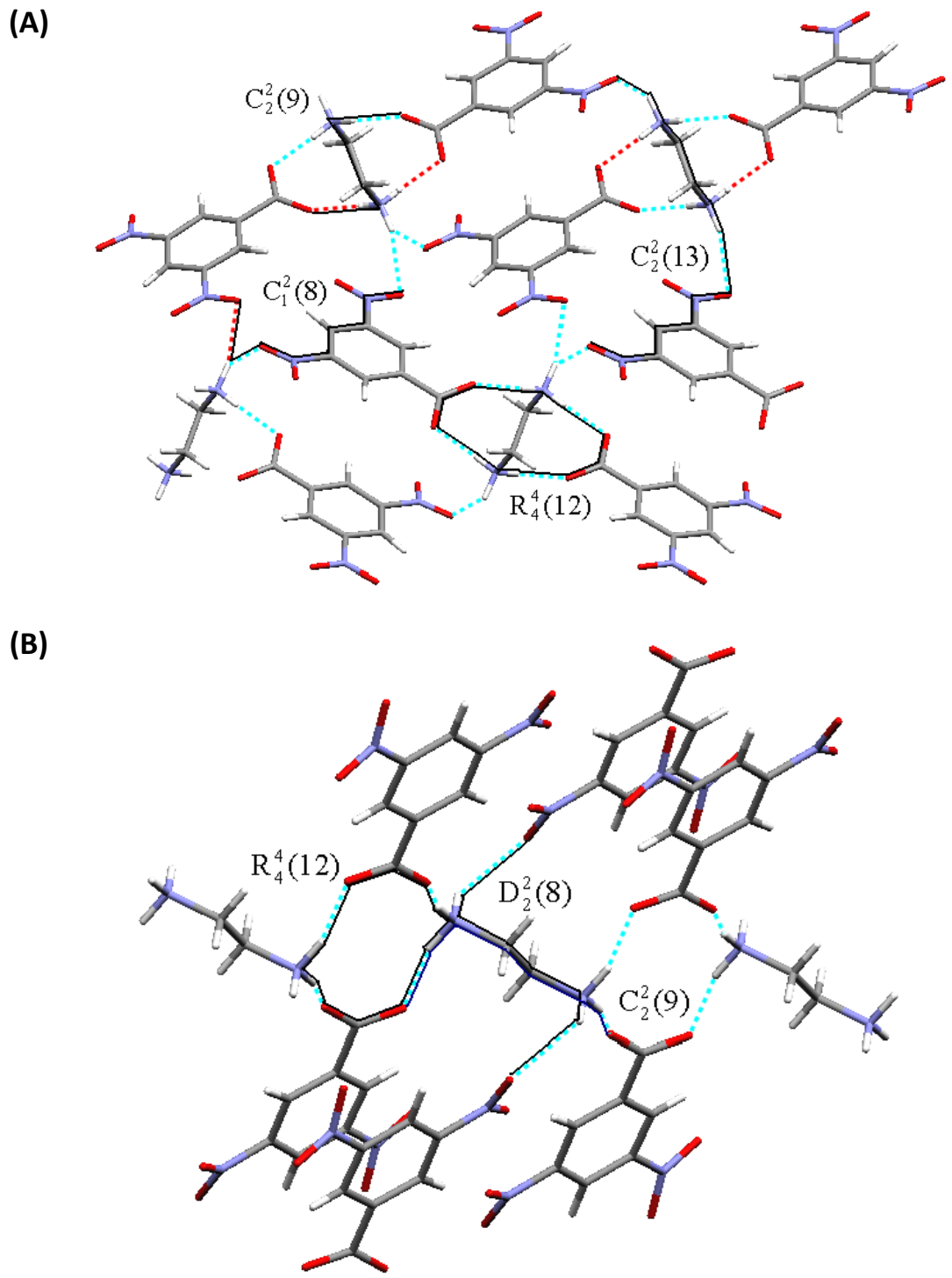

Figure 11. Crystal structure diagrams showing hydrogen bonding motifs for (A) monoclinic and (B) triclinic form of 2:1 EDNB salt [110].

4.2. EDNB speciation, solubility and supersaturation

3,5-DNBA is a monoprotic acid with a pKa value and ethylenediamine is a diprotic base with a pKa_1 and a pKa_2 value. A summary of the pKa values taken from literature and used in this work are shown in Table 2.

Table 2. Summary of literature pKa values for 3,5-DNBA and ethylenediamine [111-113].

Compound	Temperature (°C)	pKa	pKa_1	pKa_2
3,5-DNBA	25	2.82	–	–
	50	3.07	–	–
Ethylenediamine	25	–	6.86	9.92
	50	–	6.33	9.00

Knowledge of the pKa values allowed for the 3,5-DNBA and ethylenediamine speciation profiles to be plotted and shown in Figure 12.

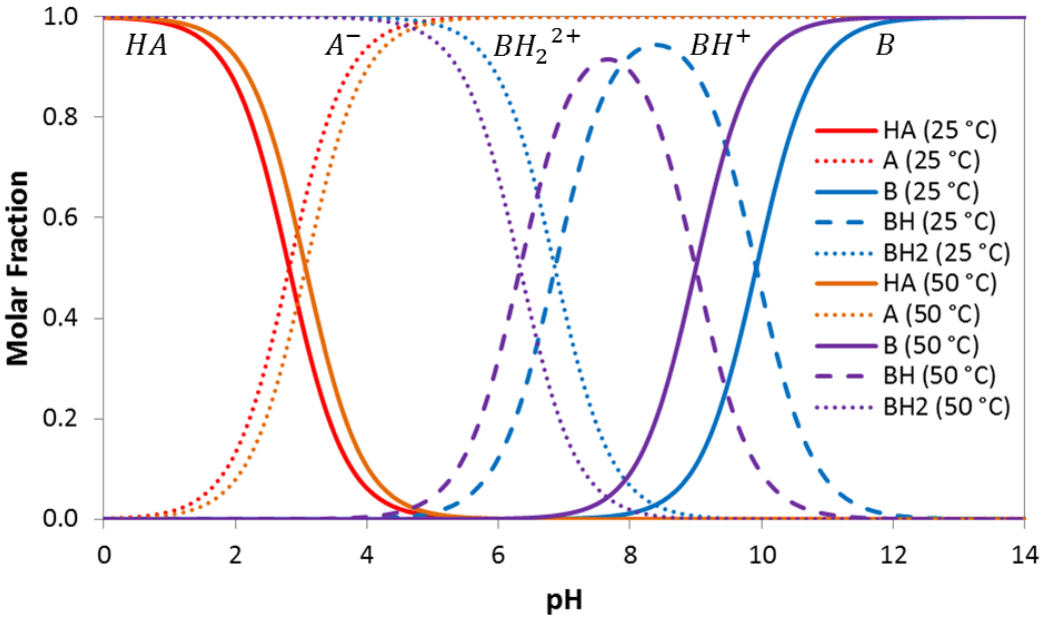

Figure 12. Speciation profiles for 3,5-dinitrobenzoic acid and ethylenediamine at 25 °C and 50 °C.

The speciation profiles illustrate the acid-base equilibria which are described by the dissociation constants in equations 11–13.

$$K_a = \frac{[A^-][H^+]}{[AH]} \tag{11}$$

$$K_{a1} = \frac{[BH^+][H^+]}{[BH_2^{2+}]} \tag{12}$$

$$K_{a2} = \frac{[B][H^+]}{[BH^+]} \tag{13}$$

When dealing with crystallisation processes it is vital to determine the solubility and supersaturation with respect to each material that has the potential to crystallise. In this system the materials of interest are EDNB monoclinic and EDNB triclinic and their solubilities are determined by equation 14.

$$Solubility = \left\{\frac{1}{4}K_{sp}\left(1 + \frac{K_{a1}}{[H^+]} + \frac{K_{a1}K_{a2}}{[H^+]^2}\right)\left(\frac{[H^+]}{K_a} + 1\right)^2\right\}^{1/3} \tag{14}$$

Knowledge of the solubility product, K_{sp}, is required to calculate the solubility and is defined for the 2:1 EDNB salt in equation 15 where each polymorph will have a different value and this will be different for each temperature (25 °C and 50 °C).

$$K_{sp} = [A^-]_{Eq}^2[BH_2^{2+}]_{Eq} \tag{15}$$

The K_{sp} values were estimated in literature by fitting experimental EDNB salt solubility measurements using equation (14. These experimental solubility measurements were observed by adding the EDNB salt to water before adding sodium hydroxide solution to

reach a desired pH and then allowing the slurry to equilibrate. A summary of the solubility products taken from literature and used in this work are shown in Table 3.

Table 3. Summary of literature values for the solubility products [109, 110].

EDNB Polymorph	Temperature (°C)	$K_{sp}\ (mol^3/dm^9)$
Monoclinic	25	5.20×10^{-5}
Monoclinic	50	3.73×10^{-4}
Triclinic	25	7.70×10^{-5}
Triclinic	50	5.20×10^{-4}

Inserting the estimated K_{sp} values into equation (14 gives the pH-solubility profiles for EDNB monoclinic and EDNB triclinic, at 25 °C and 50 °C, which are shown in Figure 13.

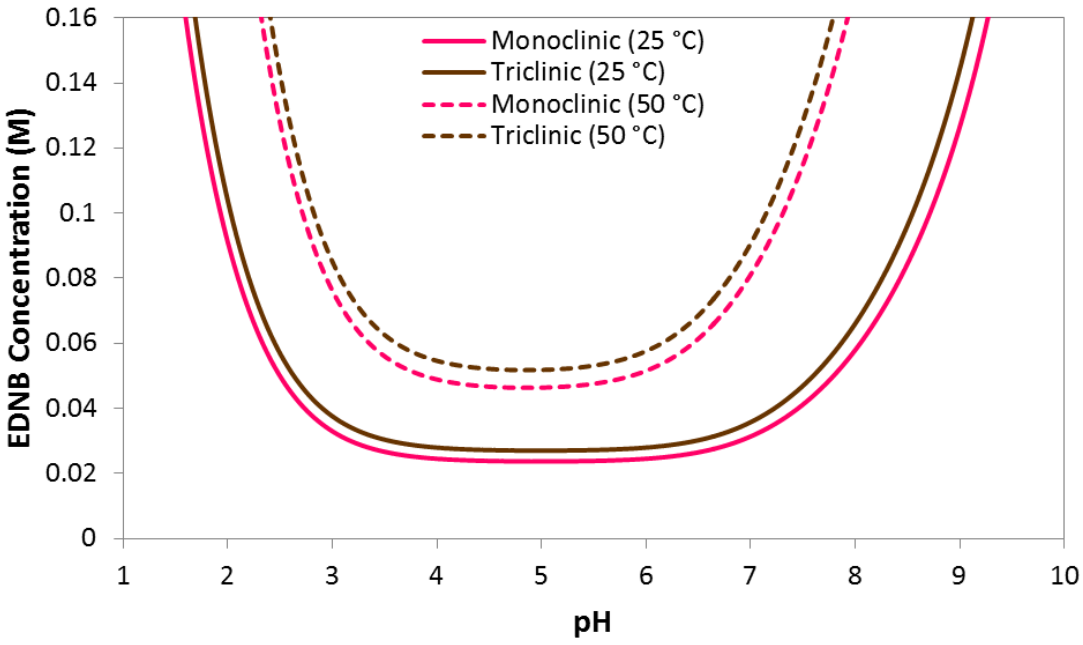

Figure 13. pH-solubility profiles for EDNB monoclinic and EDNB triclinic at 25 °C and 50 °C.

The key driving force for crystallisation, the supersaturation, of a solution of the salt $[BH_2.A_2]$ can be calculated using the solubility product according to equation 16. Here the solubility product is independent of pH whereas the concentration product is dependent on pH. It should also be noted that this definition of supersaturation implies that the solution is saturated when $S = 0$.

$$S = \ln\left(\frac{[A^-]^2[BH_2^{2+}]}{K_{sp}}\right) \tag{16}$$

Using the relationship in equation 16 the supersaturation with respect to both EDNB monoclinic and EDNB triclinic can be calculated when the speciation of each component and the solubility products are known.

Equations 14–16 assume that the solutions are dilute and exhibit ideal behaviour. When the solutions have high ionic strengths this assumption of ideal behaviour may not be valid. Therefore, activity coefficients for each species in solution must be calculated from the known ionic strength. This calculation is performed using equation 17 where I denotes the ionic strength and z denotes the ionic charge. Activity coefficients (γ) can be calculated according to equation 17 for the anion of the weak acid (γ_A), the diprotonated base (γ_B) and the hydrogen ions (γ_H) in solution in order to account for any non-ideal behaviour and correct solubility and supersaturation values.

$$-\log\gamma_i = 0.5\, z_i^2\left(\frac{I^{1/2}}{1 + I^{1/2}} - 0.3I\right) \tag{17}$$

The molar ionic strength of a solution is a function of the concentration of all ions present in that solution and is calculated using equation 18 where c_i is the molar concentration of ion i and z_i is the charge number of that ion.

$$I = \frac{1}{2}\sum_{i=1}^{n} c_i {z_i}^2 \tag{18}$$

Knowledge of all the activity coefficients allows for the activity corrected solubility to be calculated which in literature has been reported as equation 19.

$$Solubility = \left\{\frac{1}{4}K_{sp}\left(1 + \frac{K_{a1}}{[H^+]\gamma_H} + \frac{K_{a1}K_{a2}}{[H^+]^2\gamma_H^2}\right)\left(\frac{[H^+]\gamma_H}{K_a} + 1\right)^2\right\}^{1/3} \tag{19}$$

However, in this work equation 19 was deemed inappropriate for capturing the full effects of activity on EDNB salt solubility. This is discussed fully in section 5.5 where a new activity corrected solubility equation was derived. Considering activity coefficients, the solubility product in equation 15 should be written in terms of the activities of the acid (a_{A^-}) and the base ($a_{BH_2^{2+}}$) rather than in terms of the concentrations. This is shown in equation 20.

$$K_{sp} = {a_{A^-}}^2 a_{BH_2^{2+}} = [A^-]^2 {\gamma_A}^2 [BH_2^{2+}]\gamma_B \tag{20}$$

As with solubility and the solubility product, the supersaturation must be corrected due to the activity of the ions according to equation 21.

$$S = \ln\left(\frac{[A^-]^2 {\gamma_A}^2 [BH_2^{2+}]\gamma_B}{K_{sp}}\right) \tag{21}$$

Activity coefficients were needed was determined for every experiment in this work as the ionic strength of the solutions were high.

4.3. Previous knowledge of EDNB crystallisation & polymorphic transformation

In literature the EDNB crystallisation method has only ever taken the form of an evaporate crystallisation or a small scale (50 ml) batch pH-controlled crystallisation. In the small scale

batch pH-controlled crystallisations a strong base (NaOH) was used to dissolve 3,5-DNBA and ethylenediamine in an aqueous solution before a strong acid (HCl) was added to induce crystallisation of the EDNB salt [109, 110]. The pH of the initial basic solution was kept below pH 9 because above this value 3,5-DNBA is reported [114] to react with hydroxide ions to yield a red coloured solution containing 2,3-dihydroxy-5-nitrobenzoic acid and 3,3'-dinitro-5,5'-dicarboxyazoxybenzene.

The main result of the previous work is that pH, supersaturation and temperature can be utilised to control the morphology and polymorphic form of the EDNB salt. At 25 °C only EDNB triclinic was ever nucleated directly but at 50 °C the pH and supersaturation controlled which polymorph (EDNB monoclinic or EDNB triclinic) was nucleated directly. Furthermore, the pH affects the time taken for transformation from the metastable triclinic form to the stable monoclinic form with the transformation rate increasing with increasing pH. The effect of structurally similar additives on the EDNB crystallisation has also been investigated but additives were not used in this study.

5. Solubility measurements of 3,5-DNBA and EDNB triclinic

5.1. Introduction

In crystallisation processes it is vital to understand the solubility of all the compounds used. In the crystallisation of the 2:1 EDNB salt there are three solid forms which realistically may crystallise depending on the experimental conditions (temperature, pH etc.). These solid forms are EDNB monoclinic (stable EDNB polymorph), EDNB triclinic (metastable EDNB polymorph) and 3,5-DNBA (acidic starting material). In the crystallisation experiments it is desired to crystallise one of the polymorphs of the EDNB salt and avoid the crystallisation of the 3,5-DNBA starting material. Therefore, it is important to know the aqueous pH-solubility profiles of all three solid forms so that crystallisation experiments can be designed to avoid 3,5-DNBA appearing in the crystalline product. Furthermore, if 3,5-DNBA does appear in the product then knowledge of the pH-solubility profiles will allow for this to be explained.

The experimental aqueous pH-solubility profile of 3,5-DNBA couldn't be found in literature. All that was reported is that it has a very low solubility in water [115]. For this reason the aqueous pH-solubility profile is experimentally measured using the Sirius T3 automatic titrator. With knowledge of the pKa value for 3,5-DNBA the intrinsic solubility is determined by alternatively titrating an aqueous 3,5-DNBA solution with a strong acid and base to cycle between an undersaturated and supersaturated state. Knowledge of the pKa and intrinsic solubility values allows for the full aqueous pH-solubility profile to be determined. This solubility measurement is only performed at 25 °C but this should be sufficient for this work as the solubility of 3,5-DNBA depends much more on pH than temperature.

After performing some EDNB crystallisation experiments it can be observed that the experimental endpoints significantly differed from the literature solubility data, especially at lower pH values. In an effort to explain this discrepancy, solubility measurements of EDNB triclinic are performed at 25 °C so they can be compared with the literature data and with the experimental endpoints obtained in this work. This temperature and polymorph are chosen as they reflect the operating temperature and polymorphic outcome of the vast majority of the experiments. There wasn't sufficient time to obtain solubility measurements for EDNB monoclinic at 25 °C or either polymorph at 50 °C in this study but it should be performed in future work. In addition to performing solubility measurements to account for the discrepancy in solubility values, a new activity corrected solubility equation is developed and is fully discussed in this chapter.

5.2. Materials and methods

5.2.1. Materials

3,5-dinitrobenzoic acid (99%), ethylenediamine (≥99.5%), sulfuric acid (95-98%), sodium sulfate (≥99%) and sodium chloride (≥99.5%) were supplied by Sigma Aldrich. Sodium hydroxide (98%) was supplied by Fisher Scientific. Deionised water was produced using an in-house Millipore Milli-Q system. Potassium hydroxide (KOH) 1M and hydrochloric acid (HCl) 0.5M were supplied by Fisher Scientific. The HPLC grade water used to dilute the KOH solution to 0.5M was obtained using an Elga UHQ2 system.

5.2.2. Methods: Aqueous pH-solubility measurements of 3,5-DNBA

Experimental 3,5-DNBA aqueous pH-solubility measurements were made using the Sirius T3 automatic titrator, in ionic strength adjusted (ISA) water containing 0.15 M potassium chloride. Experiments were conducted at a temperature of 25 ± 0.5 °C under an argon atmosphere. The apparatus was controlled using Sirius software. The T3 set up includes an

Ag/AgCl double junction reference pH electrode, a Peltier temperature control device, with thermocouple temperature probe and an overhead stirrer (variable speed, computer controlled). The spectrophotometer was a MMS UV–Vis Carl Zeiss Microimaging spectrophotometer with an ultra-mini immersion probe attached.

Solubility determination was carried out using the CheqSol assay. 5.3 mg 3,5-DNBA was weighed into a vial and 1.5 ml ISA water was added. The first step in the experiment was to adjust the pH to 10 as it was expected that 3,5-DNBA would be completely solubilised at this point. After dissolution of the solid was complete the sample was titrated from ionisation to non-ionisation through the addition of acid until precipitation was detected. After this point more acid was added to increase precipitation before alternating aliquots of acid (HCl, 0.5M) and base (KOH, 0.5M) were added until twenty crossing points had been titrated. A crossing point is where the pH change versus time ($\Delta pH/\Delta t$) is zero [116]. The concentration at each crossing point is calculated using a series of equations [117] with the intrinsic solubility being the mean of the crossing point concentrations.

5.2.3. Methods: Aqueous pH-solubility measurements of EDNB triclinic

The EDNB aqueous pH-solubility measurements were obtained via gravimetric analysis. This was performed by one of two methods; the crystallisation method or the dissolution method. The crystallisation method involved mimicking larger scale crystallisation experiments by adding the sulfuric acid solution to the basic solution containing 3,5-DNBA, ethylenediamine and NaOH in order to induce crystallisation of EDNB triclinic. 2ml sulfuric acid solution was added to 18ml basic solution in a 28ml vial. This slurry was then stirred for a certain period of time until equilibrium was thought to be reached. The dissolution method involved dissolving EDNB triclinic in the aqueous solution of interest. Either a water, NaOH, NaCl or Na_2SO_4 solution was used. These different solutions were used to

investigate the effect of ionic strength on the EDNB salt solubility. 20ml solution was added to a particular mass of EDNB triclinic in a 28ml vial. This slurry was then stirred for a certain period of time until equilibrium was thought to be reached. The dissolution method helped confirm that the crystallisation method was allowing equilibrium to be reached.

Apart from whether the crystallisation or dissolution method was used the experimental apparatus and procedure was the same for all measurements. Once the slurry was created in the vial, a magnetic stirrer was placed inside and the vial was placed on a magnetic stirrer plate inside an incubator set at a temperature of 25 °C. Once a certain period of time had passed the vial was removed from the incubator, a pH probe was dipped into the vial to measure solution pH and then the slurry was filtered. The EDNB solid was then dried in a vacuum oven and weighed. Knowledge of the solid mass allowed for the solution concentration to be calculated at the measured pH. Different time periods were used to ensure equilibrium had been reached and each condition had repeat measurements to ensure accuracy.

5.3. Aqueous pH-solubility measurements of 3,5-DNBA

The presence of precipitate in a titration leads to a shift in the apparent pKa for the compound of interest. For this reason the intrinsic solubility of the compound can be calculated from the sample weight, equilibrium pH and the known aqueous pKa of the compound. When a weak acid such as 3,5-DNBA precipitates the pH of the solution will increase as a result of the acid being removed from solution. Conversely, when a weak acid dissolves the pH of the solution will decrease because acid is being added to the solution. For a crystalline compound such as 3,5-DNBA precipitation from, and dissolution into, solution tends to be slow. Therefore, there is a very small but measureable pH change with time during the precipitation and dissolution processes.

Measuring the pH changes with time allows for it to be determined whether the compound is precipitating or dissolving. If the pH of the solution is close to the compound's pKa then varying the pH varies the proportion of the sample which is ionised. This feature allows for the system to be cycled between an undersaturated and supersaturated state. By doing this the equilibrium pH can be determined by interpolation. Knowledge of the equilibrium pH then allows for the intrinsic solubility of the compound to be calculated by using the appropriate mass and charge balance equations.

At a low pH when 3,5-DNBA is completely neutral the apparent solubility is equal to the intrinsic solubility. The apparent solubility of 3,5-DNBA increases as the proportion of ionised species in solution increases. However, at too high a pH value the solubility measurement will no longer be valid because the 3,5-DNBA will have formed a potassium salt due to the presence of KOH from the titration. The aqueous pH-solubility profile of 3,5-DNBA is shown in Figure 14. This profile includes the experimental measurements and the extrapolated measurements but not the measurements which may have been affected by potassium salt formation.

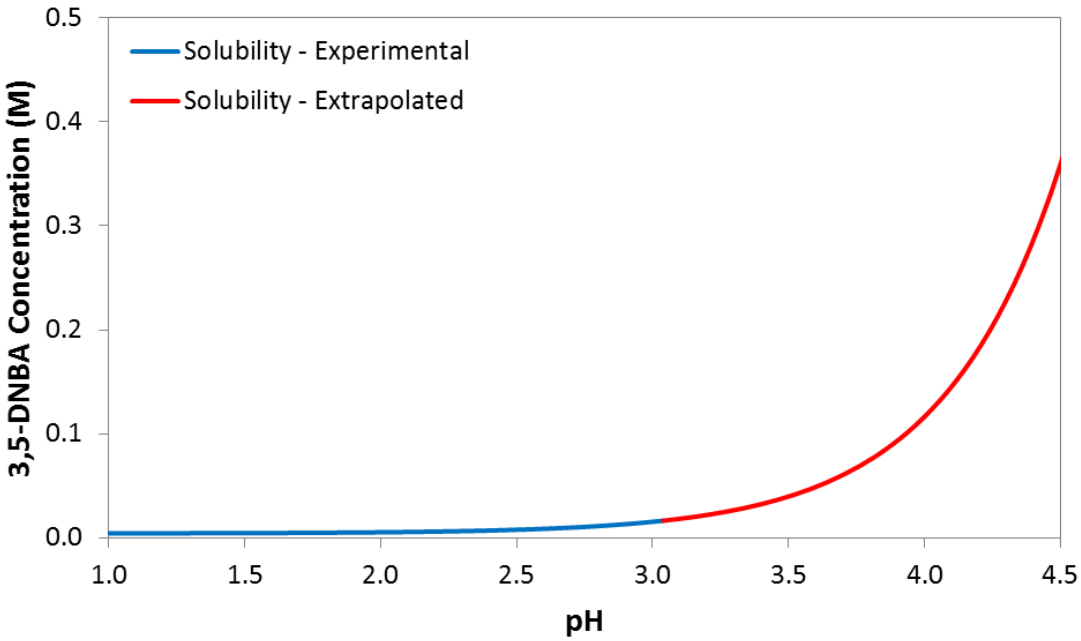

Figure 14. 3,5-Dintrobenzoic acid (3,5-DNBA) pH-solubility profile from Sirius T3 titrator.

The solubility is experimentally measured up to a pH of 3.04 and above this pH the solubility is extrapolated based on the pKa and intrinsic solubility of 3,5-DNBA. The pKa value used for the solubility measurement was experimentally measured using the Sirius T3 automatic titrator rather than the value from literature. The experimentally determined pKa value was 2.58 rather than the 2.82 value from literature. The experimentally determined intrinsic solubility value from the solubility measurement was 7.72 $mmol/L$. Knowledge of the 3,5-DNBA pH-solubility profile allows for the determination of the point in a titration where 3,5-DNBA will crystallise.

5.4. Aqueous pH-solubility measurements of EDNB triclinic

The aqueous pH-solubility measurements of EDNB triclinic at 25 °C are shown in Figure 15. The uncorrected solubility lines, in addition to the "corrected" solubility lines based on equation 19, taken from literature are also shown.

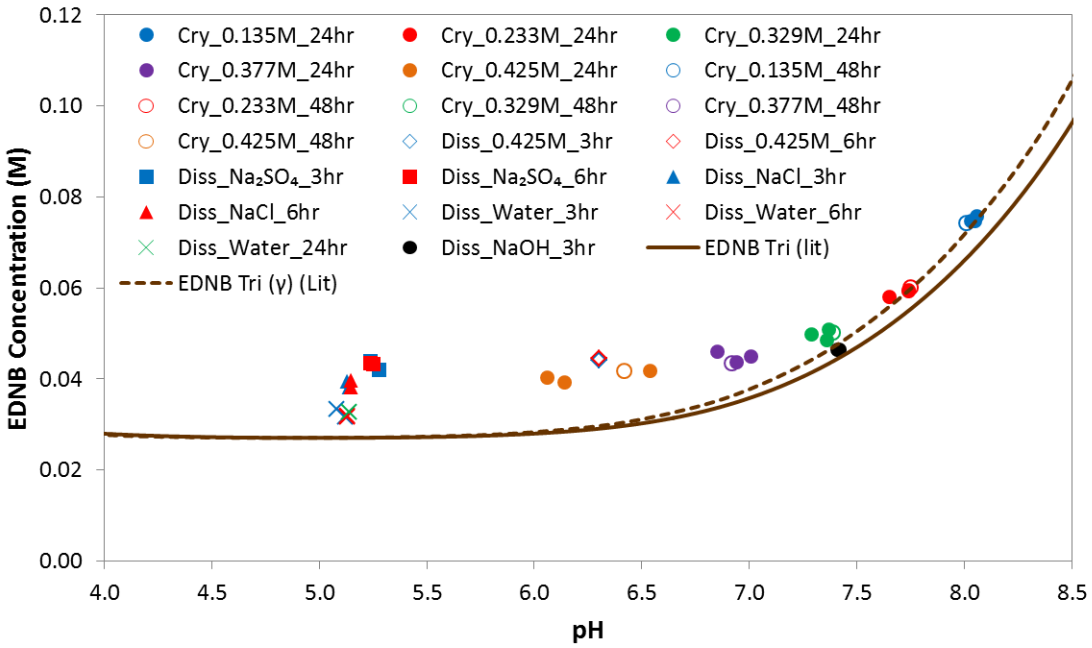

Figure 15. EDNB triclinic solubility measurements compared with literature solubility lines. Solid brown line and dashed brown line are uncorrected and activity corrected literature solubility lines respectively.

When dissolving EDNB triclinic in pure water or in NaOH solutions the solubility measurements closely match the "activity corrected" solubility profile from literature. This is because the conditions used for those measurements are very similar to those used in literature. However, when there is a significant concentration of sulfate ions in solution the EDNB triclinic solubility becomes significantly greater than the literature values. This was thought to be due to the increased ionic strength of the solution and/or possible complexation of sulfate ions with ethylenediamine ions. EDNB triclinic was also dissolved in NaCl solutions in order to check if the increase in EDNB triclinic solubility was simply due to the increase in ionic strength or if the sulfate ions in particular played some additional role. It can be seen from the solubility measurements that NaCl solutions did lead to a greater EDNB triclinic solubility relative to pure water but it still isn't as great as the solubility

obtained in the Na_2SO_4 solutions. Therefore, the sulfate ions are playing some additional role, beyond ionic strength, which is affecting the EDNB triclinic solubility.

5.5. Derivation and application of new activity corrected solubility equation for EDNB salt

The activity corrected solubility equation obtained from literature and expressed in equation 19 was obtained simply by multiplying each hydrogen ion concentration term by the hydrogen ion activity coefficient in the final form of the derived solubility equation. This proved sufficient for the work performed in literature but not for the work performed in this study. Therefore, it was decided that the solubility equation should be fully re-derived with activity coefficients for every ion present in every equation.

Fundamental acid-base equilibria, material balances and solubility relationships which contain all of the necessary activity coefficients are used for the derivation of the new activity corrected solubility equation. Firstly, the activity coefficients were simplified to being either for monovalent or divalent ions as shown in equations 22 and 23.

$$\gamma_1 = \gamma_{H^+} = \gamma_{A^-} = \gamma_{BH^+} \tag{22}$$

$$\gamma_2 = \gamma_{BH_2^{2+}} \tag{23}$$

With this simplification the expressions for the dissociation constants and the solubility product were described by equations 24–27.

$$K_a = \frac{[A^-]\,\gamma_1\,[H^+]\,\gamma_1}{[AH]} \tag{24}$$

$$K_{a1} = \frac{[BH^+]\,\gamma_1\,[H^+]\,\gamma_1}{[BH_2^{2+}]\,\gamma_2} \tag{25}$$

$$K_{a2} = \frac{[B]\,[H^+]\,\gamma_1}{[BH^+]\,\gamma_1} \tag{26}$$

$$K_{sp} = [A^-]^2\,\gamma_1^2\,[BH_2^{2+}]\,\gamma_2 \tag{27}$$

The dissociation constant relationships were rearranged in terms of the concentration of each ion from the acid and base, before being further simplified, according to equations 28–30.

$$[A^-] = \frac{[AH]\,K_a}{[H^+]\,\gamma_1^2} \tag{28}$$

$$[BH^+] = \frac{[B]\,[H^+]}{K_{a2}} \tag{29}$$

$$[BH_2^{2+}] = [BH^+]\,\frac{[H^+]\,\gamma_1^2}{K_{a1}\,\gamma_2} = \frac{[B]\,[H^+]^2}{K_{a1}\,K_{a2}}\left(\frac{\gamma_1^2}{\gamma_2}\right) \tag{30}$$

The materials balance expressions were then written with the ionic species terms being replaced as shown in equations 31 and 32.

$$[Acid] = [AH] + [A^-] = [AH]\left(1 + \frac{K_a}{[H^+]}\left(\frac{1}{\gamma_1^2}\right)\right) \tag{31}$$

$$[Base] = [B] + [BH^+] + [BH_2^{2+}] = [B]\left(1 + \frac{[H^+]}{K_{a2}} + \frac{[H^+]^2}{K_{a1}\,K_{a2}}\left(\frac{\gamma_1^2}{\gamma_2}\right)\right) \tag{32}$$

As the overall composition is assumed to be stoichiometric, and the same stoichiometry as the salt (2:1 3,5-DNBA:ethylenediamine), the total acid and base concentrations were related to each other according to equations 33 and 34.

$$[Acid] = 2\,[Base] \tag{33}$$

$$[AH]\left(1+\frac{K_a}{[H^+]}\left(\frac{1}{\gamma_1^2}\right)\right)=2\,[B]\left(1+\frac{[H^+]}{K_{a2}}+\frac{[H^+]^2}{K_{a1}\,K_{a2}}\left(\frac{\gamma_1^2}{\gamma_2}\right)\right) \quad (34)$$

The solubility product expression was then rewritten and simplified by replacing the ionic species terms from the acid and base as shown in equations 35 and 36.

$$K_{sp}=[A^-]^2\,\gamma_1^2\,[BH_2^{2+}]\,\gamma_2=\left(\frac{[AH]\,K_a}{[H^+]\,\gamma_1^2}\right)^2\,\gamma_1^2\,\frac{[B]\,[H^+]^2}{K_{a1}\,K_{a2}}\left(\frac{\gamma_1^2}{\gamma_2}\right)\gamma_2 \quad (35)$$

$$K_{sp}=[AH]^2\,\frac{{K_a}^2}{K_{a1}\,K_{a2}}\,[B] \quad (36)$$

The $[B]$ term was then replaced with an expression which contained the $[AH]$ term before being simplified as shown in equations 37 and 38.

$$K_{sp}=[AH]^2\,\frac{{K_a}^2}{K_{a1}\,K_{a2}}\,\frac{1}{2}\,[AH]\,\frac{\left(1+\frac{K_a}{[H^+]\,\gamma_1^2}\right)}{\left(1+\frac{[H^+]}{K_{a2}}+\frac{[H^+]^2}{K_{a1}\,K_{a2}}\left(\frac{\gamma_1^2}{\gamma_2}\right)\right)} \quad (37)$$

$$K_{sp}=\frac{1}{2}\,[AH]^3\,\frac{{K_a}^2}{K_{a1}\,K_{a2}}\,\frac{\left(1+\frac{K_a}{[H^+]\,\gamma_1^2}\right)}{\left(1+\frac{[H^+]}{K_{a2}}+\frac{[H^+]^2}{K_{a1}\,K_{a2}}\left(\frac{\gamma_1^2}{\gamma_2}\right)\right)} \quad (38)$$

This solubility product expression was then rewritten in terms of $[AH]$ rather than $[K_{sp}]$ according to equation 39.

$$[AH]=\left\{2\,K_{sp}\,\frac{K_{a1}\,K_{a2}}{{K_a}^2}\,\frac{\left(1+\frac{[H^+]}{K_{a2}}+\frac{[H^+]^2}{K_{a1}\,K_{a2}}\left(\frac{\gamma_1^2}{\gamma_2}\right)\right)}{\left(1+\frac{K_a}{[H^+]\,\gamma_1^2}\right)}\right\}^{1/3} \quad (39)$$

The expressions for $[AH]$ and $[A^-]$ were then inserted into one of the definitions of solubility in order to obtain an expression for solubility which only utilises the hydrogen ion

concentration, activity coefficients, dissociation constants and solubility product. This process is shown in equations 40–44.

$$Solubility = \frac{1}{2}\left([AH] + [A^-]\right) \tag{40}$$

$$= \frac{1}{2}\,[AH]\left(1 + \frac{K_a}{[H^+]\,\gamma_1^2}\right) \tag{41}$$

$$= \left\{\frac{1}{4}\,K_{sp}\left(\frac{K_{a1}\,K_{a2}}{{K_a}^2}\right)\left(1 + \frac{[H^+]}{K_{a2}} + \frac{[H^+]^2}{K_{a1}\,K_{a2}}\left(\frac{\gamma_1^2}{\gamma_2}\right)\right)\left(1 + \frac{K_a}{[H^+]\,\gamma_1^2}\right)^2\right\}^{1/3} \tag{42}$$

$$= \left\{\frac{1}{4}\,K_{sp}\left(\frac{\gamma_1^2}{\gamma_2} + \frac{K_{a1}}{[H^+]} + \frac{K_{a1}\,K_{a2}}{[H^+]^2}\right)\left(\frac{1}{\gamma_1^2} + \frac{[H^+]}{K_a}\right)^2\right\}^{1/3} \tag{43}$$

$$Solubility = \left\{\frac{1}{4}\,K_{sp}\left(\frac{1}{\gamma_2} + \frac{K_{a1}}{[H^+]\,\gamma_1^2} + \frac{K_{a1}\,K_{a2}}{[H^+]^2\,\gamma_1^2}\right)\left(1 + \frac{[H^+]\,\gamma_1^2}{K_a}\right)^2\right\}^{1/3} \tag{44}$$

Equation 44 is the final form of the new activity corrected solubility equation. A new K_{sp} value was fitted to this new equation in order to determine the actual solubility of EDNB triclinic at 25 °C for the experiments performed. This new K_{sp} value is $6.0 \times 10^{-5}\ mol^3/dm^9$. It is interesting to note that this value is similar to the corresponding literature value of $7.7 \times 10^{-5}\ mol^3/dm^3$. Figure 16 shows a comparison of the EDNB triclinic solubility measurements with the activity corrected solubility line developed in this work and the "activity corrected" solubility line from literature. The uncorrected solubility lines from this work and from literature are also shown with the only difference between them being the K_{sp} value.

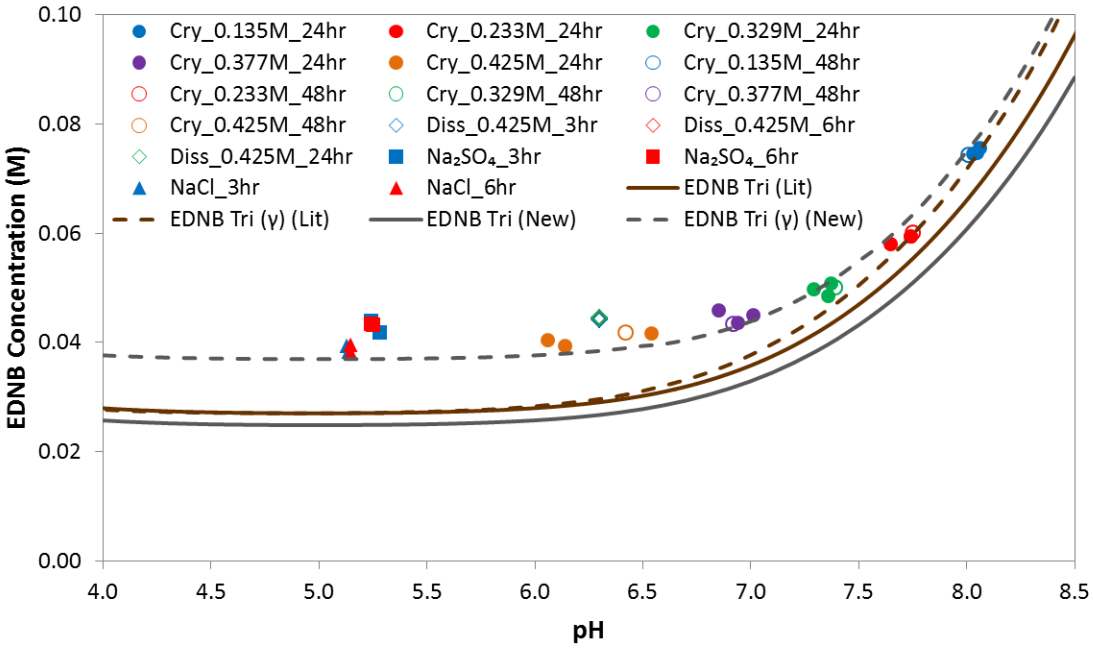

Figure 16. Comparison of EDNB triclinic solubility measurements with solubility lines developed here and from literature. Solid brown line and dashed brown line are uncorrected and activity corrected literature solubility lines respectively. Solid grey line and dashed grey line are the new uncorrected and activity corrected solubility lines respectively.

The comparison demonstrates that utilising the activity corrected solubility equation developed in this study, with the re-determined solubility product, allowed for the EDNB triclinic solubility measurements to be fitted much more closely than the literature "activity corrected" solubility equation did. Therefore, it was decided that solubility data from the new equation would be used to determine solid recovery and scrutinise experimental endpoints for the 25 °C experiments where EDNB triclinic was produced.

As the value for the solubility product for EDNB triclinic at 25 °C determined in this work was similar to the literature value it was deemed acceptable to apply the new activity corrected solubility equation to estimate the solubility lines of EDNB triclinic at 50 °C, EDNB

monoclinic at 25 °C and EDNB monoclinic at 50 °C using the literature K_{sp} values even though no experimental solubility measurements were made for these combinations of polymorph and temperature. A comparison of these activity corrected solubility lines is shown in Figure 17.

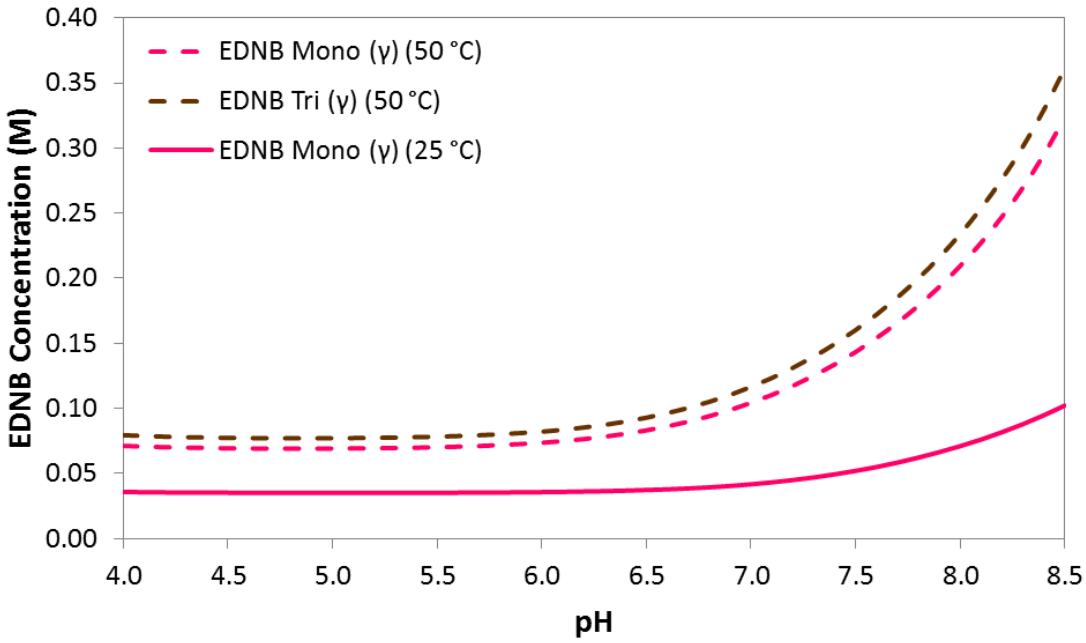

Figure 17. Comparison of solubility lines estimated from the new activity corrected solubility equation using literature solubility product values.

Based on these results it was decided that solubility data from the new activity corrected solubility equation should be used to calculate solid recoveries and scrutinise experimental endpoints for all combinations of polymorph and temperature in this work.

5.6. Conclusions

In this chapter experimental aqueous pH-solubility measurements for 3,5-DNBA at 25 °C have been presented. This is the first instance that the aqueous solubility of 3,5-DNBA has been determined over a wide pH range and reported. The results show that 3,5-DNBA

solubility is very low below pH 3 but then increases sharply above pH 3. This trend was expected due to 3,5-DNBA having a measured pKa value of 2.58. It is this sharp transition in 3,5-DNBA solubility between pH 3 and pH 4.5 which must be considered when designing EDNB salt crystallisation processes. EDNB crystallisation processes typically cover the range of pH 4 to pH 9 so if the 3,5-DNBA concentration is high enough the solution may become supersaturated with respect to 3,5-DNBA when the solution pH approaches a value of 4 which could cause it to crystallise and be present in the final product.

Experimental aqueous pH-solubility measurements for EDNB triclinic at 25 °C have also been presented. These measurements were performed to determine the solubility of EDNB triclinic in solutions with different ionic strengths and different ions present. The results show that EDNB triclinic solubility in solutions with high ionic strength is significantly higher than the solubility data reported in literature. In addition, EDNB triclinic solubility in sodium sulfate solutions was higher than in sodium chloride solutions with the same ionic strength. This suggested that the sulfate ions play an additional role beyond ionic strength which is affecting solubility. The reason for this is not known but one suggestion is that the sulfate ions are complexing with the ethylenediamine ions in solution which is altering the acid-base equilibria and EDNB salt solubility.

The discrepancy between EDNB triclinic solubility measurements and the literature solubility data lead to the derivation of a new activity corrected solubility equation to account for the full activity effects. Utilising the activity corrected solubility equation developed in this study, with a re-determined solubility product, allowed for the EDNB triclinic solubility measurements to be fitted much more closely than the literature solubility equation did. As the re-determined K_{sp} value ($6.0 \times 10^{-5}\ mol^3/dm^9$) is similar to the value from literature ($7.7 \times 10^{-5}\ mol^3/dm^9$) it was deemed acceptable to apply

this new solubility equation to estimate the solubility of EDNB triclinic at 50 °C, EDNB monoclinic at 25 °C and EDNB monoclinic at 50 °C using the literature K_{sp} values even though no experimental solubility measurements were made for these combinations of polymorph and temperature. The solubility data from the new activity corrected solubility equation was then used to calculate solid recoveries and scrutinise experimental endpoints in this work.

6. Solution speciation model applied to salt crystallisation

6.1. Introduction

In organic salt crystallisation experiments there will typically be a target pH value based on understanding of the solution speciation. Organic salt crystallisation literature covers semi-batch experiments where a strong acid is continually added to a basic solution until the desired pH level is reached [109, 110]. Some literature concerned with the semi-batch reactive crystallisation of L-glutamic acid goes further where models are utilised that have pH as an input to calculate the change in pH when a certain quantity of acid is added [118-122]. With this tool they can create an acid addition profile based on the properties of the initial L-glutamic acid solution. Elsewhere, there have been modelling studies looking at applying control strategies to the semi-batch reactive crystallisation of L-glutamic acid in an effort to control the solution concentration and particle size distribution [123, 124].

In this study we seek to build upon the current literature by developing a solution speciation model that can predict the pH and speciation of a solution containing any combination of acids and bases. The only information required is the concentration and pK_a value of each component in addition to the solvent dissociation constant at the temperature of interest. In the application of organic salt crystallisation knowledge of the solubility products for any potential salts will also allow for the supersaturation of any salt to be predicted. In a standard semi-batch process, the model would be used to calculate the pH of the initial basic solution, the volume and concentration of strong acid required to reach the target pH and the change in solution pH and composition as crystallisation initialises and progresses to completion. Therefore, this model can be utilised to explore the entire salt crystallisation design space and predict full crystallisation processes.

The results obtained from the solution speciation model which are presented in this chapter will be limited to experiments performed at 25 °C. In addition, the pKa and solubility values used were those from literature. The first result shown is from the model validation experiments to demonstrate that the model is valid. After this the model is applied to investigate different solution addition approaches. The model is then used to model batch titration, batch crystallisation of the 2:1 EDNB salt, batch crystallisation of the hypothetical 1:1 EDNB salt, batch crystallisation of the 3,5-DNBA staring material and continuous crystallisation of the 2:1 EDNB salt. As a side note different 3,5-DNBA:ethylenediamine molar feed ratios are utilised for the batch 2:1 EDNB salt crystallisation in addition to the batch hypothetical 1:1 EDNB salt crystallisation.

6.2. Materials & methods

6.2.1. Materials

3,5-dinitrobenzoic acid (99%), ethylenediamine (≥99.5%) and hydrochloric acid (37%)were supplied by Sigma Aldrich. Sodium hydroxide (98%) was supplied by Fisher Scientific. Deionised water was produced using an in-house Millipore Milli-Q system.

6.2.2. Experimental methods: Model validation via batch titration

3,5-DNBA and ethylenediamine were dissolved in an aqueous sodium hydroxide solution (NaOH) to create a basic solution where both 3,5-DNBA and the EDNB salt were undersaturated. The 3,5-DNBA, ethylenediamine and NaOH concentrations were 0.123M, 0.0615M and 0.15M respectively. 50ml of the basic solution was added to a 100ml glass beaker. Hydrochloric acid (HCl) solution, with a concentration of 12 M, was added in steps using a 1 ml syringe. A diagram and image of the 100ml beaker and pH probe is shown in Figure 18. The 100 ml beaker was from Thermo Fisher Scientific, had an outer diameter of 5 cm and had a height of 7 cm. The beaker was on a hot plate and a magnetic stirrer bar was

placed inside to provide agitation of the solution during the titration. An agitation rate of 400 rpm was utilised in all the 100 ml beaker experiments. No temperature control was used but the air conditioned laboratory was expected to be at 25 ± 2 °C.

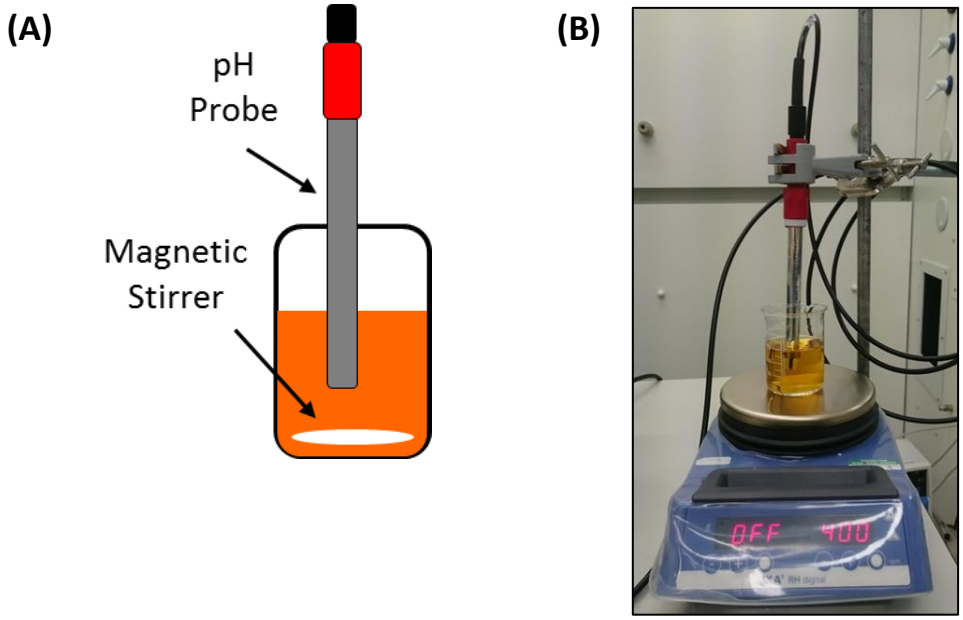

Figure 18. (A) Diagram and (B) image of 100 ml Beaker used for model validation experiments.

The pH probe was inserted into the 100ml beaker so that the pH value could be measured over the course of the titration. After each HCl addition step the solution pH was allowed to stabilise and the value was recorded. Once crystallisation was induced the experiment was stopped.

6.3. Mathematical models

6.3.1. Introduction

The equations used in the mathematical models developed here are commonly used in textbooks and other literature. However, in literature they are almost always applied to

situations where pH is known (or assumed) and are solved based on that knowledge. These mathematical models use the equations in situations where only the overall system composition is known. By solving a particular system of equations simultaneously the pH and full speciation of components in solution is calculated. It should be noted that there is no analytical solution to these systems of equations and instead they must be solved numerically. In the work MATLAB software was used to implement the numerical solving. In the present study there are 3 mathematical models applied which are described in detail. Each model describes a different physical state with different assumptions, inputs and outputs. For this reason each model has a different system of equations which needs to be solved.

6.3.2. Single phase model (liquid phase pseudo-equilibrium)

When all the components are dissolved in the aqueous solution there exists only a single phase. In order to fully model the speciation in the solution several physical phenomenon must be taken into account. These are the materials balances and acid-base equilibria associated with the weak acid and base, the dissociation of the water solvent and the overall charge balance which takes the presence of the strong acid and base into account. For the EDNB salt $[BH_2.A_2]$ made from a monoprotic weak acid, (AH), and a dibasic weak base, (B), the appropriate material balances are described by equations 45 and 46.

$$[3,5\text{-}DNBA] = [AH] + [A^-] \tag{45}$$

$$[Ethylenediamine] = [B] + [BH^+] + [BH_2^{2+}] \tag{46}$$

As the solution is completely aqueous the water dissociation constant is accounted for in equation 47.

$$K_w = [OH^-][H^+] \quad (47)$$

Finally, due to the presence of the strong base (NaOH) and strong acid (sulfuric acid) the overall charge balance is taken into account in equation 48.

$$[Na^+] + [H^+] + [BH^+] + 2[BH_2^{2+}] = [A^-] + [OH^-] + 2[SO_4^{2-}] \quad (48)$$

Equation 11–13 and 45–48 are treated as a system of 7 equations which can be solved when there are 7 unknowns. In practice this means that when the concentrations of all the components are known in addition to the dissociation constants then the proton concentration (indirectly gives pH) and speciation of each component can be determined.

6.3.3. Two phase model (liquid phase pseudo-equilibrium in the presence of solids)

When crystallisation commences the system becomes a two phase system (liquid and solid). As EDNB is crystallising 2 moles of $[A^-]$ ions are being removed from solution for every mole of $[BH_2^{2+}]$ ions. For this reason the acid-base equilibria in the solution changes as the crystallisation proceeds. This change in solution speciation can be captured in a two phase model simply by changing equations 45 and 46 so that the concentration of solid EDNB salt is incorporated into the material balance as shown in equations 49 and 50. $[EDNBx]$ is the concentration of solid EDNB in the system.

$$[3,5\text{-}DNBA] = [AH] + [A^-] + 2[EDNBx] \quad (49)$$

$$[Ethylenediamine] = [B] + [BH^+] + [BH_2^{2+}] + [EDNB_x] \quad (50)$$

This model is applied when the liquid and solid phase are not in equilibrium so the critical input must either be supersaturation or the solid EDNB concentration. Simultaneously solving the 8 equations of 11–13, 16 and 47–50 give the important outputs of proton

concentration and the speciation of each component exactly as the single phase model did with the additional output being either solid EDNB concentration or supersaturation. In practice, this model can be applied to an experiment where pH is known during the crystallisation process but concentration is not or vice versa. This allows more information to be obtained from an experiment without the use of additional probes.

6.3.4. Two phase model (solid-liquid equilibrium)

The model can be modified again when there is equilibrium between the liquid and solid phase i.e. when crystallisation is complete and the solution is completely desupersaturated. As with the non-equilibrium two phase model one must simultaneously solve the 8 equations of 11–13, 16 and 47–50. The difference here is that the supersaturation value is set to 0 according to equation 16 in order to denote saturation. When there is liquid-solid equilibrium the concentration of solid EDNB becomes an unknown which is to be solved rather than an input. In practice, this model can be used to determine the actual yield of a salt crystallisation experiment as the mass of crystals which should have been recovered is solved and the mass of crystals which are actually recovered is known.

6.4. Model validation

A series of batch titration experiments were performed in order to compare the experimental pH data with pH profiles obtained by the model. The comparison of the experimental pH data with the modelled pH profile is shown in Figure 19. Modelled boundaries were also included to show the course of the titration if the volume was ±10% of the experimentally measured value in order to account for experimental error. This magnitude of experimental error was thought to be possible as very small steps of 0.1 ml HCl solution were added using a 1ml syringe.

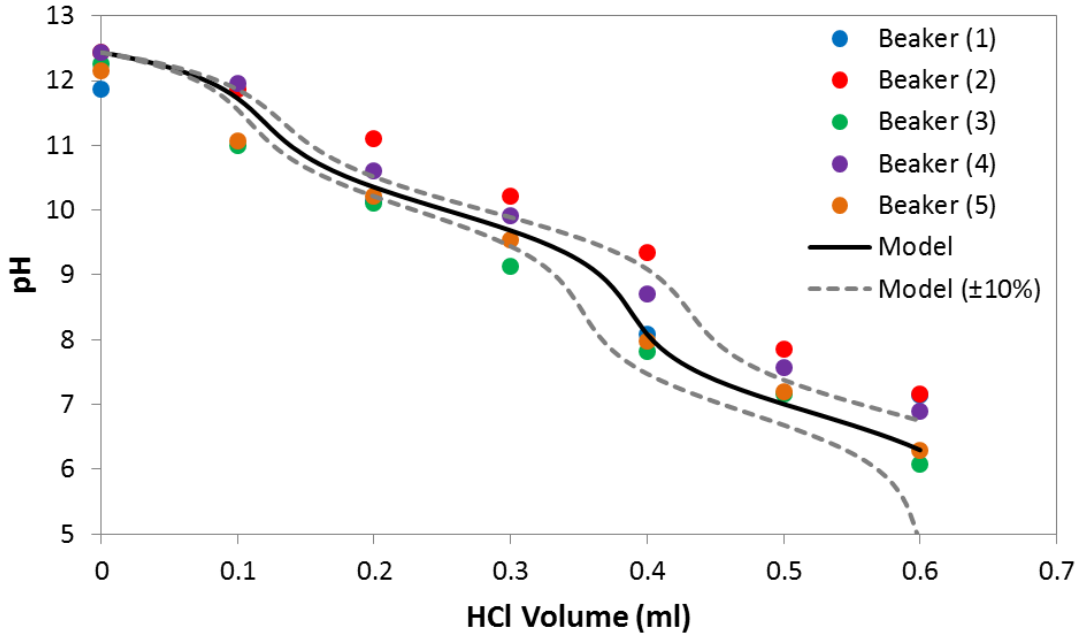

Figure 19. Comparison of experimental pH profiles with modelled pH profile in 100 ml beaker experiments.

It was determined that the modelled pH profile generally matched the experimental data although there was some significant deviation. The deviation of experimental pH data from the modelled pH profile was thought to be due to the possible volume addition errors as outlined. To further investigate the possible sources of deviation Figure 20 was generated to show how well the model matched experimental pH data over a wide range of experiments. The experiments were at 25 °C or 50 °C, utilised HCl or sulfuric acid and covered different solution concentrations and pH ranges.

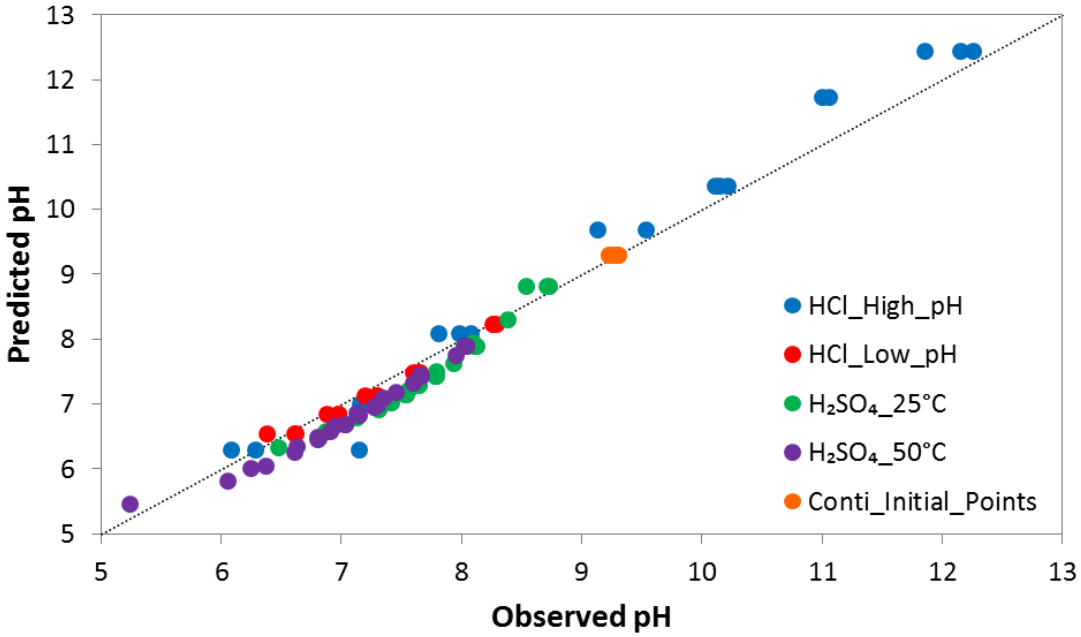

Figure 20. Plot of predicted pH values vs. observed pH values for a wide range of experimental conditions.

It can be seen that the model generally matched all of the experimental data but the experimental points deviated from the model to different extents depending on the conditions. All of the initial points in the titrations and continuous experiments matched the model most closely with them being almost identical to the predicted values. This suggests that the source of any error was the acid, whether related to its addition or its interaction with other species in solution. The pH data which deviate most from the model are from the HCl titration experiments where a high initial pH was used as shown in Figure 19. In contrast, in the HCl titration experiments where a lower initial pH was used the pH data match the model closely. This could be due to the possible decomposition of 3,5-DNBA above pH 9 which can happen according to literature. This would mean that the model isn't capturing exactly what is going on in solution. The deviation could also be due to those

experiments having a much greater NaOH concentration which significantly affects the ionic strength of the solution and makes the ideal solution assumption less valid.

Considering the ionic strength of solution this could be the reason why the pH data from the sulfuric acid titration experiments deviate from the model a little more than the pH data from the low initial pH HCl titration experiments. In other words, a diprotic acid such as sulfuric acid will have a greater contribution to ionic strength than a monoprotic acid such as HCl. The other possible reason for the increased deviation with sulfuric acid is that the sulfate ions undergo complexation with ethylendiamine ions to some extent which means that the model is no longer describing exactly what is happening in solution.

It was observed very early in this work that there is this significant deviation from the model when the initial point of the experiment is greater than pH 9. For this reason all of the crystallisation experiments were restricted to pH levels of below 9. With regards to the small deviations as a result of increased ionic strength this couldn't be avoided but it was kept in mind when designing and analysing experiments. Taking all of these points into consideration it was decided that the model was proven to be valid below pH 9 and it could be used to design and better understand experiments.

6.5. Modelling semi-batch crystallisation processes

6.5.1. Addition approaches for 2:1 EDNB salt crystallisation

The solution addition approach from literature involves adding a strong acid (HCl or sulfuric acid) to an initial aqueous solution containing 3,5-DNBA, ethylenediamine and NaOH. The initial solution composition was designed in order to have the maximum concentrations of 3,5-DNBA and ethylenediamine while keeping a stoichiometric 2:1 molar ratio of 3,5-DNBA:ethylenediamine and keeping the solution pH below 9. The solution pH should be kept below 9 because above this value 3,5-DNBA is reported [114] to react with hydroxide

ions to yield a red coloured solution containing 2,3-dihydroxy-5-nitrobenzoic acid and 3,3'-dinitro-5,5'-dicarboxyazoxybenzene. This standard solution addition approach was utilised for modelling all of the batch EDNB crystallisation processes in this study. However, alternative solution addition approaches were considered.

When considering alternative solution addition approaches several issues had to be kept in mind. Firstly, the initial solution containing 3,5-DNBA had to maintain a pH high enough to achieve reasonable solubility but not too high as to lead to decomposition. This typically meant the solution was required to have a pH value between 4.5 and 9. In addition, if 3,5-DNBA and ethylenediamine were in the same initial solution then the EDNB salt had to be undersaturated. Similarly, the final mixed solution had to be supersaturated with respect to the EDNB salt but undersaturated with respect to 3,5-DNBA. This usually meant that the initial solution containing 3,5-DNBA had a pH greater than the mixed solution pH, the other initial solution had a pH less than the mixed solution pH and the mixed solution had a pH where the EDNB salt was supersaturated.

The first approach to be considered was to remove the need for a strong acid and simply add ethylenediamine to a solution containing 3,5-DNBA and NaOH. The issue with this is that the pH of the solution containing 3,5-DNBA and NaOH had to be at least 4.5 to ensure reasonable 3,5-DNBA solubility and adding even an extremely small amount of ethylenediamine to this solution increased the pH above 8 which meant that the pH range at which the EDNB salt can be supersaturated was completely crossed over. Therefore, a strong acid needs to be used in the addition approach.

Another approach which was considered was to add ethylenediamine to an initial solution containing 3,5-DNBA, NaOH and sulfuric acid. The issue with this is that the pH of the initial solution would have too low a pH to solubilise the 3,5-DNBA due to the presence of the

sulfuric acid. An additional approach which was considered was to add a solution containing NaOH and sulfuric acid to an initial solution containing 3,5-DNBA and ethylenediamine. However, this also isn't possible as the initial solution would need a high enough concentration of 3,5-DNBA and ethylendiamine in the correct molar ratio which would result in a solution where either 3,5-DNBA and/or EDNB is supersaturated.

The most likely alternative solution addition approach was to add a solution containing ethylenediamine and sulfuric acid to an initial solution containing 3,5-DNBA and NaOH. This allowed for a high concentration of 3,5-DNBA to be dissolved in the initial solution as a reasonable pH could be maintained by using the required NaOH concentration. The stoichiometrically required concentration of ethylenediamine was then used in the other solution and the sulfuric acid concentration to be used was determined by the target pH of the mixed solution.

In order to model either the standard addition approach or the alternative addition approach a set of solution concentrations, solution volumes and a target pH of the mixed solution had to be selected. In order to compare the approaches, the initial solution (containing 3,5-DNBA and NaOH with or without ethylenediamine) had a volume of 90 ml while the titrant (containing sulfuric acid with or without ethylenediamine) had a volume of 10 ml in both approaches. Also for both approaches the mixed solution had a target pH of 6. For the standard addition approach the concentrations used in the solutions were as follows:

$$[3,5\text{-}DNBA] = 0.2\ M$$

$$[Ethylenediamine] = 0.1\ M$$

$$[NaOH] = 0.105\ M$$

$$[H_2SO_4] = 0.419\ M$$

For the alternative additions approach the concentrations used in the solutions were as follows:

$$[3{,}5\text{-}DNBA] = 0.2\ M$$

$$[Ethylenediamine] = 0.9\ M$$

$$[NaOH] = 0.2\ M$$

$$[H_2SO_4] = 0.846\ M$$

The modelled EDNB crystallisation processes for both the standard and alternative solution addition approaches, with a titration endpoint of pH 6, are shown in Figure 21.

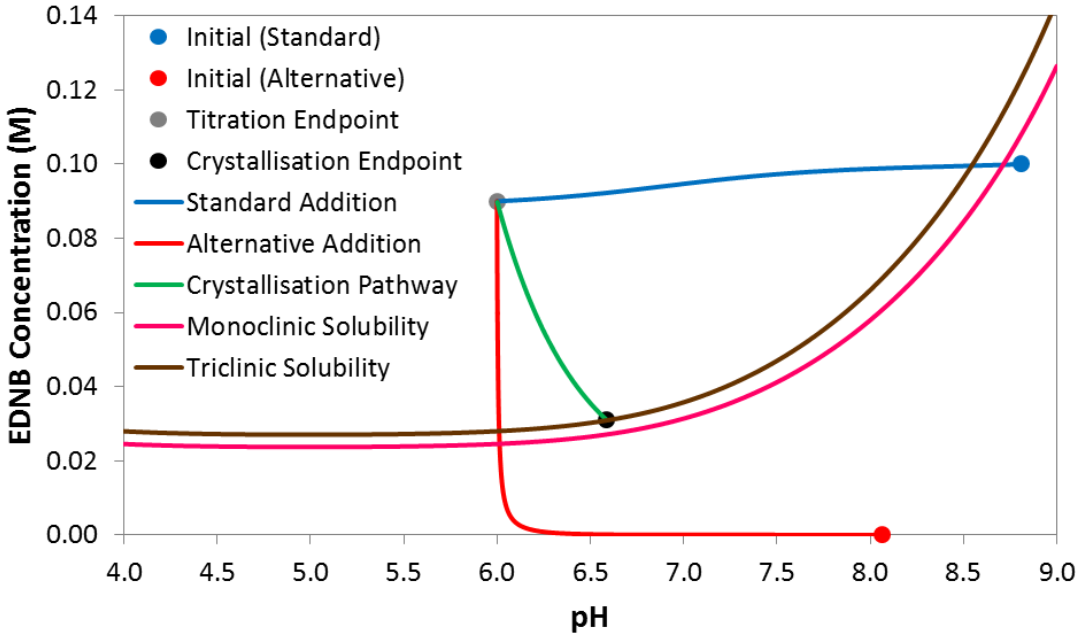

Figure 21. Modelled 2:1 EDNB crystallisation processes for both the standard and alternative solution addition approaches with titration endpoint of pH 6.

It can be seen for the standard addition approach that as the sulfuric acid is added to the initial solution containing 3,5-DNBA, ethylenediamine and NaOH, the concentration of the EDNB salt decreases to the target value (due to dilution) and the pH of the initial solution decreases to the target value. It can be seen for the alternative addition process that as the solution containing ethylenediamine and sulfuric acid is added to the initial solution containing 3,5-DNBA and NaOH, the concentration of the EDNB salt increases to the target value (due to creation of EDNB salt in solution) and the pH of the initial solution decreases to the target value. Despite these differences between the approaches the crystallisation process which occurs after the end of the titration process is the same. The alternative addition approach may be advantageous to the standard approach used in this work as the concentrations of 3,5-DNBA and ethylenediamine can be increased without the pH values of the initial solutions changing greatly. This is because the concentrations of NaOH and

sulfuric acid can be increased in each solution to counteract the pH change resulting from the increase in 3,5-DNBA and ethylenediamine concentrations. By having increased concentrations the yield of the EDNB salt can be increased. Therefore, this alternative addition approach should be investigated experimentally in the future.

6.5.2. Modelling titration curves

The solution speciation model was firstly applied to batch titration type experiments without considering crystallisation. Utilising the standard addition approach these are experiments where there exists an initial aqueous solution containing 3,5-DNBA, ethylenediamine and NaOH into which sulfuric acid is added. The model assumes perfect mixing so the vessel type, agitation method and acid addition method won't be accounted for but would of course affect the mixing efficiency of the process. The 3,5-DNBA, ethylenediamine and NaOH concentrations were 0.2 M, 0.1 M and 0.105 M respectively as they were for the addition approach comparison section. Similarly, the initial solution had a volume of 90 ml with 10 ml of the titrant being added. Using this set of 3,5-DNBA, ethylenediamine and NaOH concentrations, in addition to this volume ratio, a batch titration was modelled using a 2M sulfuric acid solution as the titrant. Such a high concentration of sulfuric acid was used in order to show the full range of possible outcomes from the titration process. The results of this modelled titration are shown in Figure 22. The pH and supersaturation profiles will correspond to those in the standard addition approach down to a pH value of 6.

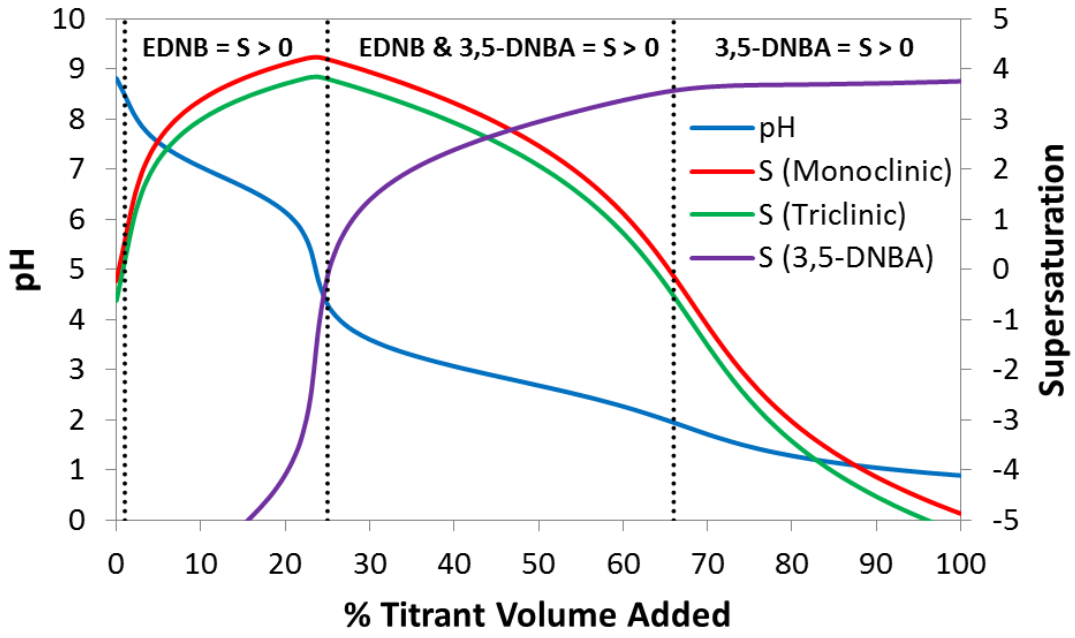

Figure 22. Plot of titration with 2M sulfuric acid solution showing different regions of interest.

The shape of the modelled titration curve demonstrates how sensitive the pH and supersaturation are to the titrant volume and concentration. Furthermore, the titration curve shows the full range of possible regions of interest and allows for the correct titrant volume and concentration to be selected in order to crystallise the desired solid form whether that be EDNB monoclinic, EDNB triclinic or 3,5-DNBA. With 0% titrant volume added both EDNB and 3,5-DNBA are undersaturated. Between 1% and 25% titrant volume added EDNB is supersaturated and 3,5-DNBA is undersaturated. Between 26% and 65% titrant volume added both EDNB and 3,5-DNBA are supersaturated. Between 66% and 100% titrant volume added EDNB is undersaturated and 3,5-DNBA is supersaturated. Therefore, to crystallise the EDNB salt without crystallising the 3,5-DNBA starting material, using this titrant concentration, between 1% and 25% of the titrant volume should be

added. The value to be chosen within this range depends on the pH, supersaturation, yield and polymorph required from the crystallisation.

Utilising the alternative solution addition approach, where the initial solution contains 3,5-DNBA and NaOH and the titrant solution contains ethylenediamine and sulfuric acid, the pH and supersaturations change as the titrant volume is added as shown in Figure 23. The 3,5-DNBA, ethylenediamine, NaOH and sulfuric acid concentrations were 0.2 M, 0.9 M, 0.2 M and 0.846 M respectively as they were for the addition approach comparison section. Similarly, the initial solution had a volume of 90 ml with 10 ml of the titrant being added.

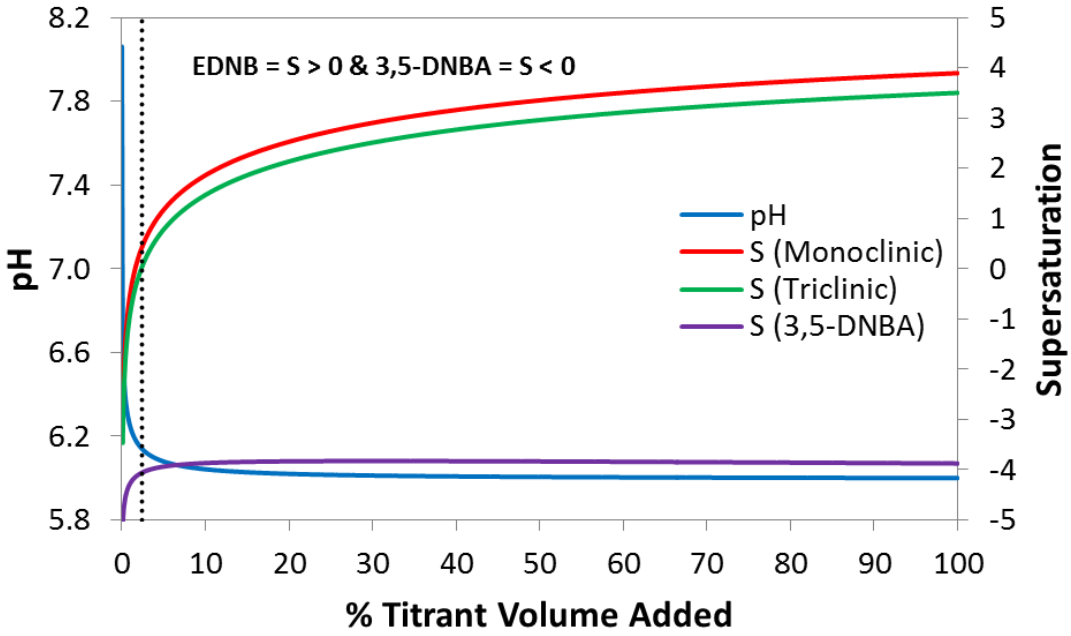

Figure 23. Plot of titration curve from alternative solution addition approach showing different regions of interest.

The pH and supersaturation profiles show how utilising the alternative solution addition approach drastically changes the titration process. Instead of a gradual decrease in pH and a gradual increase in EDNB supersaturation, the pH and supersaturation values rapidly get very close to their endpoints with most of the titration being very close to the endpoint.

Between 0% and 23% titrant volume added both EDNB and 3,5-DNBA are undersaturated. Between 24% and 100% titrant volume added EDNB is supersaturated and 3,5-DNBA is undersaturated. Due to the nature of this solution addition approach the pH range covered by the titration will change by very little when the concentrations of 3,5-DNBA and ethylenediamine are increased. This means that the only thing limiting the 3,5-DNBA concentration is the solubility at the target pH. For this reason the alternative addition approach may be preferable to the standard addition approach so will be investigated experimentally in the future.

6.5.3. Modelling 2:1 EDNB salt crystallisation

As previously mentioned the model can be applied to the two phase system which exists during the crystallisation process. Initially the model tracks solution speciation without the presence of solids as the titration progresses. Once crystallisation occurs the model starts re-calculating the solution speciation due to material being removed from solution and this continues until the solution reaches saturation because the liquid and solid phases are at equilibrium. Figure 24 shows modelled EDNB crystallisation processes with different titration endpoints. The processes can be plotted with respect to EDNB salt concentration as the molar feed ratio is the same as the salt stoichiometry throughout the entire process. The EDNB concentration will be the same as the ethylenediamine concentration and half the 3,5-DNBA concentration. The process essentially consists of two parts. The first part is the single phase titration where the titrant is added to the basic solution until completion, the second part is the crystallisation pathway showing the decrease in EDNB solution concentration until the EDNB triclinic solubility line is reached. Eventually the process would reach the EDNB monoclinic solubility line when transformation takes place but this isn't shown explicitly. Using this solubility line as the endpoint is correct as the molar feed

ratio and salt stoichiometry is maintained at all times. As with modelling the batch titration curves, the initial solution composition was as follows:

$$[3,5\text{-}DNBA] = 0.2\ M$$

$$[Ethylenediamine] = 0.1\ M$$

$$[NaOH] = 0.105\ M$$

Using this set of 3,5-DNBA, ethylenediamine and NaOH concentrations, the sulfuric acid concentration was determined by the target titration endpoint and was therefore different for each titration endpoint. The sulfuric acid concentrations used for the titration endpoints of pH 7, 6, 5 and 4 were 0.211 M, 0.419 M, 0.472 M and 0.528 M respectively. The initial solution had a volume of 90 ml with 10 ml of the sulfuric acid being added. It should be noted that EDNB crystallisation at a pH less than 4.5 in reality would be complicated by the simultaneous crystallisation of the 3,5-DNBA starting material. However, this wasn't considered in this application of the model. For the titration with an endpoint of pH 7, an alternative crystallisation pathway is shown as an example where crystallisation begins half way through titrant addition rather than at the end of titrant addition. It was assumed that the initial crystallisation moves the solution directly to saturation and adding further titrant induces further crystallisation in a way where the solution is immediately desupersaturated as the titrant is added so that the crystallisation pathway remains on the solubility line until the end of the process. The end of pH 7 process where crystallisation begins during addition is the same as the pH 7 process where crystallisation begins at the end of titration.

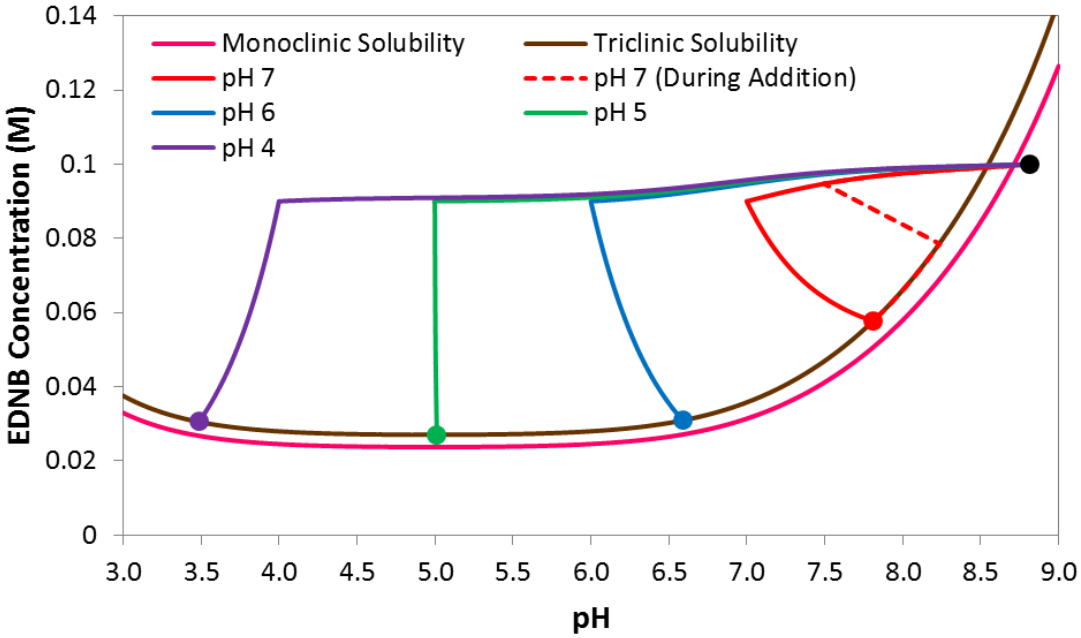

Figure 24. Modelled 2:1 EDNB crystallisation processes, using a 2:1 molar feed ratio, with different titration endpoints. Red dashed line shows crystallisation pathway for a titration endpoint of pH 7 when crystallisation begins during sulfuric acid addition.

What is most noticeable from the crystallisation pathways is how the pH changes as the crystallisation progresses. When the pH at the titration endpoint is greater than 5 then the pH will increase because although $[BH_2^{2+}]$ ions are being removed from solution, a low $[SO_4^{2-}]$ ion concentration is present and there are still $[BH^+]$ and $[Na^+]$ ions remaining in the solution. When the pH at the titration endpoint is around 5 then the pH will remain essentially constant because the $[SO_4^{2-}]$ and $[Na^+]$ ions have effectively neutralised each other and there are no $[BH^+]$ ions remaining in the solution as the $[BH_2^{2+}]$ ions are being removed from solution. When the pH at the titration endpoint is less than 5 then the pH will decrease because there is an excess of $[SO_4^{2-}]$ ions after completely neutralising the $[Na^+]$ ions and there are no $[BH^+]$ ions remaining in the solution as the $[BH_2^{2+}]$ ions are being removed from solution.

Utilising a 2:1 molar ratio of 3,5-DNBA:ethylenediamine in the feed solutions should be the most suitable method for crystallising the 2:1 EDNB salt as potentially all of the starting material can be consumed. However, other molar ratios were tested with the model in order to study the effect that it had on the crystallisation process. This exploration of the design space is useful as there may be practical benefits in using more or less of either material in the crystallisation process. When considering industrial crystallisation processes, the most notable benefit of changing the molar ratio would be to minimise the concentration of the more expensive starting material and thus make the process less costly to run. This activity is commonly performed in industry where a molar excess of the cheaper starting material will be used to ensure that the maximum amount of the more expensive material is consumed.

To demonstrate this a 1:1 molar ratio of 3,5-DNBA:ethylenediamine was used to see the effect that it had on the 2:1 EDNB salt crystallisation process. The initial solution composition was as follows:

$$[3,5\text{-}DNBA] = 0.1\ M$$

$$[Ethylenediamine] = 0.1\ M$$

$$[NaOH] = 0.005\ M$$

The 3,5-DNBA concentration was decreased from 0.2 M to 0.1 M in order to keep the ethylenediamine concentration consistent with other experiments. In order to achieve a consistent initial solution pH of 8.81 the NaOH concentration was decreased from 0.105 M to 0.005 M. The sulfuric acid concentration was determined by the target titration endpoint and was therefore different for each titration endpoint. The sulfuric acid concentrations used for the titration endpoints of pH 7, 6, 5 and 4 were 0.211 M, 0.418 M, 0.469 M and 0.5

M respectively. The initial solution had a volume of 90 ml with 10 ml of the sulfuric acid being added. Figure 25 shows modelled 2:1 EDNB crystallisation processes, using a 1:1 molar feed ratio, with different titration endpoints. As the molar feed ratio is significantly different from the salt stoichiometry the 2:1 EDNB salt solubility data no longer applies. Also, the processes are plotted with respect to the 3,5-DNBA concentration as this is the limiting component in this system. The 2:1 EDNB salt solubility line was used to determine arbitrary process endpoints.

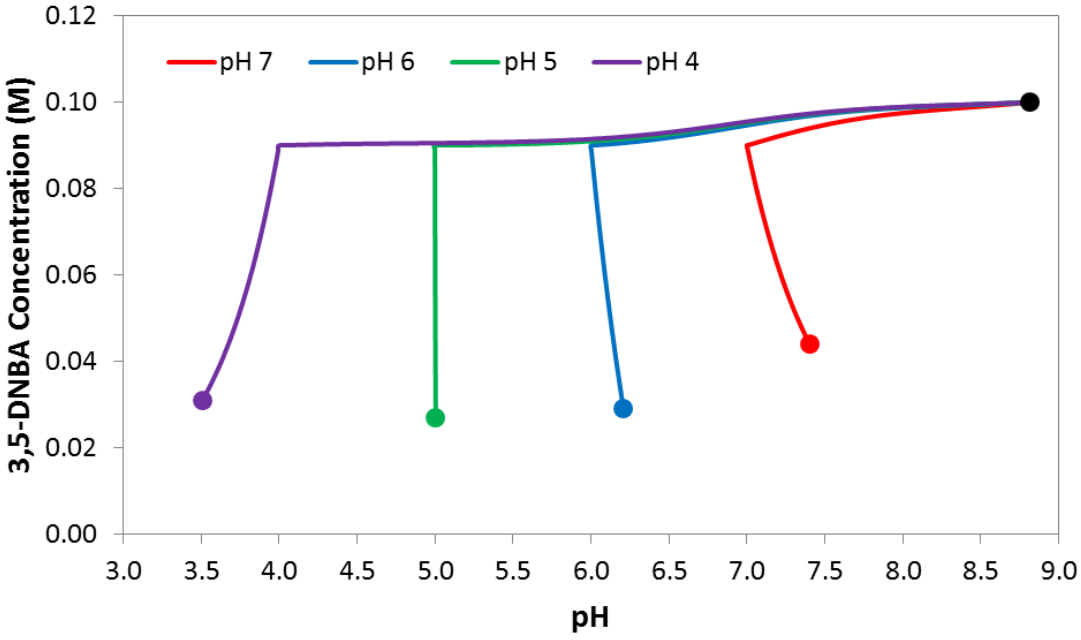

Figure 25. Modelled 2:1 EDNB crystallisation processes, using a 1:1 molar feed ratio, with different titration endpoints.

Comparing these profiles with those in Figure 24 it can be seen that changing the molar feed ratio from 2:1 to 1:1 3,5-DNBA:ethylenediamine does have a noticeable effect on the crystallisation process. The direction of the pH change during the crystallisation processes is the same but using the 1:1 molar feed ratio results in the pH change being smaller or essentially the same depending on the titration endpoint. The change is much smaller when

looking at the titration endpoints of pH 6 and pH 7 but essentially the same at the titration endpoint of pH 4. The pH is essentially constant at the titration endpoint of pH 5 for both molar feed ratios.

6.5.4. Modelling hypothetical 1:1 EDNB salt crystallisation

As an additional test to the solution speciation model, the crystallisation process of the hypothetical 1:1 EDNB salt was modelled to see how it compares with the 2:1 EDNB salt crystallisation process. A 2:1 molar ratio of 3,5-DNBA:ethylenediamine was used as with the 2:1 EDNB salt crystallisation processes. Figure 26 shows modelled 1:1 EDNB salt crystallisation processes with different titration endpoints. The same solution concentrations were used for modelling the 1:1 EDNB salt crystallisation processes and the 2:1 EDNB salt crystallisation. As with the 2:1 EDNB salt, the crystallisation process consists of two parts. The first part is the single phase titration where the titrant is added to the basic solution until completion, the second part is the crystallisation pathway showing the decrease in EDNB solution concentration. As the salt stoichiometry is 1:1 rather than 2:1, the 2:1 EDNB salt solubility data no longer applies. Also, the processes are plotted with respect to the ethylendiamine concentration as this is the limiting component in this system. Either the 2:1 salt solubility or a pH value of 3.5 was used as the arbitrary process endpoint (whichever came first) because EDNB salt crystallisation would realistically not take place below this pH value.

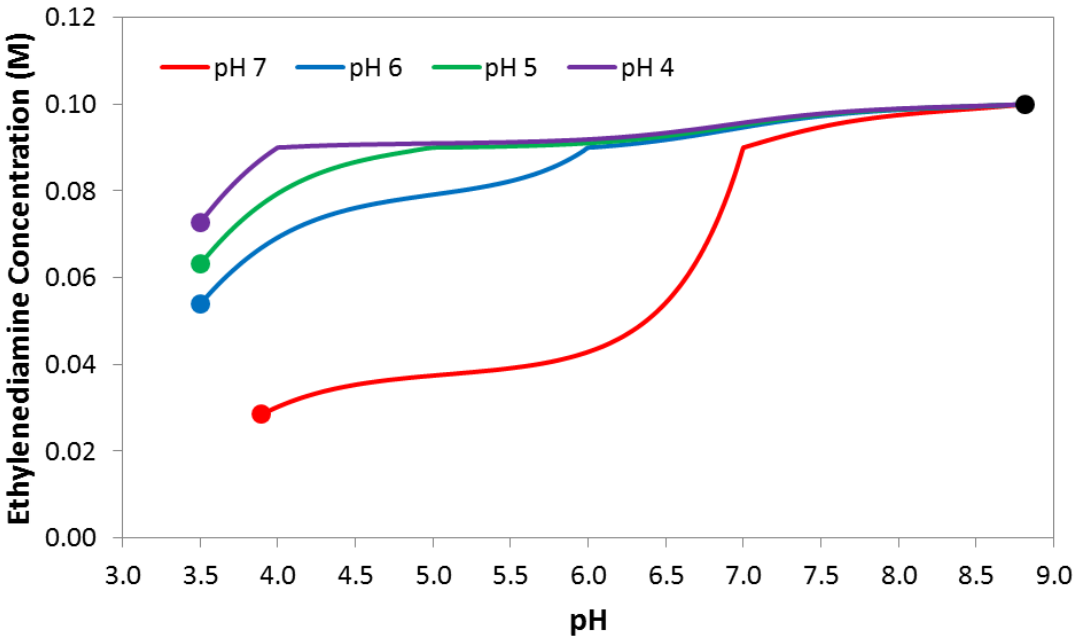

Figure 26. Modelled 1:1 EDNB crystallisation processes, using a 2:1 molar feed ratio, with different titration endpoints.

What is most noticeable from the crystallisation pathways is how the pH changes as the crystallisation progresses. Regardless of the titration endpoint the pH decreased as the crystallisation progressed. This is likely due to the fact that as $[A^-]$ and $[BH_2^{2+}]$ are being removed from solution in equal proportions, there is an increasing excess of acid in solution as the 1:1 EDNB salt is crystallising. This process results in the solution becoming more acidic and the pH decreasing.

As with the 2:1 EDNB salt crystallisation process, a 1:1 molar feed ratio of 3,5-DNBA:ethylenediamine was used with the 1:1 EDNB salt crystallisation process to see the effect that it had. The initial solution composition and sulfuric acid concentrations were the same as for the modelled 2:1 EDNB crystallisation processes using a 1:1 molar feed ratio. The initial solution had a volume of 90 ml with 10 ml of the sulfuric acid being added. Figure 27 shows modelled 1:1 EDNB crystallisation processes, using a 1:1 molar feed ratio, with

different titration endpoints. Again, as the salt stoichiometry is 1:1 rather than 2:1, the 2:1 EDNB salt solubility data no longer applies. There is no limiting component but the processes are plotted with respect to the ethylendiamine concentration. Again, either the 2:1 salt solubility or a pH value of 3.5 was used as the arbitrary process endpoint (whichever came first) because EDNB salt crystallisation would realistically not take place below this pH value.

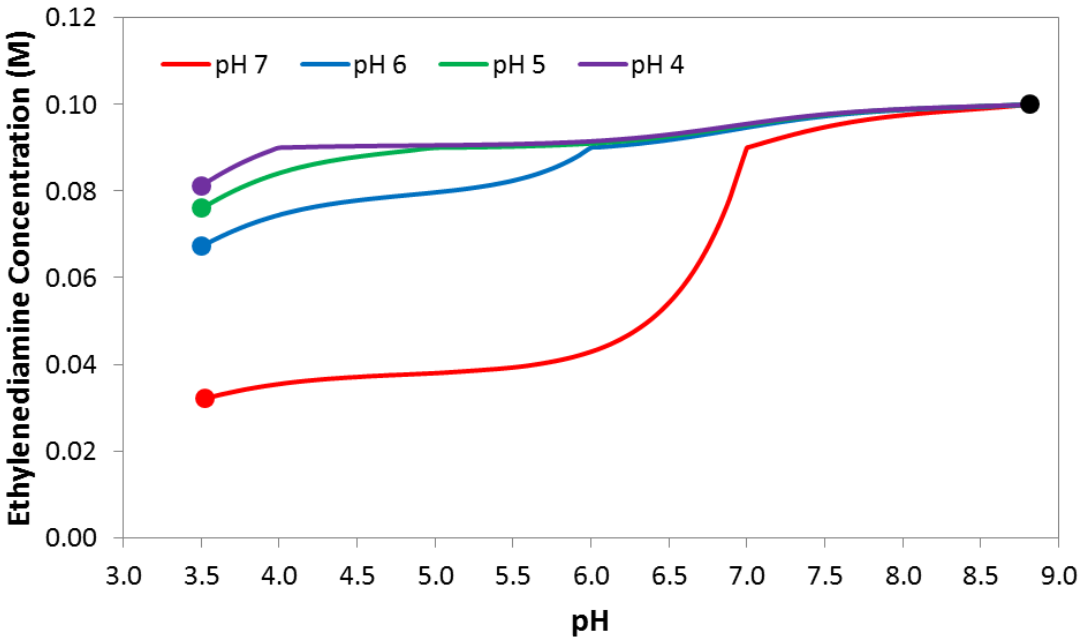

Figure 27. Modelled 1:1 EDNB crystallisation processes, using a 1:1 molar feed ratio, with different titration endpoints.

What is most noticeable from the crystallisation pathways is how the pH changes as the crystallisation progresses. Similar to the 1:1 EDNB salt crystallisation using a 2:1 molar feed ratio, regardless of the titration endpoint the pH decreased as the crystallisation progressed. $[A^-]$ and $[BH_2^{2+}]$ ions are being removed from solution in equal proportions and there is an equal concentration of 3,5-DNBA and ethylenediamine remaining in solution. However, the lower NaOH concentration in the initial solution due to the 1:1

molar feed ratio results in the $[Na^+]$ ions being entirely consumed by the $[SO_4^{2-}]$ ions in every titration. This leads to there always being an excess of $[SO_4^{2-}]$ ions in solution after titration which may be causing the pH decrease when the crystallisation begins.

6.5.5. Modelling 3,5-DNBA crystallisation

In addition to crystallising either polymorphic form of the EDNB salt, the 3,5-DNBA starting material may be crystallised instead. This typically happens when the pH drops below 4 but depends on the 3,5-DNBA concentration. Figure 28 shows modelled 3,5-DNBA crystallisation processes with different titration endpoints. As with modelling the batch EDNB crystallisation processes, the initial solution composition was as follows:

$$[3,5\text{-}DNBA] = 0.2\ M$$

$$[Ethylenediamine] = 0.1\ M$$

$$[NaOH] = 0.105\ M$$

Using this set of 3,5-DNBA, ethylenediamine and NaOH concentrations, the sulfuric acid concentration was determined by the target titration endpoint and was therefore different for each titration endpoint. The sulfuric acid concentrations used for the titration endpoints of pH 4, 3 and 2 were 0.528 M, 0.836 M and 1.304 M respectively. The EDNB salt could also crystallise at these pH values but this was ignored in this application of the model.

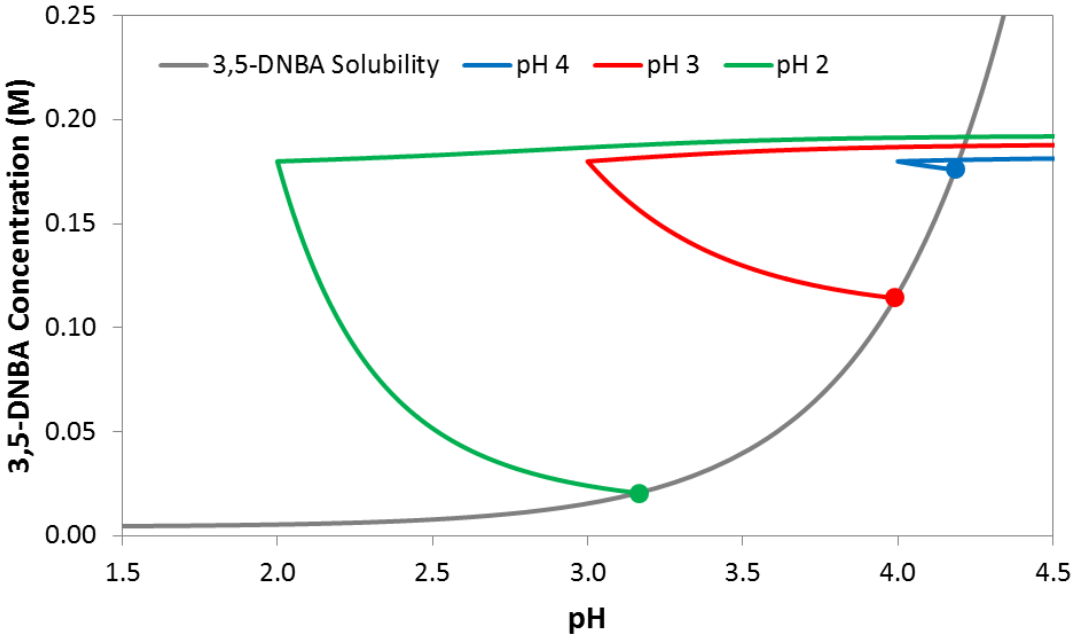

Figure 28. Modelled 3,5-DNBA crystallisation processes with different titration endpoints.

When 3,5-DNBA crystallises the pH always increases as a pure acid is being removed from the solution.

6.6. Modelling continuous crystallisation processes

6.6.1. Mixing approaches for EDNB salt crystallisation

The solution addition approach from literature, which was utilised for modelling all of the batch EDNB crystallisation processes, was directly translated to a continuous mixing approach to be used for modelling all of the continuous EDNB crystallisation processes in this work. This standard mixing approach involved continuously mixing the sulfuric acid solution with the solution containing 3,5-DNBA, ethylenediamine and NaOH. To achieve a target mixing endpoint of pH 6, the solution concentrations and volume ratio was the same as in the batch experiments. The change from the batch experiments being that instead of a gradual titration of the 10ml sulfuric acid with the 90ml initial solution, the two solutions are rapidly mixed together at a volumetric ratio of 9:1 in order to reach the mixing endpoint

immediately. Similarly to the batch experiments the model assumes perfect mixing so the mixing efficiency of the process isn't accounted for.

As with the batch EDNB crystallisation processes, an alternative mixing approach was modelled with this being a direct translation of the batch alternative addition approach. In addition, the continuous crystallisation process of the hypothetical 1:1 EDNB salt was modelled to see how it compares with the 2:1 EDNB salt crystallisation process. A 2:1 molar ratio of 3,5-DNBA:ethylenediamine was used as with the 2:1 EDNB salt crystallisation processes. The modelled continuous EDNB crystallisation processes for the standard and alternative mixing approaches for crystallising the 2:1 EDNB salt, in addition to the standard mixing approach for crystallising the hypothetical 1:1 EDNB salt, all with a mixing endpoint of pH 6, are shown in Figure 29. The 2:1 EDNB triclinic solubility line was used as the endpoint for the 2:1 EDNB salt crystallisation but an arbitrary endpoint of pH 3.5 was used for the 1:1 EDNB salt crystallisation as the solubility of the hypothetical 1:1 EDNB salt is unknown.

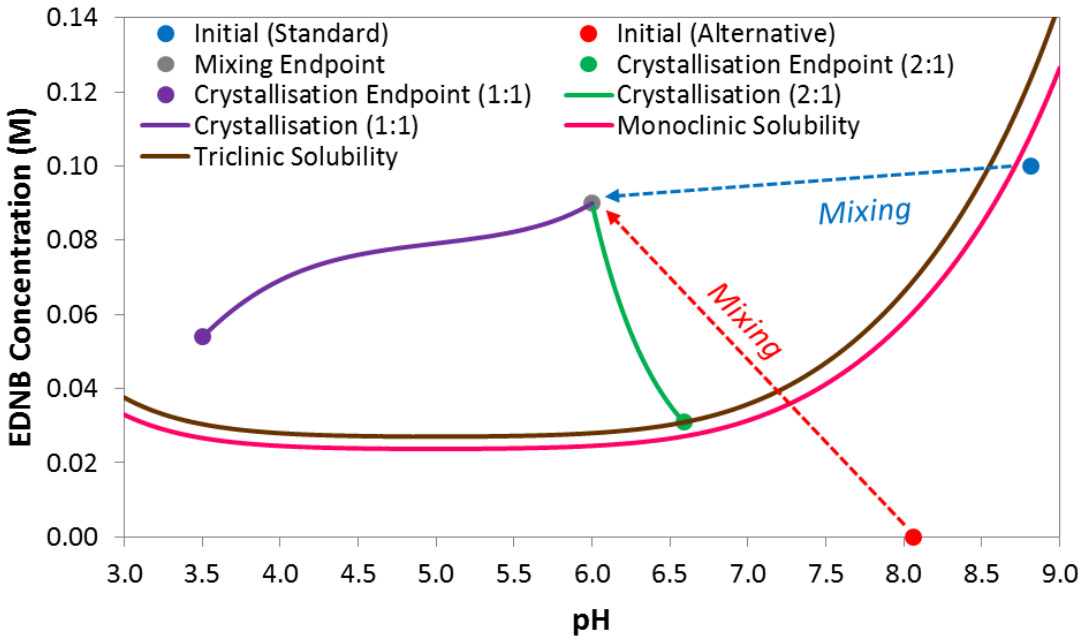

Figure 29. Modelled continuous EDNB crystallisation processes which utilised either the standard or alternative mixing approach for crystallising either the 2:1 EDNB salt or the hypothetical 1:1 EDNB salt, all with a mixing endpoint of pH 6.

The modelled continuous EDNB crystallisation process shows how continuous mixing can be used to reach the desired point on the phase diagram instantly if mixing is perfect. This means that in practice reaching any point on the phase diagram is only limited by the mixing efficiency. As with the batch alternative addition, the alternative mixing approach may be advantageous to the standard mixing approach as the concentrations of 3,5-DNBA and ethylenediamine can be increased without the pH values of the initial solutions changing greatly which allows for the yield of the EDNB salt to be increased. Therefore, this alternative mixing approach should be investigated experimentally in the future.

6.6.2. Modelling 2:1 EDNB salt crystallisation

The solution speciation model was applied to continuous experiments where an aqueous solution containing 3,5-DNBA, ethylenediamine and NaOH was continuously mixed with

sulfuric acid. Similarly to the batch experiments the model assumes perfect mixing so the mixing efficiency of the process isn't accounted for. Using the same initial solution composition as the batch experiments, the model can be used to generate surface plots showing the pH and supersaturation outcomes for a range of sulfuric acid concentrations and flow ratios. Example surface plots are shown in Figure 30.

(A)

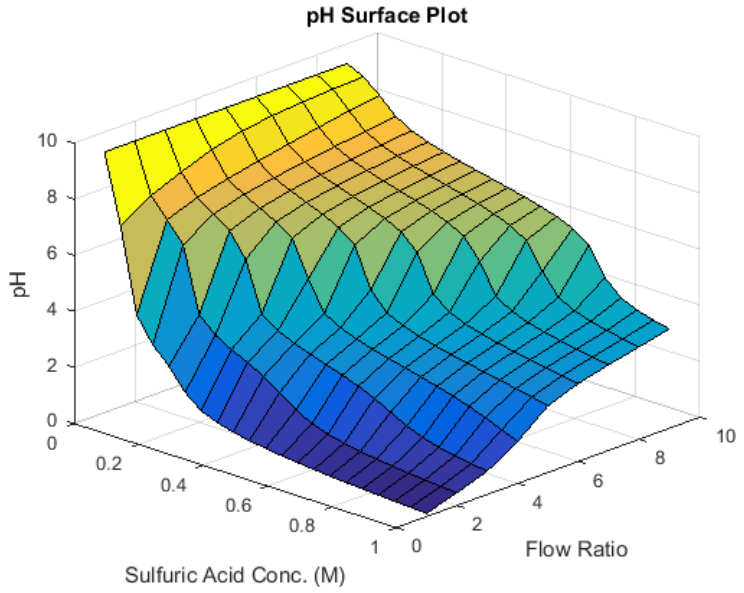

(B)

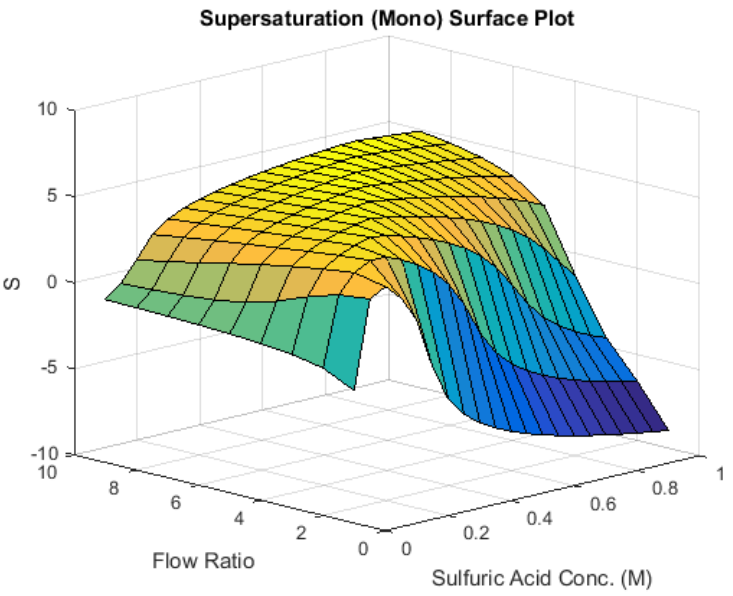

(C)

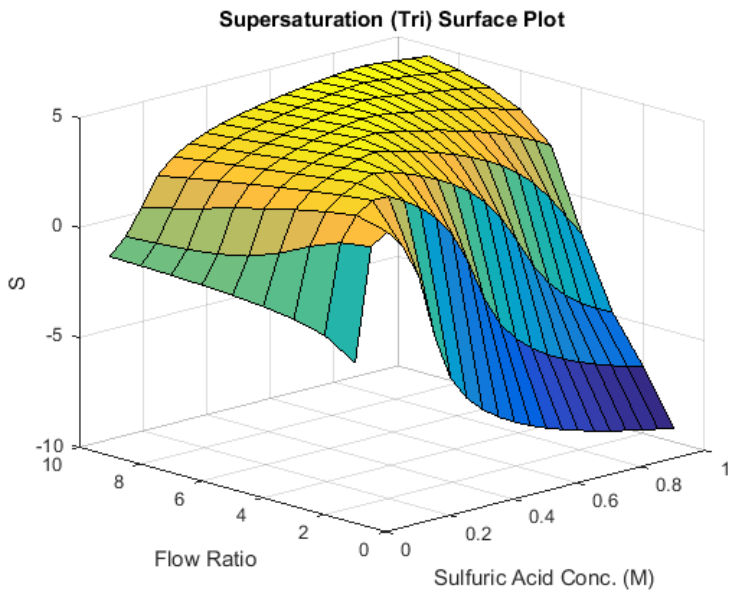

Figure 30. Surface plots of (A) pH, (B) EDNB monoclinic supersaturation and (C) EDNB triclinic supersaturation outcomes for a range of sulfuric acid concentrations and flow ratios.

These surface plots illustrate the range of pH and supersaturation outcomes that can be obtained in continuous EDNB crystallisation processes which makes them very useful for designing experiments. In this way a trial and error approach isn't required to find the best set of operating conditions. Once the required operating conditions are obtained from the solution speciation model, the full continuous crystallisation processes can be modelled in the same fashion as the batch EDNB crystallisation processes.

6.7. Conclusions

In this chapter a mathematical model of organic salt crystallisation via the addition of a strong acid to a basic solution, in either semi-batch or continuous mode, was developed. This solution speciation model utilises dissociation constants in addition to material and charge balances to predict pH and solution composition throughout a salt crystallisation process. The model in this work goes beyond what has been done in previous literature as

the models described previously either required pH as an input to determine speciation etc. or they only predicted the change in pH when an acid/base was added to an initial solution of known pH. The solution speciation model developed here was applied to the crystallisation of the different solid forms which may crystallise in the EDNB salt crystallisation process.

The model was utilised to generate the full EDNB salt crystallisation design space for semi-batch and continuous processes. This can be achieved as the outcome (in terms of pH, speciation and supersaturation with respect to each component) of mixing a basic solution (comprised of 3,5-DNBA, ethylenediamine and NaOH) with a strong acid (sulfuric acid) can be quickly calculated for a range of solution concentrations and flow ratios. Knowledge of the design space allows for the optimum outcome to be targeted by using the corresponding set of conditions provided by the model. The ability to explore the entire design space in-silico allows for easier transfer from batch to continuous salt crystallisation or to utilise continuous crystallisation directly.

Once a crystallisation outcome was targeted the model was used to compare solution addition/mixing approaches. The constraints under which this comparison was performed included not exceeding the solubility of any component in the initial solutions and not allowing either initial solution to be at too low or too high a pH. Within these constraints two main addition approaches were compared. The “standard” addition approach involved adding sulfuric acid to a solution containing 3,5-DNBA, ethylenediamine and NaOH whereas the “alternative” addition approach involved adding a solution containing ethylenediamine and sulfuric acid to a solution containing 3,5-DNBA and NaOH. The advantages and disadvantages of these two addition/mixing approaches were discussed in relation to pH ranges, maximum yields and supersaturation profiles.

Full crystallisation processes were modelled for three different solid forms which could crystallise in an EDNB crystallisation process; the target 2:1 EDNB salt, the hypothetical 1:1 EDNB salt and the 3,5-DNBA starting material. For all three solid forms, for any molar feed ratio used, the pH changed as a result of crystallisation with the direction depending on the pH at which crystallisation commenced and the molar feed ratio. Knowledge of the change in pH and solution composition from the onset of crystallisation through to saturation allows for the yield of the process to be calculated. The results show that the pH change associated with crystallisation can significantly shift the crystallisation endpoint away from what might be expected leading to a significantly higher or lower yield than expected.

7. Semi-batch EDNB crystallisation

7.1. Introduction

Semi-batch experiments are undertaken for three main purposes. Firstly, to provide experimental data that can validate the solution speciation model (discussed in section 6.4). Secondly, to replicate a section of the semi-batch experiments performed in literature to ensure consistency. Thirdly, to scale up the semi-batch experiments and utilise a wide range of conditions in order to better understand EDNB crystallisation behaviour.

The semi-batch experiments from literature were performed in a 50 ml jacketed STR, at either 25 or 50 °C, utilised different sets of 3,5-DNBA, ethylenediamine and NaOH concentrations and always used 12M HCl as the titrant. The comparable experiments performed in this work utilise one particular set of component concentrations from literature, 12M HCl as the titrant, 25 °C as the working temperature but use the 100 ml EasyMax system rather than a standard 50 ml jacketed STR. The reason for this change in equipment is that the larger volume in addition to the inherent design of the EasyMax system allows for several PAT probes to be inserted into the vessel. It's thought that inserting the pH, FBRM and PVM probes allow for the EDNB crystallisation process to be well monitored. Analysis of the data from these probes and the data from the offline techniques can then demonstrate if the EDNB crystallisation process is consistent with literature.

After consistency of the EDNB crystallisation process is ensured the semi-batch experiments can be scaled up from the 100 ml EasyMax system to the 400 ml jacketed STR. A wide range of conditions are utilised in the 400 ml STR in order to investigate the EDNB crystallisation behaviour. Experiments are performed at either 25 or 50 °C with a particular set of 3,5-

DNBA, ethylendiamine and NaOH concentrations being used at each temperature. The titrant is changed from 12M HCl to varying concentrations of sulfuric acid. Furthermore, the sulfuric acid addition rate used is either 2 ml/min or 20 ml/min. pH, UV-vis, FBRM, PVM and Raman probes are inserted into the vessel in order to monitor the crystallisation process in each of the experiments. Analysis of the data from these probes, the data from the offline techniques and the application of the solution speciation model will then provide greater understanding of EDNB crystallisation behaviour and allow for continuous EDNB crystallisation processes to be better designed.

7.2. Materials & methods

7.2.1 Materials

3,5-Dinitrobenzoic acid (99%) was supplied by either Sigma Aldrich or Acros Organics. Ethylenediamine (≥99.5%) was supplied by either Sigma Aldrich or Acros Organics. Sodium hydroxide (98%) was supplied by either Sigma Aldrich or Fisher Scientific. Hydrochloric acid (37%) and sulfuric acid (95-98%) were supplied by Sigma Aldrich. Deionised water was produced using an in-house Millipore Milli-Q system.

7.2.2. Methods: 100 ml EasyMax experiments

3,5-DNBA and ethylenediamine were dissolved in an aqueous sodium hydroxide solution (NaOH) to create a basic solution where both 3,5-DNBA and the EDNB salt were undersaturated. The 3,5-DNBA, ethylenediamine and NaOH concentrations were 0.123M, 0.0615M and 0.06M respectively. 100ml of the basic solution was added to the 100ml glass vessel inside the EasyMax 102 system from Mettler-Toledo. Hydrochloric acid (HCl) solution, with a concentration of 12 M, was added in steps using a 1 ml syringe. The EasyMax vessel had an internal diameter of 52 mm, a wall thickness of 2.5 mm and a height of 90 mm. A 45° pitched-blade overhead stirrer (with four blades) was used with an outer

diameter of 38 mm. An agitation rate of 400 rpm was used in all 100 ml EasyMax experiments. The vessel had a jacket that was used to maintain the temperature at 25 °C for all experiments. A diagram and image of the 100 ml EasyMax system and PAT tools is shown in Figure 31.

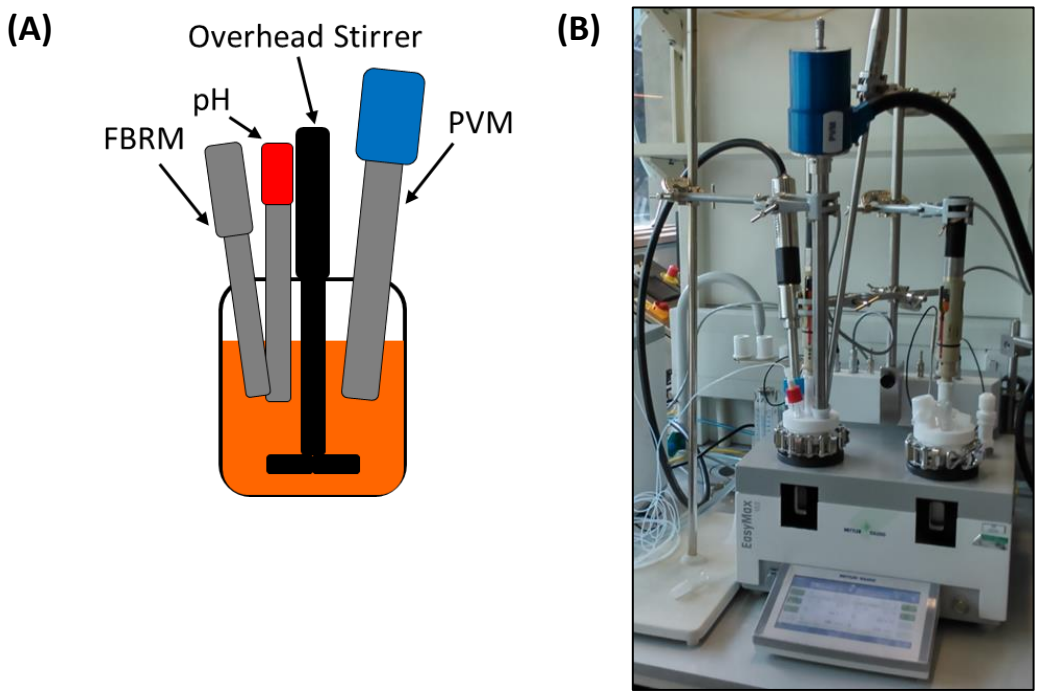

Figure 31. (A) Diagram and (B) image of 100 ml EasyMax system used for semi-batch EDNB crystallisation.

The pH probe was inserted into the 100 ml EasyMax system to measure the pH value after each addition of HCl solution. The FBRM probe was inserted to measure the CLD throughout the crystallisation process. The PVM probe was inserted to obtain images of the crystals. HCl was added until crystallisation was induced. Slurry samples were collected from the EasyMax vessel at the end of the experiment and filtered immediately in a Buchner funnel with a 0.45 µm filter paper and dried overnight at 40 °C.

7.2.3. Methods: 400 ml STR experiments

3,5-DNBA and ethylenediamine were dissolved in an aqueous sodium hydroxide solution (NaOH) to create a basic solution where both 3,5-DNBA and the EDNB salt were undersaturated. An aqueous sulfuric acid solution was prepared by diluting concentrated sulfuric acid to the desired concentration. 360ml of the basic solution was added to the 400 ml STR. The 400 ml STR had a jacket to control temperature. A three-blade retreat curve-overhead stirrer was used to agitate the system. An agitation rate of 300 rpm was used in all 400 ml STR experiments. 40ml sulfuric acid solution was fed at a constant flow rate using a peristaltic pump (Cole-Parmer Masterflex L/S). The internal diameter of the pump tubing was 1.6 mm. An image of the semi-batch setup with 400 ml STR and PAT tools used is shown in Figure 32.

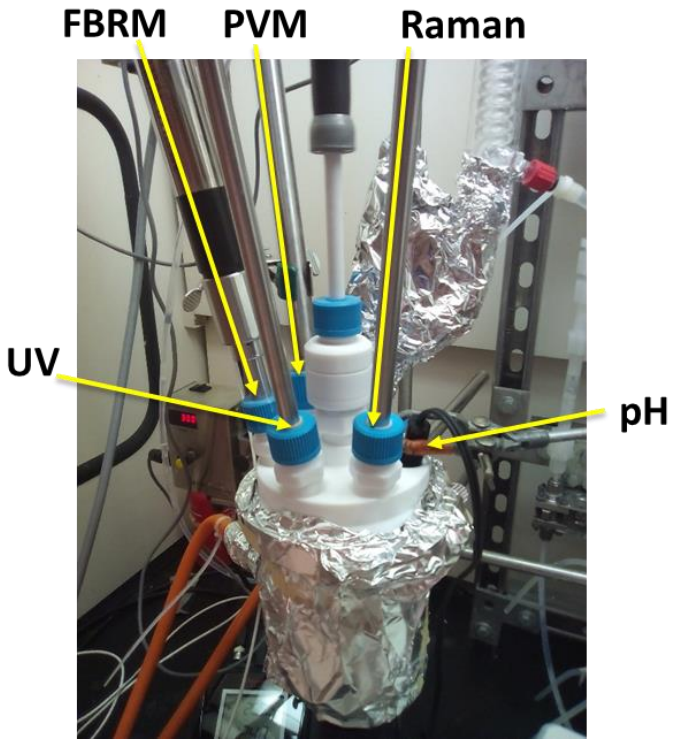

Figure 32. Semi-batch setup with 400 ml STR and PAT tools.

The pH probe was inserted into the 400ml STR to measure the pH profile during the sulfuric acid addition and EDNB salt crystallisation process. The UV probe was inserted to measure the 3,5-DNBA concentration over the course of the experiment. 3,5-DNBA is the only UV active compound in the solution and knowing its concentration indirectly gives the EDNB salt concentration. The FBRM probe was inserted to measure the CLD throughout the crystallisation process. The PVM probe was inserted to obtain images of the crystals. The Raman probe was inserted in an attempt to collect in-situ solid form data but this wasn't possible. The temperature in the STR was measured in each experiment and it was never more than 1 °C away from 25 °C in the 25 °C experiments and it was never more than 1 °C away from 50 °C in the 50 °C experiments. The volumetric flowrate of the sulfuric acid solution was either 2 ml/min or 20 ml/min in each experiment. The sulfuric acid solution concentration ranged from 0.135 M to 0.425 M in the 25 °C experiments and from 0.341 M to 0.633 M in the 50 °C experiments. Slurry samples were collected from the STR at the end of the experiment and filtered immediately in a Buchner funnel with a 0.45 µm filter paper and dried overnight at 40 °C.

7.3. 100 ml EasyMax experiments

7.3.1. pH data

The experimental pH data obtained from the 100ml EasyMax experiments, alongside the modelled pH profile, are shown in Figure 33. The pH of the initial basic solution was kept below pH 9 in order to avoid possible decomposition of 3,5-DNBA as reported in literature.

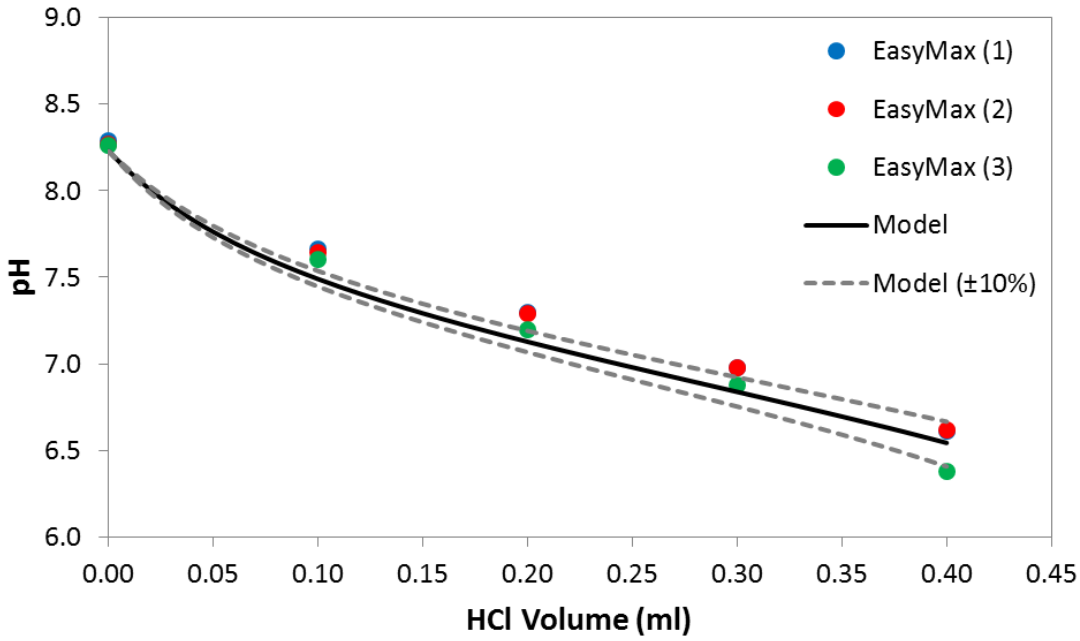

Figure 33. 100ml EasyMax experimental pH data compared with the modelled pH profile.

The modelled pH profile matches the experimental pH data closely and the experimental pH data is consistent between the three experiments which utilised the same experimental conditions. This demonstrates that the semi-batch EDNB crystallisation process is well understood and reproducible. The small deviation of the experimental pH data from the modelled profile is most likely due to the fact that a very small volume of a very strong HCl solution is being added. As the concentration of HCl is very high, even the smallest error in addition volume could lead to significant deviation.

7.3.2. FBRM results

The chord length distributions (CLDs), obtained from the FBRM, at the end of each experiment are shown in Figure 34. They are square-weighted distributions presented in the macro view.

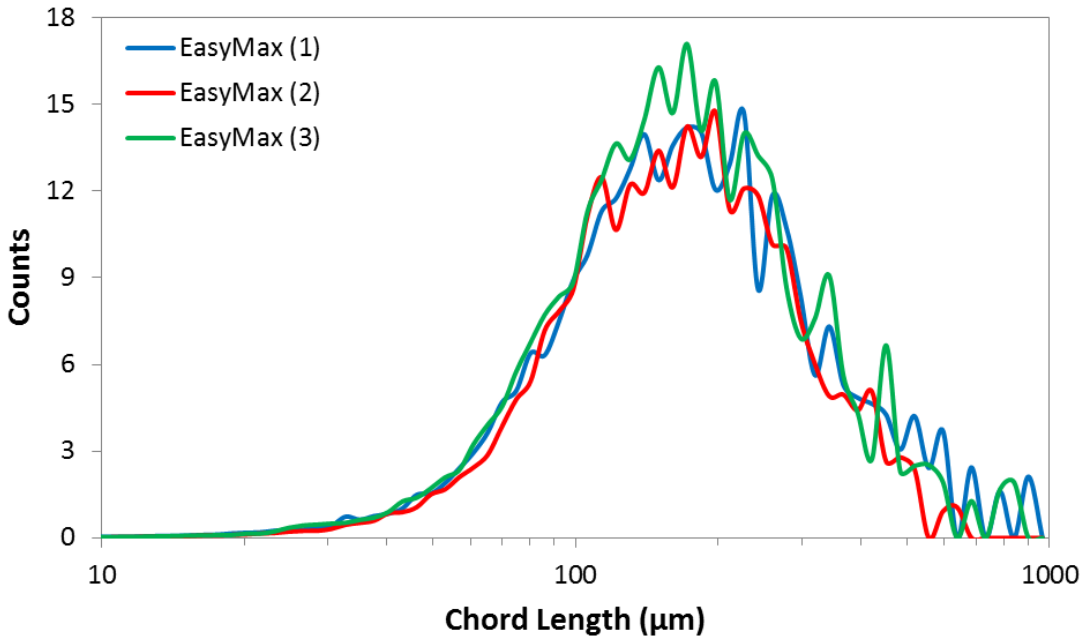

Figure 34. CLDs at the end of each 100ml EasyMax experiment.

The CLDs indicate that the particle size distribution at the end of each experiment was consistent. Based on the CLDs alone the mean particle size could be estimated to be in the region of 150 to 200 µm. However, this depends on many factors including the number of crystals and the range of crystal aspect ratios. Therefore, PVM images and offline particle sizing techniques must be utilised to obtain a better idea of the real particle size distribution.

7.3.3. PVM results

Images of the crystals, obtained from the PVM, are shown in Figure 35. The crystals had a rectangular plate shape which suggests that the triclinic form of the EDNB salt was formed which was expected.

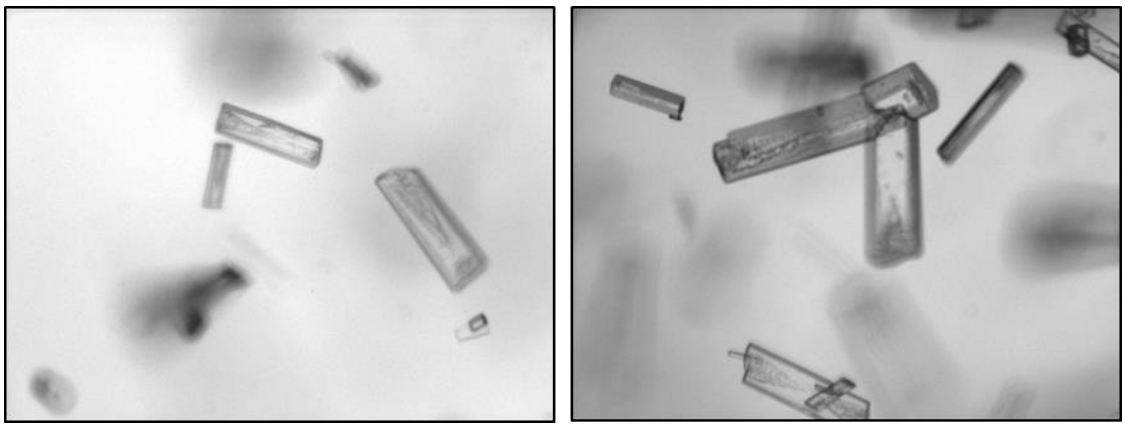

Figure 35. PVM images of the crystals obtained in the 100ml EasyMax experiments.

The fact that the crystals have a rectangular plate shape does mean that FBRM results alone can't be used to determine the particle size distribution as was suspected. The PVM images show that the crystal population has a range of lengths and widths with the crystals being mostly separate. However, there is some agglomeration with the most common form being small crystals attaching on to very large crystals. With regards to determining crystal size from the PVM images, there can be a simple estimation simply from looking at the images with the human eye or image analysis can be performed to try and achieve robustness and reliability. The issues with using image analysis to obtain an accurate particle size distribution are that there needs to be a statistically relevant number of in-focus crystals in the series of images so that a full distribution can be built and there needs to be as little as possible agglomeration or foreign particles so that the results aren't skewed in any way.

7.3.4. IR spectra of dry powder

The IR spectra of the dry powder samples, in addition to the reference spectra for EDNB monoclinic, EDNB triclinic and 3,5-DNBA, are shown in Figure 36. The characteristic infrared bands for ethylenediammonium 3,5-dinitrobenzoate are given in Table 1.

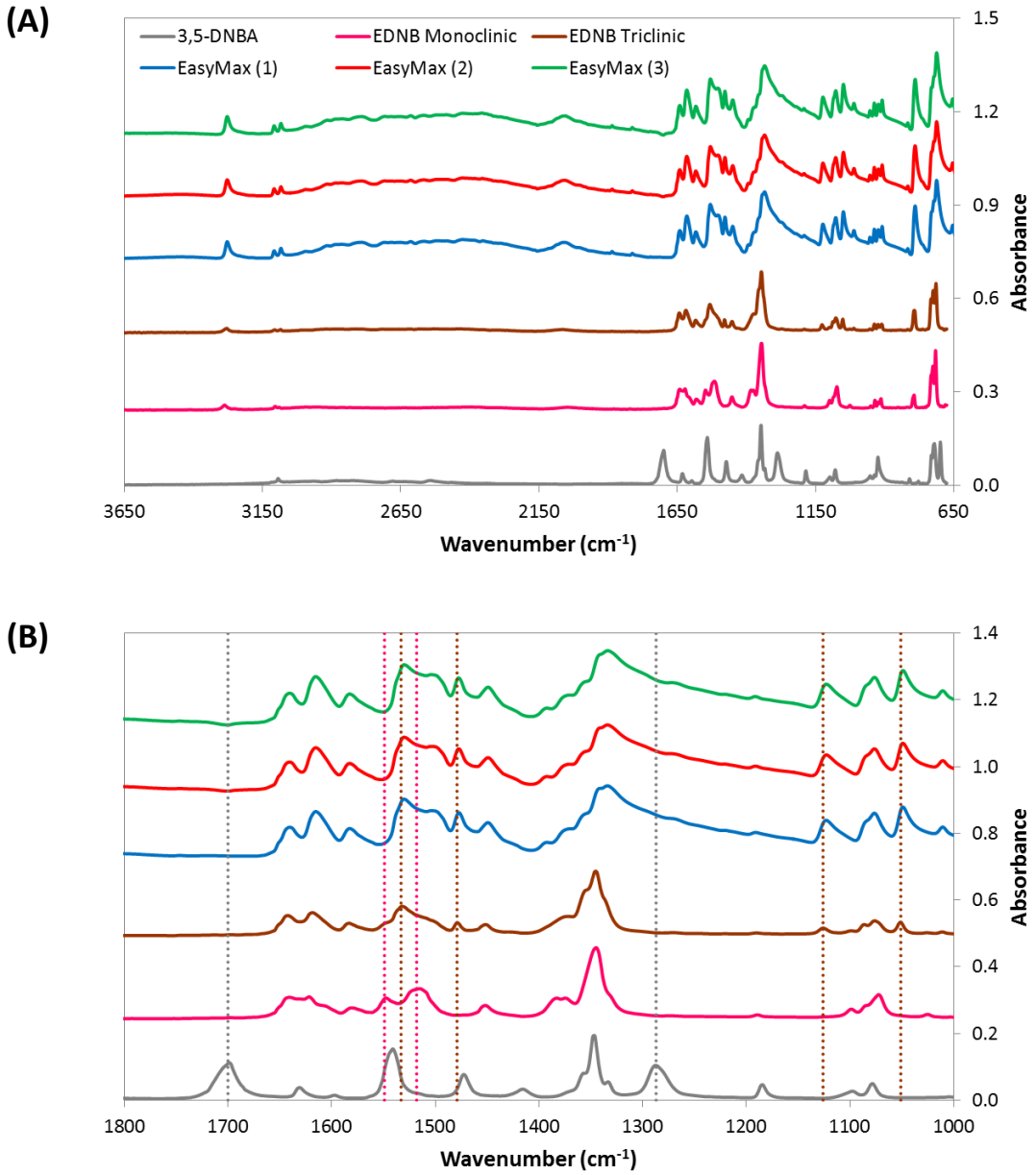

Figure 36. IR spectra of dry powder samples from 100ml EasyMax experiments presented as the (A) full range and the (B) range of interest. Dotted lines highlight the characteristic peaks of EDNB monoclinic (pink), EDNB triclinic (brown) and 3,5-DNBA (grey).

The IR spectra of the dry powder samples demonstrate that EDNB triclinic was crystallised in every 100 ml EasyMax experiment. This was to be expected as the PVM images showed the crystals to have the rectangular plate shape which is associated with EDNB triclinic. In addition, in all of the experiments performed in literature and in this study, only EDNB

triclinic was ever directly crystallised at 25 °C. Therefore, this polymorphic outcome was expected based on experience.

7.4. 400 ml STR experiments

7.4.1. Experimental conditions

The experimental conditions used in the 400 ml STR experiments are shown in Table 4.

Table 4. Experimental conditions used in the 400 ml STR experiments.

Experiment Label	Temp (°C)	Sulfuric Acid Conc. (M)	Addition Rate (ml/min)
STR_1	25	0.135	20
STR_2	25	0.233	2
STR_3	25	0.233	20
STR_4	25	0.329	2
STR_5	25	0.329	20
STR_6	25	0.425	20
STR_7	50	0.341	20
STR_8	50	0.488	2
STR_9	50	0.488	20
STR_10	50	0.633	20

A range of sulfuric acid concentrations and addition rates were utilised for experiments at both 25 °C and 50 °C. The selection of the range of sulfuric acid concentrations was informed by the solution speciation model. A wide range of pH and supersaturation values were targeted.

7.4.2. pH data

The pH profiles, from the initial pH to the end of any pH change (not the end of the experiment), for both the 25 °C and 50 °C experiments, are shown in Figure 37.

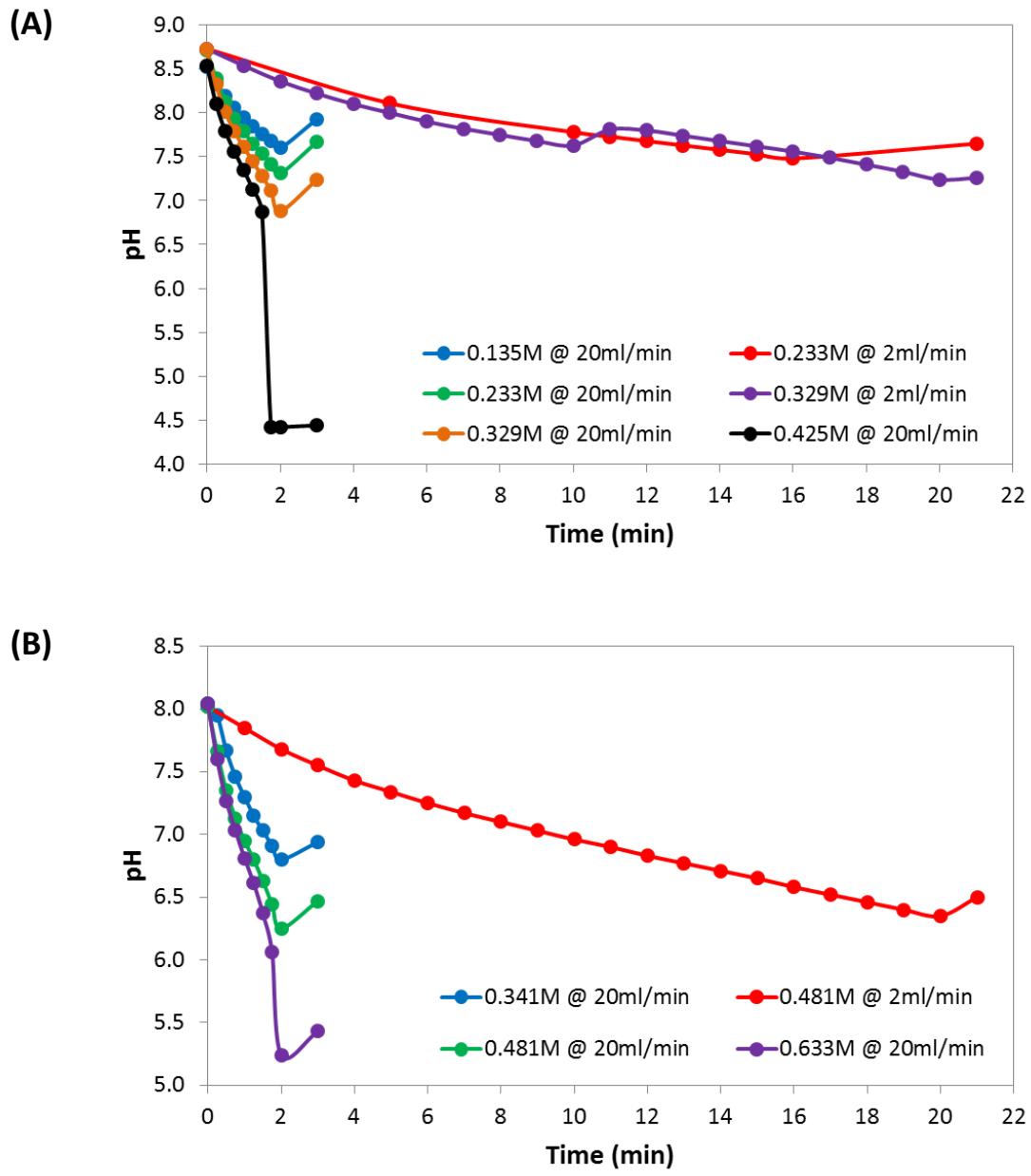

Figure 37. pH profiles for (A) 25 °C and (B) 50 °C experiments.

The different sulfuric acid concentrations allowed for different pH endpoints to be achieved. This allowed for a wide range of pH profiles, and consequently supersaturation profiles, to be explored.

7.4.3. UV probe calibration

The only UV active compound in the solution was 3,5-DNBA. This was confirmed by analysing all of the compounds used in these experiments separately. The UV probe was used with the purpose of monitoring the concentration of 3,5-DNBA throughout all of the 400 ml STR experiments. Knowledge of 3,5-DNBA concentration allowed for the EDNB salt concentration to be determined as it was known that the 3,5-DNBA:EDNB molar ratio was always 2:1 assuming only the 2:1 EDNB salt was crystallised which was the case.

The UV probe regularly measured the UV absorption spectrum for 3,5-DNBA over the time period of the experiment. A spectrum was collected every 15 seconds. A typical unprocessed 3,5-DNBA UV spectrum is shown in Figure 38.

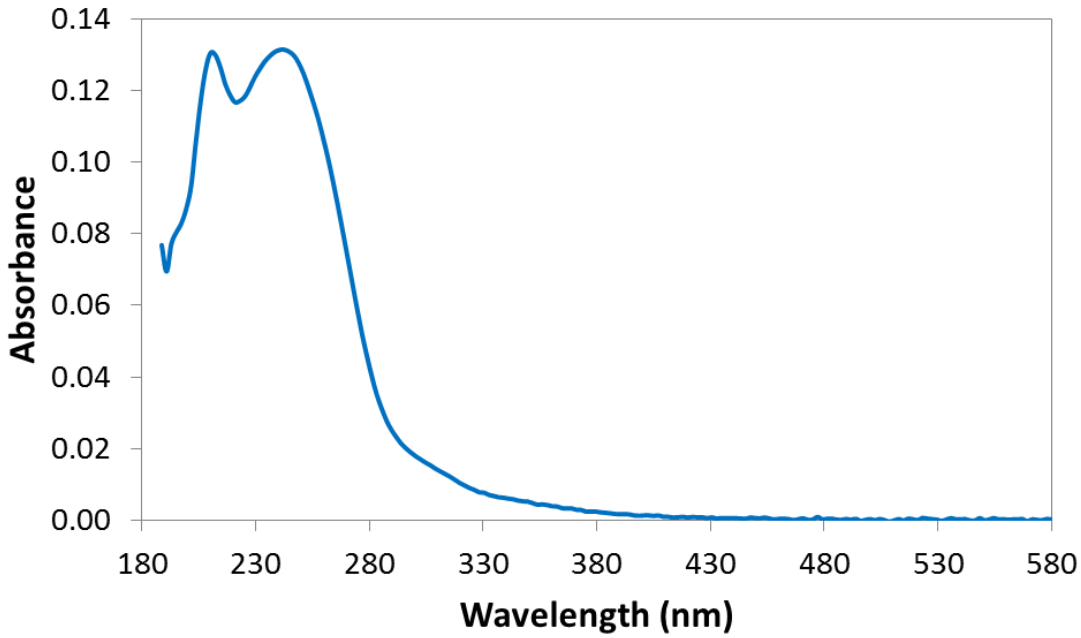

Figure 38. Typical unprocessed 3,5-DNBA UV spectrum.

It can be seen that for the unprocessed spectrum there are absorbance maxima at 210 nm and 240nm. In an effort to correct baseline drift the 1st derivative was taken of all the UV spectra before calibration models were developed. A typical 1st derivative of a 3,5-DNBA UV spectrum is shown in Figure 39.

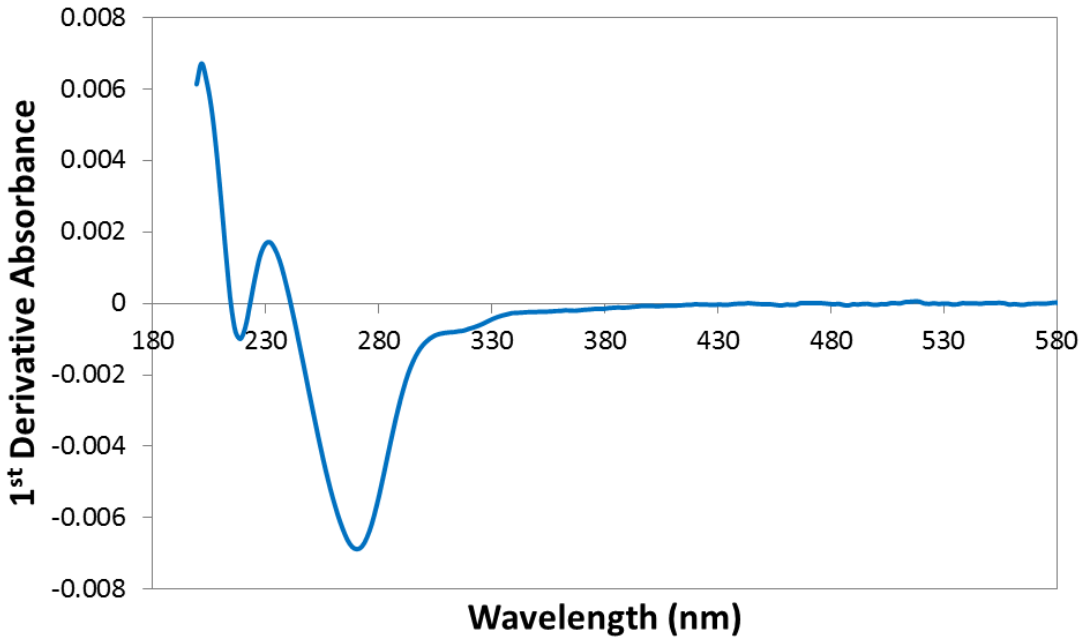

Figure 39. Typical 1st derivative of 3,5-DNBA UV spectrum.

It can be seen that for the 1st derivative of a spectrum there is one clear absorbance maximum at 270 nm. Therefore, the absorbance at this peak is used as the value for developing the calibration model and consequently for tracking the 3,5-DNBA concentration in the crystallisation experiments. In order to develop the calibration model UV spectra had to be collected for a range of 3,5-DNBA concentrations and temperatures.

In order to save time all of the required data was collected in one carefully designed experiment. It took the form of a dilution experiment with temperature cycling. In detail this meant that the 400 ml STR was filled with a solution containing 0.3 M 3,5-DNBA, 0.15 M ethylenediamine and 0.174 M NaOH. This composition was chosen to reflect the conditions of a real crystallisation experiment and to have a high concentration of 3,5-DNBA. This solution was maintained at 25 °C until a constant UV absorbance was reached. After this, the solution temperature was cycled to achieve the constant UV absorbance values at 35 °C and 50 °C. After this the solution was diluted and the temperature was

cycled again to obtain the constant UV absorbance values at these temperatures at this concentration. This process of dilution and temperature cycling was repeated until UV spectra were collected at every 3,5-DNBA concentration and temperature of interest. The overview of this UV calibration data experiment is shown in Figure 40.

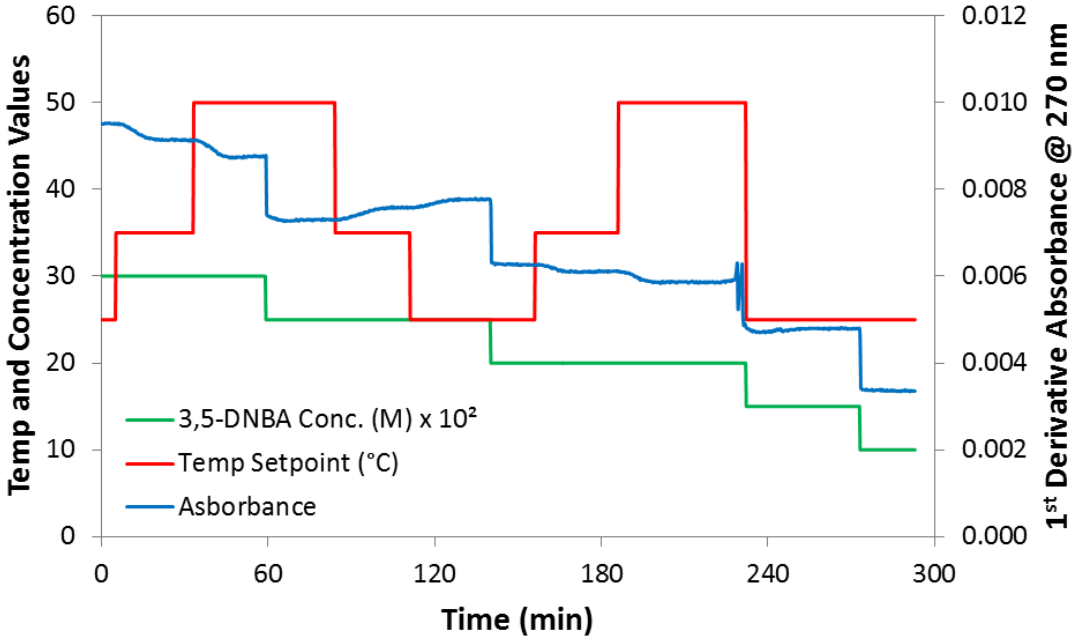

Figure 40. Overview of UV calibration data experiment.

The UV spectra were collected for 0.3, 0.25 and 0.2 M 3,5-DNBA at 25, 35 and 50 °C. In addition the UV spectra were collected for 0.15 and 0.1 M 3,5-DNBA at 25 °C.

After the absorbance profiles were obtained from the experiments it was realised that pH also has an effect on UV absorbance. No specific calibration experiment was performed to observe the effect of pH on absorbance but there was a solution to this. A calibration model was developed for each experiment which included a combination of 2 data sets; data from the calibration data experiment and the three data points from the experiment itself. These three data points from the experiment were the initial point, the point just before nucleation and the endpoint. By comparing the difference in absorbance values between

the two data sets for a common temperature and concentration point, the effect of pH on absorbance could be accounted for. The UV calibration models follow the general equation 51. This general equation is used to calculate 3,5-DNBA concentration (C) from 1st derivative UV absorbance at 270 nm (A) and pH (P) with five constants (Q_{1-5}). 3,5-DNBA concentration has units of mol/L. Temperature was constant within an experiment so wasn't accounted for in the experiment-specific calibration model.

$$C(A,P) = Q_1 + Q_2\,A + Q_3\,P + Q_4\,A\,P + Q_5\,P^2 \tag{51}$$

The values for the constants and statistics for each calibration model relating to the 25 °C experiments can be seen in Table 5. The values for the constants and statistics for each calibration model relating to the 50 °C experiments can be seen in Table 6. All these values were obtained from the curve fitting app in MATLAB.

Table 5. Values for the constants and statistics for each UV calibration model relating to the 25 °C experiments.

Exp Label	$\boldsymbol{Q_1}$	$\boldsymbol{Q_2}$	$\boldsymbol{Q_3}$	$\boldsymbol{Q_4}$	$\boldsymbol{Q_5}$	$\boldsymbol{SSE}$	$\boldsymbol{R^2}$	$\boldsymbol{RMSE}$
STR_1	0.390	-29.86	-0.062	6.717	0.0021	6.70E-06	0.9976	0.00067
STR_2	0.793	-21.09	-0.172	5.735	0.0093	3.90E-05	0.9929	0.00161
STR_3	0.057	-0.281	-0.005	3.528	-0.0002	9.48E-06	0.9984	0.00079
STR_4	0.336	4.662	-0.083	3.018	0.0049	1.75E-05	0.9987	0.00101
STR_5	0.243	14.13	-0.067	1.944	0.0044	3.36E-05	0.9973	0.00150
STR_6	0.022	23.43	-0.021	0.933	0.0020	4.90E-05	0.9963	0.00194

Table 6. Values for the constants and statistics for each UV calibration model relating to the 50 °C experiments.

Exp Label	Q_1	Q_2	Q_3	Q_4	Q_5	SSE	R^2	$RMSE$
STR_7	0.163	-1.226	-0.021	4.105	0.0003	3.54E-05	0.9911	0.00154
STR_8	-0.034	34.22	-0.019	-0.033	0.0028	2.32E-05	0.998	0.00087
STR_9	-0.135	46.64	-0.004	-1.577	0.0025	1.52E-05	0.9983	0.00195
STR_10	0.0017	24.45	-0.009	1.058	0.0012	2.46E-05	0.9976	0.00286

SSE is the sum of squares due to error which is a measure of the total deviation of the response values from the fit to the response values. A value closer to 0 indicates that the model has a smaller random error component and that the fit will be more useful for prediction. R^2 is a statistic which measures how successful the fit is in explaining the variation of the data. R^2 can have any value from 0 to 1 with a value closer to 1 indicating that a greater proportion of variance is accounted for by the model. RMSE is the root mean square error and is an estimate of the standard deviation of the random component in the data. As with SSE, an RMSE value closer to 0 indicates a fit that is more useful for prediction. The statistics show that the UV calibration models are valid and can be used to transform the absorbance profiles to 3,5-DNBA concentration profiles.

7.4.4. Concentration profiles from UV results

The 3,5-DNBA concentration profiles for the 25 °C experiments are shown in Figure 41. The 3,5-DNBA concentration was monitored with the UV probe because it was the only UV active compound in the solution.

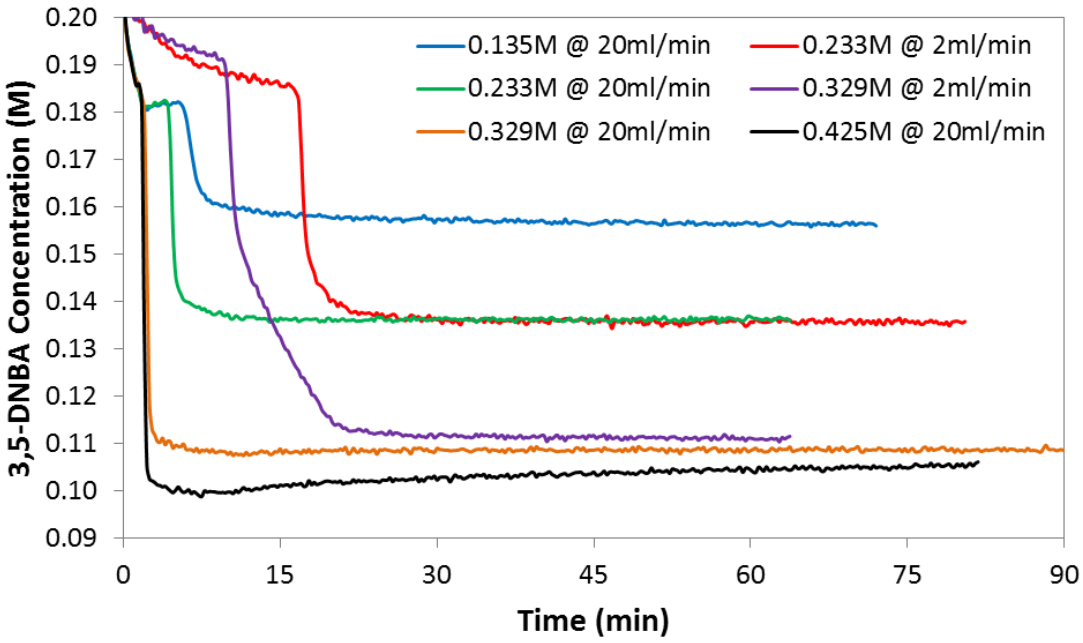

Figure 41. 3,5-DNBA concentration profiles for the 25 °C experiments.

The shape of the concentration profiles firstly depended on the sulfuric acid addition rate. For both addition rates the 3,5-DNBA concentration decreased due to dilution. If no crystallisation occurred the solution would become completely diluted after 20 minutes or 2 minutes for a 2 ml/min or 20 ml/min addition rate respectively. In the 2 ml/min experiments crystallisation took place either during addition or after addition so the full 10% decrease in concentration due to dilution wasn't always completed before crystallisation began. On the other hand, for the 20 ml/min experiments the sulfuric acid was always completely added before crystallisation began.

For the 25 °C experiments, when the 20 ml/min addition rate was used, all of the sulfuric acid was added and a certain time had to pass before nucleation occurred. This time ranged from less than 1 second with 0.425 M sulfuric acid to 4 minutes with 0.135M sulfuric acid. This nucleation event was marked by an extremely steep decrease in 3,5-DNBA concentration as was expected. These times are confirmed by the appearance of crystals in

the PVM images. After the nucleation event the 3,5-DNBA concentration decreased only slightly or not at all for the remainder of the experiment. This suggests that the process is nucleation dominated.

For the 25 °C experiments, when the 2 ml/min addition rate was used, crystallisation always began during the addition of sulfuric acid. This happened 16 minutes into the addition of 0.233 M sulfuric acid and 9 minutes into the addition of 0.329 M sulfuric acid. As with the 20 ml/min experiments there was an initial steep decrease of 3,5-DNBA concentration when nucleation first occurred. After this first nucleation event however the decrease in concentration was based on the competition between how quickly sulfuric acid was added and how quickly EDNB crystallised with further dilution also having a minor effect. When nucleation occurred 16 minutes into the 0.233 M sulfuric acid addition the 3,5-DNBA concentration decreased to a value which was close to the final concentration so there wasn't much extra crystallisation for the duration of the addition. This meant that the process was very similar to the 20 ml/min experiment when 0.233 M sulfuric acid was used. On the other hand, when nucleation occurred 9 minutes into the 0.329 M sulfuric acid addition, this resulted in a noticeably different process than the 20 ml/min experiment when 0.329 M sulfuric acid was used. After the initial steep concentration decrease due to the first nucleation event, the concentration started decreasing in a much more gradual and linear fashion. The fact that both the sulfuric acid addition and the concentration decrease were linear suggests that the sulfuric acid addition rate was limiting the EDNB crystallisation. In other words, EDNB was crystallising as quickly as supersaturation was being generated so the concentration should have been on the solubility line throughout that phase. With regards to all the 0.233 M and 0.329 M sulfuric acid experiments, it can be seen that regardless of sulfuric addition rate the final 3,5-DNBA concentration value was the same for the two 0.233M experiments and the two 0.329 M experiments. Therefore,

the final composition only depended on the concentrations of the solutions rather than the addition rates used which was expected.

The 3,5-DNBA concentration profiles for the 50 °C experiments are shown in Figure 42.

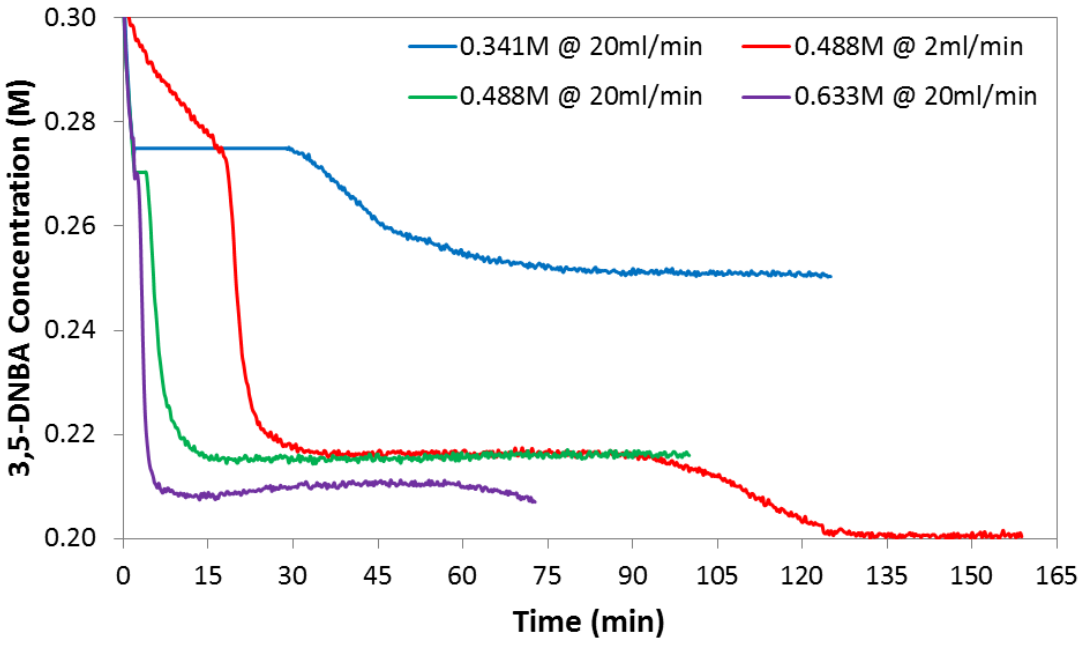

Figure 42. 3,5-DNBA concentration profiles for the 50 °C experiments.

For the 50 °C experiments, analysing the concentration profiles was a little more challenging as the concentration may have reached one value and then after a period of time decreased further to a lower value due to the transformation of the metastable EDNB triclinic to the stable EDNB monoclinic. In the 25 °C experiments, only EDNB triclinic was ever nucleated directly and it never transformed in the experiment time so there was never any further decrease once a stable 3,5-DNBA concentration was reached. The polymorph present can be determined from PVM due to the difference in shape but all the results are confirmed by offline IR analysis.

For the 50 °C experiments, when the lowest sulfuric acid concentration of 0.341 M was used, using an addition rate of 20 ml/min, all of the sulfuric acid was added before crystallisation began. In fact, the nucleation event occurred 28 minutes after sulfuric acid addition ended which was much longer than for any other experiment. This is due to the titration endpoint being at a high pH value of 6.80 which corresponds to a low supersaturation value. Furthermore, it was the only experiment where the stable monoclinic form of the EDNB salt nucleated directly which is due to the high pH and low supersaturation. As the stable monoclinic form was crystallised directly there was no transformation later in the experiment. It is also interesting to note that the decrease in 3,5-DNBA concentration is much more gradual compared to every other experiment. This suggests that after the initial nucleation event there is either additional slow nucleation or growth of the particles taking place.

Only one comparison of sulfuric acid addition rate was made in the 50 °C experiments. For the 0.488 M sulfuric acid experiments an addition rate of either 2 ml/min or 20 ml/min was used. For the 20 ml/min addition rate all of the sulfuric acid was added before crystallisation began. 2 minutes after the addition ended there was a steep decrease in 3,5-DNBA concentration corresponding to the nucleation event. There is very little concentration decrease after the nucleation event which suggests the process was nucleation dominated in the same fashion as the 25 °C experiments. This initial nucleation resulted in EDNB triclinic being formed and there was no transformation later in the experiment. On the other hand, using the 2 ml/min flow rate resulted in a different polymorphic outcome. With regards to the 2 ml/min experiment the first thing to be observed is that nucleation occurs 16 minutes into the 20 minute addition. The nucleation event resulted in a steep decrease in 3,5-DNBA concentration with very little further decrease happening afterwards as with the 20 ml/min experiment. Again, this suggests that

this is a nucleation dominated process. Similarly with the 20 ml/min experiment EDNB triclinic is nucleated directly. However, around 50 minutes after the concentration completely stabilises after EDNB triclinic has fully crystallised, a transformation begins where EDNB triclinic is changing to EDNB monoclinic. This can be seen in the concentration profile as a gradual decrease in concentration from the first stable concentration value to the final stable concentration value. This decrease is due to EDNB monoclinic having a lower solubility than EDNB triclinic. The gradual decrease took around 35 minutes so the polymorphic transformation is a relatively slow process compared to the initial nucleation and growth processes.

For the 50 °C experiments the highest sulfuric acid concentration used was 0.633 M and was added at 20 ml/min. Nucleation occurred around 45 seconds after all of the sulfuric acid was added which resulted in a very steep decrease in 3,5-DNBA concentration as expected. Once again, EDNB triclinic was nucleated directly and it seemed to be a nucleation dominated process. The interesting thing in this experiments is that the 3,5-DNBA concentration had actually started decreasing at the end of the measured concentration profile. From the offline IR analysis it is known there was EDNB monoclinic at the end of the crystallisation process. This demonstrates that the experiment was stopped during the polymorphic transformation from EDNB triclinic to EDNB monoclinic. Clearly, it wasn't known that this transformation was taking place on the day of experiment or else the experiment wouldn't have been stopped prematurely. It's interesting to note that transformation started earlier in this experiment compared with the 0.488 M experiment. This was unexpected as literature on this compound shows that transformation starts later at lower pH values. However, the same literature also describes how supersaturation can have an additional effect on transformation rate and the supersaturation profile is different

for these two experiments. Therefore, not enough information is available to know the exact causes for the differing transformation rates in the two experiments.

7.4.5. Crystallisation processes shown on EDNB phase diagram

As the full pH and concentration profiles were known in these experiments the full experimental trajectories could be plotted on the EDNB phase diagram. The crystallisation processes for both the 25 °C and 50 °C experiments, in addition to the corresponding modelled crystallisation processes, are shown in Figure 43. The modelled processed ended at the same EDNB concentration as the experimental processes.

(A)

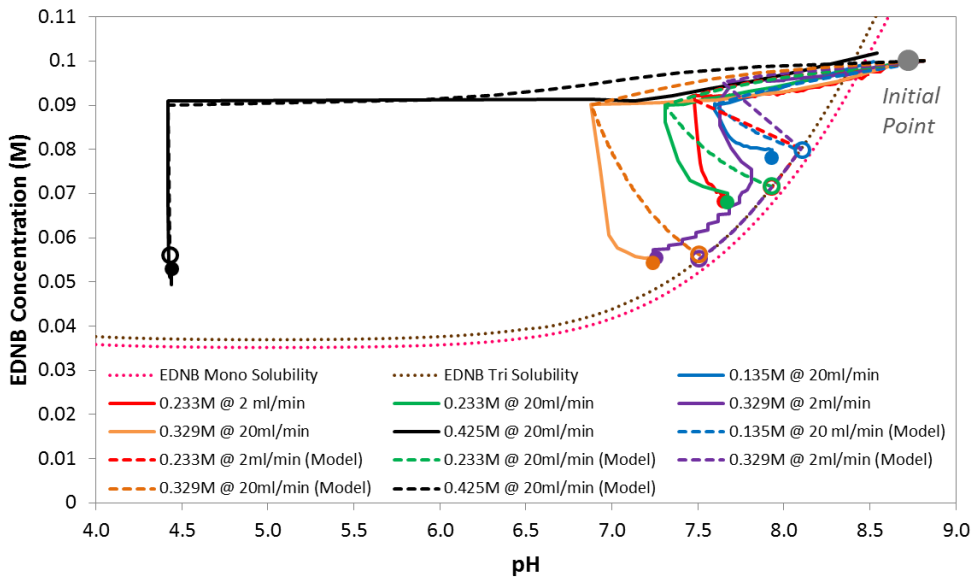

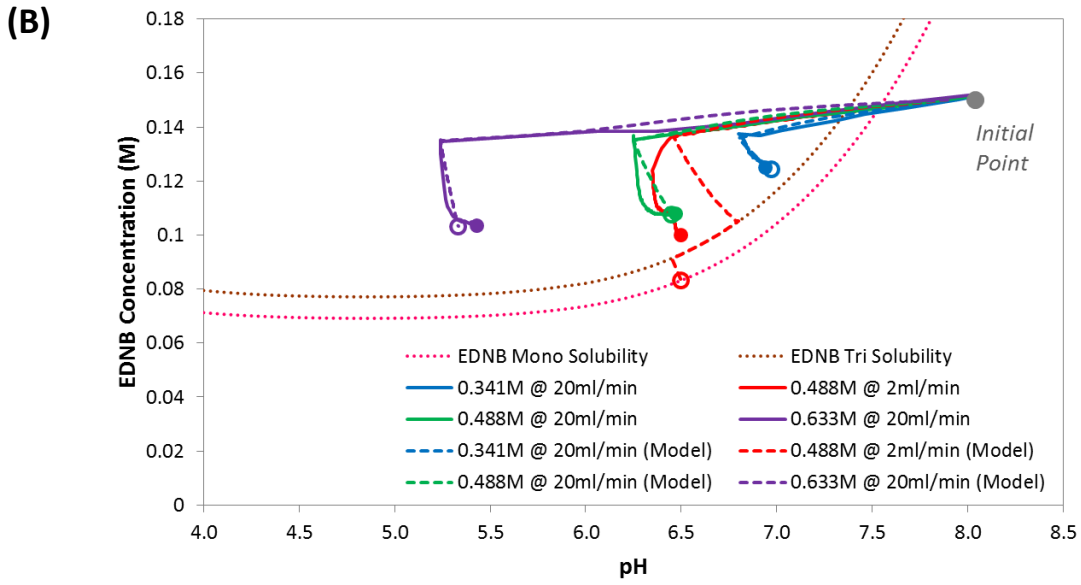

Figure 43. Experimental and modelled crystallisation processes for the (A) 25 °C and (B) 50 °C experiments. Grey closed circle is initial point for experiments. Other closed circles are experimental crystallisation endpoints. Open circles are modelled crystallisation endpoints.

The crystallisation processes essentially consisted of two parts. The first part is the single phase titration when sulfuric acid is being added to the basic solution before crystallisation commences. The second part is the crystallisation pathway which covers the period from the initial nucleation to the end of the experiment. In the experiments where crystallisation occurs after sulfuric acid addition is complete there is a clear trend of the pH decreasing during the sulfuric acid addition (alongside the small decrease in EDNB concentration due to dilution) before the pH starts increasing as a result of crystallisation (alongside the large decrease in EDNB concentration). The reason for this increase in pH during crystallisation is explained with the solution speciation model and discussed in section 6.5.

Looking at the 25 °C experiment which utilises 0.329 M sulfuric acid at a flow rate of 2 ml/min something interesting can be noted. With regards to the crystallisation phase there is a steep decrease in concentration due to nucleation followed by the profile staying on a

very specific trajectory as sulfuric acid continues to be added. As mentioned before when discussing the concentration profiles in isolation this seems to suggest that the concentration is sitting on some kind of “solubility line” with the EDNB crystallising as quickly as the sulfuric acid is being added. This invisible “solubility line” agrees well with the other experimental endpoints. At 25 °C there is some deviation between the experimental endpoints and the activity corrected solubility lines but they are close except from the endpoint at the lowest pH. As this endpoint corresponds to the experiment with the highest sulfuric acid concentration this deviation could be due to sulfate ion complexation as was discussed in section 5.4.

When comparing the experimental and modelled crystallisation processes an important point should be noted. That is, the model wasn’t applied to situations where titration and crystallisation were occurring simultaneously. Practically this meant that when crystallisation began in an experiment the model simply dealt with the whole crystallisation process first before considering the remaining titration. For this reason, in experiments where crystallisation began during titration, the experimental process shows a concentration and pH change which is the combined effect of titration and crystallisation whereas the modelled process shows a large initial decrease in concentration (and increase in pH) due to crystallisation before the concentration then follows the solubility line for whichever polymorph was crystallised due to the remainder of the titration. This modelling approach can make the modelled processes look significantly different from the experimental processes where crystallisation begins during titration. However, taking all of the experimental and modelled crystallisation processes into consideration as a whole, it can be seen that there is generally good agreement.

7.4.6. FBRM results

The chord length distributions (CLDs), obtained from the FBRM, at the end of each experiment are shown in Figure 44. They are square-weighted distributions presented in the macro view.

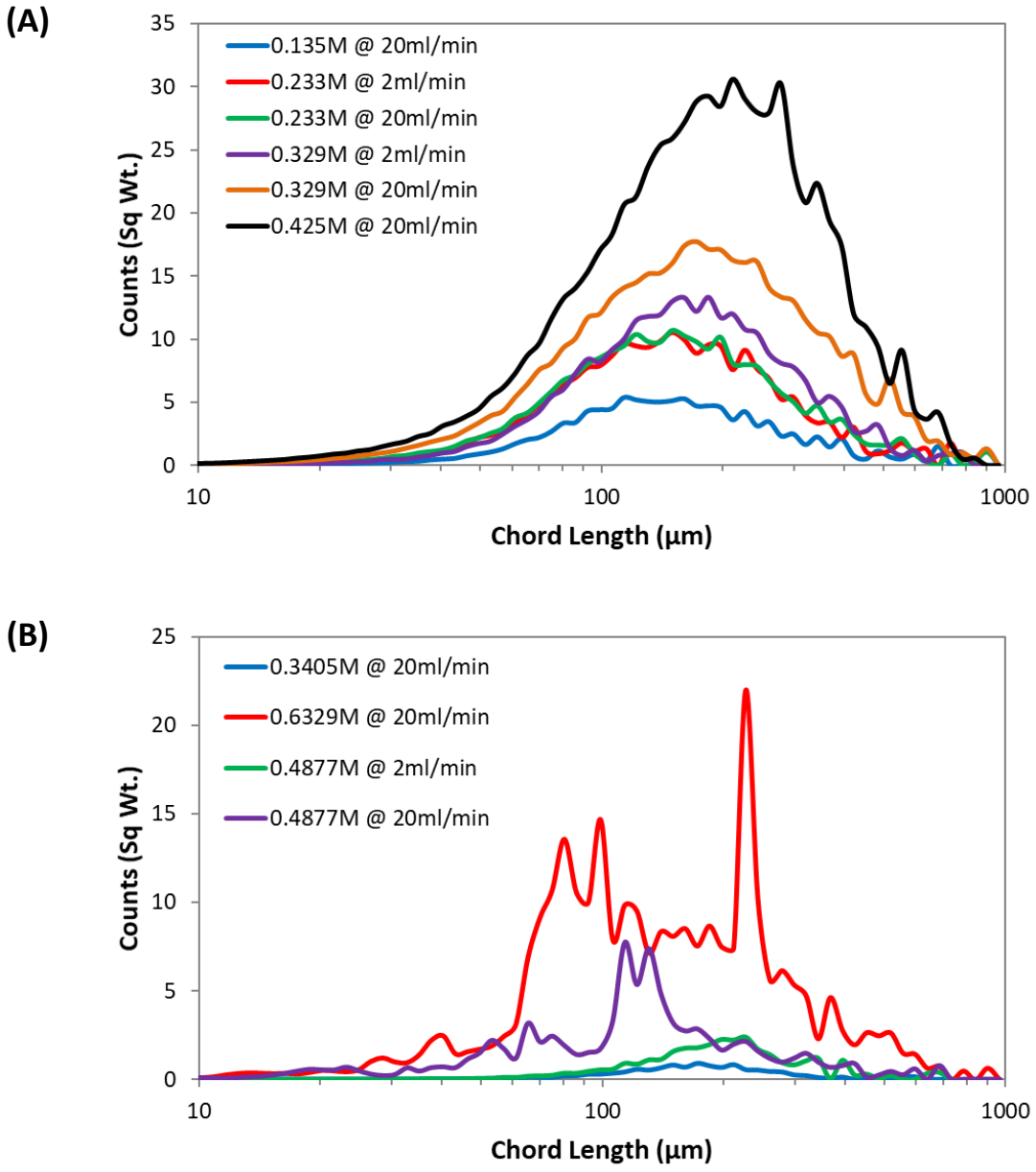

Figure 44. CLDs at the end of each (A) 25 °C experiment and (B) 50 °C experiment in the 400ml STR.

For the 25 °C experiments there is a clear trend that increasing sulfuric acid concentration results in a greater value of total counts and a shift of the CLD to the right (larger particle sizes). This is to be expected as increased sulfuric acid concentration results in a lower final EDNB concentration which means that a greater mass of EDNB is crystallised. In other words, more EDNB in the solid phase resulted in there being more EDNB crystals and EDNB crystals with a larger final size. Comparing the results of the 0.233 M experiments it can be seen that using either a 2 ml/min or 20 ml/min addition rate results in the same CLD at the end of the experiment. This is surprising as it was thought that the different supersaturation profiles would result in different CLDs. It was thought that the higher addition rate would produce smaller crystals as there would be less opportunity for crystal growth in comparison with the lower addition rate where sulfuric acid was still being added after the first nucleation event. This suggests that EDNB triclinic is much more likely to crystallise via nucleation than growth even in the presence of EDNB triclinic crystals. When using the 0.329 M sulfuric acid there actually is a difference between the CLDs of the 2 ml/min and 20 ml/min experiments. However, this is explained by the small difference in final EDNB concentration with the lower EDNB concentration corresponding to more crystals of a larger size as expected. This difference in final concentration is most likely due to minor experimental error.

For all the 50 °C experiments the CLD is too spikey or the number of total counts is too low for the measurements to be considered truly reliable. The only conclusion that could possibly be made is that the CLDs show EDNB monoclinic to have a greater mean size than EDNB triclinic. However, even this isn't for certain as the different shape of the crystals coupled with the different extents of agglomeration between EDNB triclinic and EDNB monoclinic means that this apparent difference in mean size between polymorphs could be due to a combination of other factors. Therefore, for the 50 °C experiments, and indeed for

the 25 °C experiments, the PSDs of the crystal population must be obtained from PVM or an offline sizing technique rather than from FBRM.

7.4.7. PVM results

Images of typical crystals of each polymorph, obtained from the PVM, are shown in Figure 45.

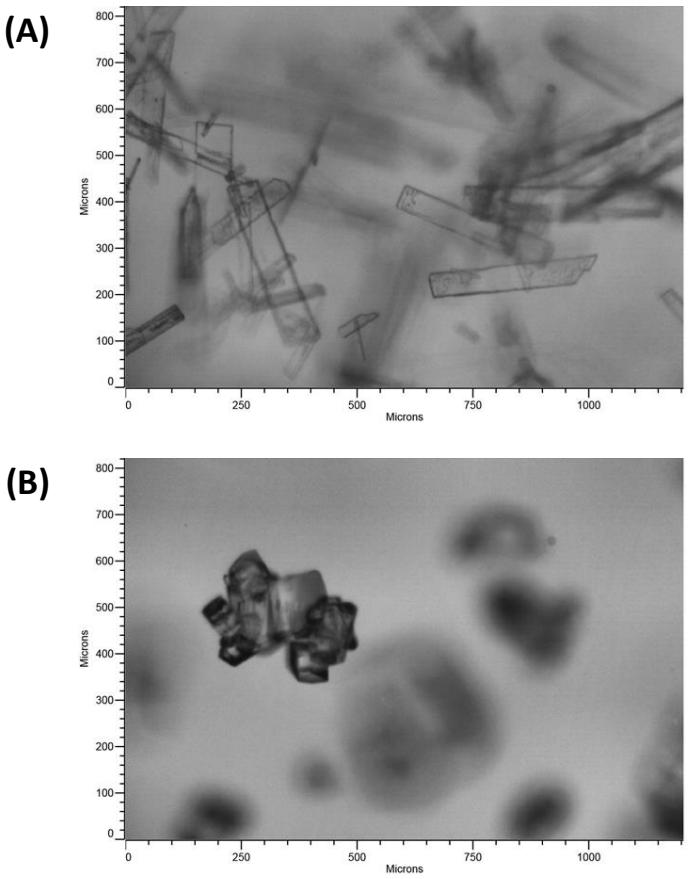

Figure 45. PVM images of typical crystals of (A) EDNB triclinic and (B) EDNB monoclinic.

The crystals in all of the 25 °C experiments had a rectangular plate shape which suggests that the triclinic form of the EDNB salt was formed as expected. In the 50 °C experiments the crystals either had a rectangular plate shape or a block shape which suggests that either EDNB triclinic or EDNB monoclinic was formed depending on the crystallisation conditions. As with the 100 ml EasyMax experiments the EDNB triclinic rectangular plates displayed a

range of lengths and widths and there was some agglomeration. With regards to EDNB monoclinic crystals the blocks had little variation with respect to shape and not a large variation with respect to size. However, the blocks did suffer more from agglomeration than the rectangular plates did. This should be kept in mind when analysing the results of particle sizing techniques, especially FBRM.

7.4.8. IR spectra of dry powder

The IR spectra of the dry powder samples from the 25 °C experiments, in addition to the reference spectra for EDNB monoclinic, EDNB triclinic and 3,5-DNBA, are shown in Figure 46. The characteristic infrared bands for ethylenediammonium 3,5-dinitrobenzoate are given in Table 1.

(A)

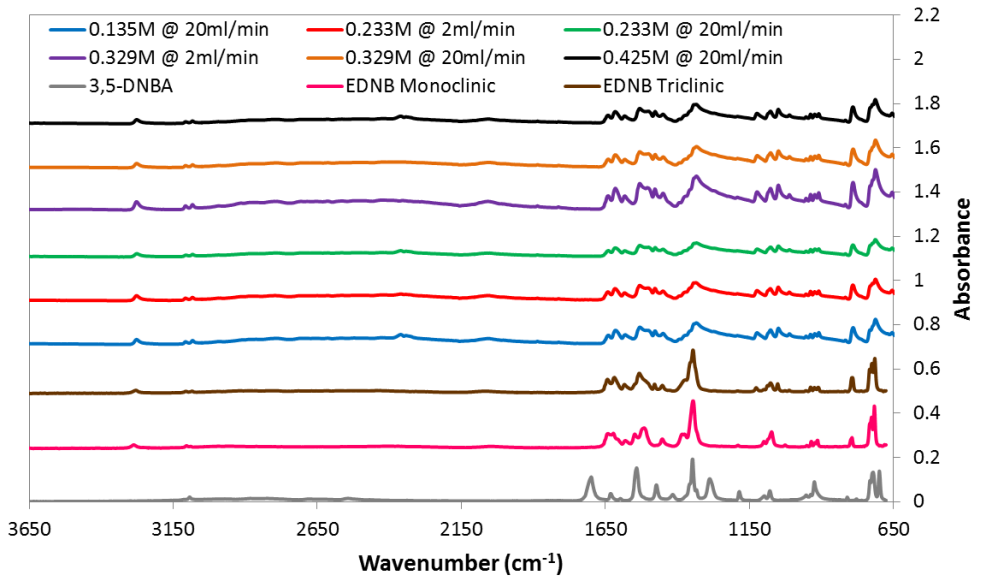

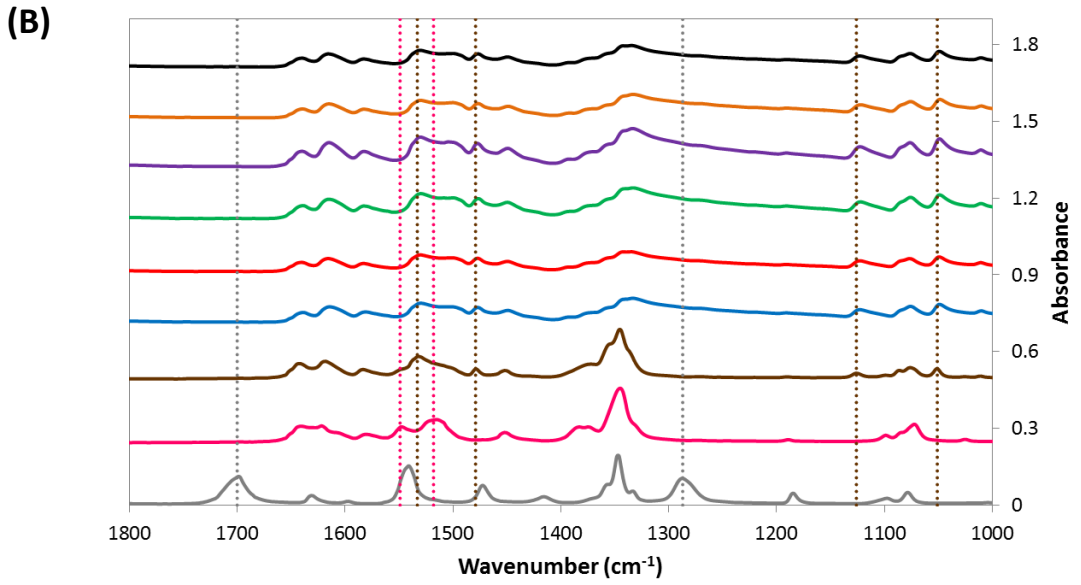

Figure 46. IR spectra of dry powder samples from 25 °C 400ml STR experiments presented as the (A) full range and the (B) range of interest. Dotted lines highlight the characteristic peaks of EDNB monoclinic (pink), EDNB triclinic (brown) and 3,5-DNBA (grey).

The IR spectra demonstrate that EDNB triclinic was crystallised in every 25 °C experiment as expected. The IR spectra of the dry powder samples from the 50 °C experiments, in addition to the reference spectra for EDNB monoclinic, EDNB triclinic and 3,5-DNBA, are shown in Figure 47.

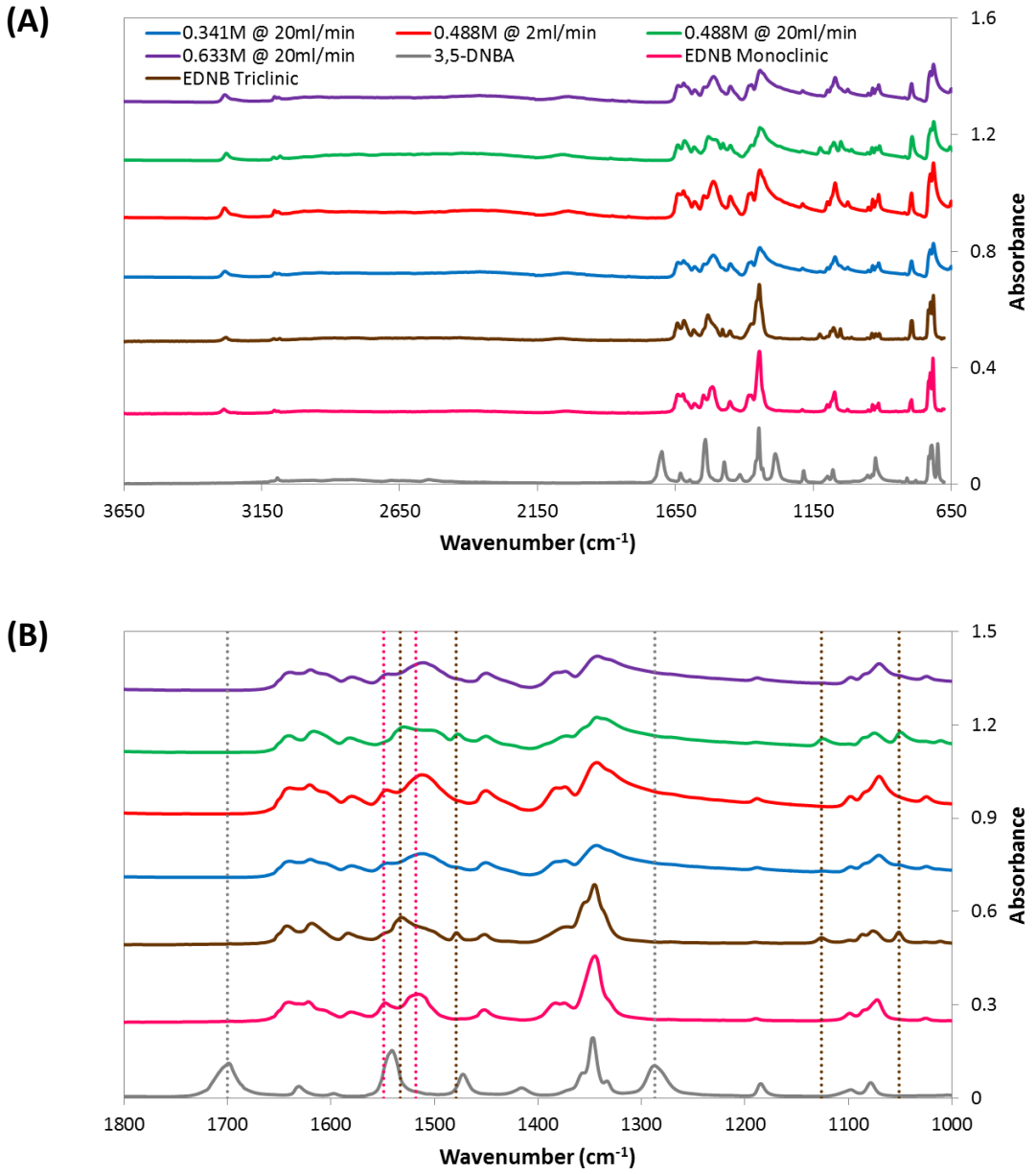

Figure 47. IR spectra of dry powder samples from 50 °C 400ml STR experiments presented as the (A) full range and the (B) range of interest. Dotted lines highlight the characteristic peaks of EDNB monoclinic (pink), EDNB triclinic (brown) and 3,5-DNBA (grey).

EDNB monoclinic was the final product in all 50 °C experiments except the experiment where 0.488 M sulfuric acid was fed at a rate of 20 ml/min. The IR results agree with the crystal shapes seen in the PVM images.

7.4.9. Yield and solid recovery data

The yield (percentage of EDNB recovered with respect to total amount of material dissolved) and solid recovery (percentage of EDNB recovered with respect to the amount of material that could be crystallised based on solubility) were calculated for each experiment. The yield and solid recovery values for each experiment are shown in Table 7. The solid recovery was calculated using the activity corrected solubility values determined in this work rather than the literature solubility.

Table 7. Yield and solid recovery values for the 400 ml STR experiments.

Experiment Label	Solid Form	Yield (%)	Solid Recovery (%)
STR_1	Triclinic	14.6	70.5
STR_2	Triclinic	27.0	80.1
STR_3	Triclinic	27.1	82.6
STR_4	Triclinic	42.8	95.5
STR_5	Triclinic	44.3	93.2
STR_6	Triclinic	46.1	78.5
STR_7	Monoclinic	7.3	28.9
STR_8	Monoclinic	25.8	67.2
STR_9	Triclinic	20.0	62.8
STR_10	Monoclinic	23.3	48.2

It can be seen that the yield is low in all of the experiments. This is because for these experiments EDNB still has a reasonable solubility in the final solution. For the 25 °C experiments the yield increased as the pH of the final solution decreased which was expected as the solubility decreases with decreasing pH. For the 50 °C experiments the

yield also generally increased with decreasing final solution pH but an additional factor is the polymorphic form present in the final slurry. This is because EDNB monoclinic has a lower solubility than EDNB triclinic so a higher yield would be expected at the same final solution pH. For example, STR_8 and STR_9 had very similar final pH values but the yield was noticeably higher from STR_8 because the product was pure EDNB monoclinic as opposed to the pure EDNB triclinic product from STR_9.

The solid recovery was significantly higher than the yield in all experiments. It may have been expected that the solid recoveries would be the same in every experiment but this is not the case. In the 25 °C experiments the yield increased as the final solution pH decreased. In other words, the yield increased when the solubility decreased (and consequently the supersaturation increased). The reason for this may be related to the inherent nature of the EDNB crystallisation process. Perhaps EDNB crystallises almost entirely via nucleation with the growth process being extremely slow at modest supersaturation values. It's possible that EDNB would nucleate from solution at a certain rate until the supersaturation reached a modest value where nucleation would stop and growth would continue the crystallisation but at a very slow rate. Since nucleation rate increases with increasing supersaturation [125], the experiments with higher supersaturation levels would crystallise more material in the initial crystallisation phase. As very little growth would have occurred in the rest of the experiment time, at the point where a sample was taken from the STR, the overall amount of EDNB crystallised would have been greater in those experiments with higher supersaturation levels.

The only exception to this observation is the experiment with the lowest final solution pH. This could be explained by the increased deviation between the salt solubility calculated from the new solubility equation and the measured salt solubility at lower pH values.

However, this could also be explained by the fact that in that low pH experiment the 3,5-DNBA starting material may have crystallised during the initial phase of the crystallisation due to the presence of local areas of supersaturation. In this case bulk supersaturation which could have been utilised to crystallise the EDNB salt would have been consumed by crystallising 3,5-DNBA and this consequently reduced the overall amount of EDNB which crystallised. The 3,5-DNBA is then dissolved by the end of the experiment time due to the establishment of pseudo-equilibrium across the vessel but as the EDNB growth rate is very slow, EDNB hasn't had sufficient time to utilise the re-generated supersaturation for crystallisation. This explanation has some evidence in the form of the 3,5-DNBA concentration profile for that experiment where a concentration minimum is reached just after the initial crystallisation phase before gradually increasing to the final, and steady, concentration value. This could suggest that 3,5-DNBA did in fact crystallise and re-dissolve.

In the 50 °C experiments the solid recovery values are relatively low and don't present a real trend. However, this is most likely due to the solubility data for 50 °C, which was only estimated in this work, not being sufficiently accurate. Future work to experimentally measure EDNB salt solubility at 50 °C should resolve this lack of accuracy in the solubility data and allow for the true solid recoveries to be calculated for the 50 °C experiments.

7.5. Conclusions

In this chapter the semi-batch crystallisation of EDNB was scaled up from 50 ml to 400 ml with PAT tools being used to develop a deeper understanding of the crystallisation process. The solution speciation model was used to design a series of experiments which covered a range of pH and supersaturation values at 25 °C and 50 °C in order to better understand EDNB crystallisation behaviour with respect to the metastable limits, desupersaturation rates and polymorphic outcomes. At each temperature the pH and supersaturation profiles

were controlled by the sulfuric acid concentration and addition rate (2 ml/min or 20 ml/min). The pH, UV-vis, FBRM, PVM and Raman probes were in the 400 ml STR to monitor the crystallisation process in each experiment.

Knowledge of the pH and concentration profiles in the 400 ml STR experiments, known from the pH and UV probes, allowed for the full experimental crystallisation processes to be determined. Combing knowledge of the experimental crystallisation processes with the modelled crystallisation processes allowed for process understanding to be developed in terms of the relative rates of titration and desupersaturation in addition to final yield. Furthermore, the FBRM and PVM data allowed for greater understanding of the particle properties for each crystallisation process. Developing this level of PAT-based crystallisation process understanding is common for the cooling crystallisation of single component systems but not for pH controlled salt crystallisations.

EDNB triclinic was crystallised in every 25 °C 400 ml STR experiment but at 50 °C the EDNB polymorphic outcome could be controlled by controlling the sulfuric acid concentration and addition rate. The results show that at 50 °C, at a high pH and low supersaturation, EDNB monoclinic was nucleated directly. Furthermore, at a lower pH and higher supersaturation, EDNB triclinic nucleated first but then transformed to EDNB monoclinic in a reasonable length of time (<150 min). These results demonstrate that the ability to selectively control which polymorph is crystallised is maintained at the larger scale of 400 ml. In addition, the use of PAT allowed for an in-situ estimation of transformation times based on the crystal shapes seen in PVM images and the concentration decrease seen in UV data.

8. Continuous EDNB Crystallisation

8.1. Introduction

The continuous experiments consist of two parts. The first part is termed the “continuous mixer” experiments which involve continuously mixing the basic solution with the sulfuric acid and collecting samples directly from the mixer outlet. This is done to directly study the effect of the particular mixer used. The second part is termed the “full continuous process” experiments which involves continuously mixing the basic solution with the sulfuric acid and having the mixed product be fed into a cascade of CSTRs. This is done to allow online monitoring of the mixed product and to demonstrate that a full continuous EDNB crystallisation process can be performed.

In the continuous mixer experiments two different mixers are evaluated. The first mixer is a bespoke co-axial mixer which consists of a narrow PEEK capillary in the centre of a larger glass tube. The second mixer is a valve mixer which is part of the modular microreactor system purchased from the Ehrfeld company. For all of the continuous mixer experiments the only analysis which can be performed is the offline analysis of the dry powder. Therefore, the main results from these experiments are yield, PSD and solid form.

In the full continuous process experiments an X-shaped static mixer is used to mix the basic solution and sulfuric acid. The mixed product is then fed into a cascade of 2 x 150 ml CSTRs. In CSTR 1 there are pH and UV-vis probes and in CSTR 2 there are pH and FBRM probes. This means that online analysis can be performed on the slurry during the experiment and offline analysis can be performed on the dry powder obtained from the samples taken at certain time points throughout the experiments. Therefore, the main results from these

experiments are in-situ pH, UV absorbance and CLD measurements in addition to the offline yield, PSD and solid form measurements.

The X-mixer and CSTR 1 used in the full continuous processes are also used for a semi-batch experiment which utilised continuous pre-mixing at 50 °C. The reason for this is to use a continuous mixing approach to directly nucleate EDNB monoclinic. An overall semi-batch approach is necessary as the low supersaturation value required to directly nucleate EDNB monoclinic is not conducive to the short residence times seen in full continuous operation. This process is preferable to traditional semi-batch experiments as the continuous mixing approach is more controlled and scalable than adding a solution from above so a more consistent product is achieved. The main results from these experiments are in-situ pH and CLD measurements in addition to the offline yield, PSD and solid form measurements.

8.2. Materials & methods

8.2.1 Materials

3,5-dinitrobenzoic acid (99%), ethylenediamine (≥99.5%) and sulfuric acid (95-98%) were supplied by Sigma Aldrich. Sodium hydroxide (98%) was supplied by Fisher Scientific. Deionised water was produced using an in-house Millipore Milli-Q system.

8.2.2. Methods: Co-axial mixer

3,5-DNBA and ethylenediamine were dissolved in an aqueous sodium hydroxide (NaOH) solution to create a basic solution where both 3,5-DNBA and the EDNB salt were undersaturated. An aqueous sulfuric acid solution was prepared by diluting concentrated sulfuric acid to the desired concentration. A diagram of the co-axial mixer with dimensions is shown in Figure 48.

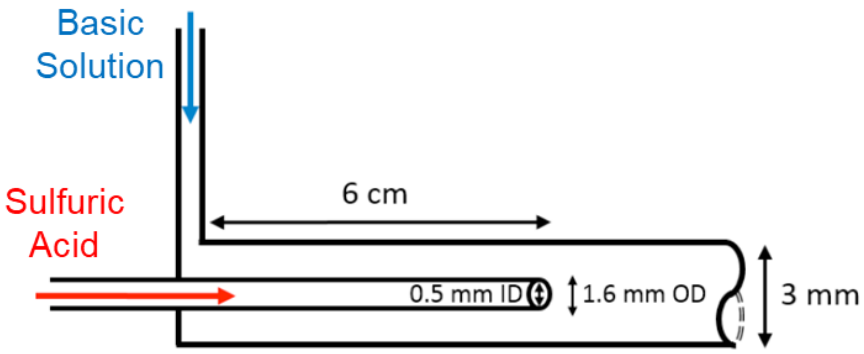

Figure 48. Co-axial mixer diagram with dimensions indicated.

The sulfuric acid was pumped through the inner PEEK capillary while the basic solution was pumped through the outer glass tube. The capillary has internal and outer diameters of 0.51 mm and 1.59 mm respectively. The outer glass tube has an internal diameter of 3 mm. The capillary stream entered into the outer tube stream 6 cm from the T-junction. The feed solutions were pumped using the Bronkhorst Mini CORI-FLOW system coupled with gear pumps allowing for accurate control of mass flow rates. The resulting slurry from the mixer was sampled 0.7 m from the mixing point. Collected slurry samples were filtered after a 15 minute holding period in a Buchner funnel with a 0.45 µm filter paper and dried overnight at 40 °C. There was no agitation during the holding time. A camera was used to visually monitor the glass tube throughout the crystallisation process to determine if there was any fouling. The temperature of both streams was measured in each experiment and it was never more than 2 °C away from 25 °C in the 25 °C experiments and it was always between 50 °C and 55 °C in the 50 °C experiments. The co-axial mixer had no temperature control but the feed solutions were placed on hot plates so that the temperature of the feeds could be controlled. The total mass flow rate through the co-axial mixer ranged from 130 g/min to 280 g/min at a basic solution:sulfuric acid flow ratio of either 6:1 or 12:1.

8.2.3. Methods: Ehrfeld modular microreactor system with valve mixer

3,5-DNBA and ethylenediamine were dissolved in an aqueous sodium hydroxide (NaOH) solution to create a basic solution where both 3,5-DNBA and the EDNB salt were undersaturated. An aqueous sulfuric acid solution was prepared by diluting concentrated sulfuric acid to the desired concentration. An image of the Ehrfeld modular microreactor system with valve mixer 30 module is shown in Figure 49.

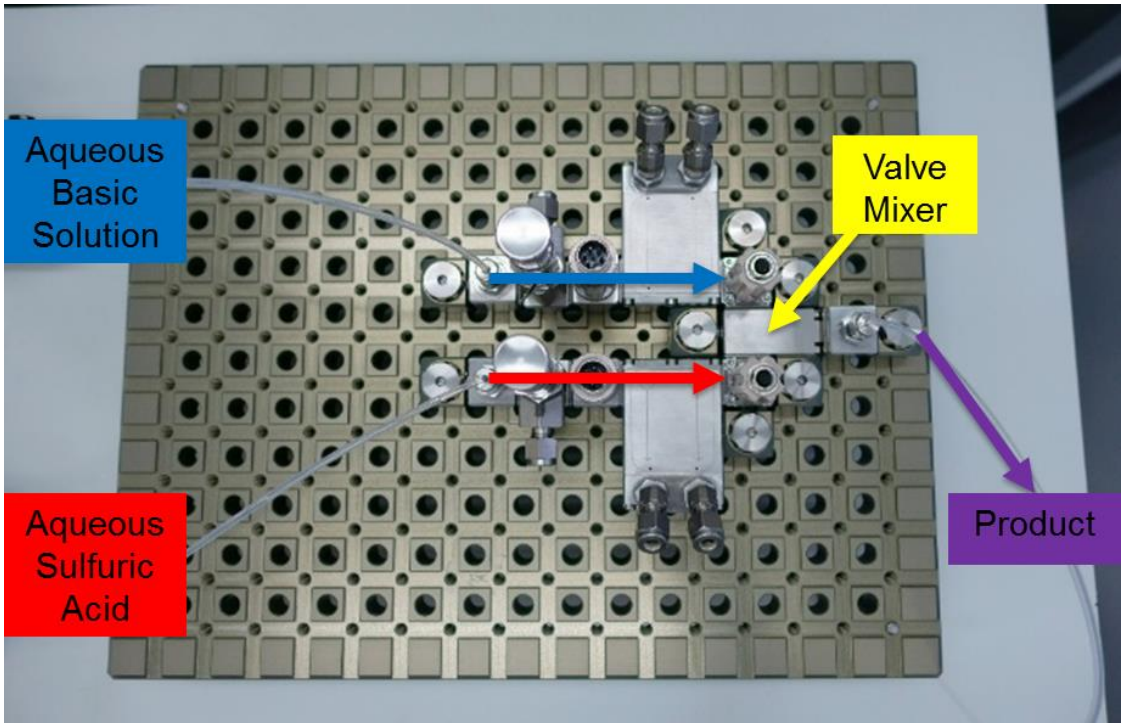

Figure 49. Ehrfeld modular microreactor system with Valve Mixer 30 module.

The feed solutions were pumped using the Bronkhorst Mini CORI-FLOW system coupled with gear pumps allowing for accurate control of mass flow rates. The resulting slurry from the mixer was sampled 0.7 m from the mixing point. Collected slurry samples were filtered after a 15 minute holding period in a Buchner funnel with a 0.45 µm filter paper and dried overnight at 40 °C. There was no agitation during the holding time. The temperature of both streams was measured in each experiment and it was never more than 2 °C away from

25 °C. The Ehrfeld system has temperature control in the base plate to maintain the valve mixer at 25 °C. The total mass flow rate through the valve mixer of the Ehrfeld system was 140 g/min with a basic solution:sulfuric acid flow ratio of 6:1.

8.2.4. Methods: X mixer & CSTR cascade

3,5-DNBA and ethylenediamine were dissolved in an aqueous sodium hydroxide (NaOH) solution to create a basic solution where both 3,5-DNBA and the EDNB salt were undersaturated. An aqueous sulfuric acid solution was prepared by diluting concentrated sulfuric acid to the desired concentration. A diagram of the X mixer & CSTR cascade with dimensions is shown in Figure 50.

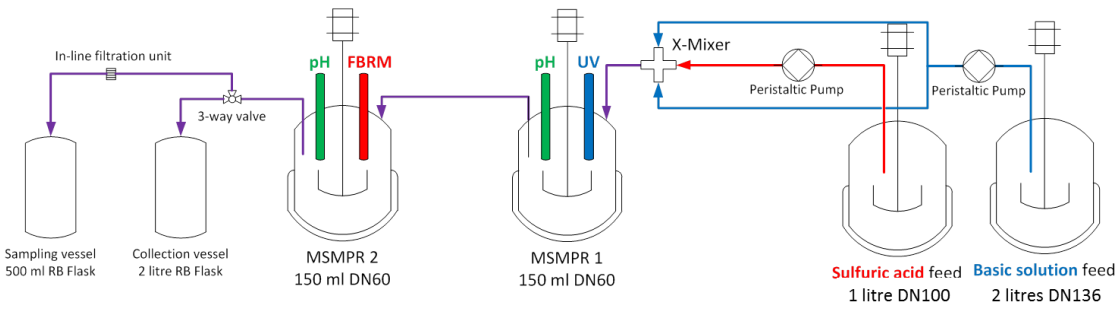

Figure 50. X mixer & CSTR cascade with dimensions indicated.

The basic solution was pumped from a glass feed vessel through a Y mixer to split it in half before it recombined in the X mixer while the sulfuric acid solution was pumped from a feed vessel through the centre of the X mixer. This approach meant that the two streams started mixing in the centre of the X mixer and the resultant mixture flowed to the CSTR cascade. The CSTR cascade consisted of two glass CSTRs which each had a volume of 150 ml and an internal diameter of 60 mm. Both CSTRs utilised three-blade retreat curve overhead stirrers to agitate the vessels. The agitation rate in the CSTRs was always 400 rpm. Both CSTRs had jackets to control the temperature. The basic solution feed vessel had a volume of 2 L and an internal diameter of 136 mm whereas the sulfuric acid solution feed vessel

had a volume of 1 L and an internal diameter of 101 mm. The X and Y mixers were both plastic and had an internal diameter of 3.18 mm throughout. The feed solutions were pumped through the X mixer to CSTR 1 using peristaltic pumps (Cole-Parmer Masterflex L/S) which were calibrated before the experiment. The internal diameter of the pump tubing was 3.1 mm. With the use of vacuum transfer the slurry in CSTR 1 was moved to CSTR 2 and then either to the collection vessel or the sampling vessel. The collection vessel was a 2 L glass round bottom flask and the sampling vessel was a 500 ml glass round bottom flask. A pH and UV probe were inserted into CSTR 1 while a pH and FBRM probe were inserted into CSTR 2. The pH probes allowed for the crystallisation process to be monitored with the UV probe measuring the UV absorbance in CSTR 1 and the FBRM probe measuring CLD in CSTR 2. An in-line filtration unit (with a 0.45 µm filter paper) was in place between CSTR 2 and the sampling vessel in order to separate the liquid and solid phases upon sampling. This allowed for both the liquid and solid phases to be analysed after the experiment. In addition to the in-line samples, slurry samples were collected from each CSTR at the end of the experiment and filtered immediately in a Buchner funnel with a 0.45 µm filter paper. All the filtered solid samples were dried overnight under a vacuum. The temperature was measured in each feed vessel and CSTR. It was never more than 2 °C away from 25 °C in the 25 °C experiments. In the 50 °C experiments the solutions in the feed vessels were always between 55 °C and 60 °C while in CSTR 1 the solution temperature was always between 50 °C and 52 °C. The total mass flow rate through the system ranged from 200 g/min to 400 g/min while the basic solution:sulfuric acid flow ratio was always 3:1.

8.3. Continuous mixer experiments with co-axial mixer or Ehrfeld valve mixer

8.3.1. Experimental conditions

The experimental conditions used in the continuous mixer experiments are shown in Table 8. All of these experiments are performed at 25 °C and the concentrations of the basic solution and sulfuric acid are the same.

Table 8. Experimental conditions used in the continuous mixer experiments.

Experiment Label	Continuous Mixer Type	Basic Solution Flow Rate (ml/min)	Sulfuric Acid Flow Rate (ml/min)	Total Flow Rate (ml/min)
Co-axial_1	Co-axial	120	10	130
Co-axial_2 (1)	Co-axial	120	20	140
Co-axial_2 (2)	Co-axial	120	20	140
Co-axial_3 (1)	Co-axial	240	40	280
Co-axial_3 (2)	Co-axial	240	40	280
Ehrfeld_1	Ehrfeld Valve	120	20	140

A range of flow ratios and total flow rates were utilised for both the co-axial mixer and the Ehrfeld valve mixer.

8.3.2. Crystallisation processes on EDNB phase diagram

In these experiments the pH and concentration data were known for the initial solution and the final slurry sample. In addition, the pH and concentration data for the fully mixed solution (before crystallisation begins) were calculated from the solution speciation model. The three points for each experiment were plotted on the EDNB phase diagram to show the

crystallisation processes. The crystallisation processes for all of the continuous mixer experiments are shown in Figure 51.

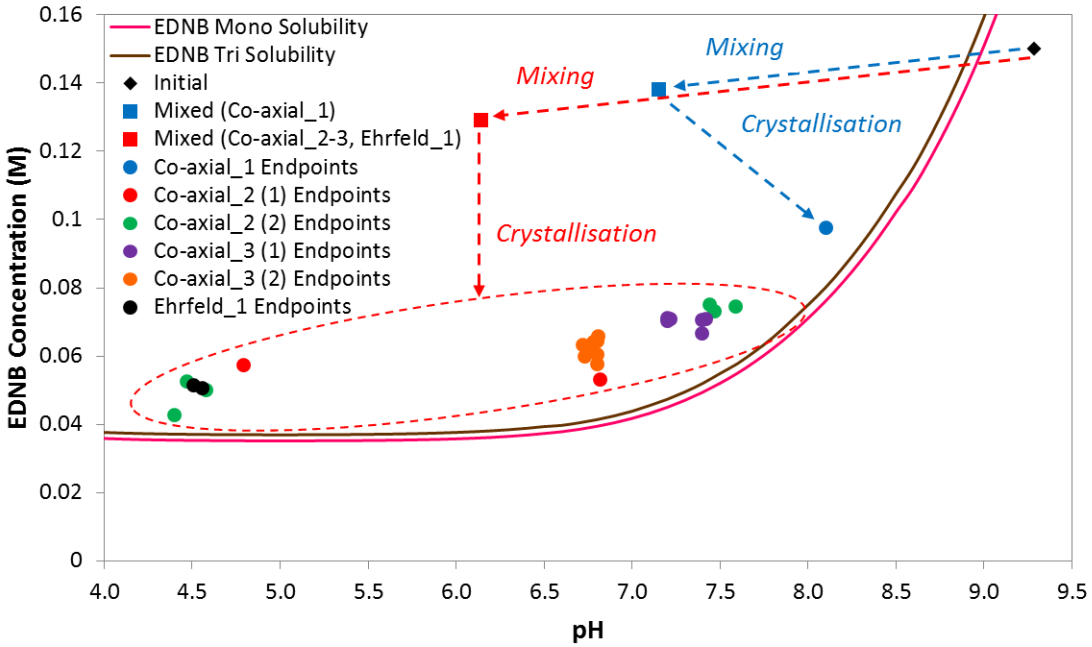

Figure 51. Crystallisation processes for all of the continuous mixer experiments.

The crystallisation processes essentially consisted of two parts. The first part is the single phase continuous mixing process when sulfuric acid is being continuously mixed with the basic solution before crystallisation commences. The second part is the crystallisation pathway which covers the period from the initial nucleation to the experimental endpoint. The first thing to note is that all of the experiments had the same mixed solution composition except from Co-axial_1 which had a mixed solution composition with a higher pH value since a greater basic solution:sulfuric acid flow ratio was being employed with the same solution concentrations.

Another thing to note is that the crystallisation endpoints cluster in two areas of the phase diagram. One area is at a pH of around 7 with an EDNB concentration of around 0.065 M. The other area is at a pH of around 4.5 with an EDNB concentration of around 0.05 M. This

separation in endpoints is due to the sensitivity of the basic solution to sulfuric acid in the pH region of 4.5 to 7 as this corresponds to the inflection point of the “titration” between the two solutions with the pKa_1 of ethylenediamine having a value of 6.86. This means that the experimental endpoints at around pH 7 relate to an experimental fully mixed solution composition which matched the calculated fully mixed solution composition very well. On the other hand, the experimental endpoints at around pH 4.5 relate to an experimental fully mixed solution composition which deviated from the calculated mixed solution composition. The deviation appears large in terms of the pH value but is actually small in terms of volume due to the sensitivity of the basic solution to the sulfuric acid as discussed.

The experimental endpoint for Co-axial_1 has significantly higher pH and EDNB concentration values than the other experiments as expected due to the increased basic solution:sulfuric acid flow ratio. All of the other co-axial mixer endpoints show a spread in pH and EDNB concentration values within a reasonable range. This spread is most likely due to the fact that mixing in the co-axial mixer isn’t perfect and this is a highly mixing sensitive process. Any deviation from the intended basic solution:sulfuric acid flow ratio will result in a solution with a different pH and EDNB concentration value. If the sample mixture has a higher pH value than expected then there is most likely an excess of basic solution and conversely if the pH value is lower than expected then there is most likely an excess of sulfuric acid. The Ehrfeld mixer endpoints show a consistency with the co-axial mixer endpoints when the same solution concentrations and flow rates are employed.

8.3.3. IR spectra of dry powder

The IR spectra of a dry powder sample from each experiment, in addition to the reference spectra for EDNB monoclinic, EDNB triclinic and 3,5-DNBA, are shown in Figure 52. Only one spectrum is shown from each experiment as all the spectra within an experiment were

almost identical. The characteristic infrared bands for ethylenediammonium 3,5-dinitrobenzoate are given in Table 1.

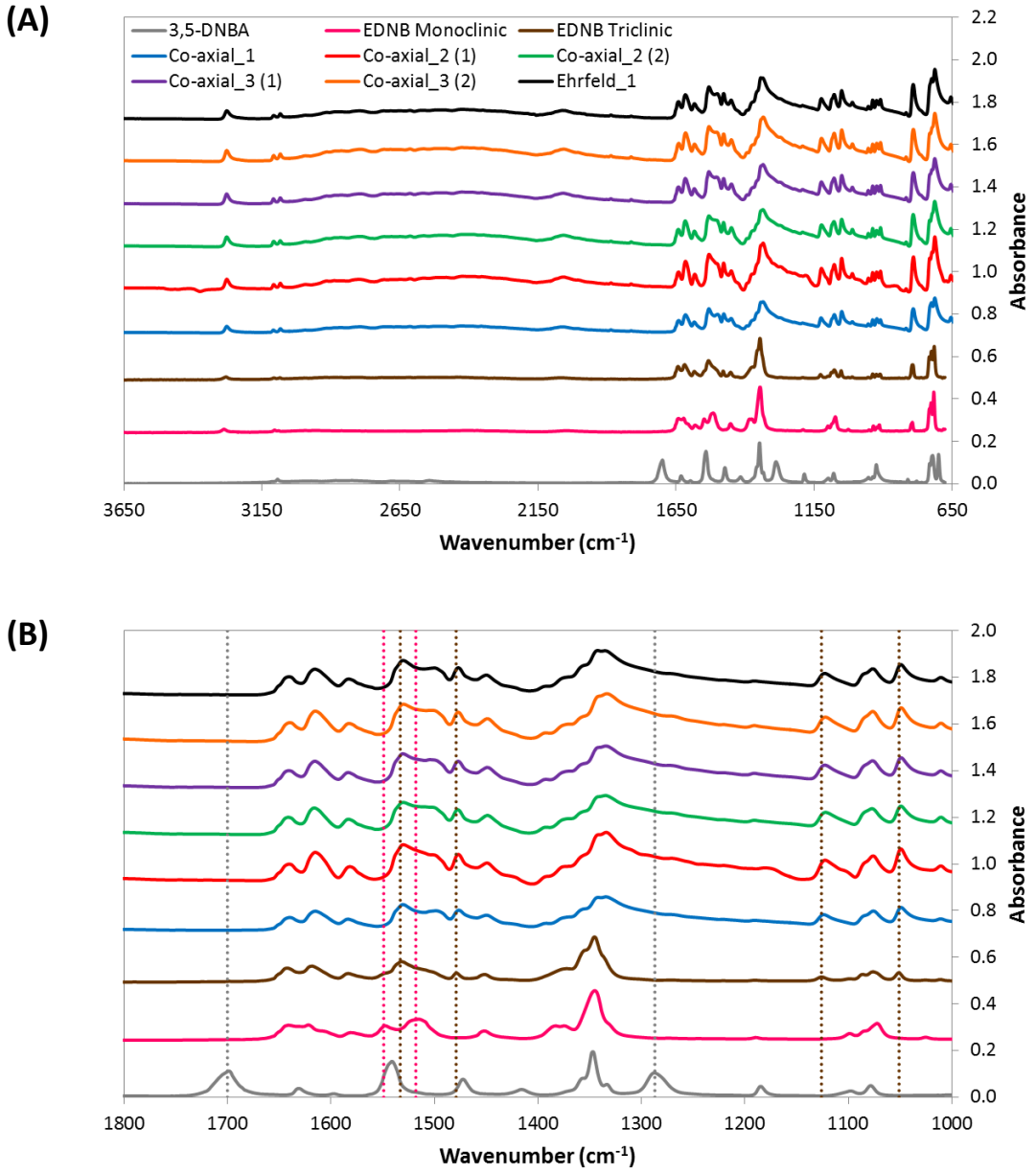

Figure 52. IR spectra of dry powder samples from the continuous mixer experiments presented as the (A) full range and the (B) range of interest. Dotted lines highlight the characteristic peaks of EDNB monoclinic (pink), EDNB triclinic (brown) and 3,5-DNBA (grey).

The IR spectra demonstrate that EDNB triclinic was crystallised in every continuous mixer experiment which was expected as all of the experiments were performed at 25 °C.

8.3.4. Yield and solid recovery data

The yield (percentage of EDNB recovered with respect to total amount of material dissolved) and solid recovery (percentage of EDNB recovered with respect to the amount of material that could be crystallised based on solubility) were calculated for each continuous mixer experiment. The yield and solid recovery values for each sample, for each experiment, are shown in Table 9. The solid recovery was calculated using the activity corrected solubility values determined in this work rather than the literature solubility.

Table 9. Yield and solid recovery values for the continuous mixer experiments.

Experiment Label	Sample Label	Final pH	Yield (%)	Solid Recovery (%)
Co-axial_1	A	8.10	29.4	71.2
Co-axial_2 (1)	A	4.79	55.4	78.1
	B	6.82	58.7	87.6
Co-axial_2 (2)	A	4.58	61.1	86.2
	B	4.40	66.7	94.1
	C	4.47	59.1	83.4
	D	7.59	41.9	77.0
	E	7.44	41.6	71.7
	F	7.47	43.2	75.3
Co-axial_3 (1)	A	7.42	44.9	76.7
	B	7.40	45.1	76.5
	C	7.40	48.1	81.7

	D	7.20	45.2	72.3
	E	7.20	44.7	71.4
	F	7.22	44.8	72.1
Co-axial_3 (2)	A	6.80	55.3	82.3
	B	6.80	52.9	78.8
	C	6.78	50.2	74.5
	D	6.73	53.5	79.0
	E	6.75	51.5	76.3
	F	6.72	50.7	74.9
	G	6.80	50.0	74.4
	H	6.80	49.5	73.7
	I	6.81	48.7	72.6
Ehrfled_1	A	4.51	59.9	84.6
	B	4.56	60.7	85.6

It can be seen that the yield is relatively low in all of the experiments. This is because for these experiments EDNB still has a reasonable solubility in the final solution. It can also be seen that the yield increased as the pH of the final solution decreased which was expected as the solubility decreases with decreasing pH.

The solid recovery is higher than the yield in every experiment as expected. Furthermore, the values for solid recovery are relatively high falling in the range of 70-95%. As with the 400 ml STR experiments, the solid recovery is higher in the experiments with lower solution pH (higher initial supersaturation) before crystallisation. Again, this is thought to be due to the higher supersaturation level resulting in a faster nucleation rate which leads to a

greater amount of EDNB crystallising in the initial phase. The modest supersaturation level present after the nucleation phase then doesn't allow crystal growth to occur in the remaining time period that the sample vial is held for. Therefore, the samples with the most EDNB crystallised via nucleation were the samples with the most EDNB crystallised overall and so the solid recoveries are higher.

8.3.5. Particle size and shape analysis with Morphologi G3

For each sample, for each continuous mixer experiment, the dry powder was analysed with the Morphologi in order to obtain the particle size and shape distributions. A low energy dispersion method was used to disperse the particles onto the glass plate before analysis took place. A low energy was used with the purpose of breaking up agglomerates but not breaking individual particles. The circle equivalent diameter and aspect ratio distributions for each sample, for each experiment, can be seen in Figure 53. All distributions are volume weighted.

(A)

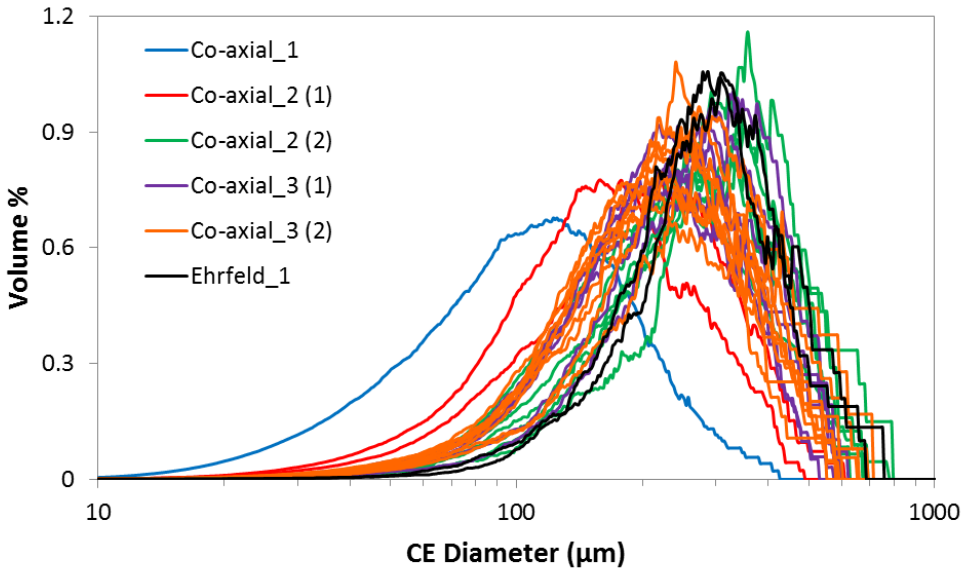

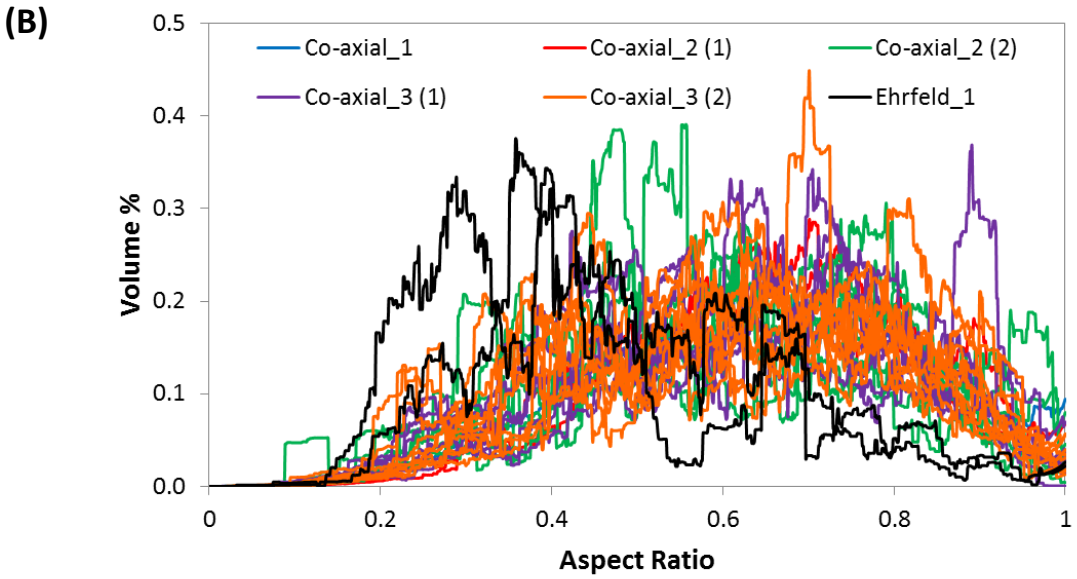

Figure 53. (A) Circle equivalent diameter and (B) aspect ratio distributions from Morphologi for continuous mixer experiments.

It can be seen from the Morphologi results that the PSDs for the continuous mixer experiments have two distinct size ranges. Almost all the samples fall in the larger size range which makes sense as in those experiments the same solution concentrations are used and similar yields are obtained. The Co-axial_1 sample PSD occupies the smaller size range which would be expected due to the lower yield of EDNB in this experiment as a result of the higher final solution pH. It is interesting to note that one of the two samples from Co-axial_2 (1) is in between the smaller size range and the larger size range even though the yield in this sample is similar to the samples in the larger size range. There is no obvious reason for this shift in PSD but a possible suggestion could be that the particles in this sample experienced greater attrition during sample preparation or powder dispersion.

Comparing the PSDs and the aspect ratio distributions it can be seen that the PSDs with fewer small particles also have more particles with lower aspect ratios. Conversely, the PSDs with more small particles also have more particles with aspect ratios closer to 1. This

result numerical confirms the images which show the crystals to grow as long rectangular plates. Co-axial_1 and Co-axial_2 (1) B have more crystals with an aspect ratio closer to 1, and both Ehrfeld_1 samples have more crystals with lower aspect ratios, but the aspect ratio distribution in every other sample is consistent.

8.4. Full continuous processes with X mixer & CSTR cascade

8.4.1. Experimental conditions

The experimental conditions used in the full continuous processes are shown in Table 10. All of these experiments are performed at 25 °C and the composition of the basic solution is always the same.

Table 10. Experimental conditions used in the full continuous processes.

Experiment Label	Sulfuric Acid Conc. (M)	Basic Solution Flow Rate (ml/min)	Sulfuric Acid Flow Rate (ml/min)	Total Flow Rate (ml/min)
X-mixer_1	0.132	150	50	200
X-mixer_2	0.132	300	100	400
X-mixer_3 (1)	0.17	150	50	200
X-mixer_3 (2)	0.17	150	50	200
X-mixer_4 (1)	0.17	300	100	400
X-mixer_4 (2)	0.17	300	100	400

A range of sulfuric acid concentrations and total flow rates were utilised for the fully continuous processes.

8.4.2. Crystallisation processes on EDNB phase diagram

In these experiments the pH and concentration data were known for the initial solution and the slurry sample taken at the end of the continuous process. In addition, the pH and concentration data for the fully mixed solution (before crystallisation begins) were calculated from the solution speciation model. The three points for each experiment were plotted on the EDNB phase diagram to show the crystallisation processes. The crystallisation processes for all of the full continuous processes are shown in Figure 54.

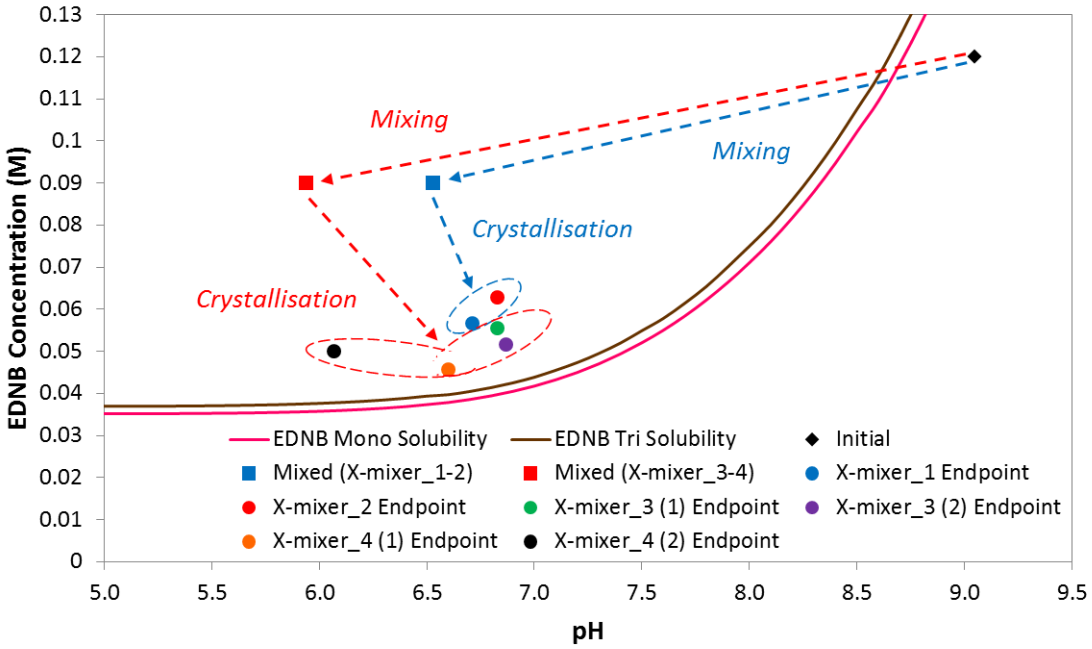

Figure 54. Crystallisation processes for all of the full continuous processes.

The crystallisation processes essentially consisted of two parts. The first part is the single phase continuous mixing process when sulfuric acid is being continuously mixed with the basic solution before crystallisation commences. The second part is the crystallisation pathway which covers the period from the initial nucleation to the experimental endpoint. The first thing to note is that as two different sulfuric acid concentrations were utilised, there were two different mixed solution compositions. X-mixer_1 and X-mixer_2 used the

lower sulfuric acid concentration which resulted in a fully mixed solution with a higher pH value than the fully mixed solution obtained in X-mixer_3 and X-mixer_4.

The experimental endpoints for X-mixer_1 and X-mixer_2 had the highest EDNB concentration values and among the highest pH values which was expected as the lower sulfuric acid concentration was used in these experiments. Despite this, all of the experimental endpoints lie within a reasonable range of pH and EDNB concentration values. The small spread in values within experiments using the same solution concentrations is most likely due to the fact that mixing in the X-mixer isn't perfect and this is a highly mixing sensitive process. Any deviation from the intended basic solution:sulfuric acid flow ratio will result in a solution with a different pH and EDNB concentration value. If the sample mixture has a higher pH value than expected then there is most likely an excess of basic solution and conversely if the pH value is lower than expected then there is most likely an excess of sulfuric acid. Therefore, different experimental endpoints were accessed by utilising different sulfuric acid concentrations, and for a particular sulfuric acid concentration the experimental endpoints were consistent across the range of total flow rates studied.

8.4.3. IR spectra of dry powder

The IR spectra of the dry powder sample from each experiment, in addition to the reference spectra for EDNB monoclinic, EDNB triclinic and 3,5-DNBA, are shown in Figure 55. The characteristic infrared bands for ethylenediammonium 3,5-dinitrobenzoate are given in Table 1.

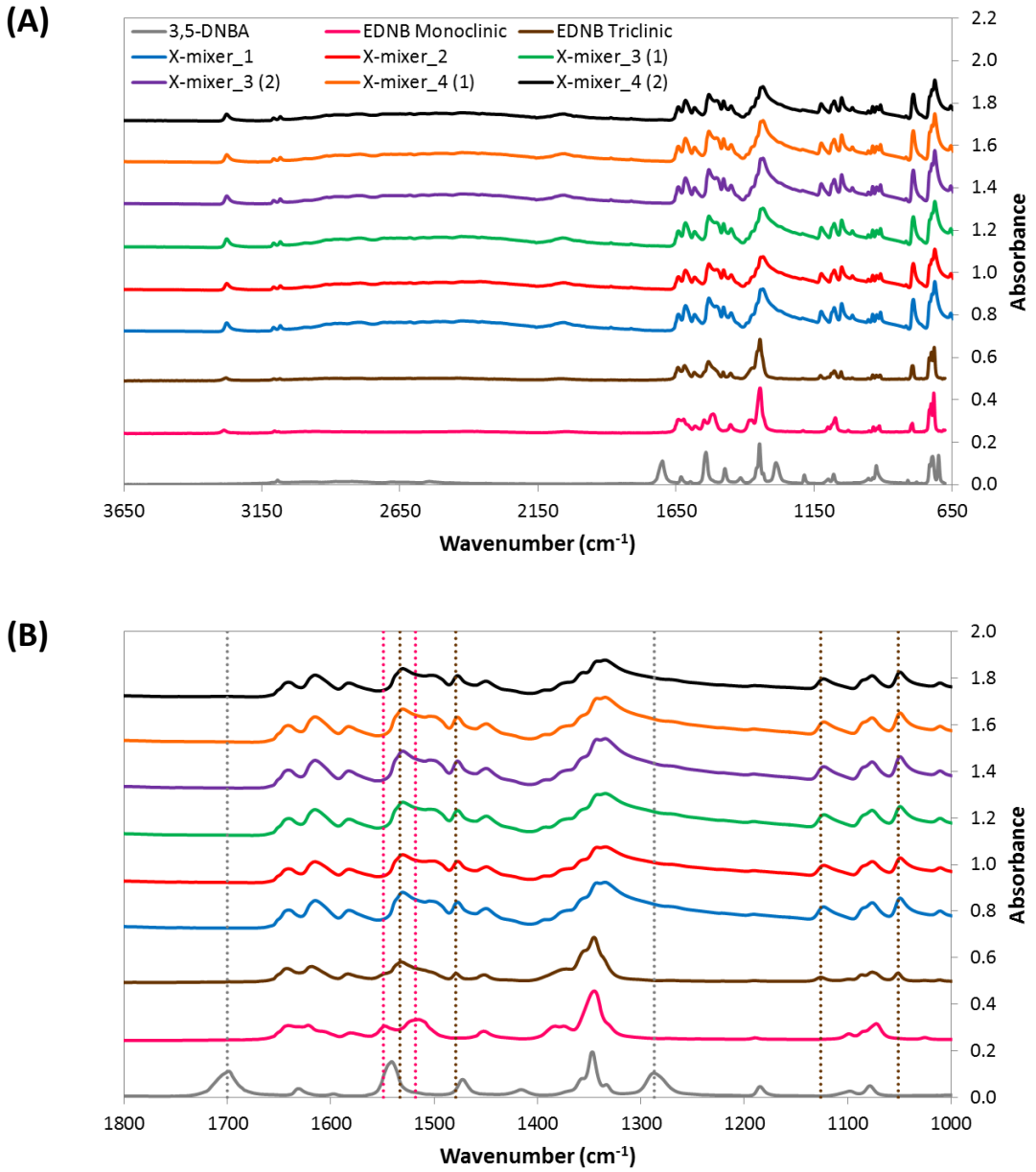

Figure 55. IR spectra of dry powder samples from the full continuous processes presented as the (A) full range and the (B) range of interest. Dotted lines highlight the characteristic peaks of EDNB monoclinic (pink), EDNB triclinic (brown) and 3,5-DNBA (grey).

The IR spectra demonstrate that EDNB triclinic was crystallised in every full continuous process which was expected as all of these experiments were performed at 25 °C.

8.4.4. Yield and solid recovery data

The yield (percentage of EDNB recovered with respect to total amount of material dissolved) and solid recovery (percentage of EDNB recovered with respect to the amount of material that could be crystallised based on solubility) were calculated for each full continuous process. The yield and solid recovery values for each experiment are shown in Table 11. The solid recovery was calculated using the activity corrected solubility values determined in this work rather than the literature solubility.

Table 11. Yield and solid recovery values for the full continuous processes.

Experiment Label	Final pH	Yield (%)	Solid Recovery (%)
X-mixer_1	6.71	52.9	80.2
X-mixer_2	6.83	47.6	73.4
X-mixer_3 (1)	6.83	53.8	82.9
X-mixer_3 (2)	6.87	57.0	88.3
X-mixer_4 (1)	6.60	61.9	92.9
X-mixer_4 (2)	6.07	58.3	85.2

It can be seen that the yield is relatively low in all of the experiments. This is because for these experiments EDNB still has a reasonable solubility in the final solution. It can also be seen that the yield was slightly higher in the experiments where the higher sulfuric acid concentration was used. This was expected as the pH of the final solution in these experiments was a little lower than the other experiments which meant that a little more EDNB should have crystallised due to decreased solubility.

The solid recovery is higher than the yield in every experiment as expected. Furthermore, the values for solid recovery are relatively high falling in the range of 73-93%. The solid recovery is higher in the experiments which utilised a higher sulfuric acid concentration due to the lower solution pH (higher initial supersaturation) before crystallisation. Again, this is thought to be due to the higher supersaturation level resulting in a faster nucleation rate which leads to a greater amount of EDNB crystallising in the initial phase. The modest supersaturation level present after the nucleation phase then doesn't allow crystal growth to occur in the remaining time period that the sample vial is held for. Therefore, the experiments with the most EDNB crystallised via nucleation were the experiments with the most EDNB crystallised overall and so the solid recoveries are higher.

8.4.5. Particle size and shape analysis with Morphologi G3

For each full continuous process, the dry powder was analysed with the Morphologi in order to obtain the particle size and shape distributions. A low energy dispersion method was used to disperse the particles onto the glass plate before analysis took place. A low energy was used with the purpose of breaking up agglomerates but not breaking individual particles. The circle equivalent diameter distribution and the aspect ratio distribution for each experiment can be seen in Figure 56. There is only one sample from the continuous phase of each experiment. All distributions are volume weighted.

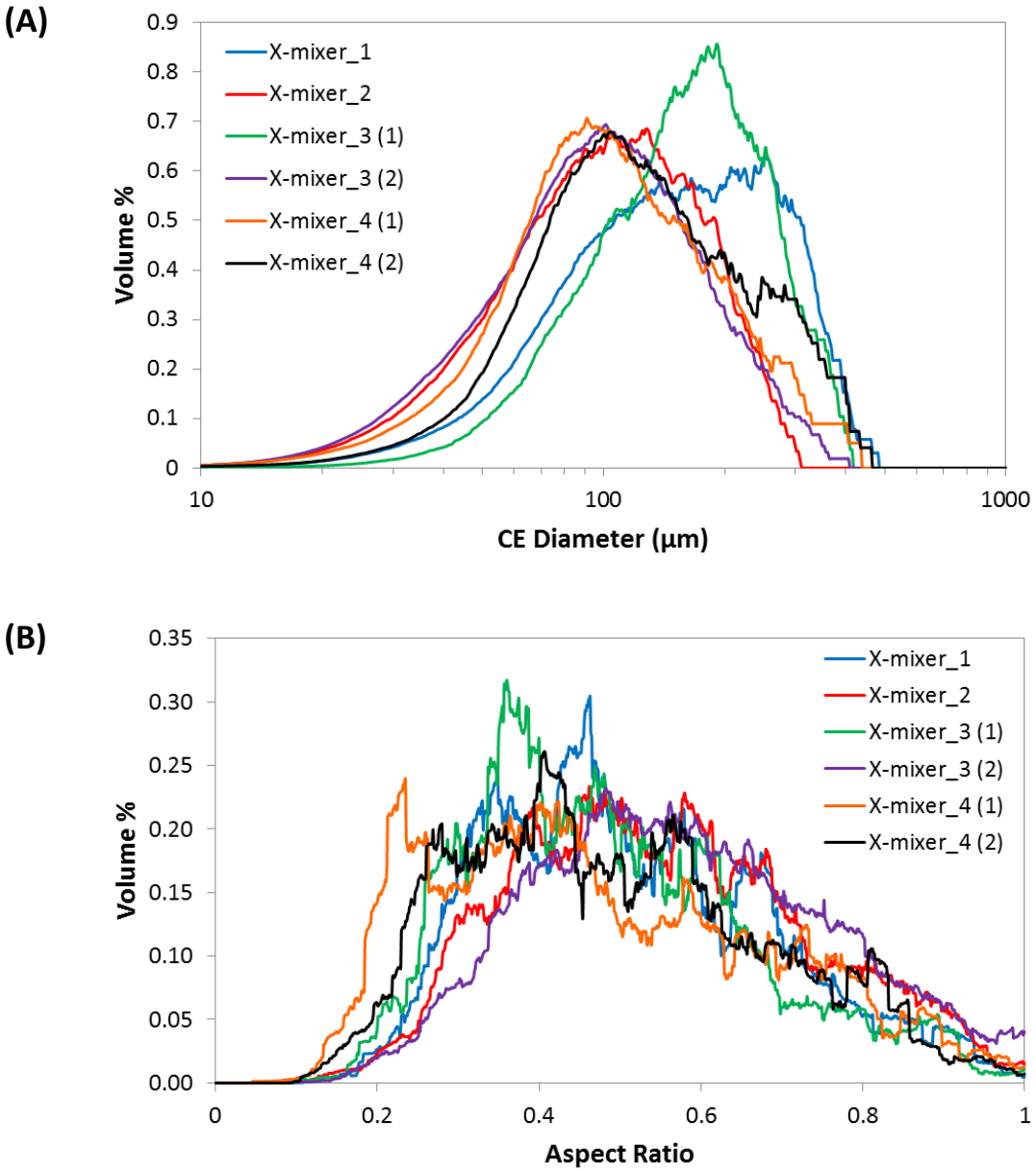

Figure 56. (A) Circle equivalent diameter and (B) aspect ratio distributions from Morphologi for full continuous processes.

It can be seen from the Morphologi results that the PSDs are similar for all of the full continuous processes but there are two distinct size ranges. X-mixer_1 and X-mixer_3 (1) appear to have fewer particles in the smaller size range so their PSDs are shifted to the right. This difference in PSDs is confirmed by the same difference in CLDs shown in Figure 60 from the FBRM results. The reason why these two processes are exhibiting this

difference in PSD could be due to the lower total flow rate being utilised which results in there being less turbulence in the system and therefore less attrition. However, this is only one possible reason which may not be the case. The aspect ratio distributions are consistent across the range of full continuous processes which suggests that the distribution of crystal shapes was essentially the same even for different distributions of crystal size. Representative microscope images of the crystal samples from X-mixer_4 (1) and X-mixer_1 are shown in Figure 57. These were obtained using the Morphologi instrument.

(A)

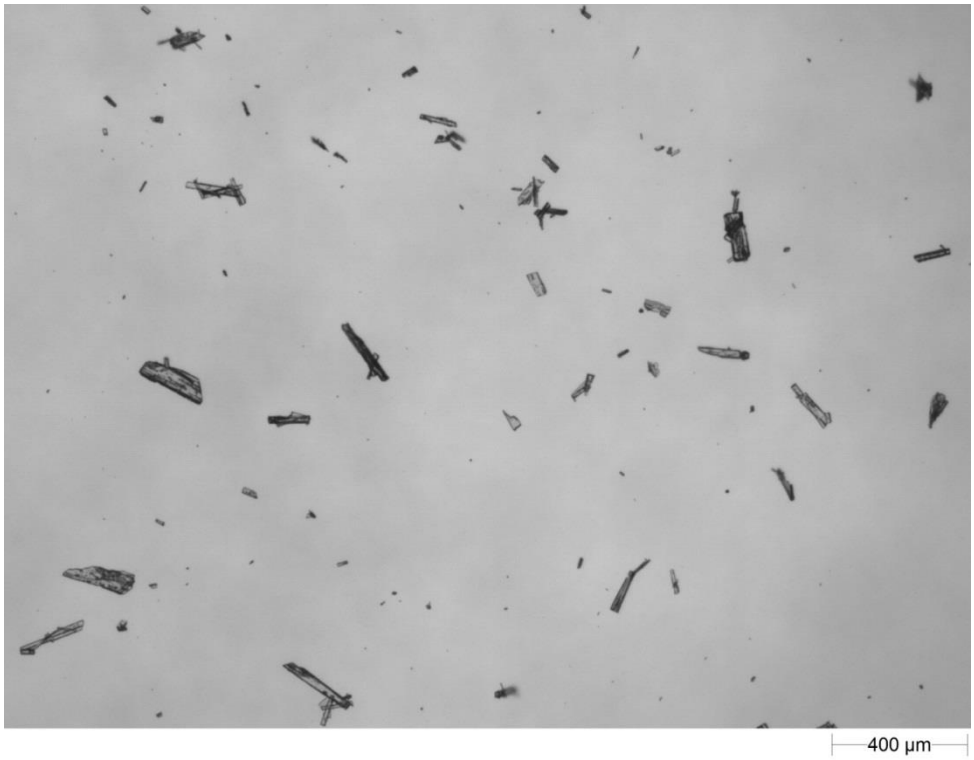

(B)

Figure 57. Representative microscope images of the samples from the (A) X-mixer_4 (1) and (B) X-mixer_1 experiments.

Images from these two experiments were chosen for comparison in an effort to better understand the cause of the two PSD size ranges obtained from the full continuous processes. It can be seen from the images that the X-mixer_1 sample contains some extremely large particles which don't appear in the X-mixer_4 (1) images. The presence of these extremely large particles could be the reason for the shift in the volume weighted PSD to the right. It is not known whether these extremely large particles broke down in the X-mixer_4 (1) experiment or if they were never present. As X-mixer_4 (1) utilised a higher total flow rate than X-mixer_1 it is possible that the greater turbulence broke the extremely large particles down to smaller sizes as discussed already.

8.4.6. PAT results (pH, UV and FBRM)

For each full continuous process, there was a pH and UV probe in CSTR 1 which monitored solution composition directly after the X-mixer. In addition, there was a pH and FBRM probe in CSTR 2 which monitored the pH and CLD of the slurry at the end of the CSTR cascade. The results from the PAT tools gave a deeper understanding of the process and demonstrated whether steady state operation was achieved or not. A comparison of the pH profiles obtained in the full continuous processes is shown in Figure 58.

(A)

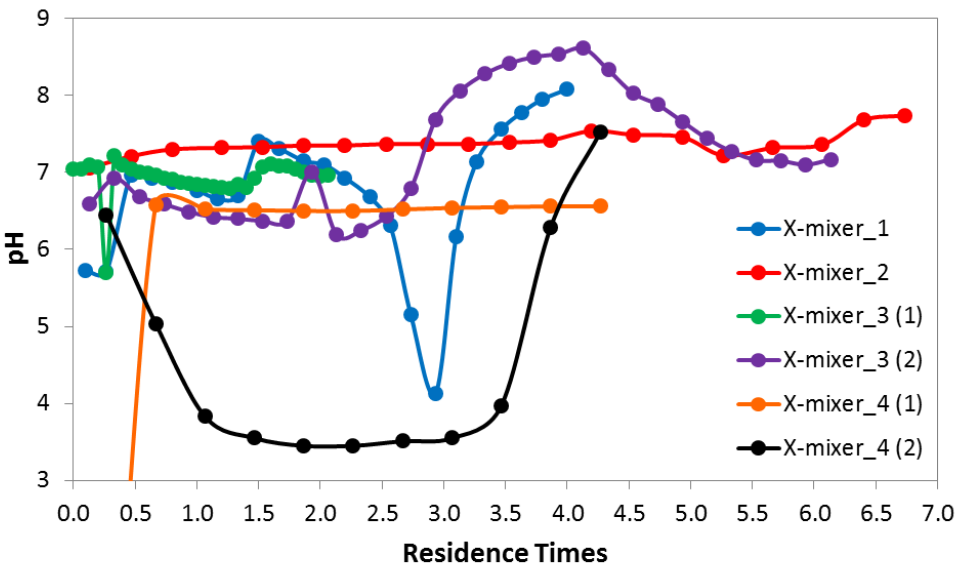

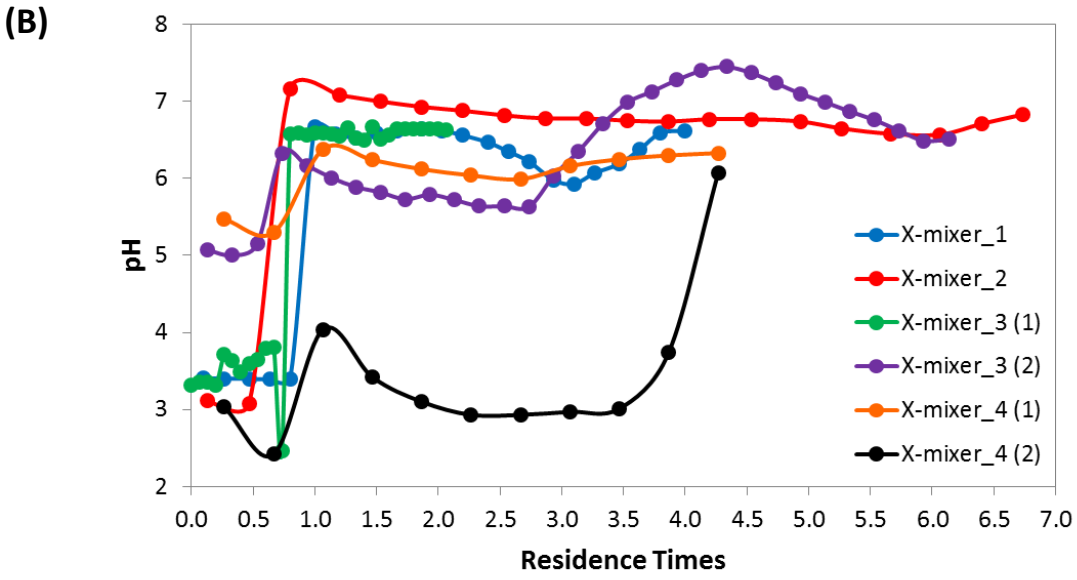

Figure 58. Comparison of pH profiles in (A) CSTR 1 and (B) CSTR 2 for full continuous processes.

The first thing to be noted is that the pH profiles in CSTR 1 and CSTR 2 follow extremely similar trajectories which suggests a completely continuous process was always maintained with good material transfer taking place. In addition, the pH value at the end of one continuous process was similar to its comparable processes. That is, in X-mixer_1 and X-mixer_2 where 0.132 M sulfuric acid was used, the final pH values were 6.62 and 6.83. In the 0.17 M sulfuric acid experiments, the final pH value ranged from 6.07 to 6.51.

Despite the similar endpoints, the full pH profiles varied between experiments with the pH values significantly fluctuating over the course of the processes. This variation between experiments is most noticeable in X-mixer_4 (2) where the pH in both CSTRs is extremely low for most of the process before sharply increasing just before the end of the process. The reason for the pH profile fluctuations, and the process to process variation, is thought to be most likely due to mixing issues caused by imperfect mixing in addition to flow issues caused by the formation of solids in the X-mixer and tubing just after the mixer. Mixing will

not be perfect, even without the presence of solids, which results in the pH of the mixed solution deviating from the expected pH value due to a deviation from the expected basic solution:sulfuric acid flow ratio. This was already discussed with regards to the continuous mixer experiments as this was also an issue there. Flow issues as a result of solid formation were a minor issue in the continuous mixer experiments but in the full continuous processes it became a more major issue. For most of the full continuous processes the experiment had to be stopped before planned due to mixer and/or tubing blockages as a result of solid formation. Clearly these flow issues may have affected the pH profiles by changing the basic solution:sulfuric acid flow ratio, reducing the overall total flow rate or by intermittently stopping and starting the flow.

A comparison of the UV absorbance profiles obtained in the full continuous processes is shown in Figure 59. Absorbance is being shown rather than 3,5-DNBA concentration as there was insufficient time to develop and implement a calibration model for this dataset in the scope of this work. It was thought that absorbance was sufficient for process monitoring without quantitative analysis.

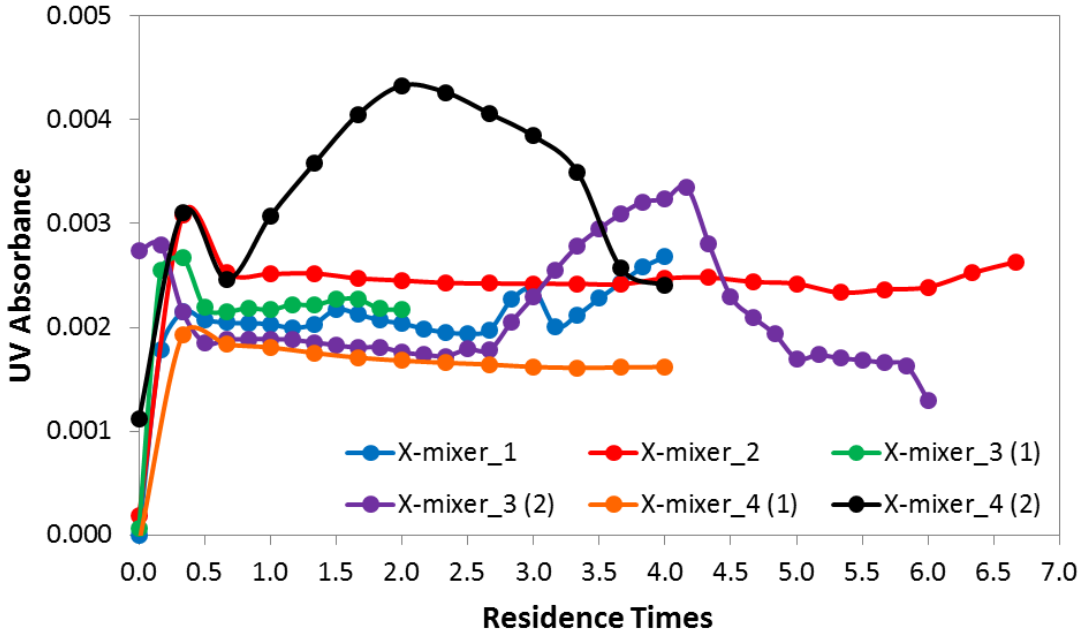

Figure 59. Comparison of UV absorbance profiles in CSTR 1 for full continuous processes.

The UV absorbance profiles correlate well with the CSTR 1 pH profiles in that the processes with a relatively constant pH value also have a relatively constant UV absorbance value. Similarly, where a significant fluctuation is seen in the pH profile, a significant fluctuation is also seen in the UV absorbance profile. As these two independent PAT tools were reporting the same trends in data this makes the overall dataset more reliable. As absorbance is observed, rather than concentration, no deeper conclusions can be made because absorbance depends on concentration, temperature and pH so any combination of these factors could cause a change in the absorbance signal.

A comparison of the FBRM data in the full continuous processes is shown in Figure 60. The profile of the total counts in addition to the slurry CLD at the end of the continuous process are shown in order to make a fair comparison. The FBRM data was collected using the S400 model of FBRM probe so only the coarse view of the particles was obtained. Therefore, this data can't be compared with the semi-batch FBRM data.

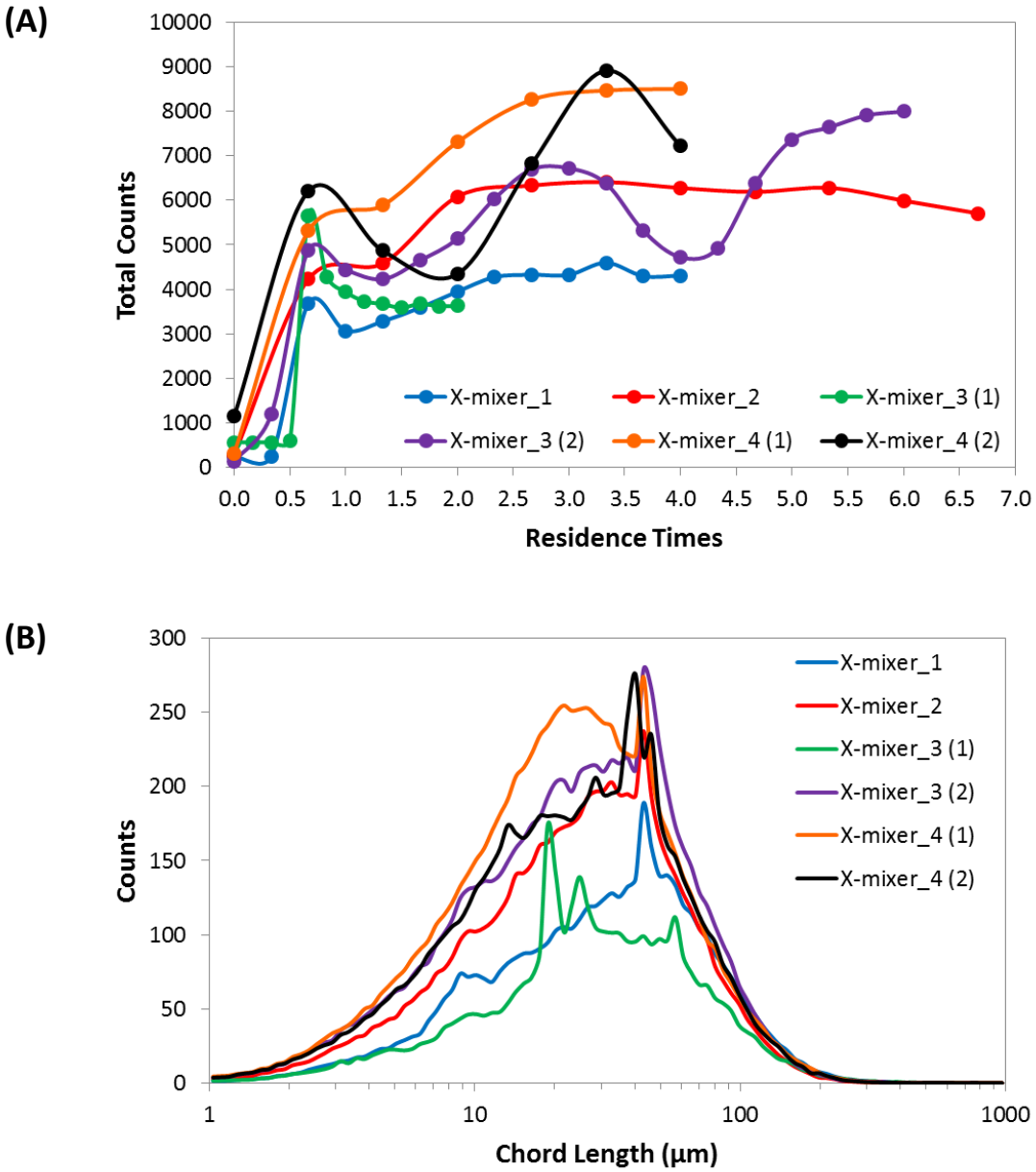

Figure 60. Comparison of (A) total counts profiles and (B) CLDs in CSTR 2 for full continuous processes.

There is significant variation between the total counts of each process ranging from 3,600 to 8,500. There is also variation, although to a lesser extent, between the CLDs of each process. Despite the CLD variation almost all of the crystals fall between a chord length of 10 and 100 µm in every experiment. There are a few spikes in the CLDs, which are thought

to be due to fouling of the probe, which aren't removed because this FBRM probe model doesn't have the "stuck particle correction" feature.

When comparing the total count profiles with the CLDs it can be seen that the experiments with lower total counts produce CLDs with fewer particles in the smaller size range which shifts the CLD peak to the right. X-mixer_1 and X-mixer_3 (1) are the processes with distinctly fewer total counts and fewer smaller particles in their CLDs. This difference in CLD is confirmed by the same difference in PSDs shown in Figure 56 from the Morphologi results. The reason why these two processes are exhibiting this difference in PSD could be due to the lower total flow rate being utilised which results in there being less turbulence in the system and therefore less attrition of the largest particles as was already discussed when analysing the Morphologi data.

Taking into account all the PAT results, the only processes which could be argued to have reached steady state operation are X-mixer_2 and X-mixer_4 (1). In both processes the pH profiles in both CSTRs quickly reached a value and remained relatively constant. This is especially true for X-mixer_4 (1) in CSTR 1. In addition, for both processes the UV absorbance profiles quickly reached a value and remained relatively constant over the course of the experiment. The total counts took some time (2-3 residence times) to increase to a relatively constant value in both processes. The CLDs for both processes evolved to, and remained at, a constant shape within a similar time period. It took longer for the particle properties to become constant, in comparison with the solution composition, due to the increased length of time required for all crystallisation processes to reach completion compared with the reactions in solution.

8.5. Semi-batch experiment utilising continuous pre-mixing with X-mixer and CSTR 1

8.5.1 Experimental conditions & method

This experimental method was implemented for one set of experimental conditions in order to directly nucleate EDNB monoclinic utilising a continuous mixing approach rather than the traditional semi-batch titration method. To achieve this polymorphic outcome the semi-batch experimental conditions of STR_7 were translated to the continuous mixing conditions of this experiment. In this way the concentrations of all the components after mixing would be equal in both experiments. The conditions of STR_7 were selected as EDNB monoclinic was nucleated directly in that experiment. Therefore, the feed solution concentrations of 3,5-DNBA , ethylenediamine, NaOH and sulfuric acid were 0.362 M, 0.181 M, 0.19 M and 0.128 M respectively. Although this experiment is still semi-batch overall, the implementation of continuous mixing (as opposed to adding sulfuric acid from above) will provide more controlled and scalable mixing of the solutions.

The method involved firstly continuously mixing the basic solution and sulfuric acid at 50 °C. This mixture flowed into CSTR 1 at a total flow rate of 400 ml/min until the 150 ml CSTR 1 was filled. The flow ratio was 3:1 basic solution:sulfuric acid as with the full continuous processes. Once the vessel was filled, the solution was held until nucleation of EDNB monoclinic occurred and the PAT signals were reading constant. A sample was taken from the vessel at this point. After sampling the cooling was initiated at a cooling rate of 1 °C/min until the slurry reached 25 °C. Cooling was employed for the purpose of increasing crystallisation yield. After cooling the slurry was held until all the PAT signals were reading constant once more. Another sample was taken from the vessel at this point.

8.5.2. Crystallisation process on EDNB phase diagram

In this experiment the pH and concentration data were known for the initial solution, the slurry sample after nucleation and the slurry sample after cooling. In addition, the pH and concentration data for the fully mixed solution (before crystallisation begins) was calculated from the solution speciation model. The four points were plotted on the EDNB phase diagram to describe the crystallisation process and this is shown in Figure 61.

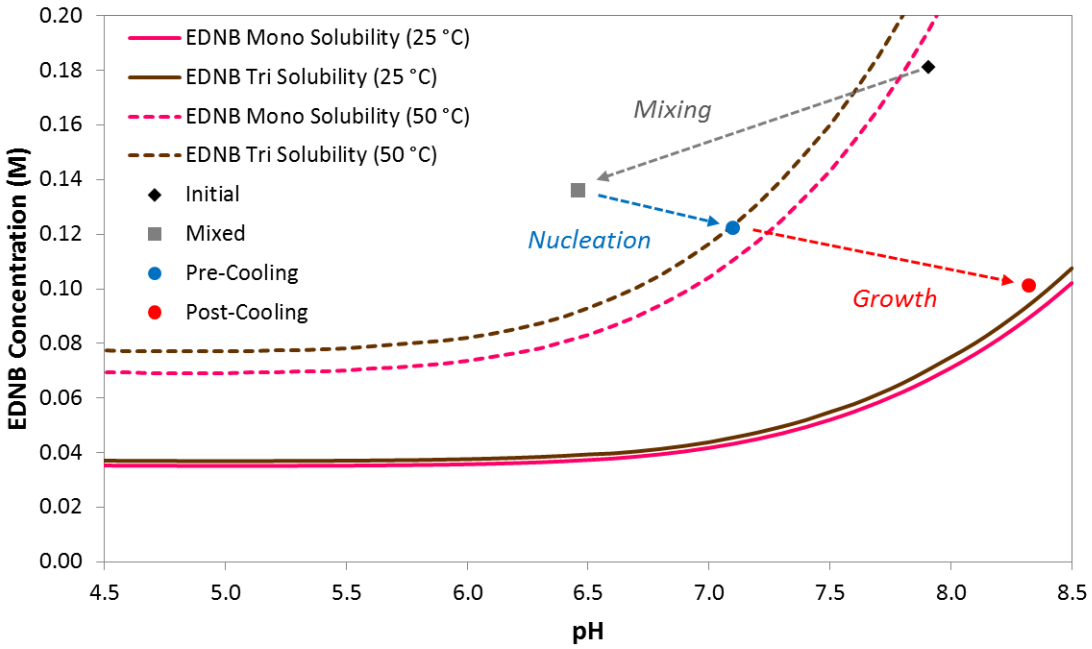

Figure 61. Crystallisation processes for the continuously pre-mixed semi-batch experiment.

The crystallisation processes essentially consisted of three parts. The first part is the single phase continuous mixing process when sulfuric acid is being continuously mixed with the basic solution before crystallisation commences. The second part is the crystallisation pathway which covers the nucleation period. The third part is the crystallisation pathway which covers the growth process during and after the cooling period. As the crystallisation process progressed the pH increased and the EDNB concentration decreased as expected.

8.5.3. IR spectra of dry powder

The IR spectra of the dry powder samples pre-cooling and post-cooling, in addition to the reference spectra for EDNB monoclinic, EDNB triclinic and 3,5-DNBA, are shown in Figure 62. The characteristic infrared bands for ethylenediammonium 3,5-dinitrobenzoate are given in Table 1.

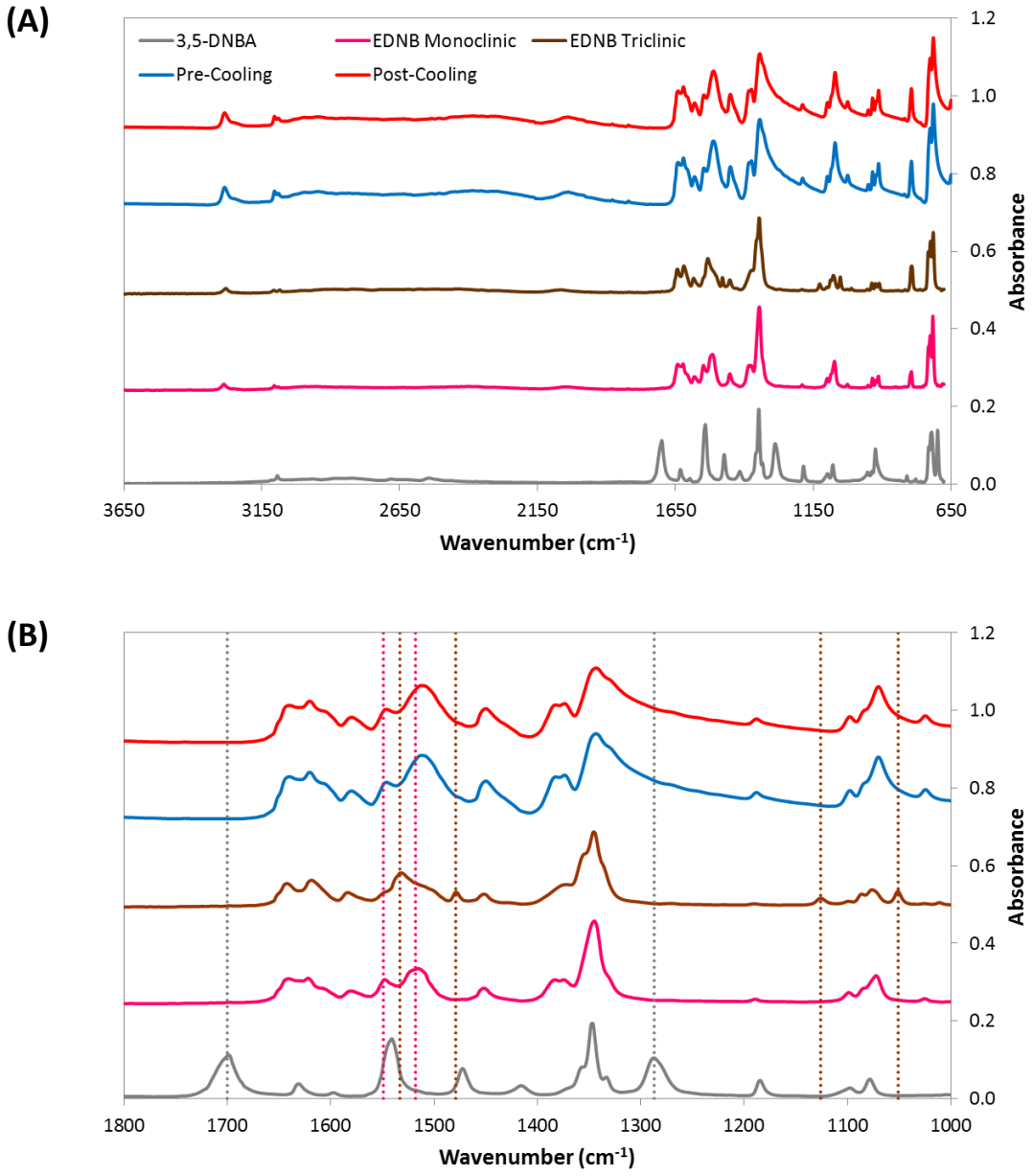

Figure 62. IR spectra of dry powder samples from the continuously pre-mixed semi-batch experiment presented as the (A) full range and the (B) range of interest. Dotted lines

highlight the characteristic peaks of EDNB monoclinic (pink), EDNB triclinic (brown) and 3,5-DNBA (grey).

The IR spectra demonstrate that EDNB monoclinic was nucleated directly and was also the only polymorph present in the final slurry at the end of the experiment. It isn't known whether or not EDNB triclinic was present at some point between pre-cooling and the end of the experiment but this was unlikely.

8.5.4. Yield and solid recovery data

The yield (percentage of EDNB recovered with respect to total amount of material dissolved) and solid recovery (percentage of EDNB recovered with respect to the amount of material that could be crystallised based on solubility) were calculated for each point in the experiment. The yield and solid recovery values for each point in the experiment are shown in Table 12. The solid recovery was calculated using the activity corrected solubility values determined in this work rather than the literature solubility.

Table 12. Yield and solid recovery values for each point in the continuously pre-mixed semi-batch experiment.

Sample	Temp (°C)	Slurry pH	Yield (%)	Solid Recovery (%)
Pre-Cooling	50	7.10	10	53.3
Post-Cooling	25	8.32	25.5	85.1

It can be seen that the yield increased after the slurry was cooled which was the purpose of the cooling step. This increase was expected to happen due to the decreased solubility at the lower temperature. However, the yield didn't increase greatly because the combined cooling and crystallisation processes increased the slurry pH which minimised the overall

decrease in solubility because solubility increases with increasing pH. The solid recovery at the end of the experiment was much higher than the yield which shows that the experiment was a success in terms of recovering the most EDNB monoclinic possible based on solubility. As a side note the solid recovery before cooling was relatively low. However, as explained previously, this was thought to be due to the solubility data for 50 °C not being sufficiently accurate as it was only estimated in this work.

8.5.5. Particle size and shape analysis with Morphologi G3

For each sample from the experiment the dry powder was analysed with the Morphologi in order to obtain the particle size and shape distributions. A low energy dispersion method was used to disperse the particles onto the glass plate before analysis took place. A low energy was used with the purpose of breaking up agglomerates but not breaking individual particles. The circle equivalent diameter distribution and the aspect ratio distribution for each point in the experiment can be seen in Figure 63. All distributions are volume weighted.

(A)

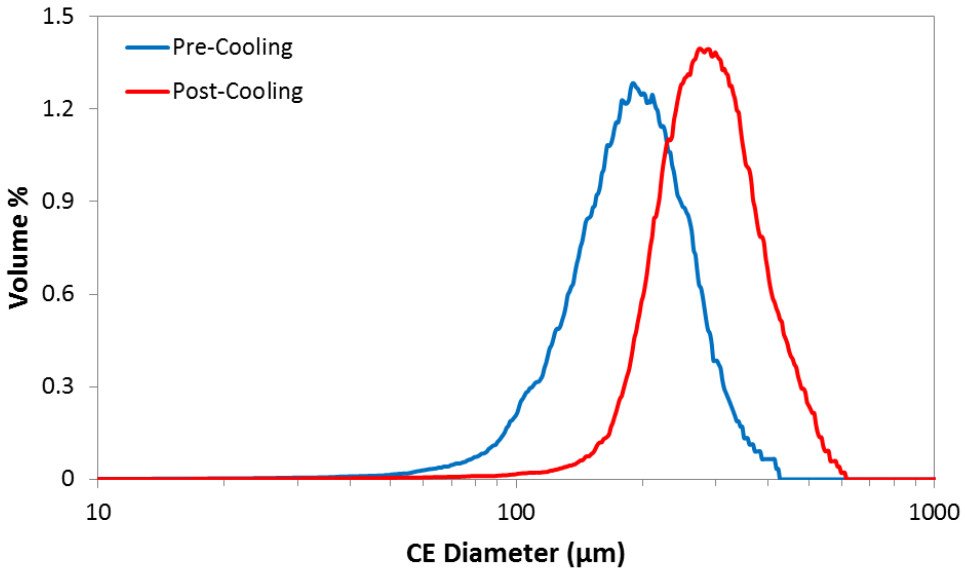

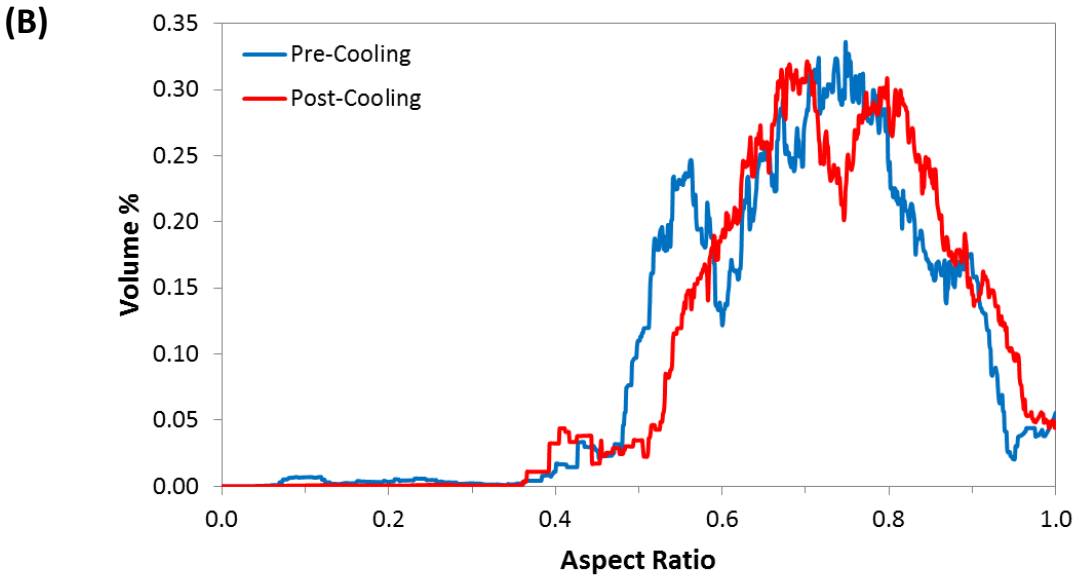

Figure 63. (A) Circle equivalent diameter and (B) aspect ratio distributions from Morphologi for continuously pre-mixed semi-batch experiment.

After cooling the PSD shifted to the right indicating there were larger particles in the slurry. This would suggest that growth of the EDNB monoclinic crystals has taken place. However, the aspect ratio distribution shows a shift in the aspect ratio distribution towards 1 after cooling which indicates that there has been increased agglomeration resulting in the particles appearing more rounded. If the small shift in aspect ratio distribution is taken into account alongside significantly increased yield and significantly increased particle sizes then it would appear that the extent of agglomeration has increased in addition to the crystal growth.

Representative microscope images of the crystal samples from the points of pre-cooling and post-cooling are shown in Figure 64. These were obtained using the Morphologi instrument.

(A)

(B)

Figure 64. Representative microscope images of the samples from the points of (A) pre-cooling and (B) post-cooling in the continuously pre-mixed semi-batch experiment.

It can be seen from both images that the block-shaped crystals of EDNB monoclinic have formed which agrees with the IR spectra obtained. In addition, there is agglomeration of the crystals in both images. The difference is that after cooling the individual crystals are larger and the agglomerate networks are larger compared with before cooling. These images confirm the CE diameter and aspect ratio distributions which suggested there was a combination of crystal growth and increased agglomeration between the points before and after cooling.

8.5.6. PAT results (pH, UV and FBRM)

For the continuously pre-mixed semi-batch process there was a pH, UV and FBRM probe in CSTR 1 which monitored the experiment from the moment the vessel was filled to the end of the experiment. The results from the PAT tools gave a deeper understanding of the process and demonstrated at which time periods constant conditions were established in the vessel. A comparison of the temperature, pH, UV absorbance and FBRM total counts profiles during the pre-cooling and post-cooling phases are shown in Figure 65. The pre-cooling phase covers the period from the beginning of the experiment to just before cooling was initiated. The post-cooling phase covers the period from when cooling was initiated to the end of the experiment.

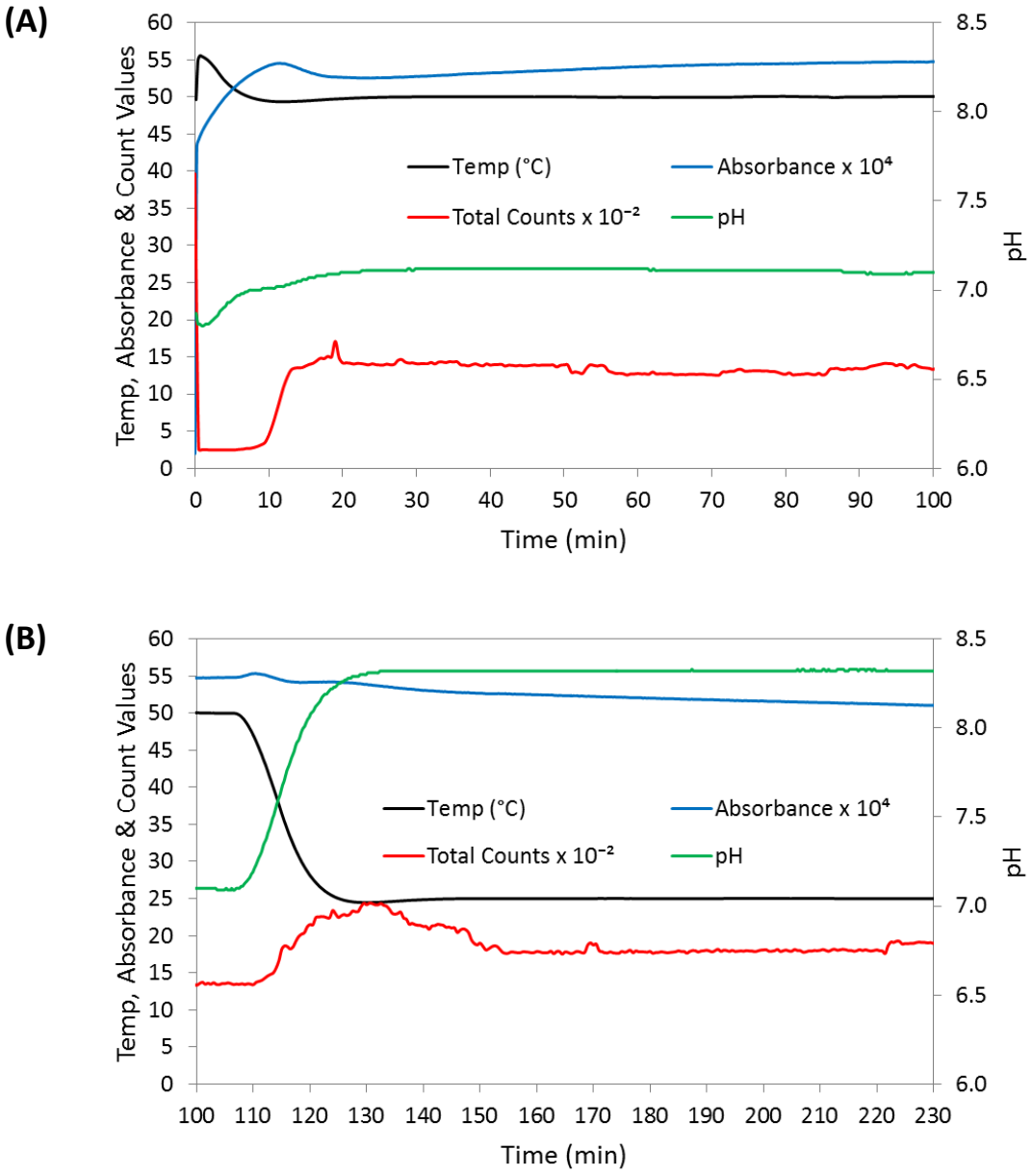

Figure 65. Temperature, pH, UV absorbance and FBRM total counts profiles during (A) pre-cooling and (B) post-cooling phases of the continuously pre-mixed semi-batch experiment.

It can be seen from the pre-cooling phase that nucleation is detected by a sharp increase in FBRM total counts. In the time after the nucleation event the pH, UV absorbance and total counts reached constant values within 60 minutes. The first sample was taken during the subsequent hold time before cooling was initiated. From the post-cooling phase it can be seen that the result of cooling was a decrease in absorbance, an increase in pH and an

initial significant increase in total counts before a gradual decrease later in time. The absorbance decreased due to a reduction in solution concentration although the overall decrease wasn't very steep because the absorbance would increase with decreasing temperature. The pH increased sharply due to the combined effect of the crystallisation and temperature decrease. In order to better understand the FBRM total counts profile the CLD progression must also be analysed. This progression is shown in Figure 66. The FBRM data was collected using the S400 model of FBRM probe so only the coarse view of the particles was obtained. Therefore, this data can't be compared with the semi-batch FBRM data.

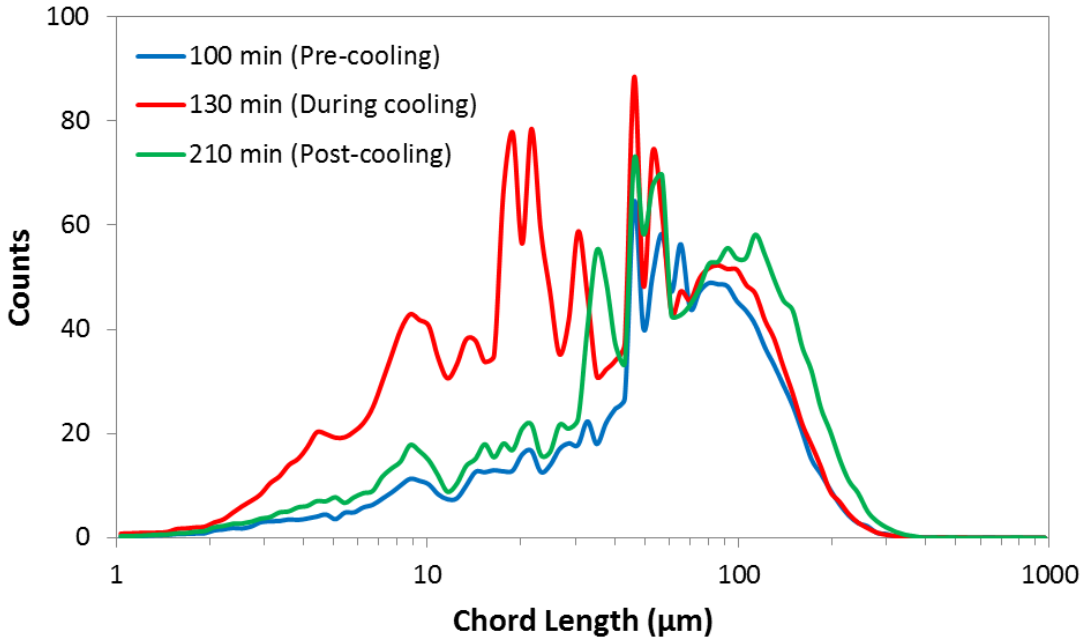

Figure 66. CLD progression for continuously pre-mixed semi-batch experiment.

The CLDs before cooling and at the end of the experiment have a very similar shape. The only differences are that at the end of the experiment the CLD is shifted to the right and is a little bigger overall which demonstrates that there are more large particles present as well as more particles overall. On the other hand, during cooling there are many more small

particles present which corresponds with the sharp increase in total counts during cooling. Analysing the FBRM data as a whole it seems likely that EDNB monoclinic initially nucleated directly before secondary nucleation of EDNB monoclinic took place during cooling before the new small particles attached to agglomerates by the end of the experiment. Therefore, the FBRM results agree with the Morphologi data which showed the shift in PSD to the right at the end of the experiment.

8.6. Conclusions

In this chapter the EDNB crystallisation has been transferred from semi-batch to continuous operation using a range of continuous mixing platforms. The solution speciation model was used to design a series of continuous mixer experiments which covered different supersaturations, total flow rates and basic solution:sulfuric acid flow ratios for two different continuous mixers; the co-axial mixer and the Ehrfeld valve mixer. Slurry samples were taken directly from the mixer outlets and filtered for offline analysis. The results show that a consistent yield and PSD was obtained across total flow rates and mixer types when the same supersaturation was used. In addition, all continuous mixer experiments were performed at 25 °C and so only EDNB triclinic was produced as expected. The consistency in solid form, yield and particle properties demonstrates a successful transfer from batch to continuous EDNB salt crystallisation with the operating conditions being selected by the solution speciation model.

Building upon the continuous mixer experiments, a series of full continuous processes were performed which utilised an X-mixer followed by a cascade of 2 x 150 ml CSTRs with PAT inserted for online monitoring of the slurry product. The solution speciation model was used to design a series of experiments which covered two different supersaturation levels and two different total flow rates. In addition to the offline sample taken from CSTR 2 at

the end of the continuous phase the entire process was monitored with 2 pH probes, a UV probe and an FBRM probe. The PAT tools, in combination with the solution speciation model, allowed for greater process understanding to be developed and for the ability to determine if the continuous crystallisation was operating at steady state. The PAT results show that only two of the six processes (X-mixer_2 and X-mixer_4 (1)) could be said to be operating at steady state with any certainty. Despite this difficulty in reaching steady state there was a consistency in yield, PSD and solid form in the offline samples at the end of the processes. All the samples were EDNB triclinic as all the full continuous processes were operated at 25 °C.

A semi-batch process which utilised continuous pre-mixing of the feeds was performed at 50 °C in order to crystallise EDNB monoclinic via a continuous mixing approach. It was necessary to have the process be semi-batch overall as the low supersaturation value required to directly nucleate EDNB monoclinic is not conducive to the short residence times seen in continuous operation. The X-mixer from the full continuous processes was used to continuously mix the feed solutions into the 150 ml CSTR 1 until the vessel was filled before the solution was then held until nucleation took place. After nucleation the slurry was cooled in order to increase the yield of EDNB monoclinic. The results from the offline analysis of the samples and the PAT (pH, UV and FBRM) showed that pure EDNB monoclinic was directly nucleated and was still present at the end of the experiment. In addition, the yield and size of EDNB monoclinic crystals increased after cooling as would be expected. This process demonstrated the ability to use continuous mixing approaches to produce a solution which directly crystallises EDNB monoclinic. This process is preferable to traditional semi-batch experiments as the continuous mixing approach is more controlled and scalable than adding a solution from above, leading to a more consistent product.

9. Heat transfer characterisation of a DN15 Continuous Oscillatory Baffled Crystalliser (COBC)

9.1. Introduction

A full scale continuous EDNB crystallisation process would involve several connected steps. The first step would be the continuous mixing of the feed solutions to facilitate the EDNB salt formation and consequent nucleation of the desired EDNB polymorph. The resultant crystal seed suspension would then be transferred to a continuous crystalliser designed for growing the seed crystals further in an effort to increase crystal size, increase process yield and/or modify crystal shape. At the end of the crystallisation process the slurry could be continuously transferred to the downstream processes if possible.

With regards to the crystallisation process, the continuous mixing and nucleation could be performed in one of the several continuous crystallisation platforms discussed in this work. The subsequent crystal growth step could be performed by one of several methods but perhaps the most practical and beneficial would be a seeded cooling crystallisation in the DN15 continuous oscillatory baffled crystalliser (COBC). The DN15 COBC has this name because it is designed to have an internal diameter of 15 mm. The first step in designing the continuous EDNB crystal growth step will be taken by characterising the heat transfer performance of the DN15 COBC.

The heat transfer performance of the DN15 COBC will be characterised through the determination of the overall heat transfer coefficients over a range of flow and oscillation conditions. Knowledge of the overall heat transfer coefficients will then allow for the implementation of a temperature profile model which predicts the temperature over a cooling process in the COBC. The ability to model the real temperature profile in the COBC

is extremely important during the design and implementation of a cooling crystallisation process as the crystal properties are directly influenced by the supersaturation profile (which is directly influenced by the temperature profile).

The temperature profile model developed here will then be applied to a theoretical case study looking at the seeded cooling crystallisation of EDNB monoclinic as a continuous process in the DN15 COBC. This case study utilises knowledge of the heat transfer performance with a typical set of crystallisation kinetics to determine the temperature and supersaturation profile which would be associated with this crystallisation process. Knowledge of the heat transfer performance will also allow for the limitations of the DN15 COBC to be discussed.

9.2. Materials & methods

9.2.1. Materials

Deionised water was sourced on-site from a Thermo Scientific Barnstead RO water purification unit.

9.2.2. Experimental methods: Temperature measurements in a COBC

Experiments were completed in a DN15 COBC platform, consisting of a series of jacketed glass tubes (straights) and non-jacketed bends, around 70 cm and 20cm in length, respectively. Fluid oscillation was provided by a fluid filled bellow unit controlled by custom electronics (housed in a control box). Peristaltic pumps (Watson-Marlow 520S) supplied the COBC with water stored in an independent stirred tank reactor (STR). The specific COBC set-up used for these temperature measurement experiments comprised of six jacketed glass straights and six unjacketed glass bends as shown in Figure 67. This smaller COBC set up was selected to simulate a typical single temperature zone of a larger COBC setup. Water

coolant was circulated through the jackets in a counter current manner by a heater/chiller (HC) (Lauda Eco RE 630S). The feed tank was controlled by an independent HC (VWR water bath 1187P) and internal flow rates were varied, alongside variation in jacket flow rates. The feed solution was maintained at either 50 or 70 °C (to simulate an undersaturated feed solution for a cooling crystallisation process) and HC controlling the shell was set to either 20 or 25 °C. Experiments were performed in an air conditioned laboratory at 20 ± 2 °C. The temperature of the solution inside the COBC and of the COBC jacket fluid was measured at 12 corresponding points along the COBC, with the use of 24 temperature probes.

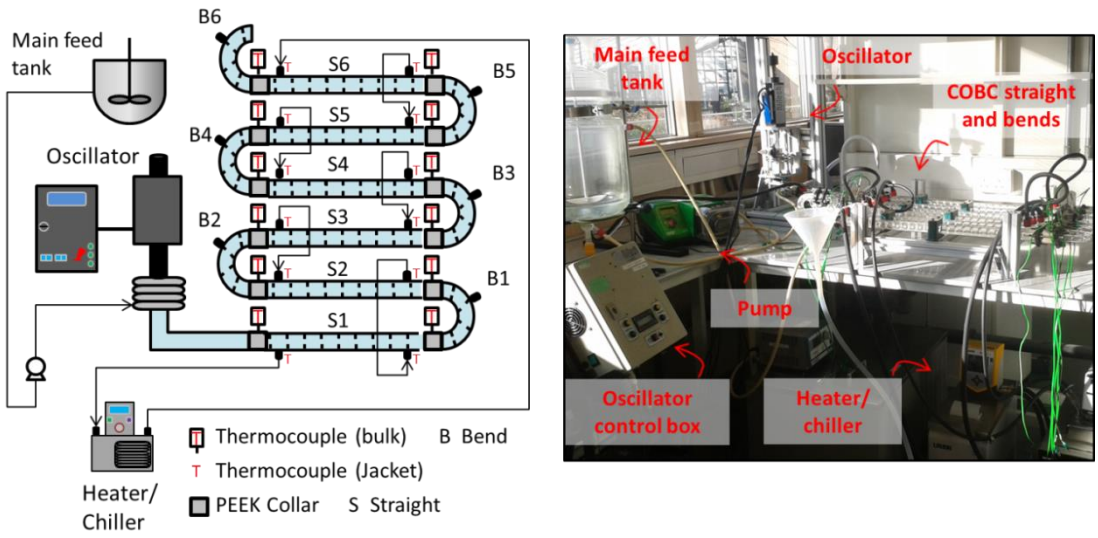

Figure 67. Schematic (left) and photograph (right) showing the COBC set-up used for heat transfer experiments operated in counter current (arrows indicate direction of flow).

Two different modes of fluid flow were used for experiments: the traditional “single oscillation” where the tube side undergoes a net flow with superimposed oscillations (with a net flow only on the shell side) and the modified “double oscillation” where the tube and shell side both experience net flow with superimposed oscillations. Within each design, the bulk solution and jacket mass flow rates were varied to investigate the effect on the temperature profile. The solution flow rate ranged from 50 to 200 g/min and the jacket

flow rate ranged from 25 g/min to 2,700 g/min. Oscillatory settings for both single oscillation (tube side) and double oscillation experiments (shell side and tube side) were set to a frequency of 1 Hz and an amplitude of 30 mm (trough-to-peak). Details of the experimental conditions can be found in Table 13.

Table 13. Experimental conditions for heat transfer studies.

Oscillation Setup	Solution Mass Flow Rate (g/min)	Jacket Mass Flow Rate (g/min)
Single	50	50
Single	50	250
Single	50	500
Single	50	750
Single	50	1000
Single	50	1700
Single	50	2700
Single	100	100
Single	150	150
Single	200	200
Single	200	1700
Single	200	2700
Double	50	25
Double	50	50
Double	100	100
Double	150	75
Double	150	81

Double	150	89
Double	150	150
Double	150	162
Double	200	200
Double	200	220
Double	200	240
Double	200	280

9.3. Heat transfer characterisation & temperature profile modelling

9.3.1. Heat transfer characterisation through the determination of overall heat transfer coefficients (U)

The overall heat transfer coefficient (U) is a measure of the overall ability of a series of conductive and convective barriers to transfer heat and is commonly applied to the calculation of heat transfer in heat exchangers. Considering that the COBC essentially takes the form of a shell-and-tube heat exchanger, the heat transfer performance of the DN15 COBC can be characterised by a set of overall heat coefficients for a range of flow and oscillation conditions [90]. The values for U can be determined from experimental temperature data. Firstly, it was considered that U can be calculated from the definition of the heat transfer rate (Q) described by equation 52.

$$Q = A\ U\ \Delta T_{lm} = Q_{sol} = m_1\ c_p\ \Delta T_{sol} \tag{52}$$

Secondly, it was considered that the log mean temperature difference (ΔT_{lm}), and the corresponding temperature differences contained within its definition, over a COBC section could be given by equations 53–55.

$$\Delta T_{lm} = \frac{\Delta T_2 - \Delta T_1}{ln\left(\frac{\Delta T_2}{\Delta T_1}\right)} \tag{53}$$

$$\Delta T_1 = T_{In} - T_2 \tag{54}$$

$$\Delta T_2 = T_{Out} - T_1 \tag{55}$$

By substituting the expression for the log mean temperature difference into the expression for Q, the overall heat transfer coefficient for a COBC section, and the corresponding area contained within its definition, are determined by equations 56 and 57.

$$U = \frac{m_1 \, c_{p1} \, \Delta T_{sol}}{A \, \Delta T_{lm}} \tag{56}$$

$$A = \pi \, d_t \, L \tag{57}$$

The values in these expressions are the mass flow rate of the solution (m_1); the specific heat capacity of the solution (c_{p1}); the total heat transfer area of the COBC section based on its inner diameter (A); the inlet and outlet temperatures of the solution (T_{In} and T_{Out}); the inlet and outlet temperatures of the jacket fluid (T_1 and T_2), the temperature difference in the solution (ΔT_{sol}) and the temperature difference in the jacket fluid (ΔT_j).

9.3.2. Temperature profile modelling

The temperature of the solution (T_1) will vary along the COBC length (x) according to a differential equation which is expressed as equation 58.

$$\frac{dT_1}{dx} = k_1(T_2 - T_1) \tag{58}$$

When the solution flows through a straight T_2 represents the temperature of the jacket fluid and when the solution flows through an unjacketed bend T_2 represents the temperature of the surrounding air. Assuming plug flow in the COBC, the constant (k_1) in

the differential equation, in addition to the heat exchange area per unit volume and the cross-sectional area contained within its definition, are given by equations 59–61.

$$k_1 = \frac{U_1\, a_1\, A_{xs1}}{m_1\, c_{p1}} \tag{59}$$

$$a_1 = 4/d_t \tag{60}$$

$$A_{xs1} = \pi\, {d_t}^2/4 \tag{61}$$

The values in these expressions are the heat exchange area per unit volume (a_1), the cross-sectional area based on the inner diameter (A_{XS1}), the mass flow rate of the solution (m_1) and the specific heat capacities of the solution (c_{p1}).

Using the overall heat transfer coefficients, and making certain assumptions, the temperature profile along the COBC can be modelled. Depending on which assumptions are made, the temperature profile model can have three levels. Level 1 assumes that the jacket fluid temperature is constant and that there are no heat losses from the jacket. Level 2 assumes that the jacket fluid varies and that there are no heat losses from the jacket. Level 3 assumes that the jacket fluid varies and that there are heat losses from the jacket. For each level, the relevant differential equations must be solved either numerically or analytically in order to model the temperature profile along the COBC.

9.3.3. Temperature profile model – Level 1

Differential equations and corresponding differential constants are given by equations 58, 59 and 62.

$$\frac{dT_1}{dx} = k_1(T_2 - T_1) \tag{58}$$

$$\frac{dT_2}{dx} = 0 \tag{62}$$

$$k_1 = \frac{U_1\, a_1\, A_{xs1}}{m_1\, c_{p1}} \tag{59}$$

The general analytical solutions are given by equations 63 and 64.

$$T_1(x) = T_2 + (T_{10} - T_2)e^{-k_1 x} \tag{63}$$

$$T_2(x) = T_2 \tag{64}$$

9.3.4. Temperature profile model – Level 2

Differential equations and corresponding differential constants are given by equations 58, 65, 59 and 66.

$$\frac{dT_1}{dx} = k_1(T_2 - T_1) \tag{58}$$

$$\frac{dT_2}{dx} = -k_2(T_1 - T_2) \tag{65}$$

$$k_1 = \frac{U_1\, a_1\, A_{xs1}}{m_1\, c_{p1}} \tag{59}$$

$$k_2 = \frac{U_1\, a_1\, A_{xs1}}{m_2\, c_{p2}} \tag{66}$$

The general analytical solutions and corresponding constants of integration are given by equations 67–70.

$$T_1(x) = C_1 + C_2\, e^{(-k_1+k_2)x} \tag{67}$$

$$T_2(x) = \frac{C_2\, e^{(-k_1+k_2)x}\, k_2}{k_1} + C_1 \tag{68}$$

$$C_1 = \frac{T_{20} - T_{10}\left(\frac{k_2}{k_1}\right)}{1 - \left(\frac{k_2}{k_1}\right)} \tag{69}$$

$$C_2 = T_{10} - C_1 \tag{70}$$

9.3.5. Temperature profile model – Level 3

Differential equations and corresponding differential constants are given by equations 58, 59, 66 and 71–74.

$$\frac{dT_1}{dx} = k_1(T_2 - T_1) \tag{58}$$

$$\frac{dT_2}{dx} = -k_2 T_1 + (k_2 + k_3)T_2 - k_3 T_a \tag{71}$$

$$k_1 = \frac{U_1\, a_1\, A_{xs1}}{m_1\, c_{p1}} \tag{59}$$

$$k_2 = \frac{U_1\, a_1\, A_{xs1}}{m_2\, c_{p2}} \tag{66}$$

$$k_3 = \frac{U_2\, a_2\, A_{xs2}}{m_2\, c_{p2}} \tag{72}$$

$$a_2 = 4/(d_s - d_t) \tag{73}$$

$$A_{xs2} = \left(\pi\, {d_s}^2/4\right) - \left(\pi\, {d_t}^2/4\right) \tag{74}$$

The general analytical solutions and corresponding constants of integration are given by equations 75–80.

$$T_1(x) = e^{(S+R)x}\, C_2 + e^{(S-R)x}\, C_1 + T_a \tag{75}$$

$$T_2(x) = \frac{1}{k_1}\left[(S+R)\, e^{(S+R)x}\, C_2 + (S-R)\, e^{(S-R)x}\, C_1 + k_1\left(e^{(S+R)x}\, C_2 + e^{(S-R)x}\, C_1 + T_a\right)\right] \quad (76)$$

$$C_1 = \frac{T_{20}k_1 - T_{10}[S+R+k_1] - T_a[-S-R]}{-2R} \quad (77)$$

$$C_2 = T_{10} - T_a - C_1 \quad (78)$$

$$S = \frac{1}{2}(-k_1 + k_2 + k_3) \quad (79)$$

$$R = \frac{1}{2}\sqrt{{k_1}^2 - 2\,k_1\,k_2 + 2\,k_1\,k_3 + {k_2}^2 + 2\,k_2\,k_3 + {k_3}^2} \quad (80)$$

The extra terms which arise in levels 2 & 3 of the temperature profile model are, m_2 = mass flow rate of jacket fluid (kg/s), c_{p2} = specific heat capacity of jacket fluid (J/kg °C), d_s = inner diameter of the shell (m), a_2 = the heat exchange area per unit volume with respect to the shell (m^{-1}), A_{xs2} = cross-sectional area with respect to the shell (m^2), T_{10} = initial temperature of solution (°C), T_{20} = initial temperature of jacket fluid (°C), T_a = air temperature (°C), k_1, k_2 & k_3 = differential equation constants (-), C_1 & C_2 = integration constants (-), and R & S = substitution constants (-).

9.4. Determining overall heat transfer coefficients (U) from experimental temperature measurements in a COBC

To assess solution temperature profiles along the crystalliser length, a series of experiments were carried out, according to Table 13, and the relative temperature was plotted with respect to COBC distance. Temperature profiles obtained from single and double oscillations setups can be found in Figure 68. As the experiments covered different temperature ranges the relative temperature was plotted against distance rather than the actual temperature so that the temperature profiles could be better compared. With this

definition of relative temperature the initial temperature has a value of 1 and the final temperature has a value of 0. The temperature data have been connected by lines only as a guide (lines do not represent the actual temperature profile).

(A)

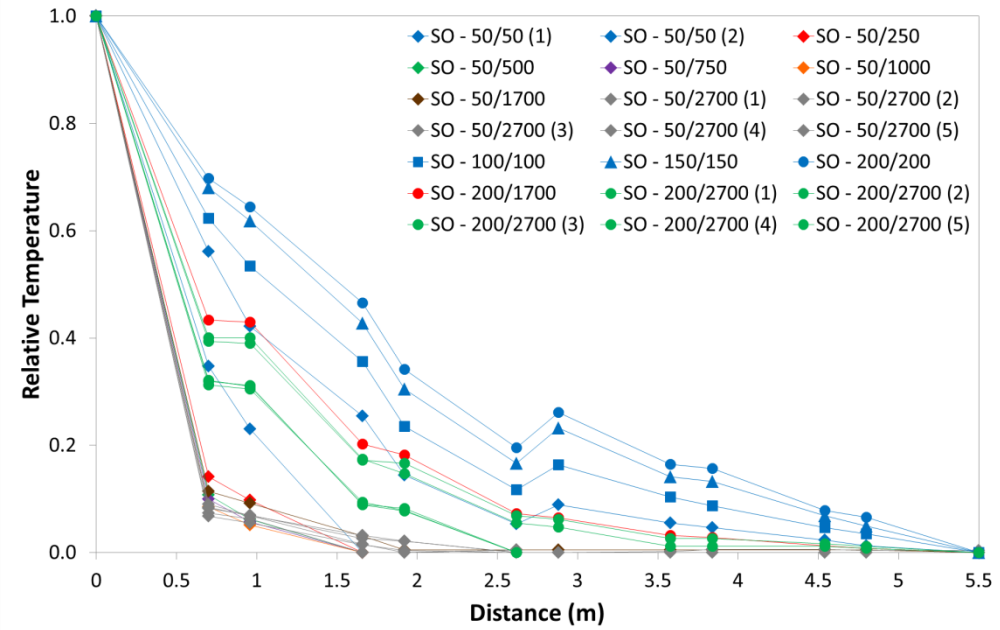

(B)

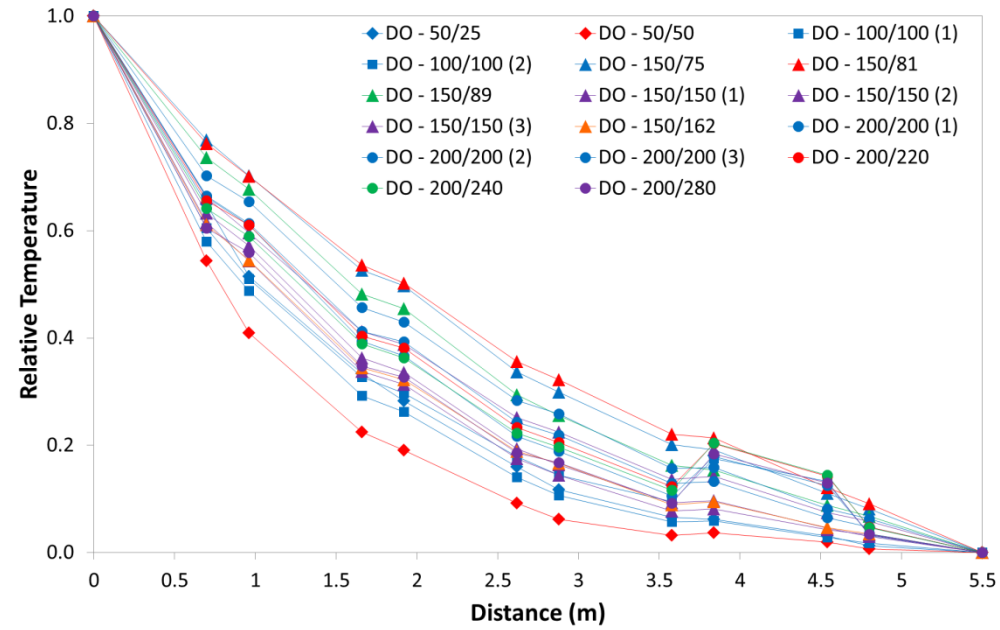

Figure 68. Experimental temperature data from (A) single and (B) double oscillation setups. The data are connected by lines as a guide only and don't represent the actual temperature profile.

The overall heat transfer coefficients (U) were calculated from the experimental temperature data using equation 56. Only U values which fulfilled two criteria were included in the final dataset. The first criterion was that the solution must be cooled by at least 1 °C in the corresponding experiment. This criterion was imposed to minimize the influence of the error in the experimental temperature measurements. The second criterion was that for each set of conditions (oscillation setup, solution mass flow rate and jacket mass flow rate) the U value must lay within 2 standard deviations of the mean U value. This criterion was imposed to remove statistical outliers. The final overall heat transfer coefficient dataset is plotted with respect to jacket mass flow rate in Figure 69.

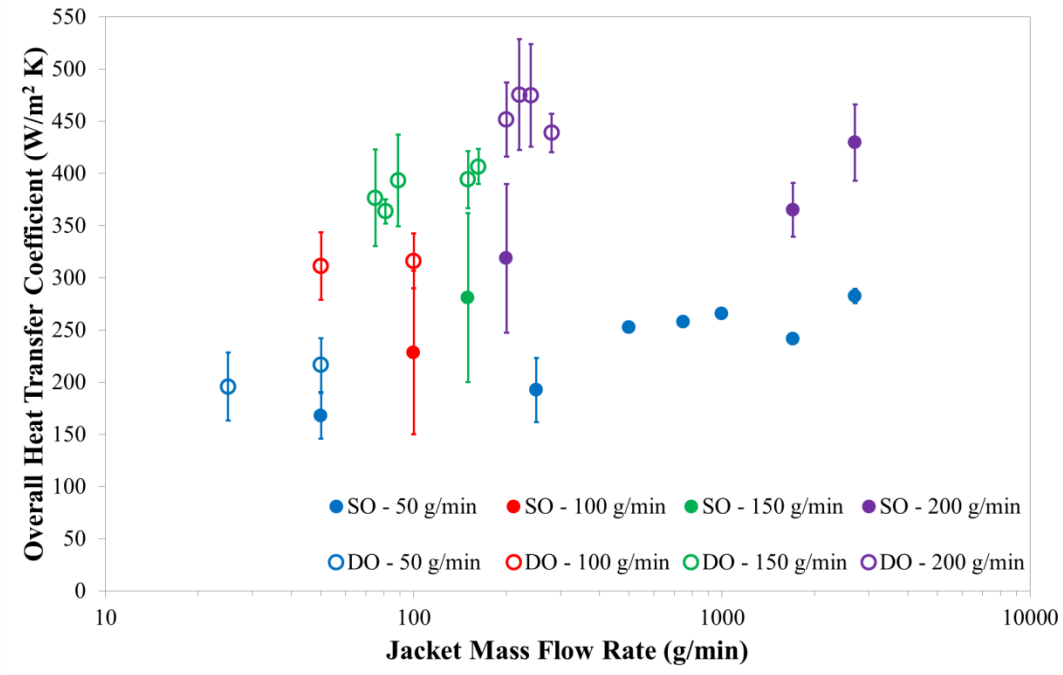

Figure 69. Overall heat transfer coefficients for the DN15 COBC with respect to jacket mass flow rate, with and without oscillation of the shell fluid. SO refers to the single oscillation

setup and DO refers to the double oscillation setup. The flow rate in the label is the solution flow rate.

For both the single and double oscillation setup, experimental temperature profiles and the overall heat transfer coefficients demonstrate that increasing the ratio of jacket mass flow rate to solution mass flow rate results in the solution cooling at a faster rate. This would be expected based on classical heat transfer theory. Furthermore, the double oscillation setup results in the solution cooling at a faster rate than the single oscillation setup. This is also to be expected as oscillation of the shell fluid increases mixing within the shell which facilitates faster heat exchange.

9.5. Temperature profile model results

In order to assess the accuracy of the overall heat transfer coefficients and the validity of the temperature profile model, experimental temperature data were compared to modelled profiles. Figure 70 shows an example of this comparison for four experiments, SO – 50/2700, SO – 200/2700, SO – 50/50 and SO – 200/200. This example utilised level 2 of the temperature profile model which assumes that although the jacket temperature varies, there are no heat losses from the jacket to the surrounding air. It should be noted that the gaps in the modelled temperature profiles correspond to the unjacketed bends.

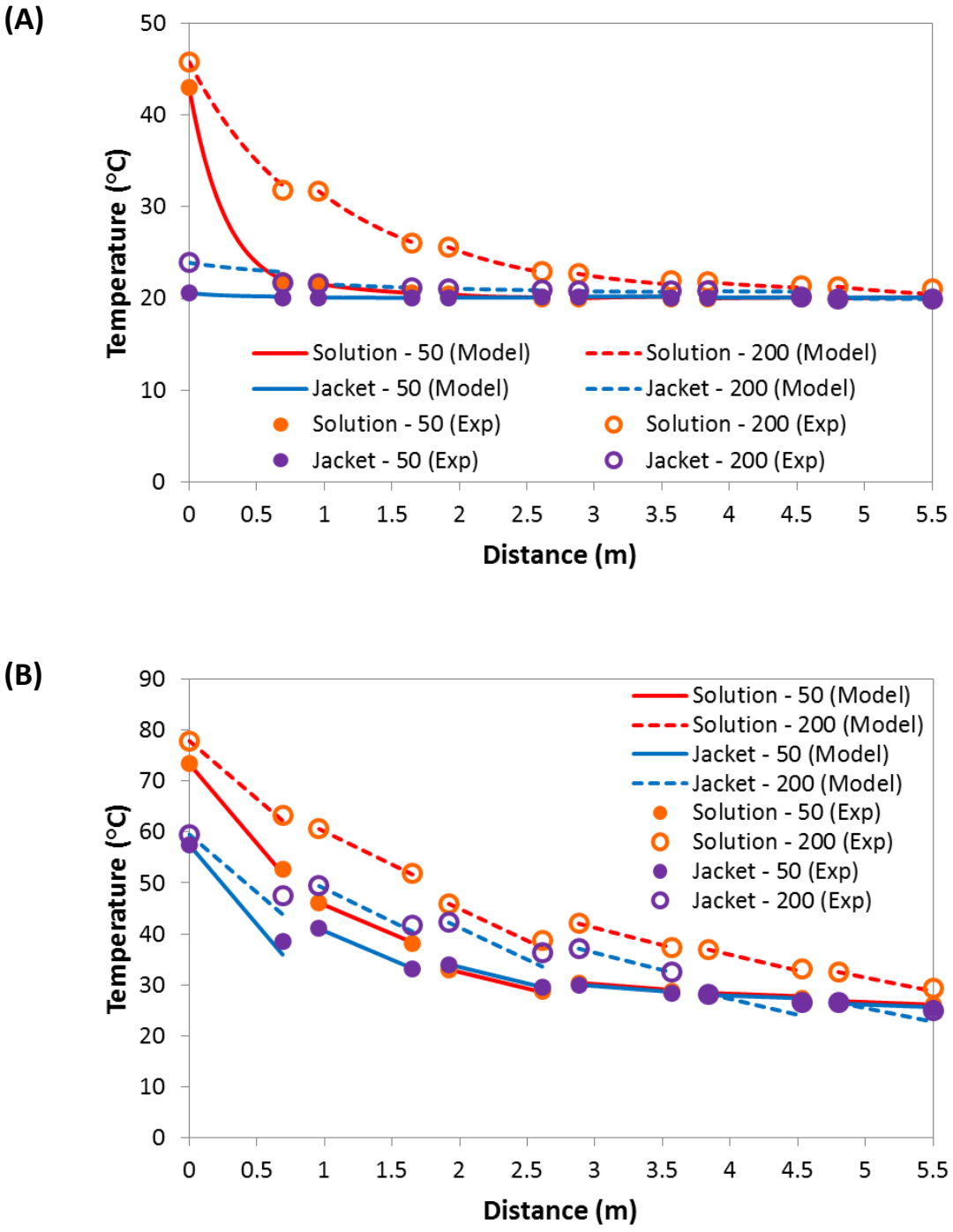

Figure 70. Experimental temperature data with modelled temperature profiles for (A) SO – 50/2700 and SO – 200/2700 in addition to (B) SO – 50/50 and SO – 200/200. SO refers to the single oscillation setup. The ratio represents solution flow rate/jacket flow rate.

It can be seen that the modelled temperature profiles are a very good fit for the experimental temperature data from the high jacket mass flow rate experiments (Figure 70 A). When a low jacket mass flow rate is used the fit is still generally good but there is some noticeable deviation between the modelled profile and the experimental data for the jacket temperature (Figure 70 B). Results suggest that at high ratios of jacket mass flow rate to solution mass flow rate the jacket is sufficiently mixed and the assumptions of the model are valid, whereas at lower ratios the mixing within the shell is poor and the assumptions of the model start to become less valid.

9.6. Jacket mixing test

To assess the hypothesis that mixing within the jacket shell is insufficient for good heat exchange at low rates, an experiment was designed where temperatures were monitored at the top and bottom of the cooling jacket during a continuous cooling experiment. Here, the solution mass flow rate was kept constant at 169 g/min whilst the jacket mass flow rate was lowered from 1702 to 77 g/min in a step-wise fashion (in order to measure the difference in temperature between the top and bottom of the jacket for each flow ratio). A single oscillation setup with oscillation conditions of 1 Hz and 30 mm were used. Figure 71 shows the temperature data that was obtained from this jacket mixing test.

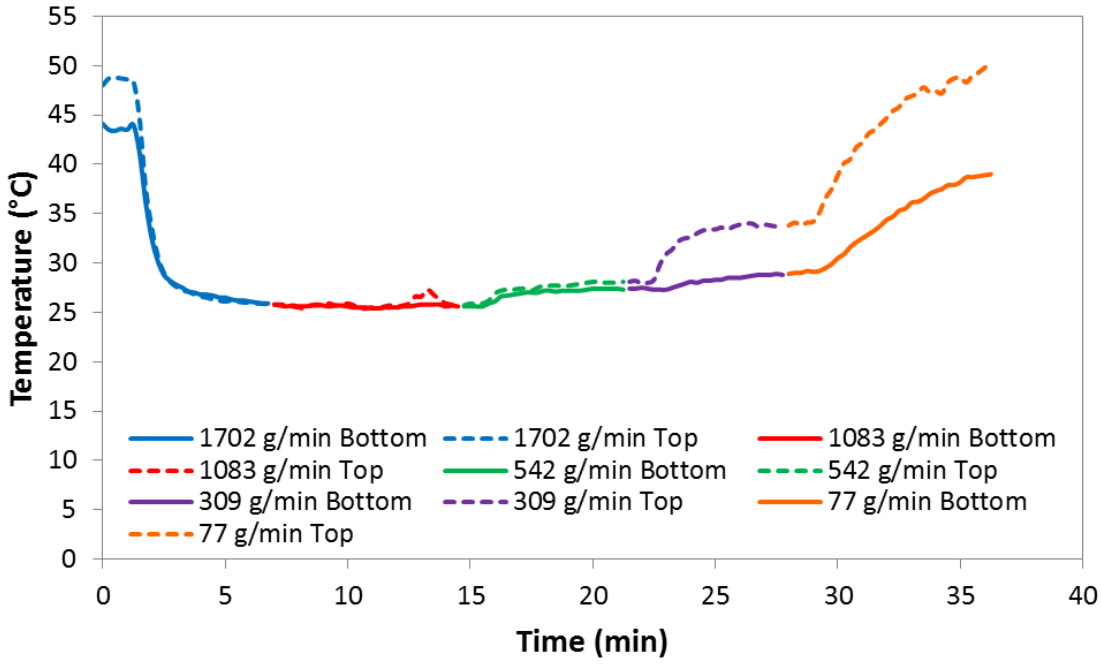

Figure 71. Results of the jacket mixing test showing the temperature on the top and bottom of a straight at various jacket mass flow rates with constant solution mass flow rate of 169 g/min.

The results show that at higher jacket mass flow rates (542 – 1702 g/min) there is a negligible temperature difference between the top and bottom of the jacket. However, when the jacket mass flow rate is lowered to 309 g/min the temperature difference between the top and bottom of the jacket increases to around 5 °C. The temperature difference increases further to around 11°C when the jacket mass flow rate is lowered to 77 g/min. These results illustrate flow separation within the shell. The top of the jacket is significantly warmer than the bottom indicating a lower flow rate at the top of the shell when compared to the bottom. Therefore, the mixing in the jacket is much poorer for low ratios of jacket mass flowrate to solution mass flowrate which causes the inaccuracy of the temperature profile model at these conditions.

9.7. Combined temperature and supersaturation profile modelling for designing continuous EDNB crystallisation

9.7.1. Introduction & modelling method

During seeded cooling crystallisation processes supersaturation levels should always remain within the metastable zone (MSZ) to control crystal growth and avoid unwanted nucleation. This can be straightforward to achieve with crystallisation systems possessing wide MSZs where small fluctuations in temperature will not move the system across the primary and/or secondary nucleation boundary. However if MSZs are narrow, a lack of understanding around temperature (supersaturation) control can result in uncontrolled crystallisation processes. Therefore, an accurate understanding of heat transfer processes along the reactor length is required to avoid operating in regions beyond the MSZ.

This theoretical case study looks at the seeded cooling crystallisation of EDNB monoclinic as a continuous process in the DN15 COBC. The model developed here applies knowledge of the heat transfer performance of the DN15 COBC with a typical set of crystallisation kinetics to determine the corresponding temperature and supersaturation profile associated with this crystallisation process. The assumptions for this case study are as follows:

- It is a seeded crystallisation process (no nucleation, only growth)
- The seed crystals are cubic, the same size and grow equally in all directions
- Growth rate constant and growth order are independent of crystal size and temperature
- The process is operating under plug flow conditions
- A counter-current cooling system is being utilised
- The jacket temperature remains constant
- pH & speciation of components remains constant

- Supersaturation can be described by the general relative supersaturation definition rather than based on the salt solubility product

In order to implement the model, the temperature dependent solubility of EDNB monoclinic in water must be known over the temperature range which is covered during the cooling. At pH 5 the solubility of EDNB monoclinic is known at the initial and final temperatures of 50 °C and 25 °C respectively but not at any other temperature. Therefore, it had to be assumed that an exponential equation could be used to fit the solubility data as the real shape couldn't be known without a data point at a third temperature. The known temperature dependent solubility data with this fitted exponential curve are shown in Figure 72.

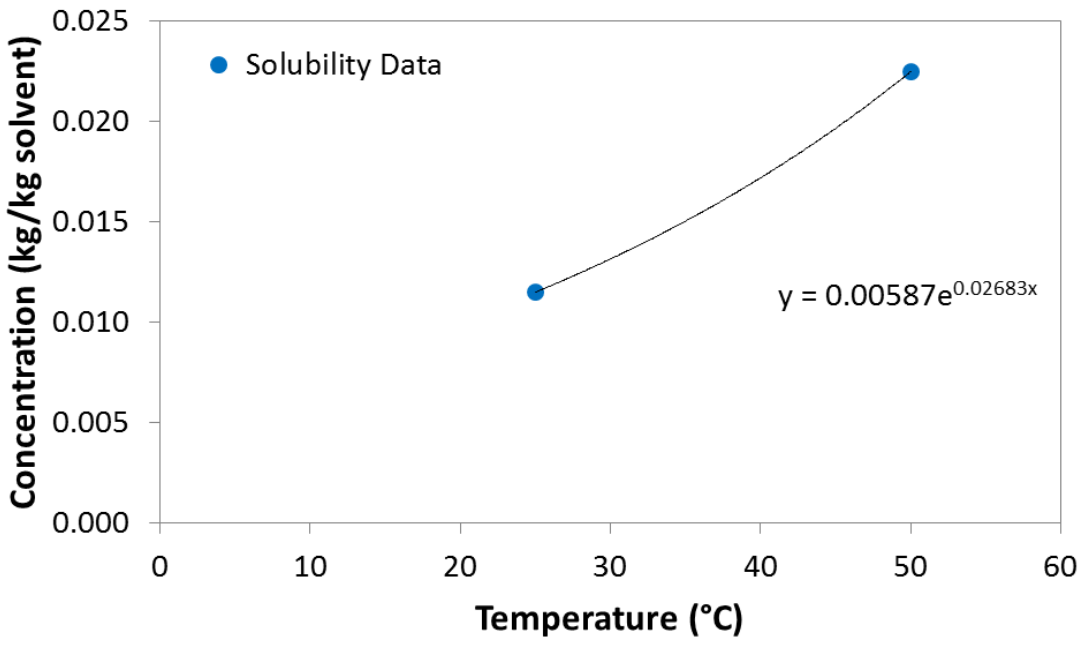

Figure 72. EDNB monoclinic temperature dependent solubility data with fitted exponential curve at pH 5.

The exponential equation used to fit the temperature dependent solubility data is described by equation 81.

$$C_S = 0.00587e^{0.02683\,T} \tag{81}$$

With consideration of both the decrease in temperature and the increase in total crystal mass with respect to time, the solution concentration (thus supersaturation) can be determined. Level 1 of the temperature profile model was utilised so the decrease in solution temperature, due to cooling, over the length of the COBC was calculated using equation 58 with a constant calculated from equation 59. The increase in total crystal mass, due to crystal growth, over the length of the COBC can be represented by equation 82.

$$\frac{dm_x}{dx} = \left((3\,k_g\,{N_T}^{1/3}\,\rho_c^{1/3}/(m_s\,C_s)^n)\,{m_x}^{2/3}\,(m_t - m_x - m_s\,C_s)^n\right)/v \tag{82}$$

In this equation, m_x = mass of API in solid phase (kg), x = COBC length (m), k_g = growth rate constant (m/s), N_T = total number of crystals (-), ρ_c = crystal density (kg/m^3), m_s = solvent mass (kg), C_s = saturation concentration (kg/kg), n = growth order (-), m_t = total mass of API (kg), and v = velocity of solution (m/s). Through simultaneous solving of equations 58 and 82 the solution concentration, and therefore the supersaturation, is known at any length of the COBC. In this case study, three different overall heat transfer coefficients were utilised with a typical set of experimental conditions in order to observe the effect heat transfer performance has on the temperature and supersaturation profile.

9.7.2 Model results & discussion

The experimental procedure involves cooling a saturated EDNB monoclinic slurry from 50 °C to a certain extent over a fixed COBC length (5.5m). Utilising a particular overall heat transfer coefficient (cooling method) will result in the solution being cooled to a particular final temperature over the COBC length. Using a basis of 1 kg solvent, the values of the constants involved in modelling the temperature and supersaturation profiles throughout the crystallisation process are shown in Table 14.

Table 14. Values for the constants used in the combined temperature and supersaturation profile model.

Constant	Symbol (Unit)	Value
Growth rate constant	k_g (m/s)	0.00001
Growth order	n (-)	1.5
Solvent mass	m_s (kg)	1
Total mass of EDNB	m_t (kg)	0.023451
Initial seed mass	m_{x0} (kg)	0.001
Crystal density	ρ_c (kg/m^3)	1,000
Initial diameter of seeds	d (m)	0.0005
Total number of crystals	N_T (-)	8,000
Solution mass flow rate	m_1 (kg/s)	0.000833
Specific heat capacity	c_p (J/kg °C)	4180
Area per unit volume	a_1 (m^{-1})	266.7
Cross-sectional area	A_{xs1} (m^2)	0.000177
Initial solution temperature	T_{10} (°C)	50
Jacket temperature	T_2 (°C)	25
Solution velocity	v (m/s)	0.004716
Overall heat transfer coefficient (1)	U_1 (W/m^2 K)	25
Overall heat transfer coefficient (2)	U_2 (W/m^2 K)	100
Overall heat transfer coefficient (3)	U_3 (W/m^2 K)	400

The variables which will change over the course of the crystallisation process as they are being determined by the model are shown in Table 15.

Table 15. Variables whose values are determined throughout the crystallisation process by the combined temperature and supersaturation profile model.

Variable	**Symbol (Unit)**
Mass of EDNB in solid phase	m_x (kg)
Solution temperature	T_1 (°C)
Solution concentration	C (kg/kg solvent)
Saturation concentration	C_S (kg/kg solvent)
Relative supersaturation	S (-)

The temperature and supersaturation profiles obtained by using the three different overall heat transfer coefficients were plotted through application of the model and are shown in Figure 73. The smallest value of overall heat transfer coefficient would be the result of utilising air cooling, the median value the result of utilising a low flow rate of cooling water and the largest value the result of utilising a high flow rate of cooling water.

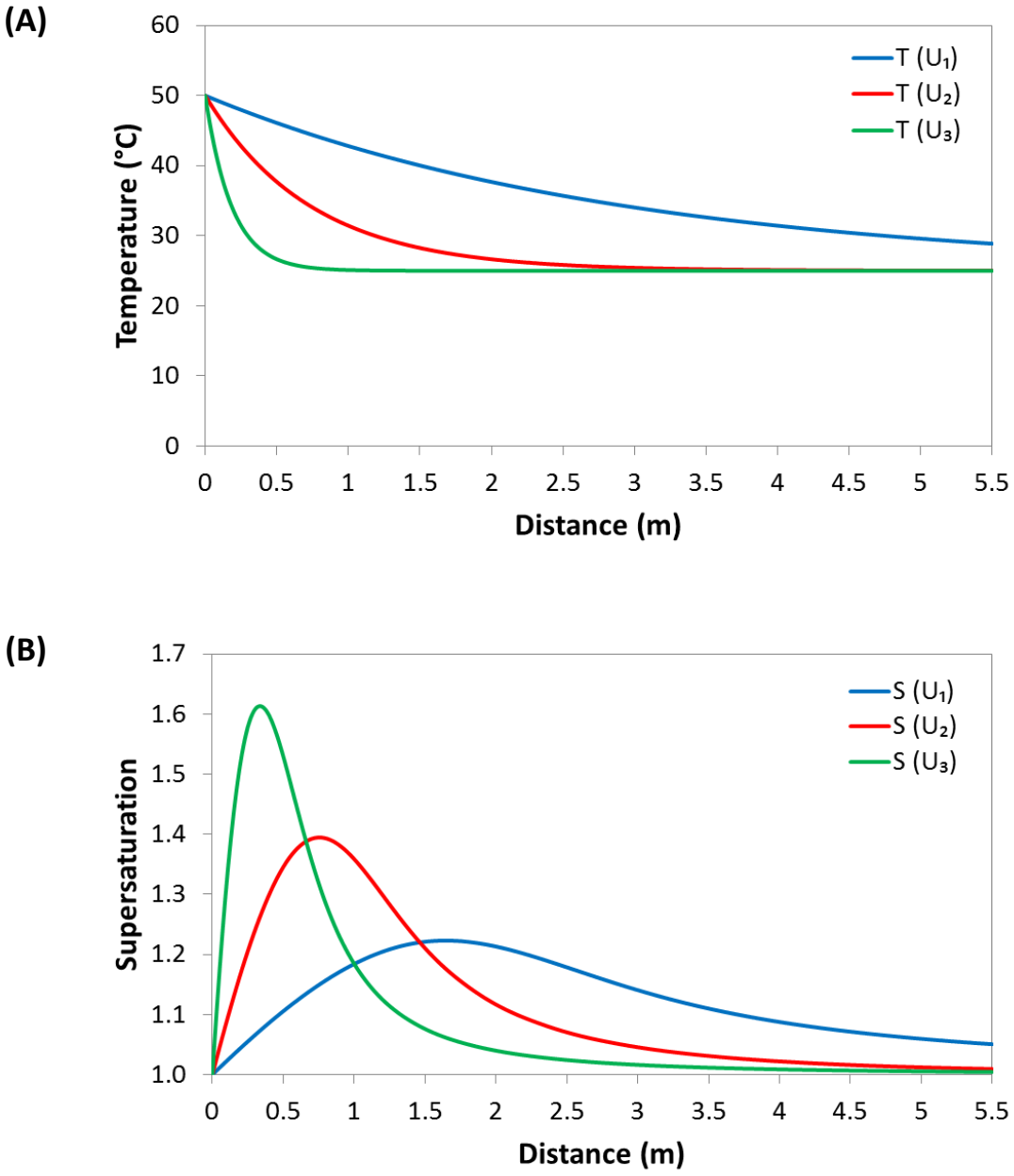

Figure 73. (A) Temperature and (B) supersaturation profiles of an experimental procedure with three different overall heat transfer coefficients. Graphs generated from model.

The plots in Figure 73 confirm that the cooling method has a significant effect on the supersaturation profile during a seeded cooling crystallisation process. That is, if this crystallisation process would leave the MSZ by exceeding a relative supersaturation value of 1.6 then the high flow rate of cooling water couldn't be utilised. Similarly, if the

crystallisation process would leave the MSZ by exceeding a lower relative supersaturation value of 1.3 then only air cooling could be utilised rather than any flow rate of cooling water.

9.8. Conclusions

In this chapter the heat transfer performance of a DN15 COBC has been characterised through determination of the overall heat transfer coefficients over a range of flow and oscillation conditions. The values of heat transfer coefficients for the jacketed straights are shown to be in the range of 150–500 $W/m^2\ K$. Heat transfer characterisation allowed for the implementation of a temperature profile model which predicts the temperature over a cooling process in the COBC. The ability to model the real temperature profile in the COBC is extremely important during the design and implementation of a cooling crystallisation as the crystal properties are directly influenced by the supersaturation profile (which is directly influenced by the temperature profile).

In addition to characterising heat transfer performance this work has uncovered the limitations of the cooling system of the COBC. Firstly, the COBC is typically operated with a very high mass flowrate in the jacket which results in the rapid cooling of the crystallisation solution and may result in a poorly controlled crystallisation process. In an effort to obtain a more gradual cooling process the mass flowrate in the jacket was substantially lowered. Although this approach did indeed produce a smoother temperature profile it resulted in much poorer mixing throughout the jacket. Poor mixing is a major issue as it may result in a large temperature difference between the top and bottom of the straights in the COBC which could result in fouling at the cold bottom and/or crystal dissolution at the warm top. Furthermore, overall heat transfer coefficients from experiments with poor jacket mixing

will be inaccurate which causes the implementation of the temperature profile model in those experiments to be inaccurate.

Knowledge of the heat transfer performance of the DN15 COBC obtained in this work was applied to a theoretical case study concerned with the seeded cooling crystallisation of EDNB monoclinic as a continuous process in the DN15 COBC. In this case study the determined overall heat transfer coefficients and a typical set of crystallisation kinetics were utilised in the temperature profile model and a basic crystal growth model in order to determine the corresponding temperature and supersaturation profiles associated with the crystallisation process. Three different sets of temperature and supersaturation profiles were obtained by using three different overall heat transfer coefficients which were intended to simulate three different modes of cooling; the smallest overall heat transfer coefficient would correspond to air cooling, the median value would correspond to a low flow rate of cooling water and the largest value would correspond to a high flow rate of cooling water. The results show that the cooling method had a significant effect on the supersaturation profile during a seeded cooling crystallisation process with the wrong cooling method possibly leading to the crystallisation process leaving the MSZ by temporarily exceeding a certain value of supersaturation. If the process did leave the MSZ then there could be uncontrolled secondary nucleation which leads to fouling and blockages in the COBC.

10. Overall conclusions and further work

10.1 Overall conclusions

Despite the great importance of organic salt crystallisation to the pharmaceutical industry there is a lack of literature describing appropriate design principles which is in stark contrast to the crystallisation of single component molecules. This is most likely because developing design principles for organic salt crystallisation requires several key challenges to be overcome. One challenge is to increase understanding of the ionic equilibria in solution and the pH-solubility of the salt. The theory of these topics is well covered in textbooks but still isn't commonly applied to designing salt crystallisation processes. For example, in the pharmaceutical industry an in-depth study of the pH-solubility of the salt typically isn't typically carried out. In order to address this lack of understanding for the EDNB crystallisation process the pH-solubility measurements of the EDNB triclinic salt and the 3,5-DNBA starting material were obtained. Furthermore, a new activity corrected solubility equation was developed and applied to properly account for the effect of high ionic strength on the EDNB salt solubility.

In addition to better understanding pH-solubility, this study also increased understanding of ionic equilibria with the development of a full solution speciation model that can be used to predict pH and solution composition during an organic salt crystallisation process. Simply with knowledge of component concentrations, dissociation constants and solubility products this tool was used to generate the entire EDNB crystallisation design space, explore different solution addition/mixing approaches and model full EDNB crystallisation processes. This allowed for the number of experiments to be minimised, easier transfer from batch to continuous crystallisation and increased process understanding.

Another key challenge in developing organic salt crystallisation processes is how to experimentally transfer from a traditional batch titration process to a continuous mixing process. From a purely experimental perspective it isn't clear how to transfer the slow addition of a strong acid in a batch vessel to a process where two solutions are continuously mixed. For this reason the first step in batch to continuous transfer should be to utilise the solution speciation model developed in this study to select suitable operating conditions with respect to the mixing approach, solutions concentrations and flow ratio. Once the operating conditions are selected a continuous mixer with a confined volume should be utilised to mix the solutions. The confined volume provides more intense, consistent and scalable mixing in comparison with larger continuous reactors (CSTRs, COBCs, etc.).

In this work several different continuous mixing platforms were utilised to perform continuous EDNB crystallisation. These included the bespoke co-axial mixer, the Ehrfeld modular microreactor system with valve mixer and the X-mixer with CSTR cascade. The results from these continuous experiments show that for a target supersaturation consistent yield, PSD and solid form is obtained across the total flow rates and mixer types. In addition, the stable monoclinic form of the EDNB salt can be crystallised in a semi-batch process which utilises a continuous mixing approach. Furthermore, in the full continuous processes PAT tools were used in combination with the solution speciation model to obtain greater process understanding and to determine if the continuous crystallisation was operating at steady state. The consistency in yield and PSD in addition to the ability to control the polymorphic outcome demonstrates the successful transfer from batch to continuous EDNB salt crystallisation which was facilitated by the solution speciation model.

A key challenge for continuous crystallisation in general is how to best control the temperature and supersaturation profiles during a seeded cooling crystallisation. During seeded cooling crystallisation processes supersaturation levels (which depend on temperature) should always remain within the metastable zone (MSZ) to ensure there is only crystal growth and no unwanted nucleation. Continuous seeded cooling crystallisation processes are commonly employed in the DN15 COBC so in this work the heat transfer performance of this device was characterised. This characterisation was performed through the determination of the overall heat transfer coefficients over a range of flow and oscillation conditions and allowed for the implementation of a temperature profile model which predicted the temperature over a cooling process in the COBC. This temperature profile model was applied to the theoretical continuous seeded crystallisation of EDNB monoclinic and demonstrated that the cooling method can have a very significant effect on the supersaturation profile with the wrong method possibly causing the process to leave the MSZ, resulting in uncontrolled secondary nucleation which leads to fouling and blockages in the COBC.

In conclusion, this work involved the development of a solution speciation model which assisted in the transfer from small scale semi-batch EDNB crystallisation to larger scale fully continuous EDNB crystallisation. By combining the use of this model with the use of PAT, the EDNB crystallisation process was better designed and better understood. Experimentally, there was a successful demonstration of transferring from batch to continuous organic salt crystallisation which allowed for the mixing of solutions to be more controlled and scalable which lead to a more consistent product in terms of the polymorphic outcome and particle properties.

10.2 Further work

In this study the pH-solubility measurements of the EDNB triclinic salt and the 3,5-DNBA starting material were obtained at 25 °C. Further work should include the experimental pH-solubility measurements of EDNB monoclinic, EDNB triclinic and 3,5-DNBA at a range of temperatures. The new activity corrected solubility equation developed in this work could then be accurately applied to account for the activity effects of at a range of temperatures for both EDNB polymorphs.

The solution speciation model developed in this study assumes perfect mixing and doesn't take salt crystallisation kinetics into account. Further work should include obtaining EDNB salt crystallisation kinetics and incorporating the crystallisation kinetics into the model. This would allow the model to predict the result of crystallising during titration which better reflects real salt crystallisation processes. In addition, the model could be used to select the required acid addition profile to obtain the optimum particle properties. Other further work involves replacing the perfect mixing assumption with a simple mixing model which accurately reflects the continuous mixing process in the mixer of interest. The data required for the simple mixing model could be obtained from mixing characterisation experiments that utilise competitive reaction schemes or optical/hyperspectral imaging. Alternatively, computational fluid dynamics (CFD) could be used to model the continuous mixer in greater detail. In any case, building a coupled speciation–mixing model would allow for the distribution of pH and salt supersaturation to be known throughout a continuous salt crystallisation process.

Some understanding of large scale metastable limits and polymorphic transformation rates were obtained for the EDNB crystallisation process. However, further work should involve performing more semi-batch EDNB crystallisation experiments which utilise different

sulfuric acid addition rates at both 25 °C and 50 °C. This would allow for the full metastable zone width (MSZW) to be determined and increase understanding of polymorphic outcome and polymorphic transformation rates. Furthermore, the data set from these experiments could be used to estimate the nucleation and growth kinetics of both polymorphs in the EDNB salt crystallisation process. The crystallisation kinetics could be incorporated into the speciation model, as already discussed, which would result in both semi-batch and continuous processes being better understood and better designed.

The main challenge to implementing continuous EDNB crystallisation in this work was the possibility of fouling and blockages. As there were regions of extremely high supersaturation in the narrow continuous mixers there was always the possibility of experiments having to be stopped early due to excessive solid formation. In this study solid formation in the continuous mixers did occur occasionally which created mixing and flow issues. Further work should include implementing heating and ultrasound in the continuous EDNB crystallisation process. For example, submerging the mixer in a heated, ultrasonic bath should result in the mixing region being undersaturated and the mixer walls being less prone to fouling. After mixing is complete the mixture would then crystallise further downstream in an area of the process which is less confined and less prone to fouling/blockages.

This work has illustrated that the issue with cooling in the DN15 COBC is that the heat transfer is often too rapid to obtain the gradual cooling profile desired in continuous crystallisation processes. The solution to this is to change the cooling method in an effort to reduce the rate of heat transfer. The most obvious way to reduce the heat transfer rate is to decrease the jacket flow rate but attempting to do this in this work lead to much poorer mixing throughout the jacket which is a major issue as the consequent large temperature

difference between the top and bottom of the COBC could result in fouling at the cold bottom and/or crystal dissolution at the warm top. Future work could involve utilising air cooling as this would correspond to a much lower heat transfer rate. Otherwise, a cooling system similar to the Cambridge Reactor Design Rattlesnake multi-orifice COBC could be used which involves having a heating coil inside the jacket in order to reduce the effect of the cooling water.

11. References

1. Schoen, H.M., C.S. Grove, and J.A. Palermo, *The early history of crystallization.* J. Chem. Educ., 1956.
2. Mullin, J., *Crystallization*. 1993, Oxford, U.K.: Butterworth-Heinemann.
3. Davey, R.J. and J. Garside, *From Molecules to Crystallizers: An Introduction to Crystallization* 2000, Oxford, U.K.: Oxford University Press.
4. Stahl, P.H. and C.G. Wermuth, *Pharmaceutical Salts: Properties, Selection and Use, 2nd Revised Edition*. International Union of Pure and Applied Chemistry (IUPAC). 2011: Wiley-VCH. 388.
5. Berge, S.M., L.D. Bighley, and D.C. Monkhouse, *PHARMACEUTICAL SALTS.* Journal of Pharmaceutical Sciences, 1977. **66**(1): p. 1-19.
6. Bastin, R.J., M.J. Bowker, and B.J. Slater, *Salt selection and optimisation procedures for pharmaceutical new chemical entities.* Organic Process Research & Development, 2000. **4**(5): p. 427-435.
7. Plumb, K., *Continuous processing in the pharmaceutical industry - Changing the mind set.* Chemical Engineering Research & Design, 2005. **83**(A6): p. 730-738.
8. Leuenberger, H., *New trends in the production of pharmaceutical granules: batch versus continuous processing.* European Journal of Pharmaceutics and Biopharmaceutics, 2001. **52**(3): p. 289-296.
9. Florence, A.T. and D. Attwood, *Physiochemical Principles of Pharmacy*. Sixth ed. 2015, London: Pharmaceutical Press.
10. Domingos, S., et al., *New forms of old drugs: improving without changing.* Journal of Pharmacy and Pharmacology, 2015. **67**(6): p. 830-846.
11. Bernstein, J., *Polymorphism in Molecular Crystals*. 2002, Oxford: Oxford University Press.

12. Childs, S.L., G.P. Stahly, and A. Park, *The salt-cocrystal continuum: The influence of crystal structure on ionization state.* Molecular Pharmaceutics, 2007. **4**(3): p. 323-338.

13. Giron, D., *Characterisation of salts of drug substances.* Journal of Thermal Analysis and Calorimetry, 2003. **73**(2): p. 441-457.

14. Serajuddin, A.T.M., *Salt formation to improve drug solubility.* Advanced Drug Delivery Reviews, 2007. **59**(7): p. 603-616.

15. Andre, V., et al., *Transforming aspirin into novel molecular salts of salicylic acid.* Structural Chemistry, 2014. **25**(3): p. 707-714.

16. Black, S.N., et al., *Structure, solubility, screening, and synthesis of molecular salts.* Journal of Pharmaceutical Sciences, 2007. **96**(5): p. 1053-1068.

17. Braga, D., et al., *Molecular Salts of Anesthetic Lidocaine with Dicarboxylic Acids: Solid-State Properties and a Combined Structural and Spectroscopic Study.* Crystal Growth & Design, 2013. **13**(6): p. 2564-2572.

18. Trask, A.V., et al., *Screening for crystalline salts via mechanochemistry.* Chemical Communications, 2006(1): p. 51-53.

19. Bernstein, J., *Polymorphism - A Perspective.* Crystal Growth & Design, 2011. **11**(3): p. 632-650.

20. Jie, L., L. Zhen, and J. Xiaolin, *Polymorphism of pharmaceutical molecules: perspectives on nucleation.* Frontiers of Chemical Engineering in China, 2010. **4**(1): p. 37-44.

21. Braga, D., et al., *Crystal Polymorphism and Multiple Crystal Forms.* Molecular Networks, 2009. **132**: p. 25-50.

22. Bond, A.D., R. Boese, and G.R. Desiraju, *On the polymorphism of aspirin.* Angewandte Chemie-International Edition, 2007. **46**(4): p. 615-617.

23. Karpinski, P.H., *Polymorphism of active pharmaceutical ingredients.* Chemical Engineering & Technology, 2006. **29**(2): p. 233-237.

24. Bardwell, D.A., et al., *Towards crystal structure prediction of complex organic compounds - a report on the fifth blind test.* Acta Crystallographica Section B-Structural Science Crystal Engineering and Materials, 2011. **67**: p. 535-551.

25. Day, G.M., et al., *Significant progress in predicting the crystal structures of small organic molecules - a report on the fourth blind test.* Acta Crystallographica Section B-Structural Science Crystal Engineering and Materials, 2009. **65**: p. 107-125.

26. Yashina, A., F. Meldrum, and A. deMello, *Calcium carbonate polymorph control using droplet-based microfluidics.* Biomicrofluidics, 2012. **6**(2): p. 10.

27. Mo, Y.X., L.P. Dang, and H.Y. Wei, *L-Glutamic Acid Polymorph Control Using Amino Acid Additives.* Industrial & Engineering Chemistry Research, 2011. **50**(18): p. 10385-10392.

28. Srinivasan, K. and P. Dhanasekaran, *Separation and nucleation control of alpha and beta polymorphs of l-glutamic acid by swift cooling crystallization process.* Amino Acids, 2011. **40**(4): p. 1257-1260.

29. Jiang, S.F., P.J. Jansens, and J.H. ter Horst, *Control over Polymorph Formation of o-Aminobenzoic Acid.* Crystal Growth & Design, 2010. **10**(6): p. 2541-2547.

30. Kordikowski, A., T. Shekunov, and P. York, *Polymorph control of sulfathiazole in supercritical CO2.* Pharmaceutical Research, 2001. **18**(5): p. 682-688.

31. Llinas, A. and J.M. Goodman, *Polymorph control: past, present and future.* Drug Discovery Today, 2008. **13**(5-6): p. 198-210.

32. Hermanto, M.W., et al., *Robust optimal control of polymorphic transformation in batch crystallization.* Aiche Journal, 2007. **53**(10): p. 2643-2650.

33. Mangin, D., F. Puel, and S. Veesler, *Polymorphism in Processes of Crystallization in Solution: A Practical Review.* Organic Process Research & Development, 2009. **13**(6): p. 1241-1253.

34. de Levie, R., *Aqueous Acid-Base Equilibria and Titrations*. Oxford Chemistry Primers. 1999, New York: Oxford University Press. 98.

35. Hou, G.Y., et al., *Development and Characterization of a Single Stage Mixed-Suspension, Mixed-Product-Removal Crystallization Process with a Novel Transfer Unit.* Crystal Growth & Design, 2014. **14**(4): p. 1782-1793.

36. Narducci, O., A.G. Jones, and E. Kougoulos, *Continuous crystallization of adipic acid with ultrasound.* Chemical Engineering Science, 2011. **66**(6): p. 1069-1076.

37. Wong, S.Y., et al., *Development of Continuous Crystallization Processes Using a Single-Stage Mixed-Suspension, Mixed-Product Removal Crystallizer with Recycle.* Crystal Growth & Design, 2012. **12**(11): p. 5701-5707.

38. Wierzbowska, B., et al., *Crystallization of vitamin C in a continuous DT MSMPR crystallizer - Size independent growth kinetic model approach.* Crystal Research and Technology, 2008. **43**(4): p. 381-389.

39. Wong, S.Y., et al., *Modeling the Crystallization Kinetic Rates of Lactose via Artificial Neural Network.* Crystal Growth & Design, 2010. **10**(6): p. 2620-2628.

40. de Paz, G.D., *Crystallization kinetics for the sugar-water-ethanol system in a continuous MSMPR crystallizer.* International Sugar Journal, 2002. **104**(1237): p. 14-20.

41. Lai, T.T.C., et al., *Continuous Crystallization and Polymorph Dynamics in the L-Glutamic Acid System.* Organic Process Research & Development, 2014. **18**(11): p. 1382-1390.

42. Ferguson, S., et al., *Characterization of the anti-solvent batch, plug flow and MSMPR crystallization of benzoic acid.* Chemical Engineering Science, 2013. **104**: p. 44-54.

43. Ferguson, S., et al., *Use of Continuous MSMPR Crystallization with Integrated Nanofiltration Membrane Recycle for Enhanced Yield and Purity in API Crystallization.* Crystal Growth & Design, 2014. **14**(2): p. 617-627.

44. Cichy, B. and E. Kuzdzal, *Obtaining Monodisperse Melamine Phosphate Grains by a Continuous Reaction Crystallization Process.* Industrial & Engineering Chemistry Research, 2014. **53**(16): p. 6593-6599.

45. Kozik, A., et al., *Continuous reaction crystallization of struvite from diluted aqueous solution of phosphate(V) ions in the presence of magnesium ions excess.* Chemical Engineering Research & Design, 2014. **92**(3): p. 481-490.

46. Gerard, A., et al., *Effect of calcium based additives on the sodium bicarbonate crystallization in a MSMPR reactor.* Powder Technology, 2014. **255**: p. 134-140.

47. Wojcik, J.A. and A.G. Jones, *Experimental investigation into dynamics and stability of continuous MSMPR agglomerative precipitation of CaCO3 crystals.* Chemical Engineering Research & Design, 1997. **75**(A2): p. 113-118.

48. Alvarez, A.J., A. Singh, and A.S. Myerson, *Crystallization of Cyclosporine in a Multistage Continuous MSMPR Crystallizer.* Crystal Growth & Design, 2011. **11**(10): p. 4392-4400.

49. Zhang, H.T., et al., *Development of Continuous Anti-Solvent/Cooling Crystallization Process using Cascaded Mixed Suspension, Mixed Product Removal Crystallizers.* Organic Process Research & Development, 2012. **16**(5): p. 915-924.

50. Lai, T.T.C., et al., *Control of Polymorphism in Continuous Crystallization via Mixed Suspension Mixed Product Removal Systems Cascade Design.* Crystal Growth & Design, 2015. **15**(7): p. 3374-3382.

51. Powell, K.A., et al., *Toward Continuous Crystallization of Urea-Barbituric Acid: A Polymorphic Co-Crystal System.* Crystal Growth & Design, 2015. **15**(10): p. 4821-4836.

52. Powell, K.A., et al., *Periodic steady-state flow crystallization of a pharmaceutical drug using MSMPR operation.* Chemical Engineering and Processing, 2015. **97**: p. 195-212.

53. Eder, R.J.P., et al., *Seed loading effects on the mean crystal size of acetylsalicylic acid in a continuous-flow crystallization device.* Crystal Research and Technology, 2011. **46**(3): p. 227-237.

54. Eder, R.J.P., et al., *Continuous Sonocrystallization of Acetylsalicylic Acid (ASA): Control of Crystal Size.* Crystal Growth & Design, 2012. **12**(10): p. 4733-4738.

55. Alvarez, A.J. and A.S. Myerson, *Continuous Plug Flow Crystallization of Pharmaceutical Compounds.* Crystal Growth & Design, 2010. **10**(5): p. 2219-2228.

56. Svoboda, V., et al., *Continuous Cocrystallization of Benzoic Acid and Isonicotinamide by Mixing-Induced Supersaturation: Exploring Opportunities between Reactive and Antisolvent Crystallization Concepts.* Crystal Growth & Design, 2017. **17**(4): p. 1902-1909.

57. MacFhionnghaile, P., et al., *Crystallization Diagram for Antisolvent Crystallization of Lactose: Using Design of Experiments To Investigate Continuous Mixing-Induced Supersaturation.* Crystal Growth & Design, 2017. **17**(5): p. 2611-2621.

58. Vacassy, R., et al., *Calcium carbonate precipitation using new segmented flow tubular reactor.* Aiche Journal, 2000. **46**(6): p. 1241-1252.

59. Stahl, M., B.L. Alund, and A.C. Rasmuson, *Reaction crystallization kinetics of benzoic add.* Aiche Journal, 2001. **47**(7): p. 1544-1560.

60. Roelands, C.P.M., et al., *Precipitation mechanism of stable and metastable polymorphs of L-glutamic acid.* Aiche Journal, 2007. **53**(2): p. 354-362.

61. Briggs, N.E.B., *Polymorph Control of Pharmaceuticals within a Continuous Oscillatory Baffled Crystalliser*, in *Strathclyde Institute of Pharmacy and Biomedical Sciences*. 2015, University of Strathclyde: Glasgow.

62. Ni, X.W., *Unwrapping the myth about plug flow.* Tce, 2006(779): p. 26-28.

63. Lawton, S., et al., *Continuous Crystallization of Pharmaceuticals Using a Continuous Oscillatory Baffled Crystallizer.* Organic Process Research & Development, 2009. **13**(6): p. 1357-1363.

64. Ricardo, C. and X.W. Ni, *Evaluation and Establishment of a Cleaning Protocol for the Production of Vanisal Sodium and Aspirin Using a Continuous Oscillatory Baffled Reactor.* Organic Process Research & Development, 2009. **13**(6): p. 1080-1087.

65. Zhao, L.H., et al., *From discovery to scale-up: alpha-lipoic acid : nicotinamide co-crystals in a continuous oscillatory baffled crystalliser.* Crystengcomm, 2014. **16**(26): p. 5769-5780.

66. McGlone, T., et al., *Oscillatory Flow Reactors (OFRs) for Continuous Manufacturing and Crystallization.* Organic Process Research & Development, 2015. **19**(9): p. 1186-1202.

67. Briggs, N.E.B., et al., *Seeded Crystallization of beta-L-Glutamic Acid in a Continuous Oscillatory Baffled Crystallizer.* Organic Process Research & Development, 2015. **19**(12): p. 1903-1911.

68. Ejim, L.N., et al., *A factorial approach to understanding the effect of inner geometry of baffled meso-scale tubes on solids suspension and axial dispersion in continuous,*

oscillatory liquid-solid plug flows. Chemical Engineering Journal, 2017. **308**: p. 669-682.

69. Agnew, L.R., et al., *Continuous Crystallization of Paracetamol (Acetaminophen) Form II: Selective Access to a Metastable Solid Form.* Crystal Growth & Design, 2017. **17**(5): p. 2418-2427.

70. Sobey, I.J., *FLOW THROUGH FURROWED CHANNELS .1. CALCULATED FLOW PATTERNS.* Journal of Fluid Mechanics, 1980. **96**(JAN): p. 1-26.

71. Sobey, I.J., *OSCILLATORY FLOWS AT INTERMEDIATE STROUHAL NUMBER IN ASYMMETRIC CHANNELS.* Journal of Fluid Mechanics, 1982. **125**(DEC): p. 359-373.

72. Stonestreet, P. and A.P. Harvey, *A mixing-based design methodology for continuous oscillatory flow reactors.* Chemical Engineering Research & Design, 2002. **80**(A1): p. 31-44.

73. Stonestreet, P. and P.M.J. Van der Veeken, *The effects of oscillatory flow and bulk flow components on residence time distribution in baffled tube reactors.* Chemical Engineering Research & Design, 1999. **77**(A8): p. 671-684.

74. Metzger, L. and M. Kind, *Influence of mixing on particle formation of fast precipitation reactions-A new coarse graining method using CFD calculations as a "measuring" instrument.* Chemical Engineering Research & Design, 2016. **108**: p. 176-185.

75. Metzger, L. and M. Kind, *On the mixing in confined impinging jet mixers - Time scale analysis and scale-up using CFD coarse-graining methods.* Chemical Engineering Research & Design, 2016. **109**: p. 464-476.

76. Zauner, R. and A.G. Jones, *On the influence of mixing on crystal precipitation processes - application of the segregated feed model.* Chemical Engineering Science, 2002. **57**(5): p. 821-831.

77. Tavare, N.S., *MIXING IN CONTINUOUS CRYSTALLIZERS.* Aiche Journal, 1986. **32**(5): p. 705-732.

78. Lewis, A., et al., *Industrial Crystallization: Fundamentals and Applications*. 2015, Cambridge: Cambridge University Press.

79. Tung, H.-H., et al., *Crystallization of Organic Compounds: An Industrial Perspective*. 2009, Hoboken: Wiley.

80. Johnson, B.K. and R.K. Prud'homme, *Chemical processing and micromixing in confined impinging jets.* Aiche Journal, 2003. **49**(9): p. 2264-2282.

81. Lindenberg, C., et al., *Experimental characterization and multi-scale modeling of mixing in static mixers.* Chemical Engineering Science, 2008. **63**(16): p. 4135-4149.

82. Lindenberg, C. and M. Mazzotti, *Experimental characterization and multi-scale modeling of mixing in static mixers. Part 2. Effect of viscosity and scale-up.* Chemical Engineering Science, 2009. **64**(20): p. 4286-4294.

83. Bourne, J.R., *Mixing and the selectivity of chemical reactions.* Organic Process Research & Development, 2003. **7**(4): p. 471-508.

84. Baldyga, J., L. Makowski, and W. Orciuch, *Interaction between mixing, chemical reactions, and precipitation.* Industrial & Engineering Chemistry Research, 2005. **44**(14): p. 5342-5352.

85. Fournier, M.C., L. Falk, and J. Villermaux, *A new parallel competing reaction system for assessing micromixing efficiency - Experimental approach.* Chemical Engineering Science, 1996. **51**(22): p. 5053-5064.

86. Falk, L. and J.M. Commenge, *Performance comparison of micromixers.* Chemical Engineering Science, 2010. **65**(1): p. 405-411.

87. Nagy, K.D., et al., *Mixing and Dispersion in Small-Scale Flow Systems.* Organic Process Research & Development, 2012. **16**(5): p. 976-981.

88. Ghanem, A., et al., *Static mixers: Mechanisms, applications, and characterization methods - A review.* Chemical Engineering Research & Design, 2014. **92**(2): p. 205-228.

89. Mackley, M.R., G.M. Tweddle, and I.D. Wyatt, *EXPERIMENTAL HEAT-TRANSFER MEASUREMENTS FOR PULSATILE FLOW IN BAFFLED TUBES.* Chemical Engineering Science, 1990. **45**(5): p. 1237-1242.

90. Mackley, M.R. and P. Stonestreet, *HEAT-TRANSFER AND ASSOCIATED ENERGY-DISSIPATION FOR OSCILLATORY FLOW IN BAFFLED TUBES.* Chemical Engineering Science, 1995. **50**(14): p. 2211-2224.

91. Solano, J.P., et al., *Numerical study of the flow pattern and heat transfer enhancement in oscillatory baffled reactors with helical coil inserts.* Chemical Engineering Research & Design, 2012. **90**(6): p. 732-742.

92. Wu, P., J. Wu, and W. Li, *A Numerical Study on the Temperature Field of Oscillatory Flow Reactor with Conic Ring Baffles.* Future Material Research and Industry Application, Pts 1 and 2, 2012. **455-456**: p. 121-+.

93. Rochow, T.G. and P.A. Tucker, *Introduction to microscopy by means of light, electrons, X-rays or acoustics*. Second ed. 1994, New York: Plenum Press.

94. Malvern. *Morphologi G3*. 2017 [cited 2017 17th June 2017]; Available from: https://www.malvern.com/en/products/product-range/morphologi-range/morphologi-g3/index.html.

95. Willen, U., *Automation in Image Analysis for Particle Size and Shape Measurement.* G.I.T. Laboratory Journal, 2008.

96. The_University_of_California_Davis. *How an FTIR spectrometer operates*. 2015 [cited 2017 17th June 2017]; Available from: https://chem.libretexts.org/Core/Physical_and_Theoretical_Chemistry/Spectroscop

y/Vibrational_Spectroscopy/Infrared_Spectroscopy/How_an_FTIR_Spectrometer_Operates.

97. Jones, H.P., *Crystallisation of Polymorphic Organic Salts*, in *Chemical Engineering and Analytical Science*. 2006, University of Manchester: Manchester.

98. George, B. and P. McIntyre, *Infrared Spectroscopy*. 1987, Chichester: Wiley.

99. Stuart, B., *Modern Infrared Spectroscopy*. 1996, Chichester: Wiley.

100. ThermoFisher. *FTIR Sample Techniques: Attenuated Total Reflection (ATR)*. 2017 [cited 2017 17th June 2017]; Available from: https://www.thermofisher.com/uk/en/home/industrial/spectroscopy-elemental-isotope-analysis/spectroscopy-elemental-isotope-analysis-learning-center/molecular-spectroscopy-information/ftir-information/ftir-sample-handling-techniques/ftir-sample-handling-techniques-attenuated-total-reflection-atr.html#.

101. Williams, D.H. and I. Fleming, *Spectroscopic Methods in Organic Chemistry*. 5th Edition ed. 1995, London: McGraw-Hill.

102. Sirius_Analytical. *Sirius T3 Titrator*. 2017 [cited 2017 25th June 2017].

103. ZEISS. *MCS 600*. 2017 [cited 2017 25th June 2017]; Available from: https://www.zeiss.com/spectroscopy/products/spectrometer-systems/mcs-600.html#downloads.

104. Avantes. *UV/VIS/NIR absorbance measurements*. 2017 [cited 2017 25th June 2017]; Available from: https://www.avantes.com/applications/measurement-techniques/item/288-uv-vis-absorbance-measurements.

105. Mettler_Toledo. *FBRM Method of Measurement*. 2017 [cited 2017 25th June 2017]; Available from: http://www.mt.com/us/en/home/library/videos/automated-reactors/Lasentec-FBRM-Method-of-Measurement.html.

106. O'Grady, D. and E. Dycus, *How In Situ Vision Simplifies Crystallization and Precipitation*. 2016.

107. Lynch, D.E., et al., *3,5-DIMETHOXYBENZOIC ACID AND THE 2ND POLYMORPH OF THE 2/1-ADDUCT OF 3,5-DINITRO-BENZOIC ACID WITH ETHYLENEDIAMINE.* Acta Crystallographica Section C-Crystal Structure Communications, 1994. **50**: p. 1259-1262.

108. Nethaji, M., et al., *STRUCTURE OF ETHYLENEDIAMMONIUM 3,5-DINITROBENZOATE.* Acta Crystallographica Section C-Crystal Structure Communications, 1992. **48**: p. 2207-2209.

109. Davey, R.J. and H.P. Jones, *The crystallisation and stability of a polymorphic salt, ethylene diammonium dinitrobenzoate.* New Journal of Chemistry, 2008. **32**(10): p. 1686-1692.

110. Jones, H.P., R.J. Davey, and B.G. Cox, *Crystallization of a salt of a weak organic acid and base: Solubility relations, supersaturation control and polymorphic behavior.* Journal of Physical Chemistry B, 2005. **109**(11): p. 5273-5278.

111. Kortum, G., W. Vogel, and K. Andrussow, 1961. **1**: p. 190-536.

112. Gupta, S.L. and R.N. Soni, Journal of the Indian Chemical Society, 1965. **42**(6): p. 377-380.

113. Hyde, D.L., *Handbook of Chemistry and Physics*. 81st ed. 2000, Boca Raton, FL: CRC Press.

114. Bolliger, A. and F.J. Reuter, *The reaction of 3,5-dinitrobenzoic acid with alkali.* Journal and Proceedings of the Royal Society of New South Wales, 1939. **72**: p. 329-334.

115. Yalkowsky, S.H. and R.M. Dannenfelser, *AQUAFAC 1: AQUEOUS FUNCTIONAL GROUP ACTIVITY COEFFICIENTS; APPLICATION TO HYDROCARBONS.* Chemosphere, 1992. **24**(8): p. 1047-1061.

116. Box, K., et al., *New Ideas about the Solubility of Drugs.* Chemistry & Biodiversity, 2009. **6**(11): p. 1767-1788.

117. Stuart, M. and K. Box, *Chasing equilibrium: Measuring the intrinsic solubility of weak acids and bases.* Analytical Chemistry, 2005. **77**(4): p. 983-990.

118. Borissova, A., et al., *Modeling the precipitation of L-glutamic acid via acidification of monosodium glutantate.* Crystal Growth & Design, 2005. **5**(3): p. 845-854.

119. Alatalo, H., et al., *In-line monitoring of reactive crystallization process based on ATR-FTIR and Raman spectroscopy.* Journal of Chemometrics, 2008. **22**(11-12): p. 644-652.

120. Alatalo, H.M., et al., *Closed-Loop Control of Reactive Crystallization. Part I: Supersaturation-Controlled Crystallization of L-Glutamic Acid.* Chemical Engineering & Technology, 2010. **33**(5): p. 743-750.

121. Hatakka, H., et al., *Closed-Loop Control of Reactive Crystallization PART II: Polymorphism Control of L-Glutamic Acid by Sonocrystallization and Seeding.* Chemical Engineering & Technology, 2010. **33**(5): p. 751-756.

122. Alatalo, H., et al., *Process Control and Monitoring of Reactive Crystallization of L-Glutamic Acid.* Aiche Journal, 2010. **56**(8): p. 2063-2076.

123. Su, Q.L., R.D. Braatz, and M.S. Chiu, *JITL-based concentration control for semi-batch pH-shift reactive crystallization of L-glutamic acid.* Journal of Process Control, 2014. **24**(2): p. 415-421.

124. Su, Q.L., M.S. Chiu, and R.D. Braatz, *Modeling and Bayesian Parameter Estimation for Semibatch pH-Shift Reactive Crystallization of L-Glutamic Acid.* Aiche Journal, 2014. **60**(8): p. 2828-2838.

125. Garside, J., A. Mersmann, and J. Nyvlt, *Measurement of Crystal Growth and Nucleation Rates*. Second ed. 2002, Rugby: IChemE.